



# University of HUDDERSFIELD

## University of Huddersfield Repository

Abdulwahab, Abubaker

Investigations on the Roll Stability of a Semitrailer Vehicle Subjected to Gusty Crosswind Aerodynamic Forces

### Original Citation

Abdulwahab, Abubaker (2018) Investigations on the Roll Stability of a Semitrailer Vehicle Subjected to Gusty Crosswind Aerodynamic Forces. Doctoral thesis, University of Huddersfield.

This version is available at <http://eprints.hud.ac.uk/id/eprint/34686/>

The University Repository is a digital collection of the research output of the University, available on Open Access. Copyright and Moral Rights for the items on this site are retained by the individual author and/or other copyright owners. Users may access full items free of charge; copies of full text items generally can be reproduced, displayed or performed and given to third parties in any format or medium for personal research or study, educational or not-for-profit purposes without prior permission or charge, provided:

- The authors, title and full bibliographic details is credited in any copy;
- A hyperlink and/or URL is included for the original metadata page; and
- The content is not changed in any way.

For more information, including our policy and submission procedure, please contact the Repository Team at: [E.mailbox@hud.ac.uk](mailto:E.mailbox@hud.ac.uk).

<http://eprints.hud.ac.uk/>

# **INVESTIGATIONS ON THE ROLL STABILITY OF A SEMITRAILER VEHICLE SUBJECTED TO GUSTY CROSSWIND AERODYNAMIC FORCES**

THESIS SUBMITTED IN PARTIAL FULFILMENT OF THE REQUIREMENTS FOR THE  
DEGREE OF DOCTOR OF PHILOSOPHY AT THE UNIVERSITY OF HUDDERSFIELD

in the  
School of Computing and Engineering

By

Abubaker Abdulwahab (Researcher)

B.Eng. Sebha University, Libya, 2001

M.Sc. University of Tripoli, Libya, 2008

NOVEMBER 2017

## **Copyright Statement**

---

The author of this thesis (including any appendices and/or schedules to this thesis) owns any copyright in it (the “Copyright”) and s/he has given The University of Huddersfield the right to use such copyright for any administrative, promotional, educational and/or teaching purposes.

Copies of this thesis, either in full or in extracts, may be made only in accordance with the regulations of the University Library. Details of these regulations may be obtained from the Librarian. This page must form part of any such copies made.

The ownership of any patents, designs, trademarks and any and all other intellectual property rights except for the Copyright (the “Intellectual Property Rights”) and any reproductions of copyright works, for example graphs and tables (“Reproductions”), which may be described in this thesis, may not be owned by the author and may be owned by third parties. Such Intellectual Property Rights and Reproductions cannot and must not be made available for use without the prior written permission of the owner(s) of the relevant Intellectual Property Rights and/or Reproductions.

## ABSTRACT

---

Threats of high crosswind gusts on running safety of modern road and rail vehicles have been reported around the world. Under high transient crosswind conditions, sudden changes in vehicle aerodynamic forces can lead to adverse effects on vehicle dynamics and stability. Moreover, due to increase in maximum speed limits and body dimensions of commercial vehicles as well as reduction in their weights, large class vehicles, in particular, are more prone to rollover accidents in strong crosswind situations, especially at cruising speeds or at exposed sites. Such crosswind accidents have been observed even at low vehicle speed of 15 m/s in adverse windy weather. It is therefore essential to conduct detailed investigations on the aerodynamic performance of commercial vehicles under crosswind conditions in order to improve their crosswind stability.

In this study, estimation of unsteady aerodynamic forces acting on a high-sided tractor-trailer vehicle have been carried out based on experiential and numerical simulations. Although natural crosswind gusts are high-turbulent phenomena, and have a large variability in types and origins, this study suggests employing two gust scenarios based on two different methods:

1. Transient wind gust scenario developed in wind-tunnel to represents a high-sided tractor semitrailer vehicle moving on a road in moderate wind condition and immediately being hit by wind gust.
2. Deterministic crosswind scenario with gusts in exponential shapes has been considered to predict crosswind aerodynamic forces of a high-sided tractor semitrailer vehicle moving through wind exposed area. This scenario is specified in the Technical Specification for Interoperability (TSI) standard, but it has been employed in this study in combination with Computational Fluid Dynamics (CFD).

A series of time-dependent crosswind aerodynamic forces acting on the tractor-semitrailer vehicle have been predicted. Moreover, to illustrate the potential influence of crosswind gusts

on a high-sided tractor semitrailer vehicle, instantaneous gust flow structures for proposed wind scenarios and wind pressure fields were presented. The results show that both wind gust scenarios have significant unsteady effects on the side aerodynamic force and the roll moment of the vehicle. Furthermore, there are significant variations in aerodynamic loads, and the flow field becomes more complicated, consistent with the gust's strength. These conclusions strongly suggested the importance of considering the unsteady aerodynamic forces in the analysis of heavy vehicle roll dynamics.

Lateral load transfer ratio (LTR) is a criterion that is often used for designing ground vehicle rollover warning technologies to indicate the vehicles rollover status. Generally, LTR index depends on road geometry and vehicle dynamic characteristics. However, as mentioned above, crosswind loads have the potential to influence the roll stability and therefore the safety of large commercial vehicles. Therefore, this thesis presents the research carried out to improve the traditional LTR for a high-sided tractor semitrailer vehicle to be more efficient in crosswind environment. For this purpose, since experimental investigations on vehicle rollover dynamics are difficult to carry out, a coupled simulation of crosswind aerodynamic forces and multi-body vehicle dynamics has been proposed. In this method, the predicted aerodynamic forces result due to the proposed wind scenarios were input into multi-body dynamic simulations of the tractor semi-trailer vehicle that were performed through Adams/Car software. Based on this coupled analysis, dynamic responses of the vehicle to fluctuating crosswind conditions have been predicted. Moreover, all parameters of the LTR index such as body roll angle and lateral acceleration were estimated through a critical turning manoeuvre with crosswind actions. The investigation results show that, in the same manoeuvre, in comparison with the traditional LTR index (i.e., in which crosswind aerodynamic forces are ignored), the improved LTR rollover (crosswind) indicator, has successfully detected wheel lift-up conditions when crosswind aerodynamic loads are

considered. Also, average values of the LTR measured under crosswind effects are about 22% higher than those of corresponding traditional LTR index. Therefore, the rollover indicator that has been improved by the proposed methodology can provide more reliable information to the warning or control system in the presence of wind conditions.

## DECLARATION

---

- The author of this thesis (including any appendices and/or schedules to this thesis) owns any copyright in it (the “Copyright”) and he has given The University of Huddersfield the right to use such Copyright for any administrative, promotional, educational and/or teaching purposes.
  
- Copies of this thesis, either in full or in extracts, may be made only in accordance with the regulations of the University Library. Details of these regulations may be obtained from the Librarian. This page must form part of any such copies made.
  
- The ownership of any patents, designs, trademarks and any and all other intellectual property rights except for the Copyright (the “Intellectual Property Rights”) and any reproductions of copyright works, for example graphs and tables (“Reproductions”), which may be described in this thesis, may not be owned by the author and may be owned by third parties. Such Intellectual Property Rights and Reproductions cannot and must not be made available for use without the prior written permission of the owner(s) of the relevant Intellectual Property Rights and/or Reproductions.

## **ACKNOWLEDGEMENT**

---

In the beginning, I would like to pay my undivided gratitude to almighty Allah for providing me the opportunity to be on this planet and take a part in the advancement of the human race with my best capability. Thereafter, I am highly indebted to my parents for their constant encouragement and support in all stages of my life. My words fall short to thank them.

I would like to express my deep thanks and sincere indebtedness to Prof. Rakesh Mishra for supervising this research and for his efforts to put the research work on the right path. I would like to thank all my colleagues at the Energy, Emissions and Environment Research group at the University of Huddersfield. In addition, I would like to acknowledge the considerable amount of help and support provided by my co-supervisor Dr. Taimoor Asim to complete this thesis.

Furthermore, sincere gratitude should get to the Libyan Government who funded my scholarship without whose support I could not achieve this study. At last but not least, I wish to thank my wife and my family, for their devoted care during my PhD journey.

# CONTENTS

---

Chapter 1 : Introduction.....	1
1.1 Background.....	2
1.1.1 Mechanics of a heavy vehicle rollover .....	3
1.1.2 Contribution of wind loads to rollover dynamics .....	9
1.1.3 Analysis of a ground vehicle crosswind stability .....	12
1.2 Motivation.....	18
1.3 Research Aims .....	21
1.4 Thesis outline.....	21
Chapter 2 : Literature Review.....	24
2.1 Vehicle crosswind aerodynamics.....	25
2.1.1 Wind-tunnel studies on moving vehicle models.....	27
2.1.2 Wind-tunnel investigation using a static vehicle model .....	30
2.1.3 Experimental simulation of gusty crosswind conditions .....	31
2.2 Wind gust modelling and CFD investigations on vehicle aerodynamics .....	35
2.2.1 Modelling of wind gust.....	35
2.2.2 CFD investigation of unsteady tractor semitrailer aerodynamics .....	37
2.3 Coupling aerodynamics to vehicle dynamics .....	40
2.4 Rollover prediction .....	46
2.5 Summary of Literature Review and gap identification.....	48
2.6 Specific Research Objectives.....	50
Chapter 3 : Methodology-Wind-tunnel experiments on aerodynamic characteristics of a high-sided tractor semitrailer vehicle in gusty crosswind conditions.....	52
3.1 Introduction.....	53
3.2 Wind-tunnel set-up .....	54
3.2.1 Wind-tunnel components.....	54
3.2.2 Aerodynamic model.....	56
3.3 Flow-speed measurements.....	57

3.4 Pressure measurements .....	59
3.5 Gust generation system.....	63
3.6 Calibration of instruments .....	66
3.7 Experimental Procedure.....	67
3.8 Experimental results .....	68
3.8.1 Reynolds number .....	68
3.8.2 Pressure coefficient.....	68
3.6.3 Values of mean aerodynamic coefficients .....	71
3.7 Accuracy of Measurement and Estimating Uncertainty .....	74
3.8 Summary.....	76
Chapter 4 : Methodology: CFD and Multi-body dynamic (MBD) Modelling .....	78
4.1 Introduction.....	79
4.2 LES governing equations.....	80
4.3 Fluent set up.....	81
4.3.1 Pre-Processing .....	83
4.3.2 Fluent solver Execution .....	87
4.3.3 Boundary condition.....	88
4.4 Solution methods and test accuracy.....	89
4.4.1 Simulation time step and Convergence Criteria .....	90
4.4.2 Mesh independent study .....	91
4.5 CFD Aerodynamic coefficients of tractor semi-trailer vehicle.....	92
4.6 Multibody dynamics modelling of tractor-trailer combination.....	94
4.6.1 Theory of multibody dynamics.....	94
4.7 Modelling of tractor semitrailer systems based on ADAMS/car application .....	98
4.7.1 Co-ordinate systems.....	98
4.7.2 Virtual prototyping modelling .....	102
4.8 Model analysis .....	107
4.9 Validation of ADAMS Tractor Semitrailer Model.....	108
4-10 Summary .....	111

Chapter 5 : Unsteady aerodynamic forces of a tractor semitrailer vehicle moving in gusty crosswind conditions.....	113
5.1 Analysis of wind-tunnel gust flow.....	113
5.1.1. Vertical velocity Profile.....	114
5.1.2 Wind-tunnel flow field.....	115
5.2 Wind speed time series .....	117
5.2.1 Parameters of wind-tunnel turbulent flow .....	119
5.3 Development of transient gusty crosswind scenario.....	123
5.3.1 Development of new mean time-varying wind gust model.....	125
5.4 Calculation of aerodynamic forces acting on a tractor-trailer vehicle in transient gusty crosswind environment .....	128
5.4.1 Relative wind speed.....	128
5.4.2 Calculation of unsteady side aerodynamic force .....	129
5.5 Deterministic modelling of extreme wind gust condition.....	133
5.5.1 Deterministic wind gust-characteristic .....	134
5.5.2 TSI Gust scenario.....	136
5.6 CFD Aerodynamics simulation of full- scale tractor-semitrailer unit under TSI gust scenario .....	140
5.6.1 Vehicle Model and Computational domain .....	141
5.6.2 TSI gust flow fields.....	143
5.6.3 The TSI wind gust pressure distribution over the vehicle .....	148
5.6.4 Unsteady aerodynamics loads due to TSI gust condition .....	152
5-7 Summary .....	154
Chapter 6 : Effects of gusty crosswind conditions on tractor semitrailer vehicle dynamics and its roll stability .....	156
6.1 Coupling unsteady aerodynamic forces to a tractor semitrailer motion .....	157
6.2 Dynamic responses of a high sided tractor semi-trailer vehicle to gusty wind conditions .....	158
6.2.1 Effect of crosswind gust on tractor semitrailer lateral dynamics.....	160
6.2.2 Effect of crosswind gust on tractor semitrailer rotational dynamics.....	163
6.3 Effects of crosswind actions on vehicle steering dynamics.....	167

6.4 Crosswind rollover index.....	171
6.4.1 Simulation results .....	174
6.5 Comparison investigation on coupled aerodynamic and dynamic method.....	179
6-7 Development of characteristic crosswind curve .....	182
6-8 Summary .....	184
Chapter 7 : Parametric and comparison study on performance of LTR index under crosswind loads .....	185
7.1 Parametric Study of Vehicle Rollover Stability.....	186
7.1.1 Effects of tractor semitrailer speed on roll stability .....	186
7.1.2 Effects of roll centre Location .....	187
7.1.3 Effects of Pressure Centre.....	189
7.1.4 Effects of Vehicle Mass.....	192
7.1.5 Effects of multi-parameters (vehicle mass and radius of road-curvature) on performance of LTR rollover indicator.....	193
7.2 Comparative analysis of Rollover Indicators for a tractor semitrailer vehicle under wind gust condition .....	195
7.2.1 Energy-Based Rollover indicator.....	195
7.2.2 Rollover Critical Factor .....	197
7.3 Evaluation of the Performance of a Passive Rollover Warning System in Crosswind Conditions .....	199
7.3.1 Description of RWS system.....	199
7.3.2 Case study .....	201
7.4 Summary.....	204
Chapter 8 : Conclusions.....	205
8.1. Research Problem Synopsis.....	206
8.2. Research Aims and Major Achievements.....	207
8.3 Thesis Conclusions .....	210
8.4 Thesis Contributions and Novelties.....	215
8.5 Recommendations for Future Work .....	217
References.....	219

APPENDIX A..... 233  
APPENDIX B..... 236  
APPENDIX C..... 237  
APPENDIX D..... 238

## LIST OF FIGURES

---

Figure 1-1 General configuration of tractor trailer units and couples used in AHVs[2].	2
Figure 1-2: Tripped and un-tripped vehicle rollover [8].	4
Figure 1-3: The free body diagram of a heavy vehicle in steady turn[11].	5
Figure 1-4: Generic roll response graph for rigid vehicle[11].	7
Figure 1-5 : Generic roll response graph for a multiple-axles vehicle [11].	8
Figure 1-6 : General force acting on vehicle in crosswind environments	10
Figure 1-7: A high-sided vehicle accidents due to crosswind actions	11
Figure 1-8: Schematic view for a ground vehicle crosswind stability approach	12
Figure 1-9 : Typical point velocity measurements in turbulent wind flow	13
Figure 1-10 : A coordinate system with the x, y, and z axes adopted for the definition of the aerodynamic forces and moments.	15
Figure 1-11 : Dynamic forces acting on an articulated vehicle. (A) Tractor of vehicle; (B) trailer with more than two axles[27]	16
Figure 2-1: Photos showing the vehicle employed for the full-scale on road tests[43].	26
Figure 2-2: Crosswind generator (on-road test facility)[47].	27
Figure 2-3: A moving vehicle device[48].	29
Figure 2-4: Device creating an oscillating flow upstream from the vehicle [59]	32
Figure 2-5: Wind-tunnel test bench for crosswind simulation[62]	33
Figure 2-6 : (A) High crosswind flow due to special topography[66];(B) rollover accident due to wind condition and site topography[63]	34
Figure 2-7 : Crosswind simulation in Lab [66].	35
Figure 2-8 : Real wind data measured by an anemometer [81]	36
Figure 2-9 : IEC wind gusts model [76]	37
Figure 3-1 : Wind-tunnel equipment	55
Figure 3-2 : Schematic of the experimental setup	56
Figure 3-3 : Tractor semitrailer model built in ADAMS/Car	57
Figure 3-4: Wind-tunnel model of tractor semitrailer (scaled- ADAMS model)	57
Figure 3-5 : Cobra probe and flow data acquisition	58
Figure 3-6 : TFI device control.	59
Figure 3-7:Data display screen in cobra probe	59
Figure 3-8: Pressure tapping points	60
Figure 3-9: Digital manometer for pressure measurements	60
Figure 3-10: Experimental design for pressure measurement	61
Figure 3-11: Pitot tube	62

Figure 3-12: Longitudinal distribution of pressure taps .....	62
Figure 3-13 : Pressure taps distribution on the model's cross-section (loop).....	63
Figure 3-14 :Mechanism of gust generatorFigure 3-15: Layout of gust generation system .....	65
Figure 3-16: Sampling point .....	66
Figure 3-17 : Mechanism of flow pressure measurement by using Pitot tube.....	67
Figure 3-18 : Values of pressure coefficients at $\beta= 90^\circ$ .....	70
Figure 3-19 : Values of pressure coefficients at $\beta=45^\circ$ .....	70
Figure 3-20 : Pressure coefficients data at $\beta= 0^\circ$ .....	71
Figure 3-21 :Comparison between pressure (triangles) and dynamometric balance (circles) measurements: (a) lateral force coefficient [129] .....	72
Figure 3-22: (A) surface area around the $i$ th tap; (B) wind-tunnel flow (main) parameters.....	73
Figure 3-23 : Side and longitudinal aerodynamic force coefficients .....	74
Figure 4-1 schematic drawing for the CFD analysis .....	82
Figure 4-2: Tractor semitrailer 3D model.....	84
Figure 4-3: CFD computational domain (without gust generator) .....	85
Figure 4-4: Mesh topology .....	86
Figure 4-5: $Y^+$ distribution over the CFD model .....	87
Figure 4-6: (a) CFD vs wind-tunnel side and drag aerodynamic coefficients; (b) data comparison ..	93
Figure 4-7: Ground Reference Frame (GRF) and a part frame[144].....	95
Figure 4-8 : ISO Vehicle Axis System .....	99
Figure 4-9 : ADAMS fixed coordinate system .....	100
Figure 4-10 : Database structure for MSC ADAMS /car .....	100
Figure 4-11: Schematic outline for ADAMS work.....	101
Figure 4-12 : Subsystems of the complete multibody dynamic model for the tractor semitrailer vehicle .....	103
Figure 4-13: Front suspension for tractor unit .....	104
Figure 4-14:Suspension of trailer axle.....	105
Figure 4-15: Road builder.....	106
Figure 4-16: Road model .....	106
Figure 4-17 : Event builder .....	107
Figure 4-18: On road experimental facilities for testing of vehicle dynamics [144] .....	109
Figure 4-19: Validation of ADAMS dynamic simulation of tractor semitrailer vehicle [144] .....	110
Figure 4-20 : Test and ADAMS simulation results for tractor semitrailer vehicle performance for validation purpose [149] .....	111
Figure 5-1: Time-average boundary layer velocity profile at sampling point in wind-tunnel without gusty flow (i.e. cobra probe velocity profile) .....	114

Figure 5-2: Boundary layer (transient) velocity profile at sampling point in wind-tunnel under gusty flow conditions .....	115
Figure 5-3: Velocity contour of wind-tunnel gust flow: a) extracted at t=1sec; b) at t=10 sec .....	116
Figure 5-4: Velocity contour of wind-tunnel flow (without gust generator) .....	117
Figure 5-5 : Longitudinal wind velocity component recorded in wind-tunnel .....	118
Figure 5-6: Lateral wind velocity component recorded in wind-tunnel .....	118
Figure 5-7: Vertical wind velocity component recorded in wind-tunnel .....	118
Figure 5-8: Longitudinal wind velocity component recorded in wind-tunnel under gust conditions	120
Figure 5-9: Time-average and time-varying mean wind speed recorded in wind-tunnel under gust condition .....	121
Figure 5-10: Discrete gusts of stochastic wind data .....	122
Figure 5-11: Transient crosswind scenario developed based on wind-tunnel data.....	124
Figure 5-12: Mean and fluctuation crosswind speed of the transient scenario .....	125
Figure 5-13: Parameters of mean time-varying wind gust model.....	126
Figure 5-14: Effects of inclination angle of gust generator on gust properties.....	128
Figure 5-15 : Longitudinal (u direction) velocity vector diagram for instantaneous wind speed (i.e., mean (U) and fluctuating ( $u'$ )): triangle ABC for the mean wind speed U, and triangle ABD includes the $u'$ , .....	129
Figure 5-16: Side aerodynamic force due to developed transient crosswind scenario .....	131
Figure 5-17: CFD computational domain and trailer model (with gust generator) .....	132
Figure 5-18: Time-varying mean aerodynamic side-force (CFD based results) .....	132
Figure 5-19: A vehicle moving through high crosswind conditions. ( Geometry analysis)[75].....	136
Figure 5-20: TSI gust scenario.....	137
Figure 5-21: 3D full-scale model of a tractor semitrailer vehicle(ADAMS model).....	142
Figure 5-22: (a) computational domain (b) mesh topology .....	143
Figure 5-23: Monitoring points over the TSI gust period.....	144
Figure 5-24: Velocity contours of the TSI gust flow.....	145
Figure 5-25 : Velocity contours of time-average crosswind flow .....	146
Figure 5-26 : Flow divergence at semitrailer edge shown by path lines colored by velocity magnitude .....	147
Figure 5-27: Local TSI gust flow .....	148
Figure 5-28: Snapshots of the total pressure distribution on sides of the trailer.....	149
Figure 5-29: Distribution of total pressure in flow field of TSI gust .....	150
Figure 5-30 : Time dependent pressure coefficients along a line on the leeward and windward sides of trailer in the TSI gust scenario.....	151

Figure 5-31: Time-history of the unsteady aerodynamic forces under effect of the TSI wind scenario .....	153
Figure 5-32: Duration of the unsteady aerodynamic rolling and yawing moments in the TSI wind scenario .....	154
Figure 6-1: Aerodynamic center on ADAMS model.....	158
Figure 6-2: Transient crosswind scenario imported to ADAMS environment to perform dynamic analysis .....	158
Figure 6-3: Schematic view of objective simulation test.....	159
Figure 6-4: Time-history of a longitudinal displacement travelled by the tractor and trailer units during straight-road maneuver in random wind-gust scenario.....	160
Figure 6-5: Lateral displacement of tractor and semitrailer units without crosswind effects .....	161
Figure 6-6: Snapshot of vehicle lateral position at the end of maneuver(under transient ( wind- tunnel) wind scenario).....	162
Figure 6-7: Lateral displacement of tractor and semitrailer units under transient crosswind scenario .....	162
Figure 6-8: Lateral displacement of tractor and semitrailer units under TSI gust model .....	163
Figure 6-9: Yaw response of tractor and semitrailer units under transient crosswind scenario.....	164
Figure 6-10: Yaw responses of tractor and semitrailer units under TSI gust model.....	164
Figure 6-11: Pitch motion of tractor and semitrailer units under transient crosswind scenario .....	165
Figure 6-12: Pitch motion of tractor and semitrailer units under TSI gust model .....	165
Figure 6-13: Variation in roll angle of tractor and semitrailer units under transient crosswind scenario	
Figure 6-14: Variation in roll angle of tractor and semitrailer units under TSI gust model	166
Figure 6-15: Variation in roll angle of tractor and semitrailer units without crosswind effects .....	167
Figure 6-16: Steering angle required for keeping the vehicle on course under transient crosswind actions.....	169
Figure 6-17: Steering angle input without crosswind effects for keeping the vehicle on course .....	169
Figure 6-18: De-activate steering input .....	170
Figure 6-19: Fluctuations in locked steering wheel.....	170
Figure 6-20: Trailer unit roll angle response in straight maneuver under transient crosswind without driver actions .....	171
Figure 6-21: Snapshot of rollover event for the trailer unit under transient crosswind conditions without driver actions .....	171
Figure 6-22: Free body diagram of the trailer body.....	172
Figure 6-23: Free body diagram for the trailer's roll model.....	173
Figure 6-24: Time dependent of the LTR index of the trailer axles (a) Crosswind ignored (b) crosswind considered .....	174
Figure 6-25: Constant radius turning maneuver .....	175

Figure 6-26: Time-history of LTR during a steady-turning maneuver without crosswind loads .....	176
Figure 6-27: Time-history of LTR during a steady-turning maneuver with transient crosswind loads .....	177
Figure 6-28: Time-history of LTR during a steady-turning maneuver under TSI gust scenario .....	177
Figure 6-29 : Differences in the trailer's LTR values for rear axle (most affected by wind forces) and LTR values of the trailer computed by traditional definition (i.e., combined axles).....	178
Figure 6-30: Co-simulation method for predicting of LTR index .....	180
Figure 6-31: Block diagram of truck ADAMS model (state parameters of tractor semi-trailer) estimated with full-order observer in Simulink .....	181
Figure 6-32: Comparison between co-simulation and ADAMS data for LTR of the trailer's rear axle .....	181
Figure 6-33: Velocity data and corresponding LTR values.....	183
Figure 6-34: Characteristic wind curve .....	184
Figure 7-1: Effects of vehicle speed on rollover indicator, LTR.....	187
Figure 7-2: Roll angle of the trailer when negotiating a curve with speed of 30 m/sec under crosswind effects.....	187
Figure 7-3: Variation in the maximum LTR with different roll center heights .....	189
Figure 7-4 Calculation of pressure center location by Fluent software .....	190
Figure 7-5 : Five intervals for calculating wind pressure centres .....	191
Figure 7-6 : V-Force elements created at location of gust pressure centres .....	191
Figure 7-7: LTR in crosswind with moved and fixed aerodynamic center .....	191
Figure 7-8 : LTR for rear axle of the trailer under TSI wind gust .....	193
Figure 7-9: Laden and empty trailer for dynamic simulations.....	193
Figure 7-10 : effects of multi-parameters on performance of LTR rollover indicator under TSI wind gust.....	194
Figure 7-11 : Critical roll condition .....	196
Figure 7-12: Behavior of Energy-Based Rollover indicator in crosswind.....	197
Figure 7-13: Behavior of RCF rollover index in crosswind conditions.....	198
Figure 7-14 :Layout of Rollover warning system [183] .....	200
Figure 7-15: Set-up of a deceleration maneuver.....	201
Figure 7-16: Location of vehicle speed monitors .....	202
Figure 7-17: (a) Performance of warning algorithm with /without wind consideration, (b) data compression .....	203

## LIST OF TABLES

---

Table 3-1: Specification of wind-tunnel rig.....	56
Table 3-2: Values of pressure measurements .....	63
Table 3-3: The estimated standard uncertainty .....	76
Table 4-1: Boundary conditions.....	88
Table 4-2: Time step calculation.....	90
Table 4-3: Mesh dependency .....	92
Table 5-1: Turbulence intensity .....	121
Table 5-2: Fixed parameters of TSI standard wind gust.....	138
Table 5-3: Pressure difference between windward side and leeward side of the tractor and semitrailer unites .....	152
Table 6-1: wind-tunnel data &LTR .....	183
Table 7-1: LTR indicator for different weights .....	202

## NOMENCLATURE

---

$A_m$	Wind gust amplitude
$a_y$	Lateral acceleration ( $m/s^2$ )
$C_D$	Aerodynamic drag force coefficient
$C_S$	Aerodynamic side force coefficient
$C_L$	Aerodynamic lift force coefficient
$C_{cs}$	Smagorinsky constant
$C_p$	Pressure coefficient
$E_{roll}$	Rotational energy of trailer body (J)
$E_{crit}$	Critical rotational energy(J)
$Eu$	Standard uncertainty
$F_L$	Vertical force applied to left tire (N)
$F_R$	Vertical force applied to the right tire (N)
$F_y$	Lateral force generated by tire (N)
$F_D$	Aerodynamic drag force (N)
$F_S$	Aerodynamic side/lateral force (N)
$F_L$	Aerodynamic lift force (N)
$F_{sr}$	Right suspension force (N)
$F_{sl}$	Left suspension force (N)
$g$	Gravity acceleration ( $m/s^2$ )
$g_p$	Expected peak factor
$h_m$	Distance between roll centre and vehicle mass centre (m)
$h_{cm}$	Height of the vehicle's centre of gravity above the ground (m)
$h_{lm}$	Vertical distance between roll centre and vehicle mass centre (m)
$I_u$	Turbulence intensity (%)
$I_{xx}$	Moment of inertia of the vehicle's sprung mass about the x-axis (N.m)
$LTR$	Load transfer ratio
$M_{TM}$	Transfer moment (N.m)
$M_{OM}$	Overturning moment (N.m)
$M_{DM}$	Displacement moment(N.m)
$M_y$	Aerodynamic yaw moment (N.m)
$M_p$	Aerodynamic pitch moment (N.m)
$M_r$	Aerodynamic roll moment (N.m)
$P$	Air pressure (Pa)
$Re$	Reynolds number
$RCF$	Rollover Critical Factor
$T$	Wind gust period (sec)
$Tr$	Track width of the vehicle (m)
$u(t)$	instantaneous wind speed (m/sec)
$\bar{U}(z)$	mean wind speed (m/sec)
$\hat{u}(t)$	Maximum wind gust speed (m/sec)
$U_e$	Potential energy (J)
$u_\tau$	Friction velocity(m/sec)
$V_{tr}$	Velocity of tractor semitrailer vehicle (m/sec)
$V_{rel}$	Wind speed relative to the vehicle (m/sec)
$V_{PC}$	Speed of the tractor at the point of curvature (m/sec)
$v_\infty$	Mean stream-wise velocity (m/sec)
$\gamma^+$	Non-dimensional wall unit

$\Delta y$	shift of the vehicle's centre of gravity
$\beta$	wind angle relative to the vehicle moving direction (°)
$\sigma$	standard deviation
$\emptyset$	vehicle's roll angle
$\kappa$	Von Karman constant
$\rho_{air}$	The air density (kg/m <sup>3</sup> )
$\tau_w$	wall shear stress (N/m <sup>2</sup> )
$\mu$	Road friction coefficient
$\nu_{sgs}$	eddy viscosity coefficient
$\nu$	kinematic viscosity of the air

## **Chapter 1 : Introduction**

---

In the design practices used for road and rail vehicles, there is an emphasis on reducing weight and lowering the aerodynamic resistance in order to minimize the vehicles' ecological and economical footprint. As well as, there is an emphasis on increasing the operational speeds of these vehicles to reduce travelling time. New designs with high speed and less overall weight of the vehicle, however, tend to increase the vehicles' sensitivity to high unsteady crosswind conditions. Hence, this chapter provides an introductory discussion regarding crosswind effects on dynamic stability of a high-sided tractor semitrailer vehicle. Furthermore, this chapter includes details of parameters, that are necessary to study and improve crosswind stability of the vehicle. Finally, the chapter includes the research motivations, the aims and contributions of the study.

## 1.1 Background

A tractor trailer is an articulated heavy vehicle (AHV); it consists of a tractor/truck which is connected to trailing units through articulation joints. The tractor unit which is controlled by the driver typically has one steerable axle, whereas the articulation joints include mechanical couplings, such as dollies, hitches, pins and fifth-wheels [1]. A trailer can be broadly classified either as a full-trailer or a semi-trailer. A full-trailer is vertically supported by running gears both at its front and rear ends. On the other hand, a semi-trailer is supported vertically by a running gear at the rear; however, its front end is vertically supported by its leading unit. Figure 1.1 shows the common vehicle units and technical hitches used in AHVs.

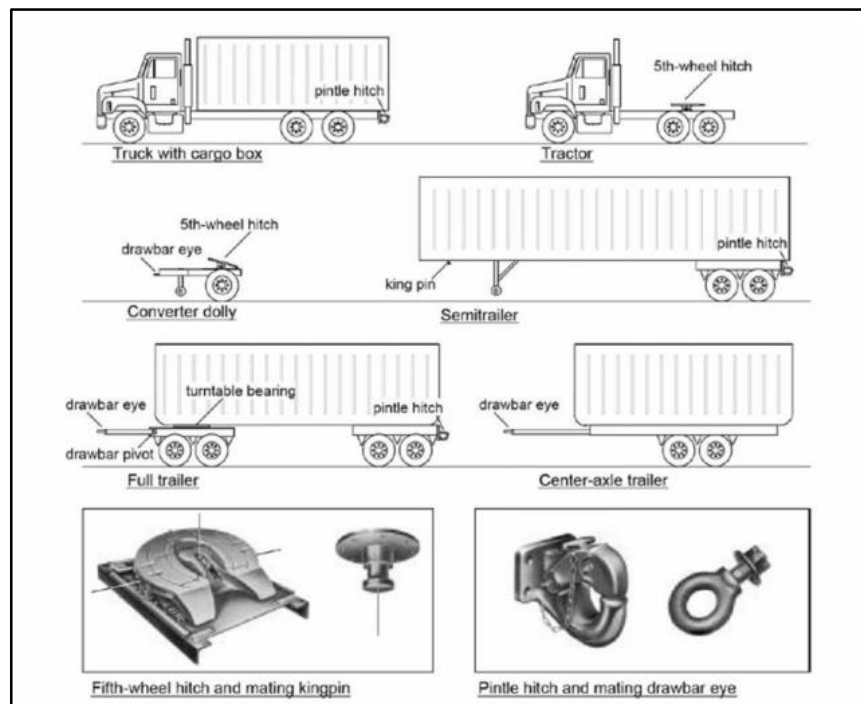


Figure 1-1: General configuration of tractor trailer units and couples used in AHVs[2].

Tractor semitrailer combinations have always been designed with utilitarian needs, and they have played a major role in the world's economic growth. According to statistics [3], in the United Kingdom, the amount of domestic freight that was moved by AHVs has increased by 69% between 1990 and 2015. As a result of this growing demand for goods and materials transportation over the past few decades, the number of on-road commercial lorries have increased worldwide. For instance, in the Great Britain, the number of licensed heavy goods

vehicles (HGV), such as tractor semitrailer lorries increased steadily from 460,000 in 2012 to 483,000 in 2015[4]. This suggests that AHVs are cost effective means of road transport in both labour requirements and fuel consumption as compared to other types of ground vehicles[3]. They also reduce greenhouse emissions owing to their large load carrying capacity. Furthermore, the recent development of transport infrastructures and highway services lead to a significant increase in average road speeds for tractor semitrailer combinations.

However, in spite of the aforementioned advantages, the safety of large class vehicles such as high-sided tractor semitrailer units remain a common concern for all roads users. These vehicles typically have a large body with a high centre of gravity and considerable loading capacity. As a result of this design, they are known to exhibit lower stability and controllability (e.g. slow brake and steering response) limits than other types of road vehicles, such as passenger cars and light trucks. Consequently, an increase in vehicle instability has adverse effects on driving performance and thus increase the risk of road accidents. In the United States, for example, 3,903 people were killed and an estimated 111,000 people were injured in road crashes involving large trucks in 2014 [5]. Most of these accidents were attributed to manoeuvre induced instabilities, such as roll instability and yaw instability [6].

In addition to its significant contribution to severe and fatal injuries, the rollover of heavy vehicles is critical owing to its association with large traffic disruption, economic loss and risks linked to the transported goods. It is also a complex event that has been the subject of repeated investigations. Therefore, predicting and analysing rollover condition requires a good understanding of vehicle roll dynamics.

### **1.1.1 Mechanics of a heavy vehicle rollover**

Vehicle body roll denotes how much the vehicle rotates about its longitudinal axis in response to lateral forces acting on its body[5]. These lateral forces can be generated under several

conditions, such as contact with an obstacle (a curb, pothole, etc.), during a turn manoeuvre on roadway or under crosswind conditions. Accordingly, rollover refers to a manoeuvre in which the vehicle rotates  $90^{\circ}$  or more around its longitudinal axis such that the body makes contact with the ground[7]. In vehicle dynamic field, rollover event has been classified into two types; tripped and un-tripped rollover[8] . Tripped rollover involves an abrupt impact with another object at vehicle's tires, which induces a rotary motion to the vehicle resulting in rollover. An un-tripped rollover is a manoeuvre induced rollover, which can occur during fast cornering, lane change manoeuvres or the avoidance of an obstacle. Under this situation, the vehicle is exposed to a gradual increase of force at tire-ground contact area which can lift off the wheel from ground, when coupled with other external forces acting on the vehicle[9].

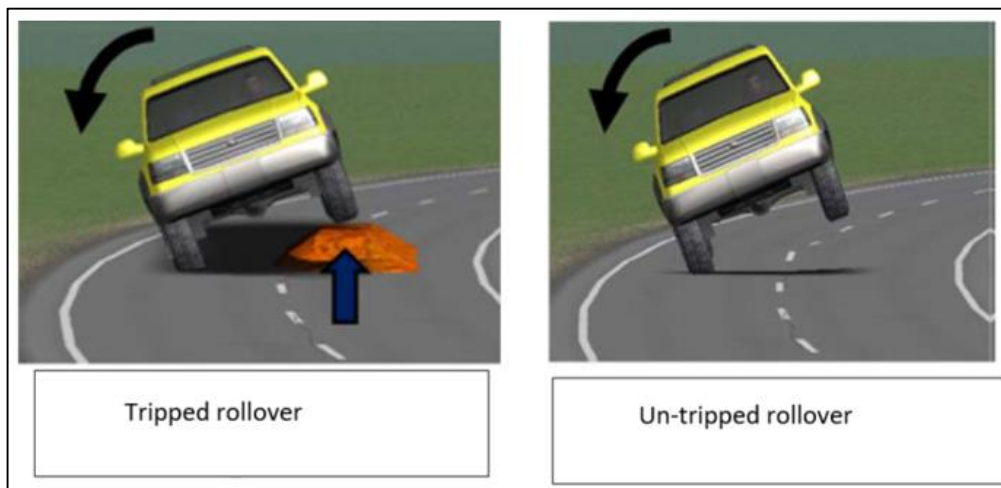


Figure 1-2: Tripped and un-tripped vehicle rollover [8]

Moreover, many systems of the truck such as tires, suspensions and steering system affect the vehicle roll response and stability. Due to this complexity, the accepted method for quantifying and estimating vehicle roll stability under particular operating conditions is to develop a vehicle rollover index/threshold [10]. For further explanation, in the following subsections, the un-tripped rollover of a rigid vehicle and a vehicle with multiple suspensions will be explained by a graphical representation of the roll angle.

### 1.1.1.1 Physics of un-tripped Rollover

When a truck makes a turn, the centrifugal force acting through the vehicle's centre of gravity, tire forces and vehicle weight acting downwards are main forces that govern the vehicle's motion. The centrifugal force pushes the truck to the outside of the curve; if the centrifugal force is sufficiently large, the truck will roll over away from the centre of the curve. This centrifugal force depends on the speed of the truck and the curvature of the road. The free body diagram of a heavy vehicle (in steady turn) is shown in Figure 1-3. This model represents the vehicle with a single roll degree of freedom, i.e. a single unit truck with a stiff frame as well as rigid suspensions and tires.

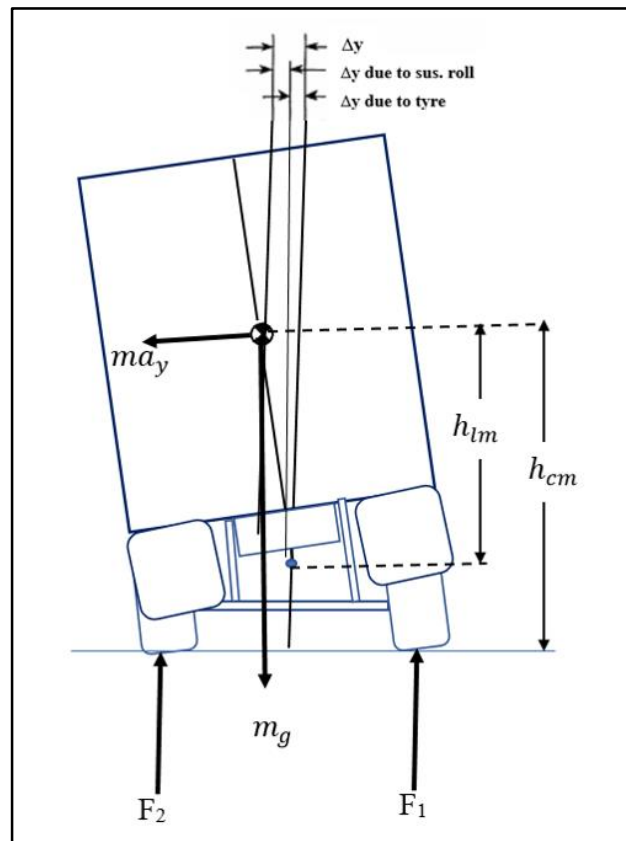


Figure 1-3: The free body diagram of a heavy vehicle in steady turn[11]

Three types of moments are applied to the vehicle with respect to a point on the ground at the centre of the track. Two of them are defined as destabilizing (overturning) moments, whereas the third one is described as a stabilizing (restoring) moment. As depicted in the Figure 1-4, the vertical forces which are exerted on the tires generate a steady-state lateral acceleration

$(a_y)$  acting towards the outside direction during cornering. This lateral acceleration causes a roll moment, which is defined as the primary overturning moment  $M_{OM}$ , and given as follows:

$$M_{OM} = ma_y h_{cm} \quad (1-1)$$

Where  $h_{cm}$  is the height of the vehicle's centre of gravity above the road surface, and  $m$  refers to the mass of the truck.

The vehicle load transfer in the lateral direction produces a moment with respect to the mid track point. It is defined as the displacement moment  $M_{DM}$  and is equal to:

$$M_{DM} = mg\Delta y \quad (1-2)$$

here,  $\Delta y$  is the lateral shift of the vehicle's centre of gravity, and it is for a small roll angle equal to:

$$\Delta y = h_{cm}\phi \quad (1-3)$$

where  $\phi$  is the vehicle's roll angle with respect to a point on the ground at the centre of the track. Another moment resulting from the vertical load transfer from the inside tire to the outside is defined as the load transfer moment  $M_{TM}$ . It is calculated as[10]:

$$M_{TM} = (F_2 - F_1) \frac{T_r}{2} \quad (1-4)$$

here  $T_r$  refers to the track width of the vehicle,  $F_1$  and  $F_2$  are the vertical forces applied to the right and left tire respectively.

When all these moments are calculated with respect to the point on the ground at the centre of track width, the following equilibrium equation is obtained:

$$ma_y h_{cm} + mgh_{cm}\phi = (F_2 - F_1) \frac{T_r}{2} \quad (1-5)$$

Equation 1-5 can be represented in the graph shown in Figure 1-4. In the case of rigid body motion, when it is assumed that the heavy vehicle is completely rigid, the load transfer moment reaches its maximum value at a very small roll angle[11]. As the roll angle grows,

the centre of gravity of the vehicle translates in lateral direction and  $y$  becomes larger. Moreover, the displacement moment increases linearly with the roll angle, and the direction of displacement moment is opposite to that of load transfer moment.

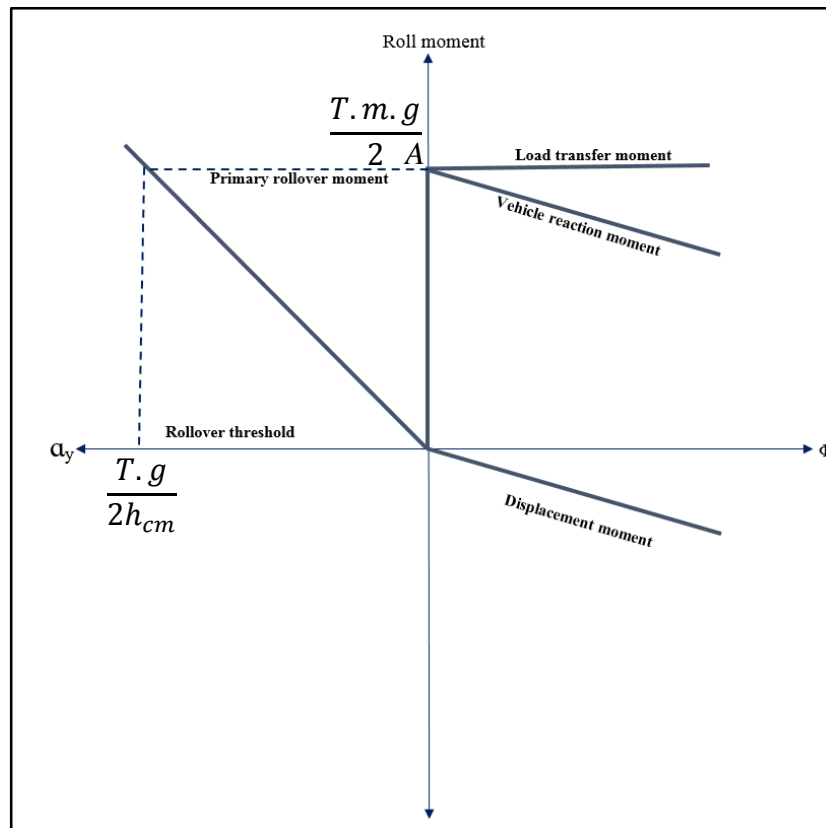


Figure 1-4: Generic roll response graph for rigid vehicle[11]

In Figure 1-4, it is also depicted that the load transfer moment remains the same after the point A, while the roll angle becomes larger. Therefore, the vehicle reaction moment attains its maximum value at zero roll angle. After the point of A (see the above figure), the slope of the vehicle reaction moment becomes negative. This implies that the vehicle inside tire lifts off and the vehicle becomes unstable. The rollover threshold is defined in terms of lateral acceleration by[12]:

$$a_y = \frac{T_r g}{2h_{cm}} \quad (1-6)$$

### 1.1.1.2 Rollover of a sprung vehicle with multiple axles

For further discussions on the mechanics of rollover, a sprung vehicle with multiple axles (e.g. a tractor semitrailer vehicle) is considered here. The three axles of a tractor semitrailer combination are studied here individually. The roll moment distribution of a typical tractor semitrailer combination is depicted in Figure 1-5. The vehicle trailer axle has the highest roll stiffness and the vehicle steer axle has the lowest roll stiffness. The vertical loads carried by the drive axle and trailer axle is similar to each other, however, is greater than the load on the steer axle.

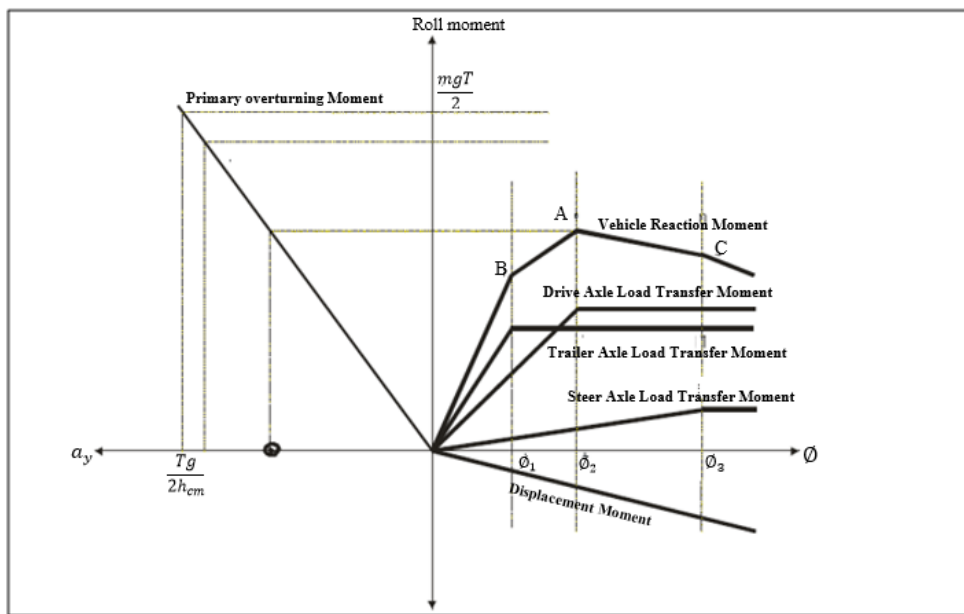


Figure 1-5 : Generic roll response graph for a multiple-axles vehicle [11]

As can be seen from Figure 1-5, when the vehicle starts rolling, firstly all vertical loads on the trailer axle completely transfer from the one side to the other side because of high roll stiffness and the trailer axle group lifts off at point B. At this point, the vehicle roll angle is described by  $\phi_1$ . After this point, the contribution of the trailer axle on the vehicle reaction moment is lost and the stiffness of total system decreases. The next tires lifting from the ground are the drive axle tires. The drive axle cannot provide any additional moment after the roll angle of  $\phi_2$  so the slope of the vehicle reaction moment again decreases. The vehicle steer axle does not produce enough load transfer moment to balance the lateral displacement moment after

the point of A" so the slope of the vehicle reaction moment becomes negative and the vehicle rolls over. As a result, the maximum reaction moment is obtained at the roll angle  $\phi_2$  and the rollover threshold is defined as the corresponding lateral acceleration. As well as, the roll angle at which the trailer axle group lifts off (point A) is lower than the corresponding angles for the tractor drive axle (point B) or the tractor steer axle (point C).

It is concluded from Figure 1-5 that the rollover threshold of sprung vehicle with multiple axles is less than the rollover threshold of the lumped system. Therefore, the optimum situation for maximizing the roll stability is that the tires lift from the ground simultaneously at all axles. It should be noted that the roll angle at which axle tires lift off is a function of both the roll stiffness of the suspension and the maximum load transfer moment of the axle. So, development of vehicle dynamic model with high level of fidelity is essential for predicting vehicles rollover[13].

### **1.1.2 Contribution of wind loads to rollover dynamics**

Crosswind is defined as a wind flow condition that has a perpendicular component to the direction of vehicle motion (Figure 1-6) [14]. Crosswind conditions can be caused by atmospheric winds or in the wake of an obstacle, for example, during passing manoeuvres or when a vehicle passes through bridge towers. Crosswind environments have adverse influences on the aerodynamic performance of a high-sided tractor semitrailer combination[15]. In the presence of a crosswind, the magnitude of the relative velocity between the truck and the crosswind increases, and its direction is skewed to the direction of motion, which means that the large side area of the trailer gets exposed. As will be discussed, vehicle aerodynamic forces increase dramatically as a result of the increase in relative wind speed or in the wind exposure area of the vehicle.

Furthermore, during high crosswinds, the lift and lateral aerodynamic forces can cause an overturning moment about the leeward side of the vehicle, as shown in Figure 1-6. The

gravitational force from the mass of the vehicle is the main stabilizing force. If the vehicle runs in a curve, the centrifugal force acting on the vehicle body will exacerbate the overturning moment when the wind blows from the inside of the curve. In addition, the aerodynamic lateral force can increase the displacement of the car body as well as the centre of gravity towards the outside of the curve due to flexibility in the suspension, which in turn, reduces the stabilizing moment.

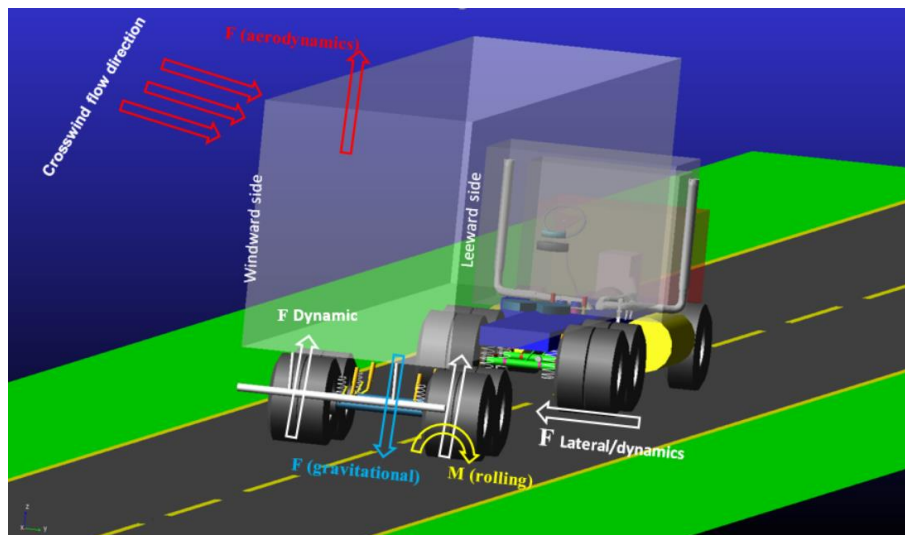


Figure 1-6 : General force acting on vehicle in crosswind environments

Therefore, high vehicle aerodynamic forces and moments result from high crosswind conditions may deteriorate the vehicle roll instability and operating safety. Moreover, three types of dynamic instability due to crosswind loads which have been observed and recorded in recent years and could result in accidents are [15, 16]:

- Overturning/rollover
- Sideslip
- Rotational



Figure 1-7: A high-sided vehicle accidents due to crosswind actions

Comparing with passenger vehicles, roll instability is more applicable to high-sided commercial vehicles like tractor semitrailer units [17]. For example, in January 2008, more than thirteen such trucks were reported to have overturned due to the prevalence of high winds on a single day[18]. More recent examples, in 2017, on Forth Road Bridge in the North of the UK, two rollover accidents of a high-sided trailer pulled by tractor unit have been recorded at this site (see the top of Figure 1-7). Such accidents are more serious for modern commercial vehicles due to reduction in vehicle weights arising out of the use of more efficient structural design and lighter materials to reduce fuel consumption. Moreover, in crosswind environment, the side force generated by the crosswind may change the driving direction and reduce the handling stability of the vehicle. Then, the drivers have to adjust the direction frequently. This may cause the drivers to get tired and increase the risk of rollover accident.

### 1.1.3 Analysis of a ground vehicle crosswind stability

A number of studies were performed over the last 20 years to develop methodologies able to evaluate the level of safety of a ground vehicle under wind conditions in terms of rollover risk. As sketched in Figure 1-8, crosswind stability is the result of complex interactions between aerodynamics, vehicle dynamics and driver actions[19]. Thereby, complete system (methodology) has to be taken into account to assess crosswind stability.

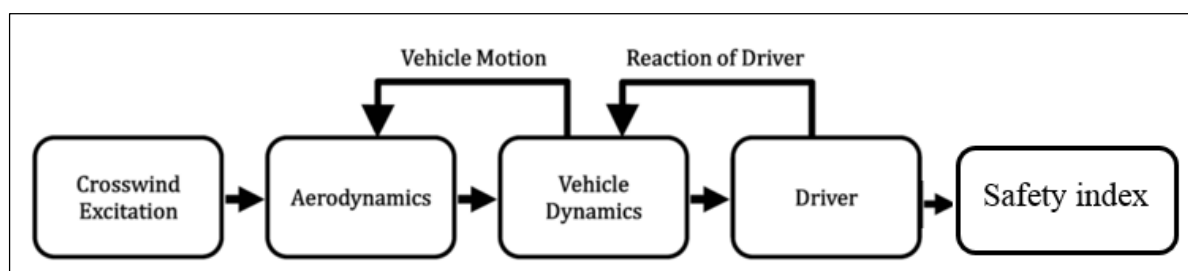


Figure 1-8: Schematic view for a ground vehicle crosswind stability approach

The first step pertains to the definition of the wind speed field; corresponding aerodynamic loads acting on the vehicle then have to be evaluated. In the next step, vehicle dynamic responses to crosswind aerodynamic forces have to be predicted. The final stage of this methodology is the definition of the rollover criteria that should include all accurate vehicle rollover parameters. Background of vehicle dynamics, vehicle aerodynamics and rollover index will be briefly outlined in the following sub-sections.

#### 1.1.3.1 Wind speed

Essentially, crosswind conditions can be classified into three types: steady crosswinds, unsteady crosswinds and so called transient crosswinds. Steady crosswinds are a result of a steady atmospheric wind condition, but in reality, they are a rare phenomenon. The inherently nature of atmospheric winds makes unsteady conditions much more likely. Transient crosswinds are attributed to a combination of one of the aforementioned conditions as well as the relative motion of a vehicle. For example, a vehicle may exit from a tunnel into a transverse wind condition, either steady or unsteady, at which point, it will be subject to a cross-wind transient [20].

The time-dependent (unsteady) wind speed occurring at any point in space  $(x, y, z)$  can be thought of as the sum of two vector components [21]:

$$u(x, y, z, t) = \bar{U}(x, y, z, t) + u'(x, y, z, t) \quad (1-7)$$

where  $u(x, y, z, t)$  is the total wind velocity at longitudinal direction  $(x)$ , lateral direction  $(y)$  and vertical direction  $(z)$ ;  $\bar{U}(x, y, z, t)$  is the non-turbulent (mean) wind velocity at a given location within the storm; and  $u'(x, y, z, t)$  is the turbulent fluctuation velocity, see Figure 1-9. Further details about wind speed analysis will be included in the Chapter Five.

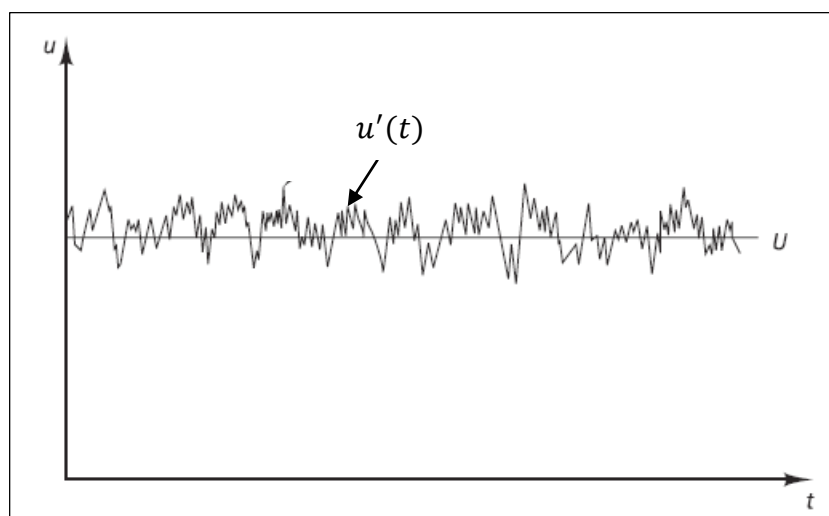


Figure 1-9 : Typical point velocity measurements in turbulent wind flow

Another wind characteristic which should be considered when evaluating crosswind stability of ground vehicles is wind gust loads. The real atmospheric wind to which a ground vehicle is subjected during on-road driving is fully turbulent and unsteady. Within a turbulent wind field, strong wind pulses can occur that are referred to as wind gusts or, more simply, gusts[22]. Under crosswind gust conditions, sudden variations in wind loads tend to have an adverse impact on the dynamic stability of road vehicles.

Modelling wind gust is a complex task since in the very short-term; the gust speed estimation becomes infeasible. However, for design purposes, gusty wind conditions can be evaluated based on the constrained simulations [23]. In this approach, extreme gusts are usually idealized as a deterministic gust, following which, it is superposed on wind turbulent

fluctuations[24]. The deterministic gust model generally describes the stochastic character of the turbulence denoting the shape of occasional occurring wind peaks[22].

### 1.1.3. 2 Definition of Vehicle aerodynamic forces

Extreme wind loads acting on a running vehicle are usually estimated adopting a quasi-steady method where in the wind forces expressed through aerodynamic coefficients are as following [25]:

$$F(t) = \frac{1}{2} \rho_{\text{air}} A_r C_i V_{\text{rel}}^2(t), i = D, S, L \quad (1-8)$$

$$M_{r,p,y}(t) = \frac{1}{2} \rho_{\text{air}} A_r h C_{mi} V_{\text{rel}}^2(t), i = r, p, y \quad (1-9)$$

where  $F(t)$  refers to the generalized aerodynamic force and  $M(t)$  is a generalized aerodynamic moment, with  $\rho_{\text{air}}$  being the air density,  $A_r$  is a reference area of the vehicle and  $h$  is a reference height (in some cases it is the height of the vehicle mass centre (C.G) above the ground). These aerodynamic coefficients pertain to drag force  $C_D$ , lift force  $C_L$  and side force  $C_S$ . In Equation 1-9, the coefficients include rolling moment coefficient ( $C_{mr}$ ), pitching coefficient ( $C_{mp}$ ) and yawing coefficient ( $C_{My}$ ). The wind speed relative to the vehicle ( $V_{\text{rel}}$ ) can be defined directly as a function of the absolute wind speed time-history  $u(t)$  as seen by the vehicle moving with a velocity of  $V_{\text{tr}}$  where  $V_{\text{rel}}$  and is defined as[19]:

$$V_{\text{rel}}^2(t) = (V_{\text{tr}} + u(t) \cos \beta)^2 + (u(t) \sin \beta)^2 \quad (1-10)$$

Where  $\beta$  is a wind angle relative to the vehicle moving direction (yaw angle).

Generally, three techniques are used for estimating both steady and unsteady aerodynamic characteristics of ground vehicles: full-scale measurements, scale model experiments and computational fluid dynamic (CFD) simulations. More details about unsteady vehicle aerodynamics are presented in Chapter 5.

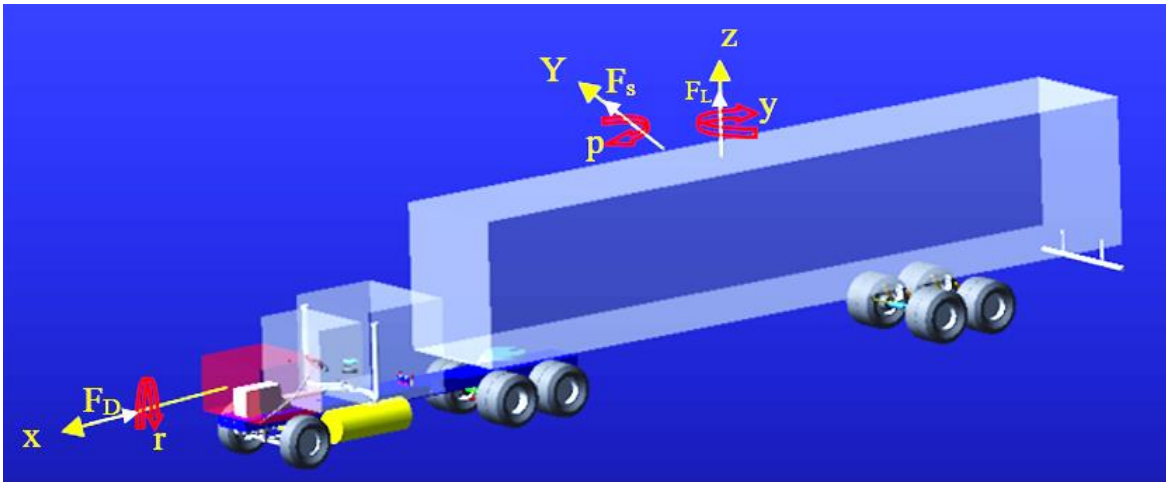


Figure 1-10 : A coordinate system with the x, y, and z axes adopted for the definition of the aerodynamic forces and moments

### 1.1.3.3 Vehicle dynamics

Development of a vehicle dynamic model that can represent the roll behaviour of tractor semitrailer vehicle is important for detecting impending rollover and for accurately applying the external vehicle aerodynamic forces[26]. Heavy truck dynamics is innately more complex than passenger cars, because trucks include more components with a higher inertia, elasticity, damping and many other dynamic features.



These equations are usually non-linear differential equations, which means that it is difficult to obtain exact analytical solutions and hence, numerical methods should be used to obtain approximate solutions[29]. Thus, in order to generate a high fidelity vehicle model to address complex roll dynamics of a vehicle, a multi-body dynamic (MBD) approach is often necessary[13].

MBD approach helps to model a real mechanical system by dividing the analysed system into separate parts, which can then be represented by elements such as rigid or flexible bodies, joints, force elements, gravity, etc. By the MBD method , a set of ordinary differential equations (ODEs) or transfer functions can be developed depending upon the choice of coordinates representing the vehicle motions[30]. Solutions of these equations within time domain can be obtained numerically by integrating the schemes with variable step-size and order, which in turn adapt themselves to system natural frequencies and guarantee a most precise solution[31].

As the complexity of the dynamic system increases, a multi-body dynamic simulation (MDS) program such as ADAMS [32] (Automatic Dynamic Analysis of Mechanical systems) becomes useful. ADAMS is used widely in the automobile industry in order to predict the vehicle's response to different manoeuvres. It allows the user to create virtual prototypes of different vehicles and analyse them like physical prototypes. In addition, ADAMS is an efficient dynamic modelling package that evaluates vehicle suspension components, which has a strong influence on vehicle roll dynamics [33]. Other advantage of using ADAMS include the possibility to produce test data that is difficult, or even impossible to measure, e.g., tire loads and chassis forces[30].

#### **1.1.3.4 Rollover index**

As discussed, vehicle rollover is a highly nonlinear event, it is attributed to large rotational motion in vehicle body, high suspension oscillation, tire nonlinearities as well as large forces acting on the wheel. Additionally, due to a plethora of reasons, rollover might not be

effectively detected by traditional vehicle driving systems, or drivers could be unaware of the upcoming rollover, especially for large class vehicles [34]. Thus, it is important to develop an effective active or a passive rollover detection system (e.g. roll stability control) for the purpose of facilitating early warning/prevention in order to avoid vehicle-rollover accidents. For example, vehicle stability control systems have become mandatory in the EU for all new commercial vehicles types since November 2011 and for all new produced vehicles since November 2014[35]. However, development of a predictor for the likelihood of a vehicle rollover poses a key challenge in the design of active/passive rollover control systems [34]. Various approaches for the detection of an impending rollover rely on the computation of the rollover index. The rollover index can be defined as a measure of the rollover status of the vehicle. A number of rollover metrics have been introduced by various researchers[8, 36, 37]. For example, a static stability factor (SSF) is one such predictor proposed by NHTSA (National Highway Traffic Safety Administration, USA ) [36] to detect vehicle rollover condition. It is a criterion defined as the ratio between one half of the wheel track width and the CG height. This system warns of an imminent rollover of the vehicle, as the lateral acceleration exceeds the SSF safety limit.

In dynamic situations, the lateral load transfer ratio (LTR) has been suggested for use in design of rollover control system. It pertains to the difference between the right vertical tire force as well as left vertical tire force of a vehicle axle divided by the vehicle's total weight. Thus, the LTR index is used to detect wheel lift-off conditions; this indicator can vary between 0 when the normal force on vehicle wheels of both sides is equal, to 1 when the wheels lift off.

## **1.2 Motivation**

In recent time, developments in road transportation have shown a trend for faster, more comfortable and more energy efficient large commercial vehicles. This also brings an increase in operating speeds, however, leading to higher aerodynamic forces acting on these vehicles

in particular, when travelling in high crosswind conditions. Due to crosswind aerodynamic forces, the dynamic stability of commercial vehicles such as the high-sided variety can be severely affected at exposed sites, and smaller vehicles can suffer handling problems[19]. Both can result in road accidents, traffic stoppage, transportation time delay, economic loss, injury, and loss of life.

Furthermore, apart from safety issues, the ambition to decrease the weight of ground vehicles imposes stronger needs for an enhanced understanding of the coupling between aerodynamic forces and vehicle dynamics properties. Thereby, investigations on the effect of strong crosswinds on vehicle stability and controllability are important for improving the safety and quality of the transportation. Recently, the crosswind stability of large class vehicles has been an object of large interest in both research and industry fields.

The real atmospheric crosswind to which ground vehicles are subjected during on-road driving is fully turbulent and unsteady. The key phenomenon of such crosswind flow over a ground vehicle is massive flow separation, which significantly affects wind pressure distribution around the vehicle's body and the vehicle aerodynamic forces. This phenomenon is more pronounced for heavy vehicles that have a boxy shape with many sharp edges, designed for carrying as much cargo as possible within regulated external dimensions. Analysis of such complex flow can be performed through experimental measurements or numerical investigations. Based on wind-tunnel tests, several unsteady crosswind experimental rigs are now available to predict vehicle aerodynamics forces. Although many valuable research results have been obtained, experimental approaches under some conditions are bound to be constrained due to their inherent limitations. For example, general vehicle shape influences the aerodynamic forces generated, due to the wind-tunnel flow created around it. As a result of this, experimental data is usually limited to the model chosen for use in wind-tunnel tests. Thus, for an accurate prediction of crosswind stability for high-sided commercial vehicles,

wind-tunnel studies (i.e. estimation of aerodynamic forces/coefficients) need to be conducted specifically for the investigated vehicle.

Furthermore, in windy environments, large class vehicles may experience a specified wind gust event. Within this gust range, wind speeds vary randomly with time, and the gust can create significant unsteady flow around the moving vehicle, with sudden variations in wind aerodynamics forces. Thereby, wind gusts are an important load condition, which can be considered for assessment of vehicle crosswind stability. However, the effects of wind gust forces on vehicle aerodynamic behaviour have received relatively little attention over the years, so more studies on vehicle aerodynamics under gusty wind conditions are encouraged. For this purpose, since naturally there are a wide variety of wind gusts in terms of their shapes, frequency, contents, and strengths, the author has particularly investigated two different scenarios of wind gust conditions. The scenarios were also developed based on two different methods in order to obtain more realistic situations.

As mentioned, it is quite evident that crosswind aerodynamic forces in gusty environments are directly related to the roll stability of a high-sided vehicle. Thus, developing a dynamic model that can represent the vehicle roll behaviour is essential for the vehicle roll control system, as well as for integrating the external vehicle aerodynamic forces into the vehicle's motion. In the review, several vehicle dynamic models have been suggested for developing active/passive roll control systems. However, the majority of these models are mathematical equations with 2 to 14 degree of freedom (DOF) derived with various assumptions and have limitations for their application.

Experimentally, field tests including rollover events under high levels of crosswind are not practicable, due to economic and safety reasons. As a result of these limitations, multi-body dynamic simulations represent an essential tool for analysing rollover stability of large class vehicles under wind conditions. Moreover, for predicting the likelihood of a vehicle rollover, a number of rollover indexes /metrics have been developed by various researchers. However,

the parameters of these rollover indexes depend either on vehicle states or on road geometry factors. There has been limited investigation into other factors affecting vehicle rollover index such as strong crosswind forces. Therefore, a rollover index needs to be developed to provide more reliable information to the warning or control system in the presence of wind conditions.

### **1.3 Research Aims**

The specific research aims formulated for this research study are described in this section, whereas the objectives for this study will be discussed after carrying out a literature review in the next chapter. Based on the motivation of this study, the research aims have been broken down into the following:

- 1- Predicting unsteady aerodynamic forces acting on a high-sided tractor semitrailer vehicle that is under gusty crosswind conditions.
- 2- Developing a methodology to incorporate crosswind aerodynamic loads into a high fidelity multi-body model of the tractor semitrailer combination, and analysing the effects of sudden crosswind conditions on its dynamic responses.
- 3- This study introduces improved LTR rollover index that can effectively detect vehicle rollover events due to impacts of extreme wind disturbances.

These research aims will cover most of the practical problems encountered in the real world as far as the crosswind stability of a tractor semitrailer vehicle is concerned, and hence can be considered satisfactory for this study. A detailed literature review is presented in the next chapter, which focuses on the aforementioned research aims, in order to find knowledge gaps in the existing literature.

### **1.4 Thesis outline**

Based on the discussion in Sections 1.1 and 1.2, this thesis presents the body of work in eight main chapters to illustrate the findings of the research conducted on the aforementioned topic. In addition to that, appendices are included to present a detailed explanation of the underlying processes.

Chapter 1 provides a concise introduction to the subject matter, as it provides an overview of the rollover dynamic for a high-sided tractor semitrailer combination, which is one of the most important road safety problems. Furthermore, this chapter focuses on providing details of a crosswind stability method, which is a multi-disciplined approach involving vehicle aerodynamics, vehicle dynamics, and driver actions. From this overview, the motivation for carrying out this research has been defined, which identifies key areas to be reviewed in Chapter 2.

Chapter 2 consists of a review of available literature that has been conducted in the field of vehicle crosswind stability. It includes the review of published literature regarding the numerical and experimental investigation of unsteady vehicle aerodynamic forces. Furthermore, a review of literature for the prediction of vehicle dynamic responses to wind actions has also been included. Details of the scope of research have been provided in the form of specific research objectives.

Chapter 3 describes the experimental facility that has been developed to evaluate aerodynamic force coefficients and pressure distribution around the vehicle's model. Furthermore, this chapter provides a detailed description of the wind gust generator mechanism that has been used in the experimental setup to develop high turbulent gust flow around the vehicle.

Chapter 4 includes the CFD and multi-body dynamic modelling for the tractor semitrailer combination. It also provides detailed explanations of LES turbulence model and meshing technique for the flow domain. Results of CFD simulations have been reported and validated against experimental data.

Chapter 5 shows detailed analysis of both wind-tunnel gust flow and a standard wind gust model based on a deterministic approach. Furthermore, aerodynamic forces on a high-sided tractor semitrailer vehicle due to the two wind gust scenarios considered have been predicted in this chapter. The scenarios represent extreme crosswind environments, which for the purpose of vehicle control design purpose, are important to predict the possibility of a rollover

event. A detailed flow field analysis of a tractor-trailer is discussed for a range of cross wind conditions.

Chapter 6 discusses how the high-sided tractor semitrailer vehicle dynamically responds to the high aerodynamic forces discussed in the current work. For this purpose, a one-way coupled simulation of unsteady aerodynamics and vehicle dynamics has been applied to the vehicle. Also, the chapter shows the improvement of traditional LTR rollover indicator for the vehicle to be more efficient under wind actions.

In Chapter 7, a parametric study is carried out to investigate the influence of various parameters on the vehicle roll crosswind stability, evaluated by using the improved LTR. A wide range of destabilising factors have been investigated. These include vehicle speed, vehicle mass, roll centre location, and effects of variation in the wind pressure centre on LTR index.

Chapter 8 presents a summary of the work carried out, recommendations for future study, and the concluding remarks that have been made by taking the planned objectives into account.

## **Chapter 2 : Literature Review**

---

After getting information regarding crosswind stability of a high-sided tractor semitrailer vehicle, and parameters affecting its rollover dynamics, a detailed literature review has been performed in this chapter. The chapter will highlight the knowledge gaps in the existing literature by presenting several methods of estimating parameters of crosswind stability. According to the main parts of this work, the review is subdivided into three parts: the first part describes previous experimental and numerical models that have been developed for predicting vehicle aerodynamic forces. Followed by discussion on vehicle dynamic modelling, and the third part provides studies vehicle rollover indicators that have been proposed by various authors. Based on the knowledge gaps found in the literature review, scope of research has been defined and research objectives of this study have been formulated.

## 2.1 Vehicle crosswind aerodynamics

As discussed, aerodynamic forces caused by strong crosswinds affect the roll stability and controllability of high-sided vehicles. To that end, the first and the most important step to develop effective tools that reliably evaluate vehicle crosswind stability is to estimate the unsteady aerodynamic forces acting upon the vehicle. For this purpose, many research projects have been conducted to examine the effects of crosswinds on vehicle aerodynamics since the 1960s [38-40]. In general, there are three ways of investigating aerodynamic characteristics of a ground vehicle that operates under strong crosswind conditions: the first method entails conducting wind-tunnel tests on scale-model; whereas the second approach is to use computational fluid dynamics (CFD) for simulating the air flow over the vehicle's body numerically. The third possibility is to perform on-road measurements to account for vehicle dynamics and obtain realistic wind conditions[41].

Adopting on-road approach, Cooper[42] develop a model of train in a scale of 1/5 to investigate aerodynamic characteristics of the model. The examinations were carried on the moving vehicle in a field of natural crosswind. Under such natural conditions, the length of test rig was 950 m, and the train model was connected to a van vehicle by push and outrigger rods, then propelled along the track. The force measurements were deployed to obtain the component forces and moments acting upon the vehicle model under wind environment. In spite of the vehicle model has a high Reynolds number, the researcher finally stated that “moving model experiments in the open air are expensive and difficult to perform, and there is insufficient control over the experimental situation”. Instead, he recommended to simulate wind conditions by carrying out experiments in wind-tunnel based on moving models. Similar to study of Cooper[42], Sterling et al.[43] undertook aerodynamic measurements on a full-scale commercial vehicle (see Figure 2-1) on-road conditions. In this study, relations between wind yaw angle and vehicle aerodynamic coefficients were predicted. However, the main

purpose of this research was to compare vehicle aerodynamic forces predicted by three methods. These approaches are wind tunnel measurements, CFD simulations and on-road (full-scale) tests. The results show that wind velocity mean profile (i.e., low and stream-wise velocity) can be correctly simulated based on all three techniques. However, many difficulties arise from on-road measurements, for instance: wind turbulences are very changeable and strong, this can cause equipment failures. Moreover, not always wind blows from the required direction, this means significant periods of time are wasted. As a result of such uncontrollable environmental conditions, experiments are rarely undertaken on a full-scale vehicle in the atmospheric boundary layer [44].



Figure 2-1: Photos showing the vehicle employed for the full-scale on road tests[43]

Apart from performing on-road measurements with atmospheric crosswinds, mounted fans at the side of the road may be used to produce a more repetitive and controllable crosswind [45]. However, fans will give a swirling flow, which impart a different flow behaviour over the vehicle than atmospheric crosswinds[46].

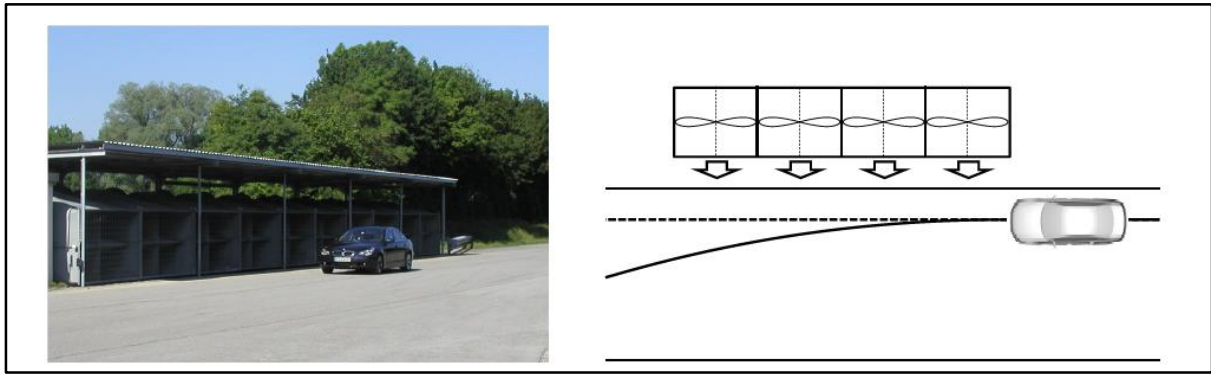


Figure 2-2: Crosswind generator (on-road test facility)[47].

As stated before, the actual wind conditions in which a vehicle operates during on-road driving are highly unsteady due to atmospheric turbulence, landscape variations, or in situations where it overtakes another vehicle or exits a tunnel. These different origins naturally imply a wide variety of wind gusts in terms of gust period, gust shape, frequency contents and gust strengths. To examine the effect of unsteady cross winds on vehicle dynamic forces and moments, we need to generate an unsteady crosswind model as experienced by the vehicle. Despite the inherent limitations of experimental facilities to accurately represent an atmospheric boundary layer and wind gusts, a number of unsteady crosswind experimental benches have been developed. Currently, all wind-tunnel tests on vehicle models can be classified into two major types: stationary vehicle model tests and moving vehicle model tests [48].

### 2.1.1 Wind-tunnel studies on moving vehicle models

Due to aforementioned difficulties of accurately predicting of vehicle aerodynamics forces based on full-scale measurements, a number of studies have attempted to simulate on-road tests in wind tunnel based on moving scale model technique. Baker [49] and Humphreys [50] designed a device for wind-tunnel experiments to measure vehicle aerodynamic forces under moving condition with a scale of 1/50. In this technique, four elastic ropes were used to pull the scaled model to slid on a guideway. Sliding speeds were between 5 m/s and 20 m/s, and force balance system was employed to estimate the aerodynamic loads and moments.

However, this rig requires the opening of a big slot below the under-body of the vehicle model, which could disturb the characteristics of wind flow and cause some measurement errors. Additionally, a long guideway across the wind-tunnel is typically required in order to provide adequate travel distance for the vehicle model to complete the acceleration and deceleration processes. Bocciolone [51], developed a U-shape moving vehicle device, which could move in a speed about 4 m/s. When the vehicle model moves over the U-shape trajectory, it can realize the acceleration and deceleration of the vehicle by gravity. Such an experimental device avoids the interference of open slots, but the moving speed remains too low for vehicle models to minimize the effects of Reynolds number. In a large wind-tunnel, Li et al.[52] proposed and set-up a moving model technique to predict vehicle aerodynamic forces .As seen in Figure 2-3, the model was simple box pulled by a rope on a bridge with a length of 18.0 m. in this experiments a device can measure both aerodynamic forces of the vehicle and bridge models at the same time. However, wind flow around the vehicle can be affected by the guideway and other attachments of the wind tunnel equipment. Additionally, it was very difficult to control the vibration of the vehicle model when it was running on the guideway by using long connecting bars and under wind-tunnel air flow. as result of this, such techniques often lack accuracy and there is a continuing search for an accurate method of estimation of vehicle aerodynamics based on moving model.



Figure 2-3: A moving vehicle device[48]

Recently, Dorigatti et al.[53] tested the pressure distribution of a moving vehicle model. They obtained the aerodynamic coefficients from the discrete integral of the mean pressure coefficient distributions. This method escapes the error caused by the model's inertia forces in force balance tests. Also, D Quinn et el. [53], compared two approaches to determine the rolling moment on a stationary vehicle: direct measurement using load cells, and indirect measurement that was obtained from the integration of vehicle surface pressures. The results obtained using both methods are shown to agree within the acceptable limits.

As a type of relatively new technology, experimental studies on moving vehicles in wind-tunnel, however, continue to face some technical challenges [53]: Firstly, if the vehicle model goes along a guideway, the track irregularity is inevitable and will generate the inertia force, affecting the accuracy of force measurements. Therefore, the signal noise caused by track irregularity needs to be minimized for appropriate force measurements. Secondly, the aerodynamic interference between vehicle testing equipment in motion and the bridge deck

or tunnel surface underneath the vehicle model (e.g. cutting slots in test section) needs to be minimized. Finally, it is extremely difficult to maintain full contact between the guideway and vehicle model's support. This may cause considerable vibrations in the vehicle model, which is unfavourable for force balance measurement.

### **2.1.2 Wind-tunnel investigation using a static vehicle model**

Static tests are conventional methods of determining vehicle aerodynamic coefficients by static methodology, with vehicle models remaining fixed in the wind-tunnel statically. The static tests do not simulate the relative motion between vehicles and ground or bridge decks; hence, they do not take into account, the effect of vehicle dynamics on aerodynamics characteristics.

Experimental investigations based on wind-tunnel static tests have also been extensively used for investigating aerodynamic stability in crosswinds [53-56]. Howell [54] and Sanquer et al. [55] have been predicted vehicle aerodynamic characteristics by measuring external pressure distribution over the surfaces of a vehicle model. Their experiments were based on static model technique and reasonable agreement between their results and results of CFD approach have been noted. In Howell investigations, it was identified that for a passenger car, the A-pillar region of the vehicle body contributes most towards overall side force and its nose contributes mainly towards the yawing aerodynamic moment. However, this analysis was specific to the car that was being investigated. Moreover, no comment was made on the variation of pressure distribution with relative flow velocity.

For investigation the behaviour of high-side vehicles in steady crosswind conditions, Baker [15] conducted wind-tunnel experiments on a model of articulated truck at scale of 1/25. static model in a low turbulence flow has been considered, but atmospheric turbulence effects were not simulated [56]. The test results for these aerodynamic force coefficients were fitted with simple analytical curves. The comparison of this formulation to the earlier study [17] shows

close values and similar trends in some cases, but also captures significant difference of magnitudes in other cases.

Similar to [15], Coleman and Baker [57] performed wind-tunnel investigations on vehicle-trailer model at scale of 1/50 on a bridge deck. The authors aim was to gain a basic understanding of the flow mechanisms developed around large ground vehicles in crosswind environment. Their studies demonstrated that in general, the magnitude of side force fluctuations are mainly depend on direct effects of upstream turbulence. However, the magnitudes of lift force fluctuations are largely determined by body induced flow oscillations. However, this investigation was restricted to the analysis of the flow field around the tractor-trailer vehicle (i.e. vehicle aerodynamic coefficients were not considered). Baker and Humphreys [58] reviewed the side force coefficients acting on a large lorry and a railway container of different static wind-tunnel experiments. They found out that the side force coefficient can be determined accurately by scale model tests. However, the lift coefficients from different studies have a large scatter, because it is strongly dependant on free-stream turbulence level as well as the nature of the wind-tunnel test.

Moreover, the findings arising from the past wind-tunnel experimental campaigns by using static and moving methods are inconclusive. For example, Cooper [42] and Bocciolone et al.[51] found similarity in results of moving and static techniques for both lift and side aerodynamic coefficients, while some differences emerged in other investigations.

### **2.1.3 Experimental simulation of gusty crosswind conditions**

Although one of the most studied research topics in commercial vehicle design has been the reduction of aerodynamic resistance, more importance has been attached to the knowledge about a vehicle's aerodynamic behaviour when confronted with a side unsteady flow, such as wind gusts. Previous works in the field of experimental gust generation show a great diversity of techniques. Schröck et al [59] upgraded a generic car model similar to the Ahmed body

[60]and wind-tunnel facility by implementing oscillating flaps (active turbulence generation systems) positioned upstream of the model, as per Figure 2-4. In this setup, the flaps generated sinusoidal gusts. The periodic shedding vortices can result in fluctuations within the pressures around the bluff body, which is characterized by the Strouhal number. The Reynolds number stood at  $Re = 4.5 \times 10^6$  and the Strouhal number varied according to the excitation of the flaps. The flaps generated sinusoidal gusts, and it is reported that unsteady yaw moment amplitude tends to exceed the steady value at maximum angular positions of the flaps. The differences between unsteady and steady loads are dependent on the Strouhal number as well as the yaw amplitude. Despite being a well-documented technique, the objective of this work was to study only the yawing moment acting on simple one-box vehicle, and provides little information about the unsteady phenomena of the interaction between the gust and the vehicle.

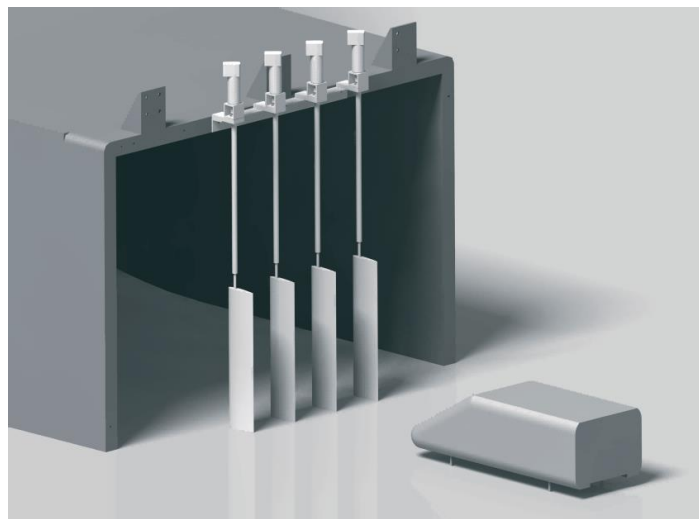


Figure 2-4: Device creating an oscillating flow upstream from the vehicle [59]

Another interesting kind of test bench that used to model unsteady crosswind effects is the side jet facility proposed by Ryan and Dominy [61]. In their experiments, characteristics of moving model were completely simulated, but based on static model. For this purpose, two wind-tunnels produce an unsteady side wind were employed. The main wind-tunnel is classically used to simulate stream-wise vehicle motion, while the econdary tunnel placed at a  $30^\circ$  angle to the axis of the main working section produces the wind gust, see Figure 2-5.

The passage of the auxiliary air flow within the measurement region is driven by an actuated shutter mechanism. On integrating the results from surface pressure tapings, it is seen that the transient side force coefficient exceeds the corresponding steady state values by between 10 and 20 per cent. However, the tests are limited for investigating the effects of wind angles on side aerodynamic force. Although this method allows for large flow yaw angles, the opening and closing mechanism is unable to produce a smooth gust profile.

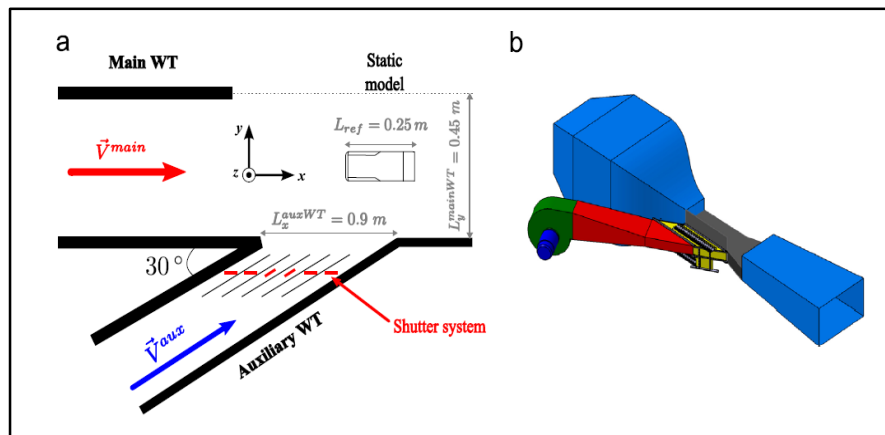


Figure 2-5: Wind-tunnel test bench for crosswind simulation[62]

Moreover, some locations with special topography are generally dangerous for truck running safety. In particular, the wind flow can be amplified by mountainous terrain cliffs and hills adjacent to the road and therefore, will increase the possibility of strong crosswinds[63]. Terrain is normally classified by the general slope of the ground across the highway alignment [64]. Liu et al[65] investigated effects of sloppy terrain on the aerodynamic performance of a high speed rail vehicle. Based on the CFD results, they conclude that running stability of a train vehicle will affect dramatically at the site when the leeward side of the cutting went downhill.

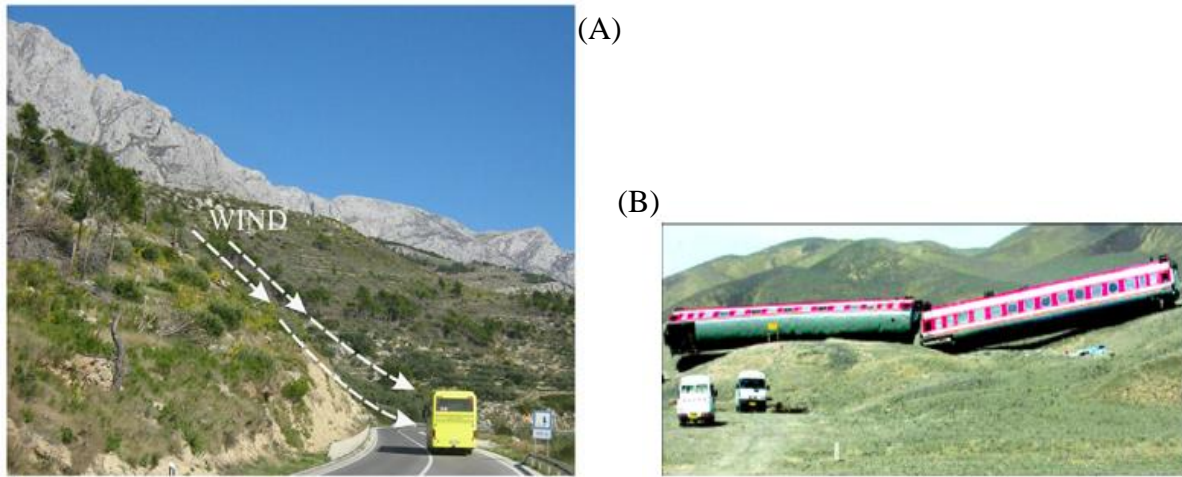


Figure 2-6 : (A) High crosswind flow due to special topography[66];(B) rollover accident due to wind condition and site topography[63]

Furthermore, in laboratory conditions, H. Kozmar et al. [66] developed a wind gust environment to mimic down slope crosswind gusts impacting vehicles on a bridge. The simulation was carried out in wind-tunnel by placing the vehicle-bridge model immediately downwind from the exit of the wind-tunnel. The side force and overturning moment of the vehicle were studied in greater detail, as reported in Figure 2-7. The results of this study showed that a higher vehicle instability risk exists at lower vertical wind incidence at angles up to  $30^\circ$ . Also, vehicle aerodynamic loads in downwind traffic lanes are largely due to shed vortices that are a consequence of the bridge architecture. However, in this work, the relevance of these results to real-world situations was observed to be fairly limited. This is attributed to the significantly simplified vehicle model used in the experiments which comprised of only one discrete box. According to Cooper [42], well detailed models are necessary if full-scale behaviour is to be predicted. Although this study represents an initial study on impulsive wind gusts on vehicles, the author has recommended experiments in other flow conditions to further confirm the observed gusty wind loading phenomena.

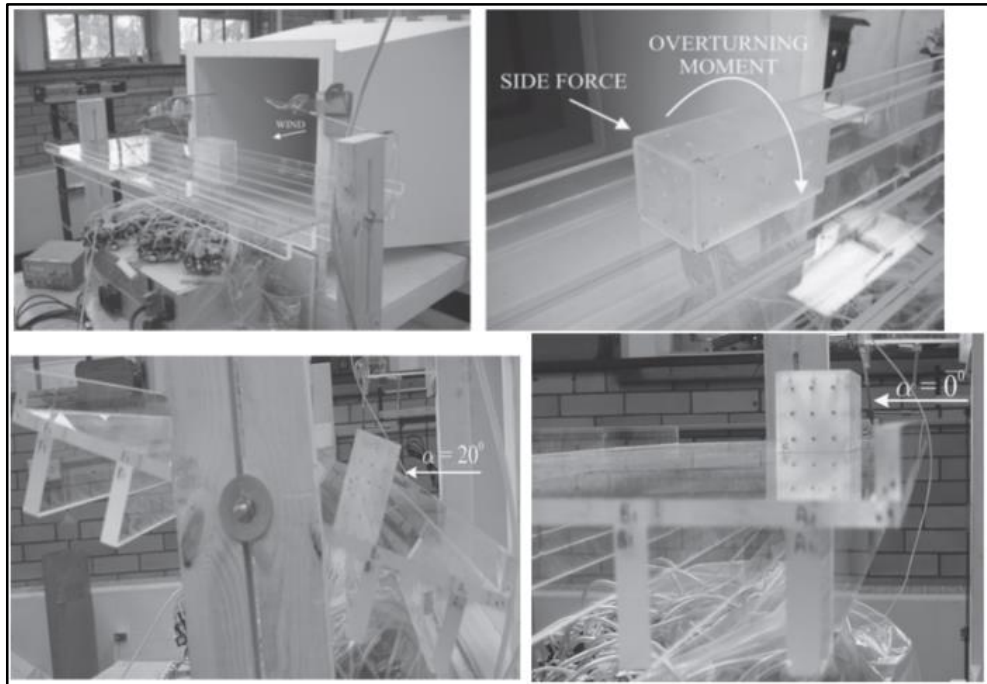


Figure 2-7 : Crosswind simulation in Lab [66]

## 2.2 Wind gust modelling and CFD investigations on vehicle aerodynamics

This section discusses on methods for modelling and estimation of wind gust speed. It also includes a brief review on CFD based numerical simulation techniques which are used for estimation of. vehicle aerodynamic forces.

### 2.2.1 Modelling of wind gust

Wind gust events are complex phenomenon; for design purposes, two approaches have been developed for the modelling of gusty wind conditions namely, deterministic and stochastic approaches. In the former, extreme gusts are usually idealized as a deterministic gust, and then superposed into wind turbulent fluctuations [24]. According to A. Carrarini [67], an ideal or a deterministic wind gust can be defined as “a variation of the wind velocity defined by a simple, usually analytical, function of time. Such variation occurs in the same direction of (or “following”) the main wind speed (longitudinal gust)”. Baes on Taylor's frozen turbulence hypothesis(Taylor, 1938 #257), the ideal gust can be also assumed as non-evolving phenomena and transported with mean longitudinal wind speed ( $\bar{U}$ ) [67].

Gust models based on deterministic methodology are applied in different scientific and technical fields. Within the rail vehicles field, a large European research project TRANSAERO[68] and the DEUFRAKO cross wind program[69] contributed towards the standard in the form of the Technical Specification for Interoperability (TSI) [70] and the EN 14067-6[71]. According to these standards, the wind scenario prescribes a deterministic gust model based on a bi-exponential function, which is also referred to as a “Chinese hat”. A number of studies have utilized the TSI gust scenario to model certain extreme wind conditions on rail vehicles (e.g. [72],[24],[73],[74] and[75]). Another example of deterministic wind gust scenario is the famous ‘Mexican hat’ model, which is described in the IEC-standard [76]as extreme wind load conditions. It is used to calibrate the gust magnitude for the wind turbine design. Apart from TSI and IEC wind gusts, ideal wind gust has also been adapted by different simple shapes. These are for example, the ramp function[77], ‘1-cos’ gust shape[78], and a sinusoidal function[79].While some standards preferred ‘1-cos’ gust shapes, there are strong theoretical arguments [80] in favour of an exponential shape of the gust. Figure 2-9 shows an example of the famous ‘Mexican hat’ gust model.

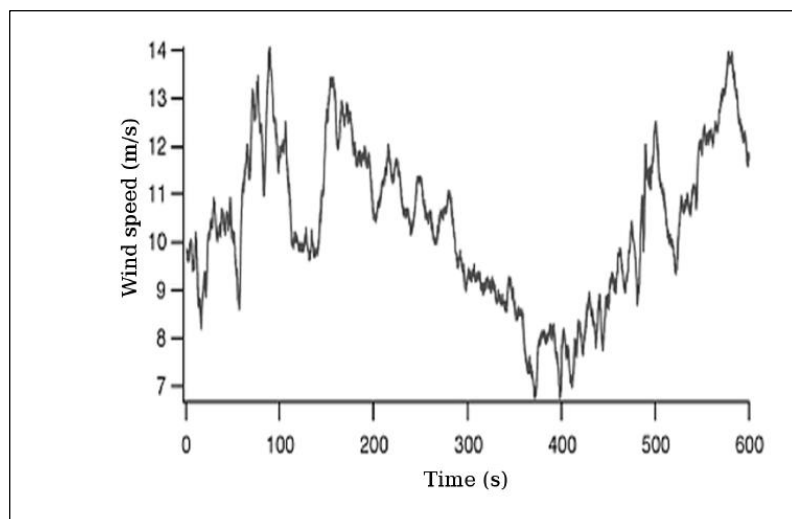


Figure 2-8 : Real wind data measured by an anemometer [81]

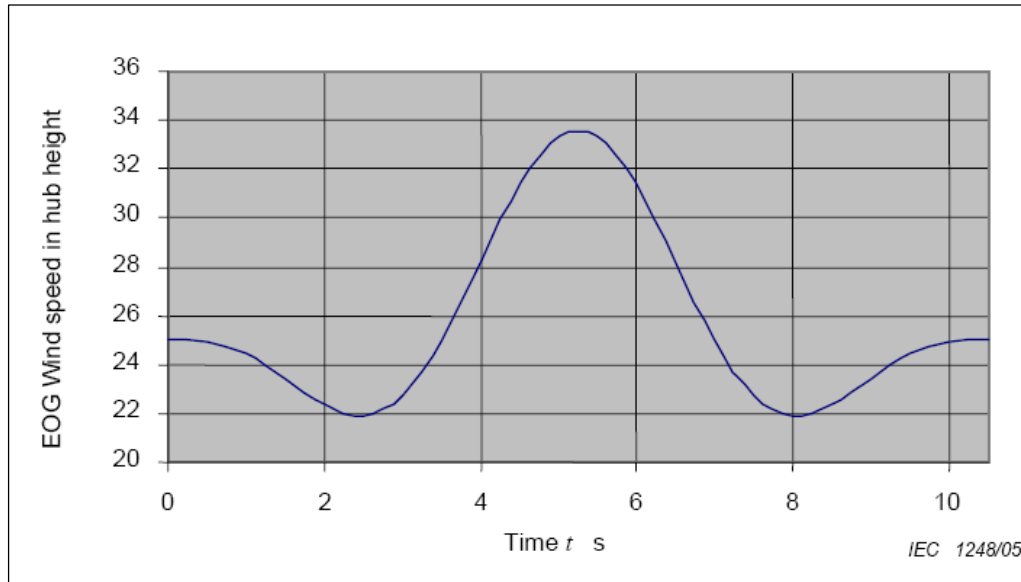


Figure 2-9 : IEC wind gusts model [76]

### 2.2.2 CFD investigation of unsteady tractor semitrailer aerodynamics

In addition to wind-tunnel techniques, Computational fluid dynamics (CFD) is one of the branches of fluid mechanics that use numerical methods and algorithms to solve and analyse problems that involve fluid flows[82]. It is an attractive approach for such problems by providing a large amount of transient data and detailed three-dimensional information about the flow field, in order to elucidate the comprehensive mechanisms of unsteady aerodynamics of road vehicles. In brief, for implementation of the CFD method, a computational domain around flow boundaries should be developed. Then, based on control volume theory, the domain divides into small volumes/cells and the fluid flow is modelled for each cell. After which, flow equations for each cell/mesh are created and solved by numerical iterations. As in general all fluid flows are turbulent, different methods are suggested by using CFD for simulating the turbulences [83]. The most popular are: turbulence models that developed for solving turbulent formulas of Reynolds-Averaged Navier-Stokes (RANS), Large Eddy Simulation (LES) model, Lattice Boltzmann method (LBM), and Direct Numerical Simulation (DNS) .

Using numerical method such as CFD should depend on the purpose of the investigation (i.e., steady flow, turbulent flow, etc.), vehicle geometry and boundary conditions. The idea of using RANS technique is that this turbulent model enable the splitting of the flow field variables  $u$ , into a mean part,  $\bar{U}$ , and a fluctuating turbulent part  $u'$ :  $u = \bar{U} + u'$ . Also, the resulting time-averaged Navier–Stokes equations gives rise to a new terms known as Reynolds stresses, after which they are then modelled with non-linear or linear eddy viscosity models. Pantakar and Spalding[84] introduced the  $k$ - $\varepsilon$  model and then Markatos [85] applied this model to vehicle aerodynamics. Another commonly used two-equation model is the  $k$ - $\omega$  model, which behaves better near the wall region when compared with the  $k$ - $\varepsilon$  model, which is suited better for free stream flow. Then, Menter [86] introduced the SST model, which can combine with both models mentioned above with a set of empirical blending functions.

However, the conventional Reynolds-averaged Navier-Stokes (RANS) simulation is not suitable for transient analysis, especially in cases where the fluctuating incoming flow interacts with the wake turbulence of the vehicle [79]. As well as, DNS does not use a turbulence model; it computes all turbulent velocity fluctuations and therefore, demands both small time steps and cells necessitating substantial computer resources.

LES was established in the 1960s [87]; however, the computational power to process this model was not available until recently for industrially relevant problems. LES is good at resolving certain time dependent features of turbulence with no additional equation since it is inherent in its own formulation. Furthermore, LES attempts to reduce the number of grid points necessary for computing the turbulent flow by modelling the small scales of motion and resolving only large, energy-carrying structures.

LES has been successfully applied in a number of unsteady aerodynamic analyses of vehicle body. N. Patel et al.[88] carried out Large-Eddy Simulations (LES) on the flow around a 1:25 scale model truck travelling in headwinds and in 30-degree yaw wind. The Subgrid scales (SGS) was modelled using a standard Smagorinsky model. LES results compared well with

the experimental data collected in a previous study by Quinn et al [89]. However, the discussion on these results obtained for the vehicle aerodynamic coefficient has been limited to the effects of lifts and drag coefficients. There is a lack of information about time histories of lateral aerodynamic coefficients. Also, the analysis of truck crosswind aerodynamics, and flow structures within the computational domain has been considered only in the 30° yaw wind.

Hemida and Baker [90] used LES for investigation crosswind flow around a train unit and the flow blows at 90° yaw angle. The unit was assumed to be away from sources of any asymmetrical flow that may generated by other train components. As well as, in this investigation, for representing the effect of adjacent train units on the wind flow, periodic boundary conditions were employed. Although many results and analysis data have been reported, validation was not performed against physical experiments, thus affecting the reliability of the results.

LES has been successfully applied in number of unsteady wake analyses of vehicle body. Tsubokura et al. [79] used LES to investigate the vehicle in transient crosswinds, and the results of aerodynamic forces and moments showed good consistent results with the experimental. Krajnovic[91] used LES to study the drag reduction of an Ahmed body, which also showed good consistency with the experiments. However, a few examples of using a deterministic gust model in combination with CFD approach can be found in the literature.

Favre [92] carried out the CFD study to analyse the flow around basic car geometry under crosswind gust conditions. In this investigation, a deterministic wind gust represented by a continuous and smooth step-like function was used. Vehicle aerodynamic forces were obtained using commercial software, and the results were compared against two different types of mesh. His work reveals that deterministic gust models can be applied to simulate crosswind aerodynamic forces on a ground vehicle based on CFD method. However, the study was conducted on a simple small car model, which is less sensitive to the crosswind as

compared to trains or high-sided lorries[93]. In addition, the author recommends further investigation on other types of wind gusts. Similar to[92], a rectangular crosswind profile was considered by Tsubokura et al.[94]. The study carries out a numerical simulation of unsteady aerodynamics of full-scale truck model under wind gust by implementing the LES technique. Numerical values of drag and side coefficients were validated by wind-tunnel tests, with the results showing a good agreement. However, the maximum gust strength applied stood at 4.43 m/s, which is relatively small as compared to the strength of the gust in reality.

Sterling et al.[43] compared the wind-tunnel experiments, CFD simulations with a full-scale field measurement of aerodynamic forces and moments for a high sided lorry. They found out that all three methods can correctly simulate the mean side aerodynamic force coefficient. However, the lift coefficients obtained from CFD simulations were larger than the values obtained from the other two methods; their result can be attributed to the difficulty in simulating the near ground flow.

### **2.3 Coupling aerodynamics to vehicle dynamics**

As discussed, developing a vehicle dynamic model is an essential part in predicting methodology of vehicle crosswind stability. The difficulty in creating the vehicle dynamic model comes from determining the appropriate level of detail that will accurately represent the dynamics behaviour of the vehicle. Lozia[95] compared the rollover threshold acceleration obtained from truck models with different levels of detail; ranging from simple static equilibrium of a single body to a 14 degree of freedom (DOF) model with step input steering wheel excitation. The author discovered that the differences in results between a simple vehicle dynamic model and the model with high DOF up to 38%.

Thereby, mathematical models are useful for analysing simple models; but for more complex ones such as tractor semitrailer model, an analysis might be time consuming or even beyond human capabilities. As a result, the field of Multi-Body Simulation (MBS) software has

witnessed great progress during the past 30 years. The biggest advantage of using MBS software is that it enables the user to accurately develop models of complex systems in almost any possible scenario. In the rollover study for example, the results presented by Shim and Ghike [96] indicate that when compared to a complex multi-body model, the simple 14-DoF model lacked accuracy at extreme roll angles and after wheel lift-off, because it did not account for the changes in the suspension geometries. Dahlberg[97] used a full vehicle model of articulated vehicle by using ADAMS application in order to test the Dynamic Rollover Threshold (DRT). The author included the flexibility of the trailer in the MBS simulation and he concluded that kinematic properties of the vehicle system should be considered when analysing the rolling dynamics. Hussain et al.[98] employed the multi-body simulation software ADAMS for studying the phenomenon of rollover of articulated vehicles. The authors noted that MBS software enables the user to account for not only the suspension kinematics, but also all sources of compliance. The use of multi-body dynamic simulation of road vehicles has been demonstrated in detail in a number of studies (e.g, Rahnejat [99], Hegazy [100], and Blundell[101]) . However, these studies mainly investigated vehicle dynamic in terms of handling and ride behaviour.

For assessment of a ground vehicle crosswind stability, coupling of vehicle aerodynamic forces with vehicle dynamic and kinematic model based on multibody method is important. Based on the literature survey it is found that there are limited investigations on integration methods of a high-sided trailer vehicle dynamics and aerodynamic forces. The following table summarises recent published studies on current development of crosswind stability on large vehicles.

<b>Authors</b>	<b>Study highlights and results</b>	<b>Gaps and limitations</b>
M Batista and M Perkovič [115]	<p>In this study, the researchers carried out theoretical investigations on safety of road vehicles under crosswind conditions. Critical wind speed for rollover accident have been defined by using a static model (i.e., for aerodynamic evaluation). The model was developed based on basic equations and it was assumed that the vehicle travels on a uniform straight road. The results report that for rollover accident, the mathematical formula provides lower critical wind speed for road vehicle than that of the Baker model [16]. For validation, numerical calculations were conducted and the outcomes were compared with the observations of test drives that were carried out on 6-km long section on the Slovenian highway H4. Good agreement has been obtained between the results, and the authors reported that the suggested method is reliable for analysing vehicle crosswind stability.</p>	<p>1- Wind speed formulas that developed for predicting wind-induced accidents were for a simple two-axle vehicle model driving in a straight line at a uniform speed.</p> <p>2- The authors state that “the model simplifies the real situation because many factors, especially the non-stationary conditions for sudden wind gusts, are ignored.”. Furthermore, vehicle aerodynamic coefficients were not considered which are very important parameters for evaluation of vehicle crosswind stability.</p>
Proppe, C., & Zhang, X [116]	<p>The crosswind stability of ground vehicles (rail &amp; road) has been investigated in this work. A stochastic model has been proposed for the analysis, and uncertainties were taken into account. The model has been developed based on nonstationary wind turbulence and an artificial gust model. The proposed method has been used to investigate the crosswind stability of both railway and road vehicles. The study also considers vehicles motion on curved and straight ways. Failure probabilities were predicted and a risk analysis was conducted.</p> <p>The study concluded that there was a significant correlation between ground vehicle crosswind stability and amplitude and duration of wind gusts. Also, the observations show that the most important variables</p>	<p>1- In wind model, turbulent wind speed has been calculated by the von Karman power spectral density, and the weakness of this model is its inability (or it is very complicated) to describe the three-dimensional wind flow.</p> <p>2- Wind forces (i.e., vehicle aerodynamics) have been calculated based on wind spectrum of a fixed point in space, and no flow domain has been considered. As a result of that, most properties</p>

	<p>affecting the crosswind stability of ground vehicles were radius and cant of curved way and aerodynamic lateral forces.</p>	<p>of wind flow were not taken into account.</p> <p>3- No validation study has been undertaken to verify the wind model and data obtained.</p>
<p>Alonso- Estébanez, A et al. [117]</p>	<p>In this investigation, numerical modelling has been developed to analysis the crosswind stability of truck vehicle. During the simulations, the vehicle was located on the crest of an embankment in order to consider the most possible scenarios in which the truck crosswind instability can be affected. For the modelling, the CFD (RANS) equations along with the <math>k-\omega</math> turbulence technique were used to predict the behaviour of turbulent crosswind flow. The crosswind aerodynamic coefficients of the truck were evaluated for the embankment with or without the wind fences installed.</p> <p>The numerical results show that the distance between the vehicle position and the wind fence has quite strong influence on the rollover coefficient. Furthermore, after comparison analysis of vehicle aerodynamics forces under different heights of wind fence, it observed that the wind fence can provide a reasonable level of protection against rollover accident.</p>	<p>1- Effects of wind loads on stability of a high-sided truck were analysed only in terms of vehicle aerodynamic forces and moments, and contribution of vehicle dynamics or driving manoeuvres on vehicle crosswind stability were not considered .</p> <p>2- No validation study has been undertaken to verify the data obtained from CFD simulations.</p>
<p>Wang, B et al. [118]</p>	<p>The aims of this study were to explore the dynamic reliability of a road vehicle (tractor semitrailer) subjected to turbulent crosswinds conditions. For this purpose, the dynamic responses of a road vehicle are simulated based on a nonlinear vibration model. To look at influences of random variables including the vehicle weight, road friction coefficient and driver parameter on vehicle crosswind stability, Monte Carlo simulation with Latin Hypercube sampling have been used in the study. The wind-induced safety in crosswinds considering these</p>	<p>1- In this study, a safety indicator developed for prediction of vehicle instability in crosswinds was based on only a single parameter, which can be chosen from parameters of vehicle dynamics or aerodynamics. For this reason, acceptance of safety status is restricted to the selected parameter.</p>

	<p>random variables and a distribution model of the dynamic reliability is introduced to evaluate the safety of the running vehicle. It observed that the proposed method provides a conservative result for the rollover reliability and reliability for course deviation condition of the vehicle. This reliability decreases with the increase in the mean wind velocity, the vehicle speed, and the road roughness height.</p>	<p>2-The authors state that “corresponding experimental data are few to give an adequate verification, which is a general limitation for the simulation of such complex wind-vehicle effects”</p>
Zhang, X. [74]	<p>In this research project, the crosswind stability of ground vehicles has been analyzed by using a probabilistic method. Also, wind-induced risk assessment of vehicles in high crosswind conditions have been evaluated based on nonstationary wind turbulence. For this purpose, the researcher also considered a stochastic gust model to be applied on the vehicles. To calibrate the gust model, realistic wind data that has been recorded at the exposed road section are utilized.</p> <p>The gust variables and aerodynamic coefficients are considered as random parameters. It is observed that the failure probability will become larger with higher (high-sided) vehicle and high wind speed. Also, the study has concluded that for different vehicle types, strong crosswind has significant influences on their running stability. In addition, the wind angle has reported to be essential factor that should be considered to maintain the crosswind stability of vehicles at accepted level.</p>	<p>1- Effects of driver actions (i.e., vehicle manoeuvres ) on vehicle crosswind stability which are very important factor are not consider.</p> <p>2- Vehicle aerodynamic forces were analysed as concentrated forces and moments, and the researcher recommended further and more detailed study on vehicle aerodynamics based on CFD , full-scale and wind-tunnel tests.</p>
Nakashima, T et al.[120]	<p>In this work the researchers have evaluated the crosswind stability of a full-scale truck vehicle by developing an unsteady aerodynamic simulator. Based on this model, a fully coupled analysis of vehicle motion and transient crosswind vehicle aerodynamic forces has been conducted. For this purpose and to reproduce the unsteady crosswind</p>	<p>1- For vehicle dynamics analysis, it was assumed that the vertical motion of the truck is restrained.</p>

	<p>event, CFD method based on a large-eddy simulation (LES) technique has been used. The results were validated against results obtained by a conventional quasi-steady method.</p> <p>The outcomes show that the influences of the unsteady aerodynamics on driver's perception variables are significant. Also, in crosswind region, it was observed that the truck begins to deviate strongly from its initial position on the road. Based on their results, the researchers reported a positive relationship between crosswind aerodynamics and wind-induced truck accidents. They strongly recommend further estimation and analysis of unsteady aerodynamic loads acting on motion of high-sided vehicles.</p>	<p>2- Pitching and rolling dynamic moments were assumed to be constant and balanced statically.</p> <p>3- In validation analysis, differences in the truck yaw angle obtained by the two methods were observed.</p>
<p>Grm,A., &amp; Batista, M[121]</p>	<p>This study employed CFD simulation method to predict truck aerodynamic stability running in high crosswind condition. Essential CFD parameters like boundary conditions, mesh type, turbulence technique are considered and discussed in detail. Simulation results were fit to a piece-wise function <math>g(x)</math> which was proposed for validation purposes. There is a lower bound path defined within the fit models. Critical aerodynamic stability of the vehicle has been estimated base on the simulation data and fit model. Instability conditions such as rollover, rotation and side-slip were acquired. It was also observed that lower bound predictions for critical wind-vehicle speeds are the most significant data. The authors suggest that it is possible to develop worst-case scenario for estimating critical wind-vehicle speeds and analyzing of wind safety regulations. For this purpose, from the developed model, marginal path can be used as indicator.</p>	<p>1- Estimation of vehicle crosswind stability is strongly based on truck aerodynamic parameters.</p> <p>2- The authors state that "the relationship between vehicle and wind speed is implicit, and requires a numerical solution."</p>

However, it must be noted that the range of investigations in the above studies of crosswind stability are limited to simple vehicle dynamic models. Simple models however, cannot be used to accurately predict complex interactions between aerodynamics, vehicle dynamics and the driver (i.e. under different driving manoeuvre).

## **2.4 Rollover prediction**

In the late 1980's, Harwin and Emery [105] developed a database called CARS (Crash Avoidance Rollover Study) which included data from about 3,000 single vehicle rollover crashes in the state of Maryland over an eighteen month period. Data was collected by specially trained Maryland State Police who worked with NHTSA engineers. The authors developed the system based on environmental and driver factors that contributed to the accidents. Their results were divided into five files: accident, vehicle, driver, passenger, and tire. The authors concluded that over 50% of the skidding type of rollover accidents were caused by going too fast around a curve in the road and 24% of the rollover accidents were caused by severe steering input while on a straight road.

Typically, a real-time rollover index is utilised in the system to address the detection of vehicle dynamic rollover threat. Recently, number of rollover indices have been developed based on different parameters and published in vehicle dynamics and automotive journals (e.g., [106], [8], [37], [111] and [108]). Chen and Peng [108] proposed a dynamic rollover warning algorithm based on the time-to-rollover (TTR) metric. The TTR can dynamically record the predicted time from the current time to the rollover moment and selected the roll angle of the centre of gravity (CG) of the vehicle as the dynamic warning threshold. However, a real-time vehicle model is needed in this metric to predict future vehicle states, which is extremely difficult under sudden crosswind actions. As well as, as the inherent vehicle nonlinearities are neglected, the work range and accuracy of TTR are limited.

In addition, Preston et al.[37] suggested a lateral Load Transfer Ratio (LTR) to judge the rollover stability for heavy vehicles. As mentioned before, this index is a function in vertical loads on the left and right tires of the vehicle. However, the author stated that there is no simple method for directly measuring the normal wheel loads. In order to resolve this problem, several studies[8, 26, 34, 109, 110] were conducted to obtain the implementable version of the LTR index. Rajamani et al.[26] developed algorithms to estimate state and parameters of a vehicle for reliable computation of the LTR index. The investigated algorithms include a sensor fusion algorithm that utilized a low-frequency tilt angle sensor and a gyroscope, and a nonlinear dynamic observer using only a lateral accelerometer and a gyroscope. Hyun and Reza [109] also proposed another solution, a predictive model was used to determine a rollover threat index associated with tractor-semitrailers. The authors used the LTR coefficient for which, several key parameters were obtained using system identification techniques.

Moreover, the dimensionless RI was developed by Yoon et al.[111] via the wheel lift threshold in the roll angle and roll rate ( $\phi - \dot{\phi}$ ) phase plane. Chou and Chu [34] combined the original RI with a classic Grey Model (GM (1, 1)) to predict the future trends of vehicle dynamics and proposed the Grey RI (GRI).

Nalecz et al.[112] proposed a method using the rollover prevention energy reserved (RPER) to warn about the possibility of rollover. RPER function measures the difference between the potential energy required to bring the vehicle to the static tip over position and the rotational kinetic energy of the vehicle created after impact with the curb. Sensitivity analysis involved finite difference measures of changes of RPER with respect to vehicle parameters. A complication of this technique is that changing vehicle parameters invariably changes the severity of the vehicle's trajectory, thus the finite difference derivatives are not partial derivatives of RPER taken for the same vehicle trajectory.

Furthermore, Yu et al.[113] has proposed a two-axle vehicle stability model for studying the behaviour of a vehicle under cross wind for roll-over accidents and course deviation. This model evaluates the vertical reactions at the four wheels by analysing the forces and moments associated with the vehicle inertial reference frame. This stability model consists of six equations which aim to predict rollover as well as side-slip stability of heavy vehicles. However, the mathematical model that was used for developing the rollover warning system, ignores most nonlinearities that arises from suspension, tire and steering models of the vehicle. Due to this assumption, the accuracy of the system is not sufficient for predicting rollover event of more complicated dynamic models such as tractor semitrailer dynamic model. From the above discussion, it can be seen that parameters of the rollover reported in literature have been predicted based on either on vehicle states or road geometry factors. However, not a lot of research investigations have been carried out for other factors affecting , in particular, vehicle rollover index such as strong crosswind forces[114]. Crosswind effects become critical when the vertical load on one or more wheels is already low due to the other effects described here.

## **2.5 Summary of Literature Review and gap identification**

For the modern design of road and rail vehicles, assessment of crosswind stability is an important criterion. This assessment involves four stages:

- 1- Development of artificial or simulation data for crosswind flow conditions.
- 2- Prediction of vehicle crosswind aerodynamic forces.
- 3- Coupling of vehicle aerodynamic forces to high accurate vehicle dynamic model.
- 4- Development of vehicle rollover indicator.

In this chapter the research works on each stage were reviewed from the published literature. The reviews have identified the specific research problems and there are a number of consistent results and important points which are:

- Investigations on the influence of crosswind aerodynamic forces on a moving vehicle are important for the vehicle safety and stability. Currently major research and industrial projects do not carry out significant unsteady aerodynamic development in extreme wind conditions because the traditional steady state approach continues to be sufficient. However, the previous studies show that as a vehicle get lighter/larger with less rotational inertia, it can produce high roll and yaw moments. As a result of this, high-sided vehicles are more sensitive to unsteady or transient aerodynamic forces than the passenger cars. Thus, these forces should be estimated in order to avoid their effects on vehicle rollover conditions.
- The review of previous studies reveals that a reliable prediction model for gusty crosswind aerodynamic acting on road vehicles is still far from established. This is due to the complicated nature of the problem related to scaling rules, flow simulation, the effects of local topography and infrastructure, as well as the limitations of wind-tunnel technology. Therefore, different institutions have developed a test method/mechanism for investigation of vehicle unsteady aerodynamic forces. These studies are also depending on several hypotheses and specific geometric parameters, and no single method finding overall favour.
- There have also been limited investigations of using a deterministic gust model in combination with CFD approach to predict aerodynamic forces in gusty crosswind conditions.
- In previous wind-tunnel experiments, aerodynamic forces were obtained either with force balance technique or by integrating surface pressure distributions over the vehicle.

- For evaluating the running safety of a high-sided commercial vehicle subjected to crosswinds, it is important that the entire system of wind loads, vehicle and driving dynamics are considered. However, limited work is available in the literature in which such comprehensive method with high crosswind actions has been applied to high-sided commercial vehicles.
- Although, experimental investigations for examination of a large vehicle rollover are expensive and difficult to carry out, very few of previous studies have performed dynamic simulations to capture the effects of crosswind loads on a rollover event during critical manoeuvre.

## **2.6 Specific Research Objectives**

The primary contribution of this research is to improve the traditional LTR rollover index for predicting rollover event of a tractor semitrailer vehicle subjected to transient aerodynamic forces due to gusty crosswind conditions. After review of the research literature on vehicle crosswind stability, following objectives are defined to achieve the aims of this project:

- 1- To conduct wind-tunnel experiments on static vehicle model to:
  - a. Measure the crosswind time-averaged aerodynamic force coefficients of a high-sided tractor semitrailer vehicle (ADAMS model).
  - b. Develop a methodology for wind gust generation to predict the aerodynamic loads acting on the high-sided tractor semitrailer vehicle passing through gusty crosswind conditions.
- 2- To Develop transient wind gust scenario based on wind-tunnel data.
- 3- To conduct CFD simulations in combination with the TSI deterministic gust scenario to predict the extreme wind loads that large ground vehicles at exposed locations such as bridges or embankments, are likely to experience.
- 4- To understand the wind-tunnel (empirical) and TSI gust flow field behaviour and its pressure distribution around a full-scale tractor semitrailer vehicle.

- 5- To establish a coupled analysis of unsteady aerodynamic forces and a realistic full vehicle model based on multibody method.
- 6- To investigate dynamic responses of a high-sided tractor semitrailer vehicle subjected to two different transient wind gust scenarios during straight manoeuvre.
- 7- To investigate dynamic responses of the tractor semitrailer during curve negotiation that is subjected to two different time-dependent wind gust scenarios.
- 8- To propose a predictive lateral load transfer ratio (LTR) that incorporated gusty crosswind actions.
- 9- To carry out a parametric study for investigating the influence of various road and vehicle parameters on the roll stability (rollover index) of the vehicle.

### **Chapter 3 : Methodology-Wind-tunnel experiments on aerodynamic characteristics of a high-sided tractor semitrailer vehicle in gusty crosswind conditions**

---

Wind-tunnel experiments have been carried out to investigate the aerodynamic characteristics of a tractor semi-trailer unit under extreme crosswind environments. For this purpose, an artificial wind gust scenario has been developed in a wind-tunnel. This scenario represents the situation of a lorry running on a flat terrain, and wind gusts originated due to a sloped topology of surroundings hitting the truck body perpendicularly ( $\beta=90^\circ$ ). The test apparatus, experimental set-up, characteristics of the flow (e.g., pressure variation acting on the tractor semi-trailer) are presented in this chapter.

### 3.1 Introduction

Wind-tunnels are a significant research apparatus used in vehicle aerodynamic investigations to study for example the effects of air moving past a ground vehicle body. In general, wind-tunnels are equipped with a fan that blows the air onto a test model, which is located in the test section of the tunnel. Compared to full-scale measurement, the cost of wind-tunnel tests is much lower. In addition, under controllable laboratory conditions, tests are repeatable, thus ensuring the accuracy of the results compared with on- road tests. So, wind-tunnel tests remain the most popular measure to obtain wind-related information. However, it should be noted that variations can exist between model data obtained from different tunnels, even when the same model is used[115]. This is because of that estimation of vehicle aerodynamic characteristics is strongly dependent on air flow around the vehicle's body. Additionally, exact actual air flow pattern generated in wind tunnels is not standardised or lack reproducibility. This disadvantage arises from uncontrollable flow turbulences that generated by wind tunnel fans and effects by both tunnel walls and surrounding equipment.

In this study, there are two main aims of the experimental work. The first aim is to assess the steady aerodynamic parameters of a stationary tractor semi-trailer vehicle in a crosswind. It is important to point out that a rigid model was used during the tests. This means that the geometric characteristics of the tested vehicle are reproduced, but not its inertial, stiffness and damping properties. Thus, the dynamic interaction between the vehicle and the wind can not be experimentally evaluated. The second aim is to develop a gusty wind flow for modelling the worst operational scenario, which is essential to assess tractor semi-trailer rollover events under crosswind conditions.

## 3.2 Wind-tunnel set-up

The experimental measurements detailed in this work were collected in the wind-tunnel observation room at the University of Huddersfield. This section provides information about the set-up of the tests.

### 3.2.1 Wind-tunnel components

The wind-tunnel is an open circuit type, with a cross-sectional area of 600 x 600mm and the total length of the test section (from the nozzle inlet to the section outlet) is 1,500 mm. It is a low speed tunnel, able to produce a maximum wind velocity of 20m/s, and minimum turbulence intensity of about 13%. As shown in Figure3.1, apart from test section, the wind-tunnel consists of several components most of these are:

- 1- Settling chamber: this is also called the entry section. This part is important to create a smooth flow that can be managed and hence generate the required turbulence structure.
- 2- Honeycomb: large, turbulent eddies of the inlet flow in the test section are reduced by using a honeycomb. This is placed perpendicular to the flow direction at the end of the settling room part and has a hexagonal shape with a thickness of 12mm.
- 3- Contraction section: the entry and contraction sections were bolted to each other. The purpose of the contraction sections is to decelerate the flow to the desired velocity in the test section.

The experimental facilities and the layout of the experimental set up are depicted in Figure 3-1 and Figure 3-2 respectively. As can be seen from Figure 3-1, the bottom of the test section was provided with mounting holes and openings for inserting flow measuring devices. The wind-tunnel also has a fixed floor and, according to Cooper [116] one can

conclude that a fixed floor with a thin boundary layer is sufficient for current automotive and commercial vehicle applications. Furthermore, Table 3-1 contains technical information about the wind-tunnel components.

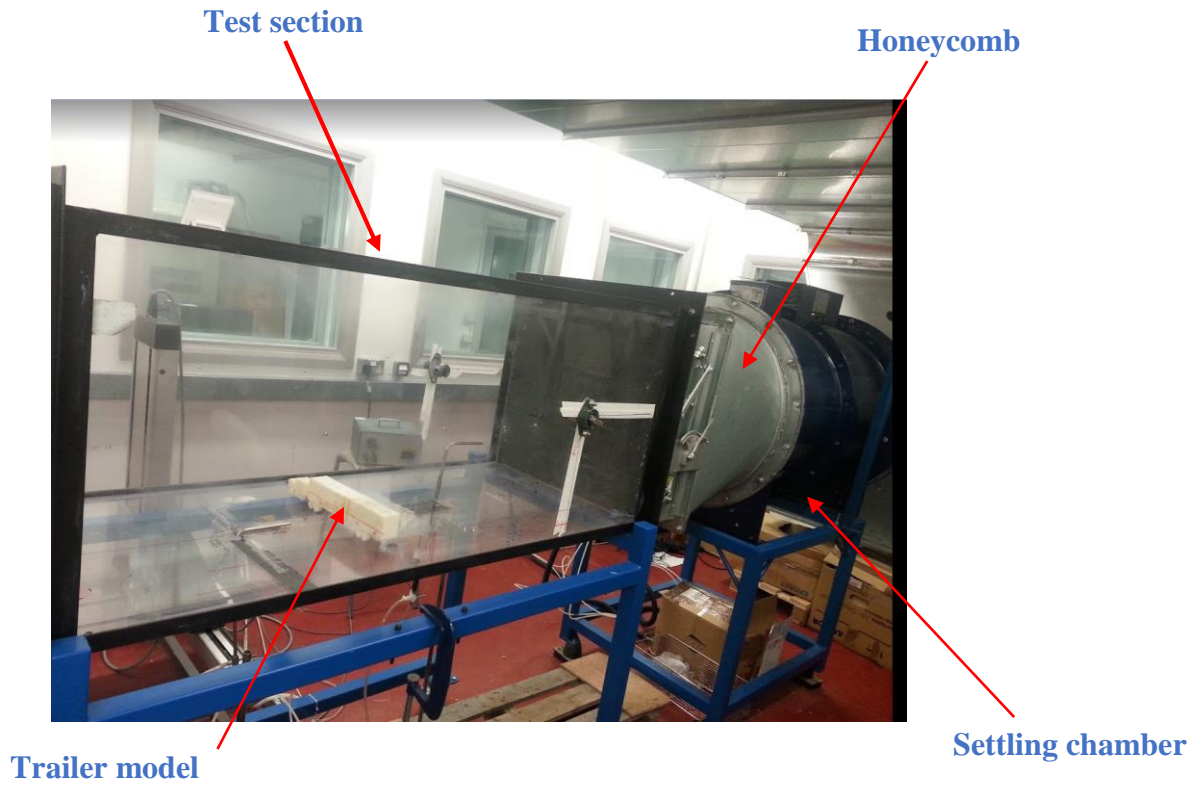


Figure 3-1 : Wind-tunnel equipment

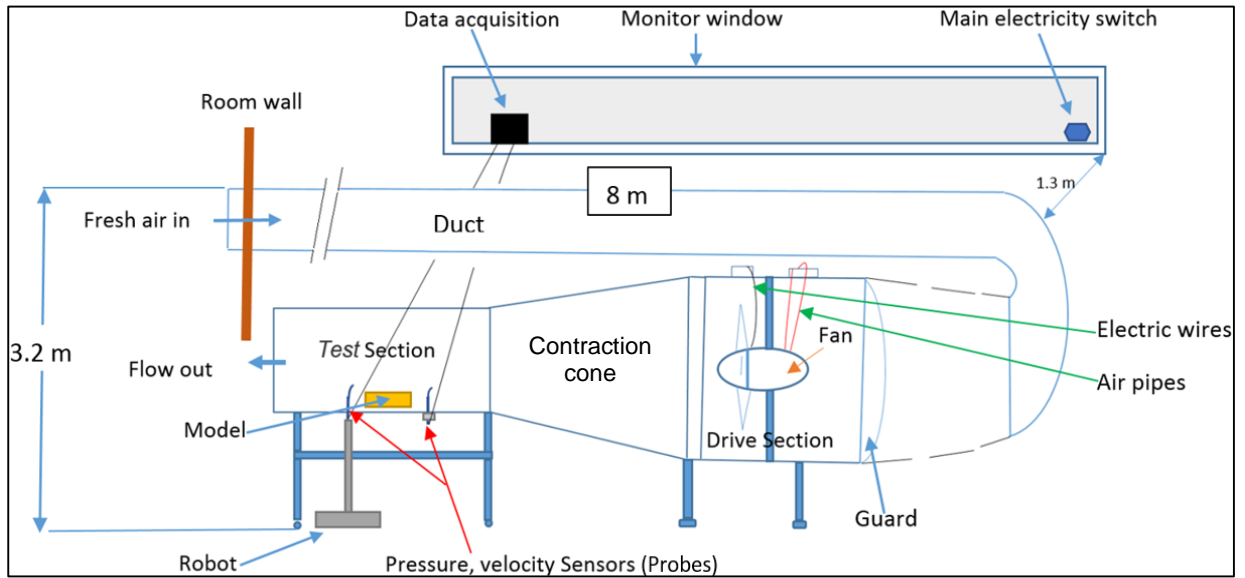


Figure 3-2 : Schematic of the experimental setup

Table 3-1: Specification of wind-tunnel rig

Technical parameters	Technical data
Type	Open-circuit wind tunnel 71KG 40 A
Drive section	Electric impeller (fan) with pneumatic system
Operating voltage	380/420 v
Maximum fan speed	2950 R.P.M
Operating air pressure	1.76 kg/cm <sup>2</sup>
Electric motor specifications	3 phase, 13 kw, 50 Hz, 25 A (at full load)

### 3.2.2 Aerodynamic model

In general, unsteady wind conditions must be modelled according to the configuration of the body with which it interacts [117]. Therefore, in order to facilitate the accuracy needed for predicting vehicle dynamic responses to wind actions through dynamic simulation, the

geometry of a tractor semi-trailer vehicle, built in ADAMS /Car software version 2015.1.1, was developed for wind-tunnel tests. The geometry of the vehicle's model is based on configuration of a real commercial vehicle (more details about model dimensions are in the next chapter) , and the 3-D model is shown in Figure 3-3. The model was downsized to 1:54 scale (Figure 3-4) to maintain the blockage ratio of the model to the cross-sectional area of the wind-tunnel test section at less than 10 % [124] .



Figure 3-3 : Tractor semitrailer model built in ADAMS/Car



Figure 3-4: Wind-tunnel model of tractor semitrailer (scaled- ADAMS model)

The model has been made from compacted powder using a 3D printer. Dimensions of the model are 400mm  $\times$  47.6mm  $\times$  78.9mm (length  $\times$  width  $\times$  height). The wheels of the model were stationary, and the model was rigidly fixed on the bottom of the test section using the support outside of the test section to avoid eventual disturbances of the flow.

### 3.3 Flow-speed measurements

The airflow in the wind-tunnel is generated by an axial blower fan (powered by an electric motor of 13kW) with pneumatically adjustable variable blade pitch. The range of air speeds

possible in the wind-tunnel was from 11m/s to 20m/s (without gust generator). Instantaneous velocities and turbulence intensities of the airflow were measured using a multi-hole pressure probe called Cobra probe (from Turbulent Flow Instrumentation Pty Ltd, or TFI)[118], see Figure 3-5. The Cobra probe provides three component velocities (magnitude and direction), turbulent turbulence intensity and local static pressure measurements in real time. The probe has a frequency response of up to 5,000 Hz, and it measures the flow field within a range of  $\pm 45$  degrees from its axis [119].

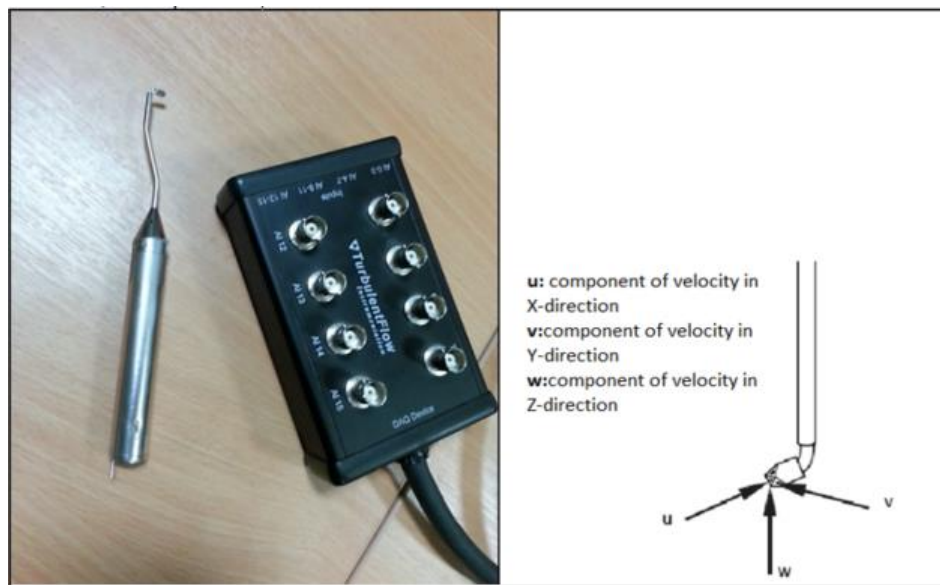


Figure 3-5 : Cobra probe and flow data acquisition

The computer set-up inputs the raw voltage from the probe to a data acquisition interface unit, which is connected to the computer using a data acquisition card. As shown in Figure 3-6, TFI device control software is used to control the probe and analyse the raw output.

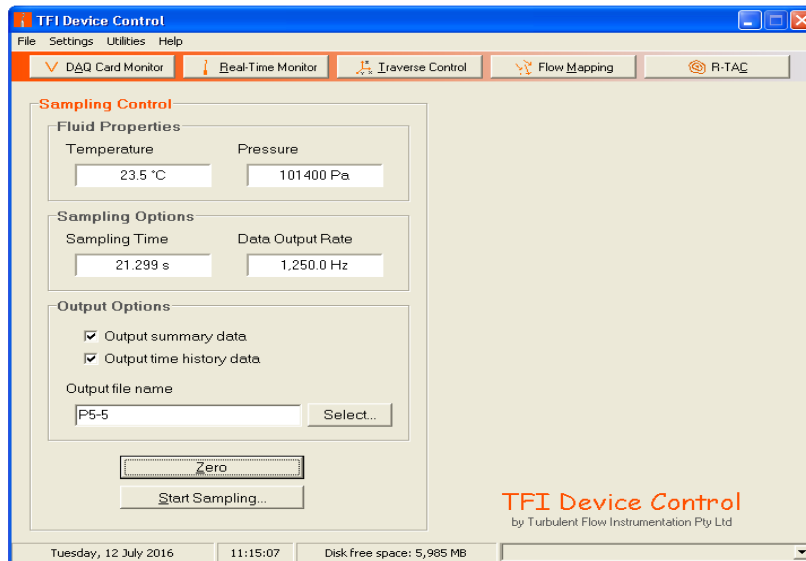


Figure 3-6 : TFI device control



Figure 3-7: Data display screen in cobra probe

### 3.4 Pressure measurements

Wind pressures were also recorded in the experiment to quantify vehicle aerodynamic loads. Measurements of pressure on the trailer's surface were made using 20 pressure-tapping points drilled through the vehicle body and vinyl tubes were placed in these holes, as reported in Figure 3-8. The tapping points were distributed across the faces of the model in four cross-sections, one of them coincides with the model midsection. The surface pressures were

measured relative to the working section static pressure. For this purpose, digital manometers (see Figure 3-9) were placed outside of the wind-tunnel test section, and the vinyl tubes connected between the tapping points and manometers.

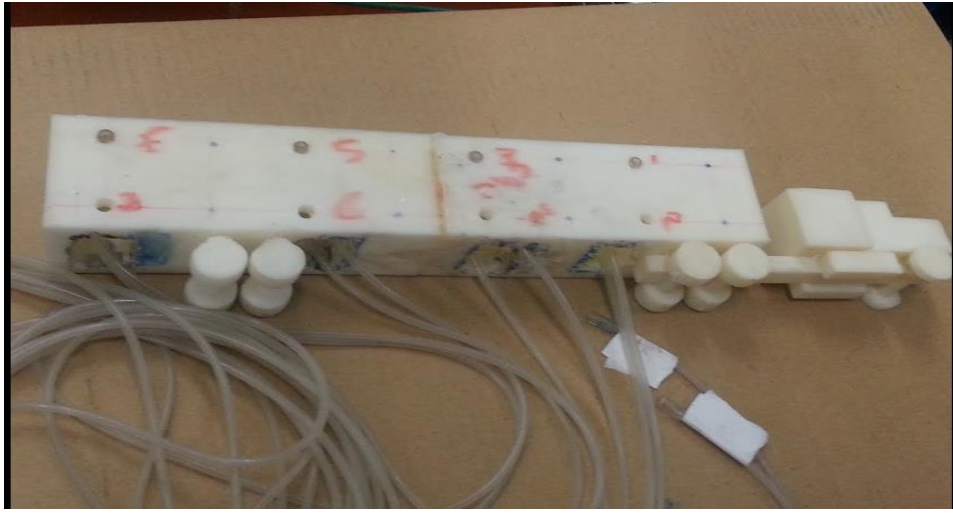


Figure 3-8: Pressure tapping points



Figure 3-9: Digital manometer for pressure measurements

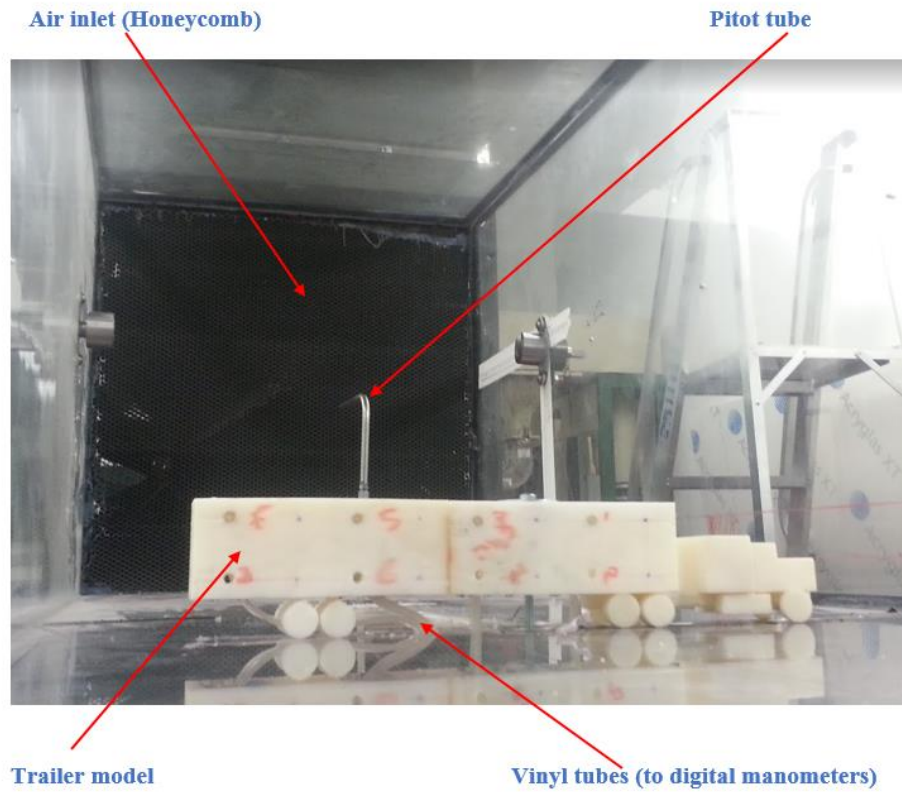


Figure 3-10: Experimental design for pressure measurement

In order to obtain pressure measurements in the flow field as well, a pitot tube (Figure 3-10) measuring the static pressure of the airflow was mounted on a stand and fixed to the test section floor. It is located upstream from the model and at height of 0.8m (just above the model's height), this location has been selected in order to measure the flow pressure out of the boundary layer.



Figure 3-11: Pitot tube

As it will discuss later, the time-average pressure value corresponding to each pressure tap was recorded in order to determine the pressure coefficient. This values are listed in the table 3-2.

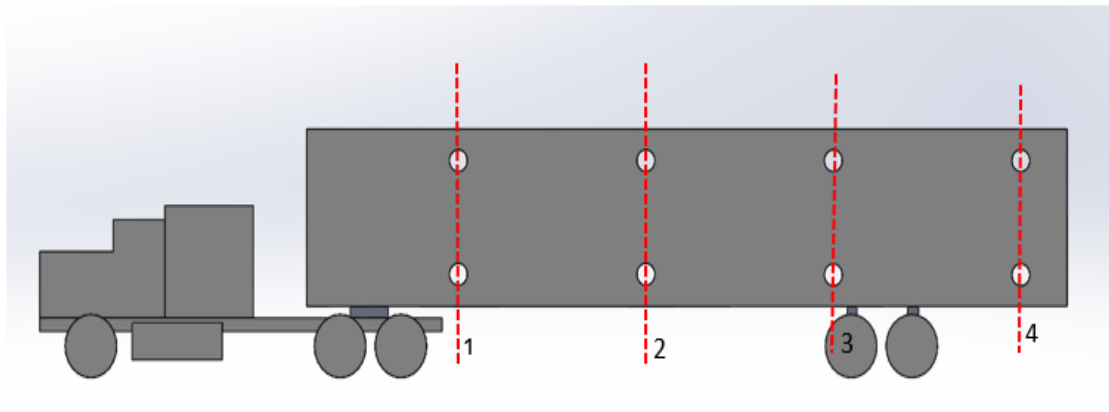


Figure 3-12: Longitudinal distribution of pressure taps

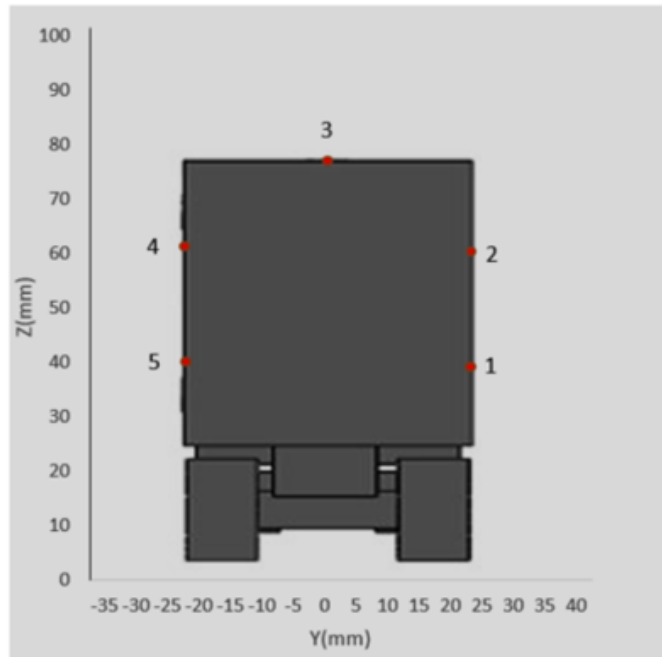


Figure 3-13 : Pressure taps distribution on the model's cross-section (loop)

Table 3-2: Values of pressure measurements

Pressure at taps (digital manometer pressure) (kPa)					Flow field pressure (kPa)
Tap	Loop1	Loop2	Loop3	Loop4	
					<b>0.878</b>
<b>1</b>	<b>0.36</b>	<b>0.42</b>	<b>0.27</b>	<b>0.31</b>	<b>0.878</b>
<b>2</b>	<b>0.38</b>	<b>0.47</b>	<b>0.28</b>	<b>0.34</b>	<b>0.878</b>
<b>3</b>	<b>0.07</b>	<b>0.054</b>	<b>0.065</b>	<b>0.072</b>	<b>0.878</b>
<b>4</b>	<b>0.21</b>	<b>0.28</b>	<b>0.19</b>	<b>0.13</b>	<b>0.878</b>
<b>5</b>	<b>0.18</b>	<b>0.15</b>	<b>0.13</b>	<b>0.14</b>	<b>0.878</b>

Even though the surface pressure measurements would benefit from more pressure taps placed at various positions around the model to capture high-pressure gradients, it is believed that this would not change the overall trend in aerodynamic loads experienced by the vehicle model [121].

### 3.5 Gust generation system

Wind speeds can be increased considerably by natural and man-made topography in the form of escarpments, embankments, ridges, cliffs and hills. The basic idea for generating gusts in a steady flow tunnel is to modify the boundary conditions, in an unsteady manner, at the flow

inlet (i.e., upstream of the model). Generation of wind gusts by using of wind-tunnel facility has been traditionally carried out by active or passive techniques, such as boundary layer and grid turbulence. In this work, the gust generation mechanism is based on the concept of achieving a quick change of the wind flow speed in the test section. By this mechanism, the gust is produced due to the wake vorticity of a flat plate, which was positioned within a section of the wind-tunnel upstream of the model, see Figure 3-14. The passive gust generation technique used in this thesis has been inspired by the experimental bench test of Butler and Kareem [122], as well as a numerical study carried out by the authors[123] .

The subsequent change induced by the flat plate was that the flow is forced to quickly accelerate in the regions above and below the plate, recreating a gust flow condition in those regions. The flat plate is fixed with angle of  $\theta=30^\circ$  to the approaching flow, this angle is among the range of critical wind incidence angles for vehicle instability under gust loads[66].In addition, the blockage ratio (the ratio of the projected area of the model to the cross-section area of the test section) without plate is 5.94%, and with plate is 8.23%. According to previous researches, a blockage ratio lower than 10% is acceptable in practical engineering[124]. Figure 3-14 shows the general set-up of the flat plate (gust generator) fixed in the wind-tunnel test section. Main dimensions of the measurement domain are indicated by the layout in Figure 3-15, where  $d=27\text{ cm}$  is the height of the opening and  $\chi = 30^\circ$ .



Figure 3-14 :Mechanism of gust generator

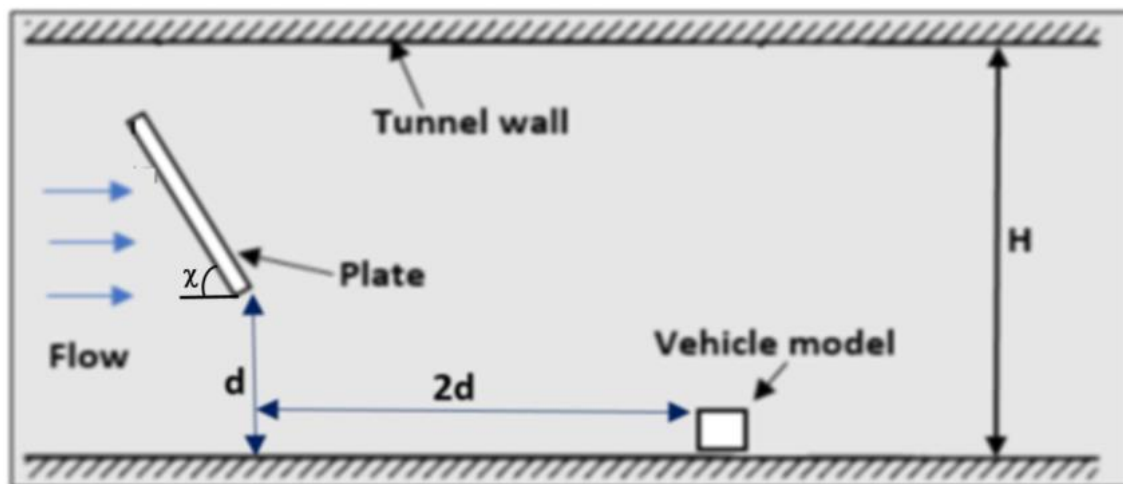


Figure 3-15: Layout of gust generation system

Moreover, in these experiments, the time series of crosswind velocity ( $u(t)$ ) was sampled at a point within the region of accelerated flow (gust regime. The point position close to (just above) the trailer's centre of gravity (Figure 3-16) where the most critical conditions occur [125]. Furthermore, in gusty flow test cases reported in this study, the wind flow was perpendicular to the side of the vehicle.

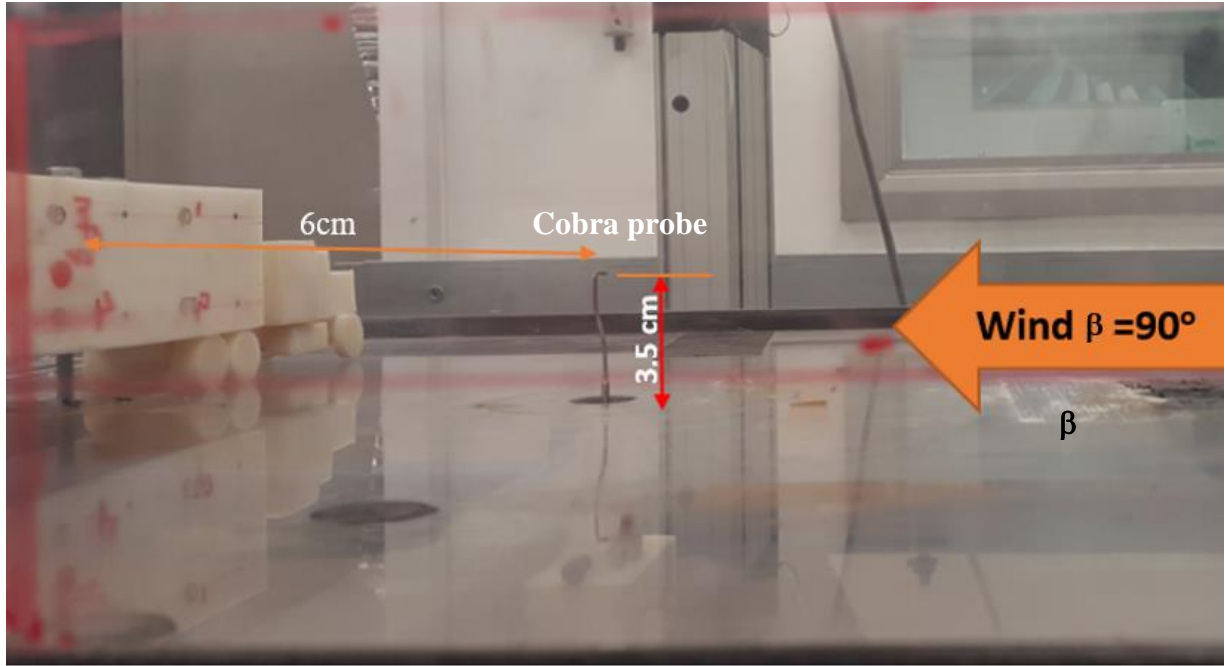


Figure 3-16: Sampling point

### 3.6 Calibration of instruments

The Cobra probe is the main device used in this experiments, it has an accuracy of  $\pm 1.6 \frac{ft}{s}$  ( $\pm 0.5 \frac{m}{s}$ ) and  $\pm 1$  degree for pitch and yaw angles [120]. The sensor and TFI device control software are also calibrated in the factory; therefore no initial calibration was required[120]. In spite of that, the Cobra probe reading has been calibrated against air velocity that calculated based on Pitot tube measurements. For this purpose, the Pitot tube has been fixed in wind flow at centre of test section cross- section facing upstream. Bernoulli equation has been used to determine the wind speed, as follows:

$$V_{pit} = \sqrt{\frac{2(p_o - P)}{\rho_{air}}}$$

Where  $V_{pit}$  is air speed measured by Pitot tube,  $P_o$  is stagnation pressure show in Figure 3-14 ,  $P$  is static air pressure and  $\rho_{air}$  is the air density. The data regarding calibration of wind-tunnel air speed measured by the Cobra probe and Pitot tube at the same point and flow conditions are:

$$V_{pit} = 17.657 \text{ m/sec}$$

$$V_{cobra} = 17.875 \text{ m/sec}$$

Therefore, this calibration shows an excellent match between the two instruments.

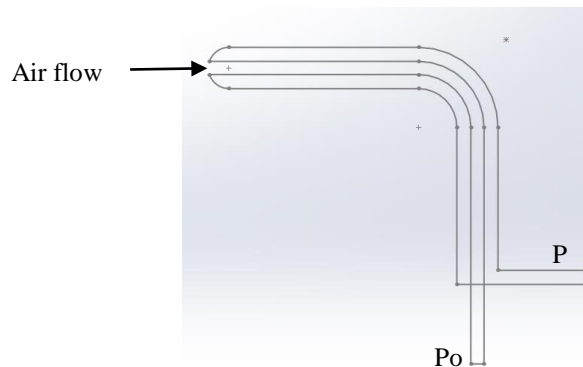


Figure 3-17 : Mechanism of flow pressure measurement by using Pitot tube

Moreover, the digital manometers come with calibration certificate originating from the factory (Dwyer Instruments Limited). During the experiments, the range of accuracy of the digital manometer is  $\pm 0.5\%$  FS, at 20 to 78°C.

### 3.7 Experimental Procedure

In this investigations, the experimental work was conducted according to the procedure below:

1. Place securely the trailer model in the wind tunnel test section, and set the longitudinal axle of the model at desired angle (e.g., 0°, 45°, 90°) to the flow direction.
2. Fixed the cobra probe at selected sampling point.
3. Enter the room temperature and static pressure to TFI device control.
4. Set the pneumatic supply pressure to the fan blades at constant value that should does not exceed 26psi.
5. Connect all vinyl tubes to the digital manometers.
6. Turn on the wind tunnel fan.
7. Once the air flow condition become steady, record the pressure at tapping points and freestream pressure reading from pitot tube.
8. Record the flow velocity components (longitudinal, lateral and vertical) at sampling point using copra probe.

9. Calculate the trailer aerodynamic coefficients as explained in section 3-8.
10. For gusty flow condition, place the gust generator in its position and repeat the steps 1-6 and 8.

### **3.8 Experimental results**

This section discusses time-average aerodynamic characteristics of the vehicle model. For this purpose, a flow with a constant wind velocity have been generated in the test section (without gust generator). The range of air speeds possible in the wind-tunnel was from 7m/s to 19.2m/s.

#### **3.8.1 Reynolds number**

Determination of the Reynolds number requires knowledge of the oncoming airflow velocity and the characteristic dimension of the model. Therefore, the Reynolds number is determined as:

$$Re = \frac{VL}{\nu} \quad (3-1)$$

where V, L, and  $\nu$  are the airflow velocity, the characteristic dimension of the body, and the kinematic viscosity of air ( $\nu = 1.46 \times 10^{-5} \text{ m}^2/\text{s}$ ) respectively. For time-average vehicle aerodynamic characteristics, the benchmark tests were conducted at a wind-tunnel speed of 12m/s. This speed, leading to a Reynolds number of about  $3.28 \times 10^5$  based on the model's length [126]. This, along with the full-scale Reynolds number of  $1.97 \times 10^7$ , is sufficiently high and so, in the turbulent regime, therefore, no Reynolds corrections were applied[124].

#### **3.8.2 Pressure coefficient**

In this section, the results of the measured flow pattern around the vehicle are reported in terms of non-dimensional pressure coefficients (mean pressure coefficients,  $C_P$ ). The pressure coefficient is an essential parameter that directly relates to the distribution of wind loads over

the vehicle's body[117]. Therefore, analysis of this parameter helps to understand the differences in aerodynamic force coefficients.

The mean pressure coefficient at the  $i$ th measured tap on the model surfaces ( $C_{Pi}$ ) is defined as [53]:

$$C_{Pi} = \frac{P_i - P_\infty}{0.5 \rho v_\infty^2} \quad (3-2)$$

where  $P_i$  is the pressure at the  $i$ th measured tap,  $P_\infty$  is the reference static pressure (measured by the pitot tube in the laboratory well away from the jet pressure),  $\rho$  is the air density, and  $v_\infty$  is the mean stream-wise velocity at the sampling point (Figure 3-10).

Figures 3-18,3-19 and 3-20 show the distribution of pressure coefficients around the vehicle cross-sections corresponding to loops 1–4 (see Figure 3-12), at yaw angles of  $0^\circ$ ,  $45^\circ$  and  $90^\circ$  respectively. The data was recorded in smooth wind (without gust generator), with a flow velocity of 12m/sec. As can be seen, a region of negative pressure can be observed on the leeward and top surfaces of the trailer under flow of  $90^\circ$  yaw angle. Whereas, on the windward surface, values of pressure coefficients are positive. This differences are due to the shape of the trailer edges, as sharp edges of the trailer's box produce a separation flow zone on the trailer's roof [127]. This separation zone creates a recirculating flow field behind the trailer with negative pressure. This flow feature (i.e., high pressure on windward side and low pressure on leeward side) could increase the side aerodynamic and aerodynamic overturning moment of the vehicle. For flow with yaw angle of  $0^\circ$ , variations in pressure coefficients are observed over the trailer surfaces. All coefficients are smaller than those of at  $90^\circ$  yaw angle with negative values. As the yaw angle is increased above  $40^\circ$ , the results agree that the flow changes from that associated with a slender body to a bluff body with vortex/separated flow behind the lateral side of the vehicle.

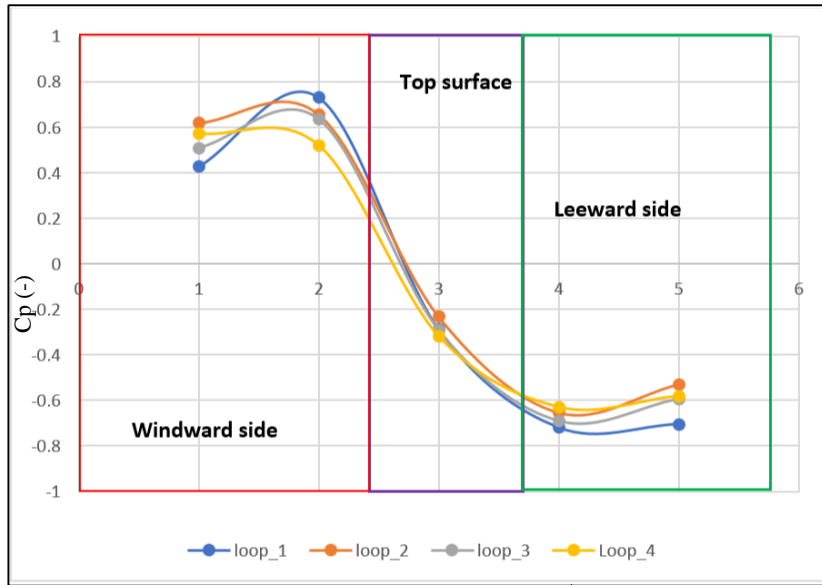


Figure 3-18 : Values of pressure coefficients at  $\beta=90^\circ$

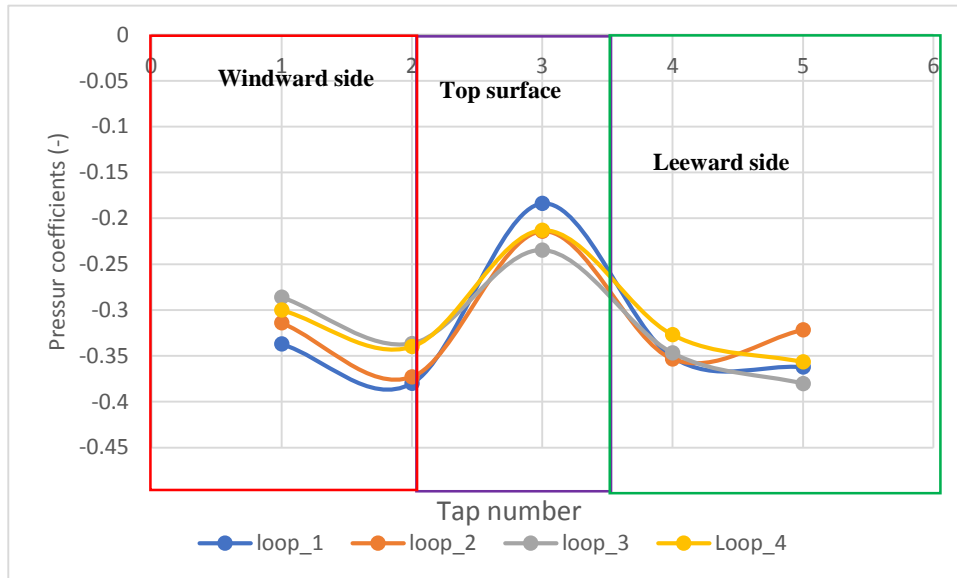


Figure 3-19 : Values of pressure coefficients at  $\beta=45^\circ$

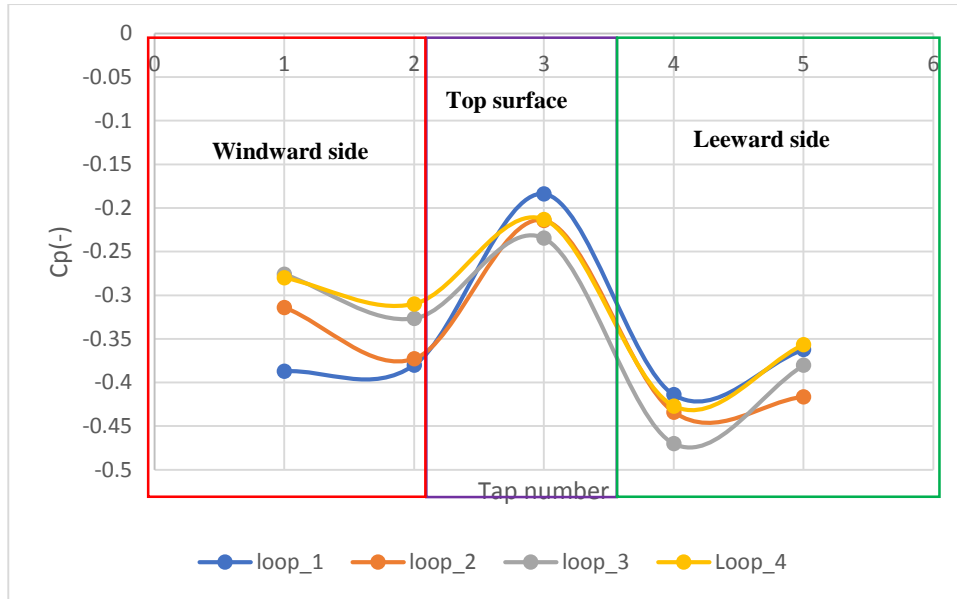


Figure 3-20 : Pressure coefficients data at  $\beta=0^\circ$

Note: due to there being some experimental limitations for measuring the air pressure on the tractor unit of the laboratory model, the pressure coefficient has been measured on the trailer surfaces.

### 3.6.3 Values of mean aerodynamic coefficients

A vehicle crosswind stability is influenced mainly by the side aerodynamic forces [128]. Usually, two approaches are used to determine mean aerodynamic forces/coefficients in wind-tunnel experiments:

1. Design a static force balancing system using load cells placed under the test section for direct measurement of aerodynamic forces.
2. Indirect measurement obtained from the integration of vehicle surface pressures.

For example, experimental results obtained by Rocchi et al.[129] shown in Figure 3-16, compare the lateral force coefficient measured by the dynamometric balance and by integrating the pressure distribution around the vehicle. A good agreement can be noticed between the two measuring systems, allowing the conclusion that the adopted pressure tap

distribution is able to capture all the information to reconstruct global forces. The maximum error between the two measuring systems is in fact generally lower than 7% for the lateral force. Furthermore, according to Quinn et al.[89], results obtained using both methods are shown to agree within acceptable limits.

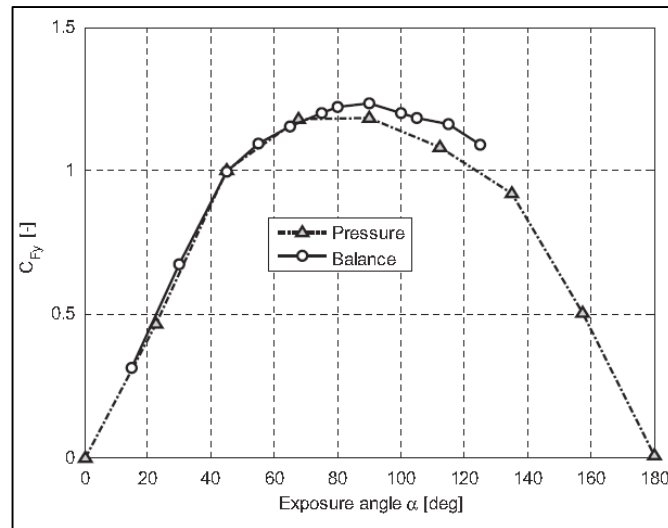


Figure 3-21 :Comparison between pressure (triangles) and dynamometric balance (circles) measurements: (a) lateral force coefficient [129]

Therefore, in this experiment, from the measured pressure distributions, the side and drag aerodynamic force coefficients were calculated. These coefficients are defined as[130, 131]

$$C_D = \sum_i C_{pi} A_i \cos \beta_i / A_t \quad (3-3)$$

here,  $A_i$  is an elementary surface area near the  $i$ th tap,  $A_t$  is the total surface area of the trailer,  $\beta_i$  is an angle between the normal direction of a prism surface on which the  $i$ th cell belongs and wind direction, see Figure 3-22.

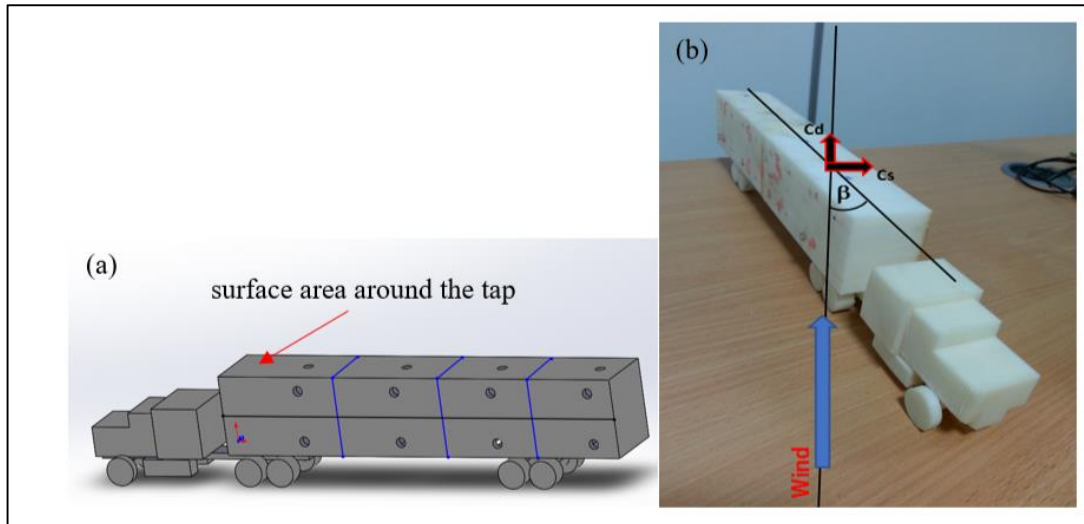


Figure 3-22: (A) surface area around the  $i$ th tap; (B) wind-tunnel flow (main) parameters

To observe variations of aerodynamic coefficients with wind direction, the wind-tunnel model is turned in respect to the upcoming flow by a yaw angle  $\beta$  of  $0^\circ$ ,  $45^\circ$  and  $90^\circ$ . The time-averaged aerodynamic coefficients with respect to the flow direction are shown as points in Figure 3-18. As expected, the lateral force coefficient grows with an almost linear trend; the coefficient also increases with the yaw angle and reaches the maximum value at the high yaw angle of  $90^\circ$ . The same observation (trend) for an articulated lorry was reported in several experimental findings(e.g.,[18, 38, 43, 58, 125]). This result also indicates that a critical wind direction for a high-sided vehicle due to which it suffers higher wind loads is  $90^\circ$ .

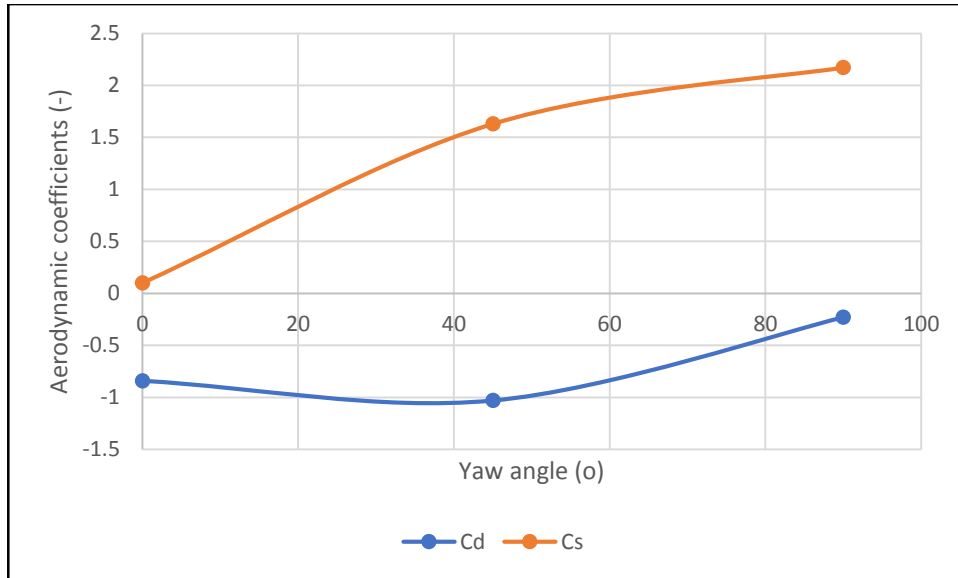


Figure 3-23 : Side and longitudinal aerodynamic force coefficients

Therefore, the author has considered this angle (as worst case scenario) when developing the vehicle crosswind rollover index. Furthermore, Figure 3-18 shows that the longitudinal force coefficient is negative at all yaw angles, with moderately increases with an increase in yaw angle. Values of this coefficient are lower than those observed in side coefficient and take minimum value at around  $\beta=90^\circ$ .

### 3.7 Accuracy of Measurement and Estimating Uncertainty

Uncertainty of measurement can be defined as the amount of errors or fluctuations in the measurement mainly due to human error. For the experiment performed above, such human errors can be reflected in measuring the pressure and velocity of the steady and gusty flow generated by wind-tunnel. These measuring errors are brought in by different instruments, which are not necessarily operate under ideal measuring conditions.

In order to estimate uncertainty first, the sample mean should be computed. The sample mean,  $\bar{X}$  is obtained by taking the average of the sampled values. The average value is computed by summing up the values sampled and dividing them by the sample size,  $n$  as shown in Eq. (3-4)[132].

$$\bar{X} = \frac{1}{n} \sum_{i=1}^n X_i \quad (3-4)$$

where,  $\bar{X}$  is mean value,  $X_i$  is sample value and  $n$  is number of sample. After that, we compute the sample standard deviation. The sample standard deviation provides an estimate of the population standard deviation. The sample standard deviation,  $\sigma_x$ , can be computed follows:

$$\sigma_x = \sqrt{\frac{1}{n-1} \sum_{i=1}^n (X_i - \bar{X})^2} \quad (3-5)$$

The value  $n-1$  is the degrees of freedom for the estimate, which signifies the number of independent pieces of information that go into computing the estimate. In a case of Absence of any systematic influences during sample collection, the sample standard deviation will approach its population counterpart as the sample size or degrees of freedom increases. The degrees of freedom for an uncertainty estimate are useful for establishing confidence limits and other decision variables.

Finally, from Eq. (3-5) the estimated standard uncertainty can be calculated.

$$Eu = \frac{\sigma_x}{\sqrt{n}} \quad (3-6)$$

Based on the results, which have been obtained from experimental tests, are included in Appendix D, the above-mentioned equations (3-4), (3-5) and (3-6) are used to calculate the value of uncertainty in this experiment work. A sample calculation of the uncertainty in the measurement of air velocity at sampling points as follows[133]:

- The mean inlet velocity (longitudinal) can be calculated by:

$$\bar{U} = \frac{1}{131072} \sum_{i=1}^{131072} u_i = 18.4 \text{ m/sec}$$

- Sample standard deviation:

$$\sigma_x = \sqrt{\frac{1}{n-1} \sum_{i=1}^n (u_i - \bar{U})^2} = \sqrt{\frac{1}{131072-1} \sum_{i=1}^{131072} (u_i - 18.4)^2} = 7.17 \text{ m/sec}$$

- Estimated standard uncertainty:

$$Eu = \frac{\sigma_x}{\sqrt{n}} = \frac{7.17}{\sqrt{131072}} = 0.02 \text{ m/sec}$$

- The mean estimated standard uncertainty

$$\overline{Eu} = \frac{1}{n_t} \sum_{i=1}^{n_t} Eu_i = \frac{0.02 + 0.036 + 0.016}{3} = 0.024 \text{ m/sec}$$

where  $n_t$  is number of tests. Moreover, to estimate the repeatability of pressure measurements and the accuracy of the procedure, the tests were repeated three times (i.e.,  $n_t = 3$ ) and the mean values have been obtained and listed in the Table 4-3. for the detailed analyses Based on this calculation procedure the uncertainty of pressure measurements at each pressure tap are calculated, which are shown in the Table 1-3 (details of loops and taps are shown in figures 3-11 and 3-12).

Table 3-3: The estimated standard uncertainty

	Loop 1					Loop 2					Loop 3					Loop 4				
	P1	P2	P3	P4	P5	P1	P2	P3	P4	P5	P1	P2	P3	P4	P5	P1	P2	P3	P4	P5
Mean standard uncertainty	0.23	0.26	0.31	0.25	0.22	0.21	0.23	0.27	0.18	0.2	0.23	0.26	0.33	0.26	0.24	0.22	0.29	0.34	0.25	0.25
Percentage error %	±0.64	±0.66	±0.69	±0.68	±0.64	±0.63	±0.66	±0.68	±0.65	±0.64	±0.67	±0.68	±0.72	±0.64	±0.67	±0.61	±0.64	±0.69	±0.67	±0.65

It was observed that the data corresponding to air pressures were collected by setting the data acquisition system to acquire 20 segments (sample points) in about 70 sec. Under this conditions, the maximum error in the pressure measurement were expected to be 0.72% (i.e., less than 1%). This means, the results are highly reliable across the experiments and stable.

### 3.8 Summary

This chapter provides a detailed overview of the experimental work conducted in this study by explaining the equipment, the test rig and the data acquisition system. Pressure distributions over the surface of the vehicle's model in steady flow conditions were measured. After that, the pressure measurements were presented as (aerodynamic) pressure coefficients experienced by the vehicle. Based on these coefficients, drag and side aerodynamic

coefficients were predicted too. The results show that due to the large lateral area of the vehicle, the mean aerodynamic side force coefficient is higher than drag force coefficient, and it is nearly linear with increases in the wind direction (wind angle of attack).

Moreover, a trailer model exposed to transient aerodynamic forces were experimentally simulated utilizing gust generator method based on passive (i.e., fixed) mechanism. This type of generated turbulent flow represents gusty wind conditions, blowing perpendicular to the vehicle moving direction. After explaining the experimental work, next chapter will illustrate the CFD techniques for predicting of aerodynamic forces acting on the high-sided trailer. The numerical model will be verified against the experimental findings by following the procedure and setup mentioned in this chapter.

## **Chapter 4 : Methodology: CFD and Multi-body dynamic (MBD) Modelling**

---

Based on the research objectives of this study that have been identified in the previous Chapter 2, advanced CFD techniques have been used in order to computationally simulate and analyse the vehicle crosswind aerodynamics. The use of the CFD techniques for the prediction of aerodynamic forces, along-with a multibody dynamic modelling for tractor semitrailer systems (i.e., suspension dynamics, steering dynamics, tire dynamics, etc) has been presented in this chapter. For CFD simulations, appropriate solver settings and the boundary conditions prescribed in the present study, have been mentioned. Furthermore, road and driving modelling that are used to perform dynamic simulation of the vehicle under different manoeuvres have been developed. The numerical experiments conducted for this research study have been identified.

## 4.1 Introduction

The airflow in the lower region of the atmosphere, where the transport infrastructure is located, is characterized by turbulent and unsteady flow [117]. The strength and structure of the atmospheric wind field around ground vehicles is very complex, as well as its effects on vehicle aerodynamics being difficult to quantify accurately [134]. In experimental set-ups, for example, limited knowledge about unsteady vehicle aerodynamics can be acquired owing to the difficulty of capturing the unsteady flow parameters and aerodynamic forces due to restricted wind-tunnel size. As previously explained, CFD is an attractive approach for such problems – it can provide a large amount of transient data and detailed three-dimensional information about the flow field. In this numerical method, the continuity and Navier-Stokes (N-S) equations are believed to describe the behaviour of fluid motion in differential form, as long as the fluid can be regarded as a continuum. These equations describe the conservation of mass and momentum, respectively. For an incompressible unsteady turbulent flow (without the body forces), the one dimension, time-averaged continuity and N-S equations (for one direction) are respectively as follows [135]:

$$\frac{\partial u_i}{\partial x_i} = 0 \quad (4-1)$$

$$\frac{\partial u_i}{\partial t} + u_i \frac{\partial u_i}{\partial x_j} = -\frac{1}{\rho} \frac{\partial P}{\partial x_i} + \frac{\partial}{\partial x_j} \left( \nu \frac{\partial u_i}{\partial x_j} - \overline{u_i u_j} \right) \quad (4-2)$$

Where  $u$ ,  $P$ ,  $\rho$ ,  $\nu$ , respectively, are the velocity vector, pressure, density and kinematic viscosity of the fluids. These equations have no closed-form analytical solution for a generalized case, with only a select few highly simplified boundary conditions having direct analytical solutions. Therefore, numerical discretization is utilized to approximate the solution to equations (4-1) and (4-2). Furthermore, the term  $\overline{u_i u_j}$  in the equations is known as the Reynolds stress or simply turbulent stress. As discussed in the literature review, there are

different turbulence models available, each model depending on how the turbulent stress is modelled. The LES method is principally suitable for the simulation of vehicles subjected to crosswind [79]. Therefore, in this work, the LES technique was employed to solve Navier-Stokes equation.

## 4.2 LES governing equations

LES methods solve the spatially averaged Navier-Stokes equations. The flow variables are split into a term ( $\bar{u}$ ) (representing the part of the flow that can be discretised within the given computational mesh) and a term  $u'$  (representing the fluctuations that are not captured by the grid due to their small size). Furthermore, the governing LES equations are the incompressible N-S and the continuity equations filtered with the implicit spatial filter of characteristic width (the grid resolution). This means that all the turbulent scales which are larger than the filter width are resolved while those smaller are modelled. For an incompressible unsteady turbulent flow (without the body forces), the filtered continuity and N-S equations are as follows [79]:

$$\frac{\partial \bar{u}_i}{\partial x_i} = 0 \quad (4-3)$$

$$\frac{\partial \bar{u}_i}{\partial t} + \frac{\partial (\bar{u}_i \bar{u}_j)}{\partial x_j} = -\frac{1}{\rho} \frac{\partial \bar{P}}{\partial x_i} + 2 \frac{\partial \bar{u}_i}{\partial x_j} (\nu + \nu_{sgs}) \bar{S}_{ij} \quad (4-4)$$

Here,  $\bar{u}$  and  $\bar{P}$  are the resolved velocity and pressure, respectively, and the bar over the variable demonstrates the spatial filtering operation for LES. The filtered strain rate tensor  $\bar{S}_{ij}$  and  $\bar{P}$  in the equation 4-4 are expressed as:

$$\bar{S}_{ij} = \frac{1}{2} \left( \frac{\partial \bar{u}_j}{\partial x_i} + \frac{\partial \bar{u}_i}{\partial x_j} \right) \quad (4-5)$$

$$\bar{P} = \bar{p} / \rho + \frac{\bar{u}_i \bar{u}_j - \bar{u}_i \bar{u}_j}{3} \quad (4-6)$$

As mentioned, the non-resolved part of the flow is modelled through a so-called sub-grid scale model, which determines the so-called turbulent viscosity. In equation 4-4, the final term on the right represents the result of sub-grid scale (SGS) turbulence, and the eddy viscosity coefficient was modelled based on the traditional Smagorinsky model as [136]:

$$v_{sgs} = (C_s f_d \Delta)^2 \sqrt{2\bar{S}_{ij}\bar{S}_{ij}} \quad (4-7)$$

Here,  $C_s$  is Smagorinsky constant, which is dependent on the type of flow and has been determined to be  $C_s = 0.23$  for homogenous turbulence by Lilly [136]. The filter width  $\Delta$  is given as the cube root of each numerical mesh, and  $f_d$  represents the damping effect of SGS turbulence in the region of the solid wall; in this study, a van Driest type damping function is considered, which given as[79]:

$$f_d = 1 - \exp\left(-\frac{l^+}{25}\right) \quad (4-8)$$

where  $l^+$  is the gap from the solid wall in the wall coordinate normalised by the surface resistance and kinetic viscosity.

### 4.3 Fluent set up

Fluent® is a general-purpose commercial CFD package for modelling fluid flow over complex geometries. This software uses the finite volume technique to solve numerically the N-S equations. Fluent provides a simple use of their interface to do steady and transient flow analysis. The three basic simulation procedures adapted by Fluent and through which the fluid flow problem is analysed are:

1. Pre-processor
2. Solver
3. Post-processor

The schematic drawing of CFD modeling procedure for simulation of vehicle aerodynamics by using Ansys Fluent is shown in Figure4-1.

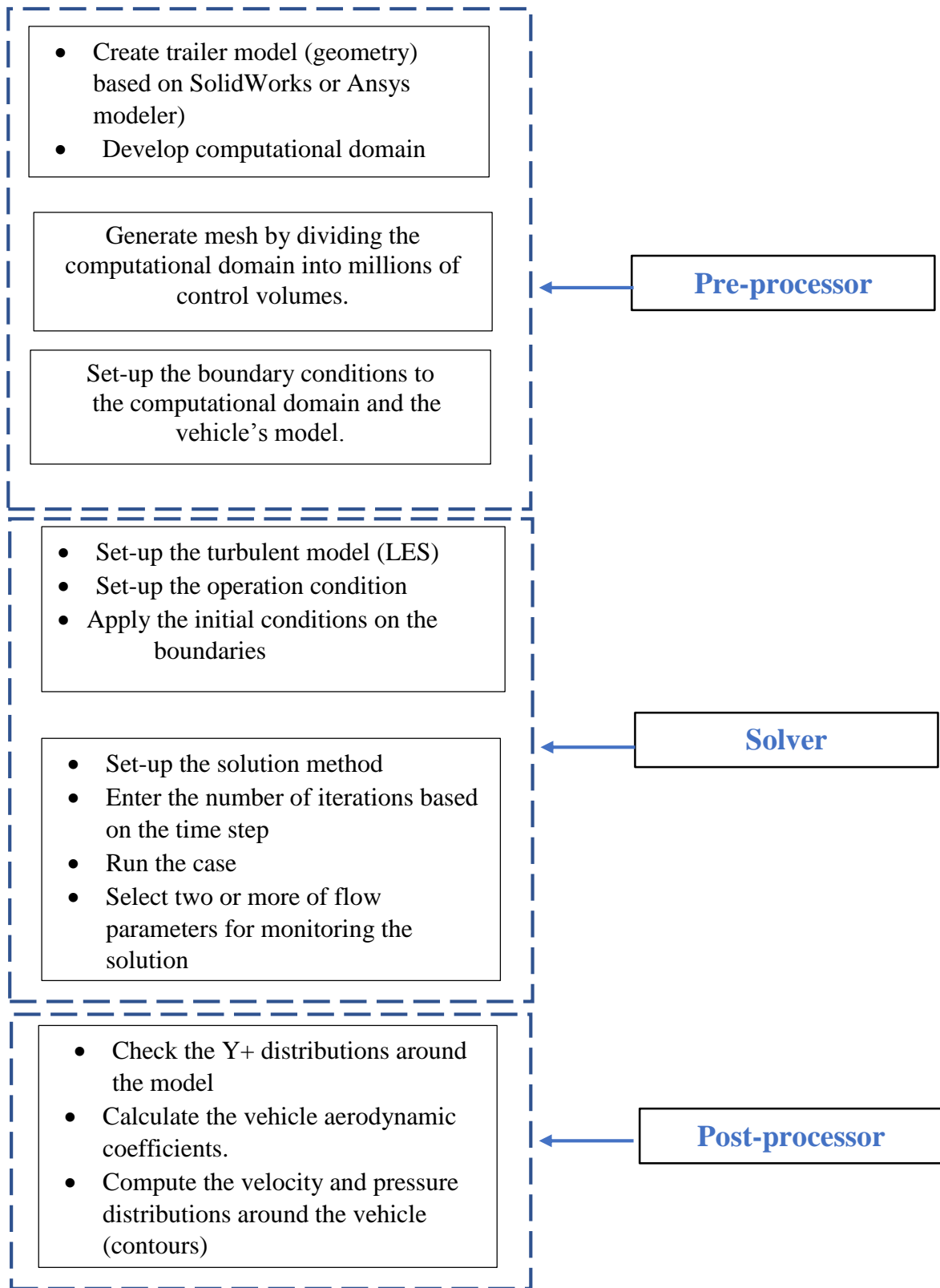


Figure 4-1 schematic drawing for the CFD analysis

As shown in the figure, in the pre-processing stage, a user can prepare the object for solution. This can be done by creating the geometry of the object's model and the fluid flow domain. Once the geometry is modelled, the next step is creating a mesh. This involves subdividing the flow domain into individual cells or control volumes so that the N-S equations can be integrated numerically on a cell-by-cell basis to generate discrete algebraic equations. All variables, including velocity components and pressure, are averages applied to a control volume. Fluent software supports different mesh types, including both 2D triangular and quadrilateral, along with 3D tetrahedral, hexahedral, pyramid, wedge and hybrid mesh. After successfully reading the meshed file within FLUENT solver, using the set boundary conditions, the flow field is initialised by the solver and the solution is calculated. Furthermore, based on a convergence criterion, the iterations are carried out until a solution is obtained. The post-processor then allows writing the case and data files along with displaying and printing the simulation results. The Fluent procedures are described in more details in the following sections.

### **4.3.1 Pre-Processing**

#### **4.3.1.1 Geometrical details**

To facilitate the validation of the experimental measurements, the same vehicle model used in the wind-tunnel tests was developed for numerical simulations. Figure 4-2 shows the 3D model of tractor semi-trailer vehicle; its length, width, and height are 400mm, 47.6mm, and 78.9mm, respectively. The CAD model was exported from SolidWorks in IGES format directly into ANSYS Workbench for further processing by the Fluent pre-processor tool.

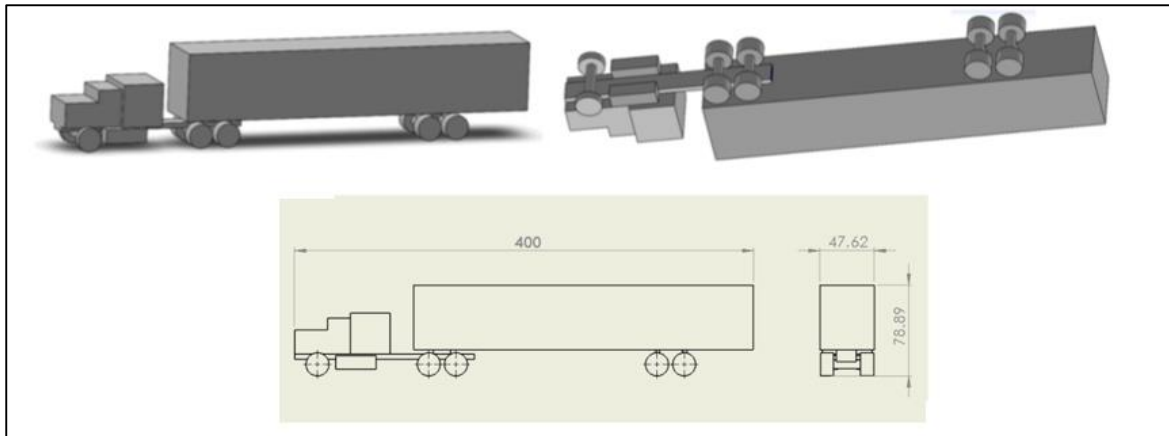


Figure 4-2: Tractor semitrailer 3D model

#### 4.3.1.2 Flow Domain and discretisation (meshing) setup

After the geometry of the tractor semi-trailer has been modelled, the next step is mesh generation for the flow domain. As shown in Figure 4-3, this domain is a rectangular duct similar to the analysis domain used in the wind-tunnel tests. Moreover, dimensions of the domain accurately match the wind-tunnel test section, with a height of 0.6 m, width of 0.6 m, and length of 1.5m. The vehicle model can be rotated about the z-axis by the required yaw angle for the simulations. The distance between the model and the inlet boundary is about 0.8m, which is large enough to ensure that the velocity and pressure fields are uniform at the inlet [137]. The model is also sufficiently far from the top and side walls to minimize near wall effects.

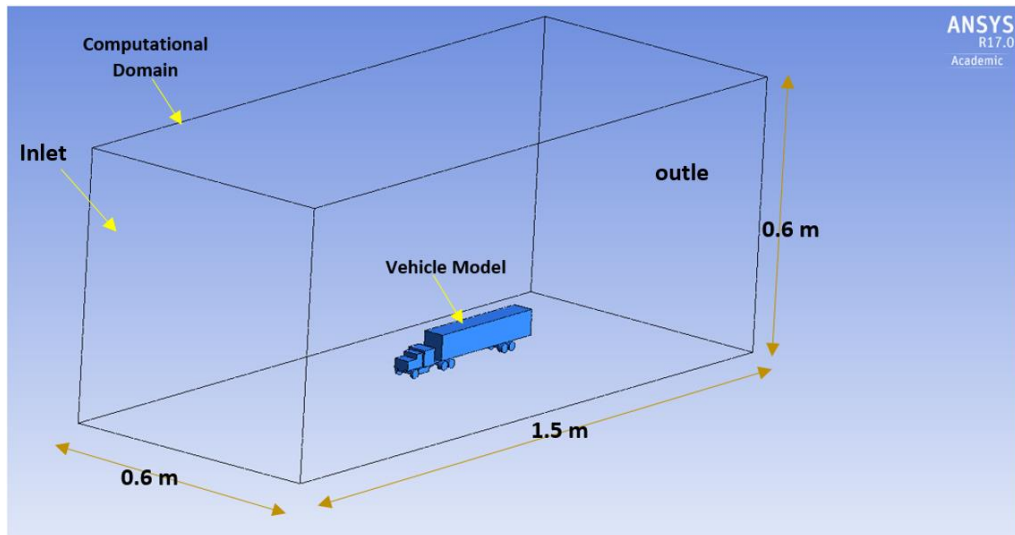


Figure 4-3: CFD computational domain (without gust generator)

The flow domain is meshed with the tetrahedral unstructured grid. This type of mesh has been used in the past for the LES (e.g., [94]) and the DES (e.g., [92]), with success. The complete meshed model comprised 26,5437 nodes and 3,400,344 elements. As will be discussed, the number of elements has been chosen after several meshes were tested to check the grid's independence. The topology of these control volumes is illustrated in Figure 4-4. From the figure, it can be seen that the mesh density is varied depending upon its location: the mesh near the vehicle model is reduced in size in comparison to the larger cells further from the model. The fine cells around the vehicle are created to capture the small flow structures around the vehicle. In the CFD process, the quality of meshing plays a vital role. A measure of the quality of the cells in the computational domain is determined by the cell skewness. The overall range of skewness is from zero to one, where the best is zero and worst is one [138] . The maximum skewness must be below 0.98 or the solution will easily become a divergence error and will not converge as desired [139]. For this simulation, the resultant mesh achieved a maximum skewness of 0.76 for over 95% of the elements and an aspect ratio between 1 and 2 for over 99% of the elements.

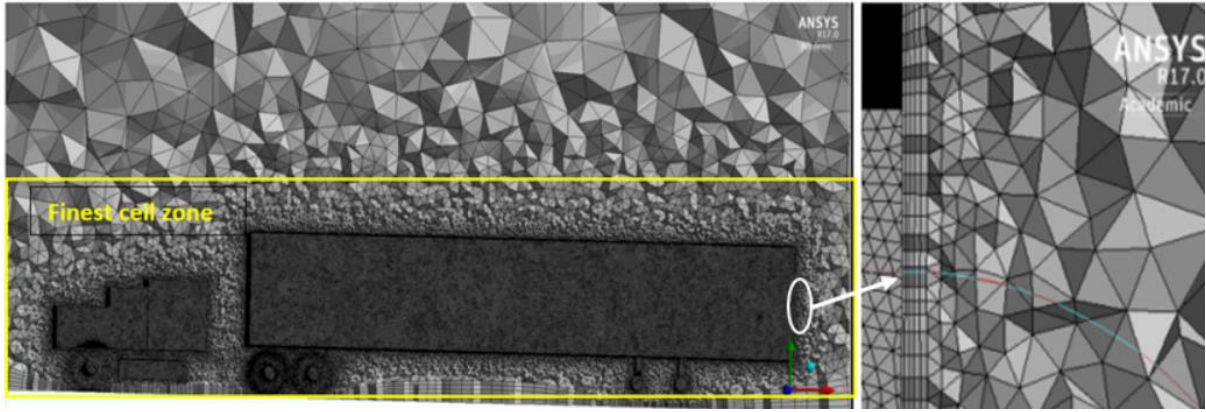


Figure 4-4: Mesh topology

Furthermore, in order to capture the fluid flow phenomena accurately in the boundary layer region, a non-dimensional wall unit,  $y^+$ , was considered. This describes the boundary layer for turbulent flows as [115]:

$$y^+ = \frac{u_\tau y}{\nu} \quad (4-9)$$

where  $y$  the normal distance to the surface and  $u_\tau$  is the friction velocity given by

$$u_\tau = \sqrt{\frac{\tau_w}{\rho}} \quad (4-10)$$

The wall shear stress ( $\tau_w$ ) is usually determined after the simulation has been completed and usually the engineers must assume a value and then check it with the simulation results. For standard or non-equilibrium wall functions, each wall-adjacent cell's centroid should be located within the log-law layer,  $30 < y^+ < 300$  [116]. In this study, five prismatic cell layers of constant thickness were added to the volume mesh on the solid walls. The layers have a starting cell height of 2mm and a growth of 20%, which with five layers of prisms generate a total height of around 12.5mm. This distance corresponds to a  $y^+$  of about 55, which meet the requirements of  $y^+$ . Figure 4-5 shows distribution of instantaneous  $y^+$  values for LES, at the windward side of the trailer, where  $y^+$  has its highest value of about 84. The vast majority of the values seem to satisfy  $y^+$  values between approximately 30 and 75.

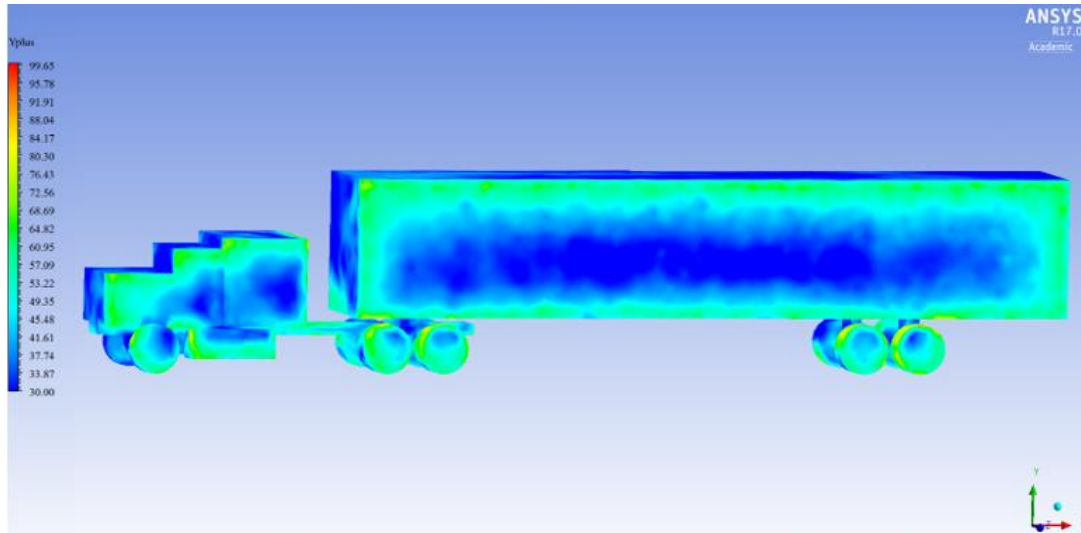


Figure 4-5: Y+ distribution over the CFD model

### 4.3.2 Fluent solver Execution

In this stage, the mesh generated in ANSYS 17.0 was imported into the Fluent solver. A double-precision solver was used with up to 12 parallel processors employed, depending on server CPU availability. The details of the solver settings used in the present study are presented in the following section.

#### 4.3.2.1 Selection of the physical models

The airflow around the tractor semi-trailer was assumed to be an incompressible flow [135], i.e., the air density is assumed to be constant. Therefore, a pressure-based solver has been nominated for the wind flow diagnostics. In this method, the primary fluid flow parameters that are being calculated iteratively are the pressure and velocity within the flow domain. Furthermore, as previously discussed in section 4.1, turbulence of wind flow in the simulations is modelled by the LES technique.

#### 4.3.2.2 Defining material Properties and Operating Conditions

The fluid medium within the computational domain has been defined as air with a density of  $1.225\text{kg/m}^3$  and dynamic viscosity of  $1.7894 \times 10^{-6}\text{ kg/m}\cdot\text{sec}$ . The vehicle model that has

been used in the current study is made of aluminium with a density of 2,719kg/ m<sup>3</sup>. Additionally, the operating conditions (reference conditions) being given to the solver are the operating pressure of 101,325Pa (i.e., atmospheric pressure).

### 4.3.3 Boundary condition

As with any partial differential equation, solution of the full 3D Navier-Stokes equations requires applying boundary conditions on the flow domain (or zones). Table 4-1 relates the type of boundary condition imposed to each of the zones present in the model.

Table 4-1: Boundary conditions

Boundary Name	Boundary Type
Inlet	Velocity Inlet (12 m/sec)
Outlet	Pressure outlet
Ground surface	Moving wall
Domain surfaces ( Sides and top)	Symmetry boundary conditions
Truck surfaces	No-slip wall
Wheels	No-slip wall

As can be seen from the table above, CFD analyses have been performed at the same wind speed conditions considered during the experimental work. Also, a low turbulence intensity ( $I_u=13\%$ ) is considered at the boundary inlet and outlet, reproducing the wind-tunnel test conditions. For simulating a static wind-tunnel test, No-slip boundary conditions were applied at the vehicle surfaces.

Moreover, symmetry boundary conditions were applied on the top and side walls. On the outlet, a homogeneous Neumann boundary condition is applied, meaning the pressure gradient is equal to zero. This will let the flow pass through the outlet without affecting the upstream flow, provided that the upstream distance to the aerodynamic body is large enough. The bottom face of the flow domain was defined as a moving wall, synchronized with the inlet

flow velocity at 12m/s in the stream -wise direction to avoid formation of its own boundary layer, which could otherwise modify the flow under the vehicle model.

#### **4.4 Solution methods and test accuracy**

Once boundary conditions were set, the solution methods can be specified. Fluent provides a list of solver formulations. From these methods, a pressure-velocity value is required to predict the pressure distribution in the flow domain with reasonable accuracy. In the present study, SIMPLE algorithm (Semi-Implicit Method for the Pressure-Linked Equation) was employed for pressure-velocity coupling. This algorithm has the ability to converge the solution faster and is often quite accurate for flows around bluff bodies such as tractor semi-trailer vehicles. Additionally, in SIMPLE algorithm, velocities are corrected and a new set of conservative fluxes is calculated [135].

Green-Gauss Node-based gradient evaluation has been selected for computing secondary diffusion terms and velocity derivatives at the cell faces. This scheme is more suitable than the cell-based gradient option for unstructured meshes [135], as it reconstructs exact values of a linear function at a node from surrounding cell-centred values on arbitrary unstructured meshes. Furthermore, the 2<sup>nd</sup> order implicit method was used for performing the time integration. This method was blended with a second-order upwind scheme for interpolating the variables on the surface of the control volumes. It should be noted here that use of the first-order upwind should be avoided, whenever possible, in LES due to the excessive amount of numerical dissipation introduced [79].

The Fluent solutions are provided in the ‘Results’ task page, where the user can set up and display the results of the CFD simulation. The graphical results that let the users visually inspect the results are also generated using Fluent. Those graphical results include contours, vectors, path lines, particle tracks, animations and plots. In addition, the user also has the

ability to get the numerical solutions for the drag, side and lift forces from the ‘Reports’ task page.

#### 4.4.1 Simulation time step and Convergence Criteria

The CFL number (Courant-Friedrichs-Lewy condition) is a mathematical convergence condition used when solving partial differential equations. In Fluent, the CFL number relates velocity with time and length of the computational cell size and is given as [140]:

$$\frac{v \Delta t}{\Delta x} \leq CFL \quad (4-11)$$

where  $\Delta x$  is minimum length side of the mesh in the domain and  $\Delta t$  is time step.

In order to acquire a correct and steady solution, the CFL number should be smaller than 1 [140]. To achieve this condition, side aerodynamic coefficient ( $C_s$ ) of the vehicle is obtained using three time steps based on different lengths of the computational cell, and constant CFL of 0.92 are compared in the Table 4-2. It is observed that there are almost no differences between the results from the first and second tests. Therefore, a constant time step of  $\Delta t = 14 \times 10^{-3}$  sec was used in the following numerical simulation. Also, 20 iterations were performed for each time step to have good convergence.

(Note: all calculations have been done for a flow angle of  $45^\circ$ )

Table 4-2: Time step calculation

CFL	At iteration number	Time step (sec)	Minimum $\Delta x$ (mm)	$C_s$ (-)
0.92	8000	$10 \times 10^{-3}$	130 mm	-1.08
	8000	$14 \times 10^{-3}$	182 mm	-1.1
	8000	$19 \times 10^{-3}$	250 mm	-0.67

In addition, in numerical CFD method, only a converged solution can be treated as the solution of the flow problem. The converged solution indicates that the solution has reached a stable state and the variations in the flow parameters and iterative process of the solver have died out. The default convergence criterion for the continuity, velocities in three dimensions and the turbulence parameters in ANSYS 17 is 0.001. This means that when the continuity changes, velocities and turbulence parameters drop down to the fourth place after the decimal, and then the solution is treated as a converged solution. However, in many practical applications, the default criterion does not necessarily indicate that the changes in the solution parameters have died out. Hence, it is often better to monitor the convergence rather than relying on the default convergence criteria [135].

In this simulation, static pressure on the leeward and windward surfaces of the trailer unit has been monitored throughout the iterative process. The solution has been considered converged once the static pressure at both these surfaces has become stable. Here a stable solution can be either one in which the pressure fluctuations have died out completely or have become cyclic, having the same amplitude in each cycle.

#### **4.4.2 Mesh independent study**

A grid sensitivity analysis for the model was performed to confirm the precision of the results, and to identify the most effective mesh sizing in order to achieve an appropriate mesh discretisation. This type of analysis must be performed to reduce the influence of the number of nodes on the computational results, since the solution must be independent of the mesh resolution in the computational domain. For this purpose, the numerical simulation is run using three different mesh sizes [141]. The first mesh comprises of 3,346,646 elements, the second mesh of 6,172,308 elements, and the third mesh of 7,709,906 elements. The mesh distributions over the trailer surfaces and the height of first layer grid over the walls were kept

constant. The computed average drag force from these three simulations is listed in Table 4-3. It has been observed that the time-average drag force is well predicted by both the second and the third mesh schemes, and the obtained results do not show significant changes. Therefore, this study employs the third mesh (comprising of 7,709,906 mesh elements) to investigate the aerodynamic forces acting on the tractor semi-trailer vehicle. Furthermore, the mesh independence test indicates that five layers of inflation are sufficient for this study.

(Note: all calculations have been carried out for a flow angle of 45°)

Table 4-3: Mesh dependency

Min size	Number of iterations	Elements	FD (N)	$\Delta$
70 mm	2500	3,346,646	3761	6.6%
100 mm	2500	6,172,308	3898	2.2%
182 mm	2500	7,709,906	3903	0.01%

#### 4.5 CFD Aerodynamic coefficients of tractor semi-trailer vehicle

It is essential to verify the numerical and experimental models of the system prior to the analysis of the data. The benchmark test is one of the approved methodologies for comparing the numerical results against experimental findings. Conducting this test also ensures the model's capability to capture the actual physical phenomenon for the full-scale model [149]. Thus, the computed aerodynamics coefficients of the trailer unit are plotted in Figure 4-5 and compared with wind-tunnel test results. It can be seen that, within the test range (i.e., yaw angle of 0°, 45° and 90°), the varying pattern in CFD drag and side coefficients are similar to those of the wind-tunnel.

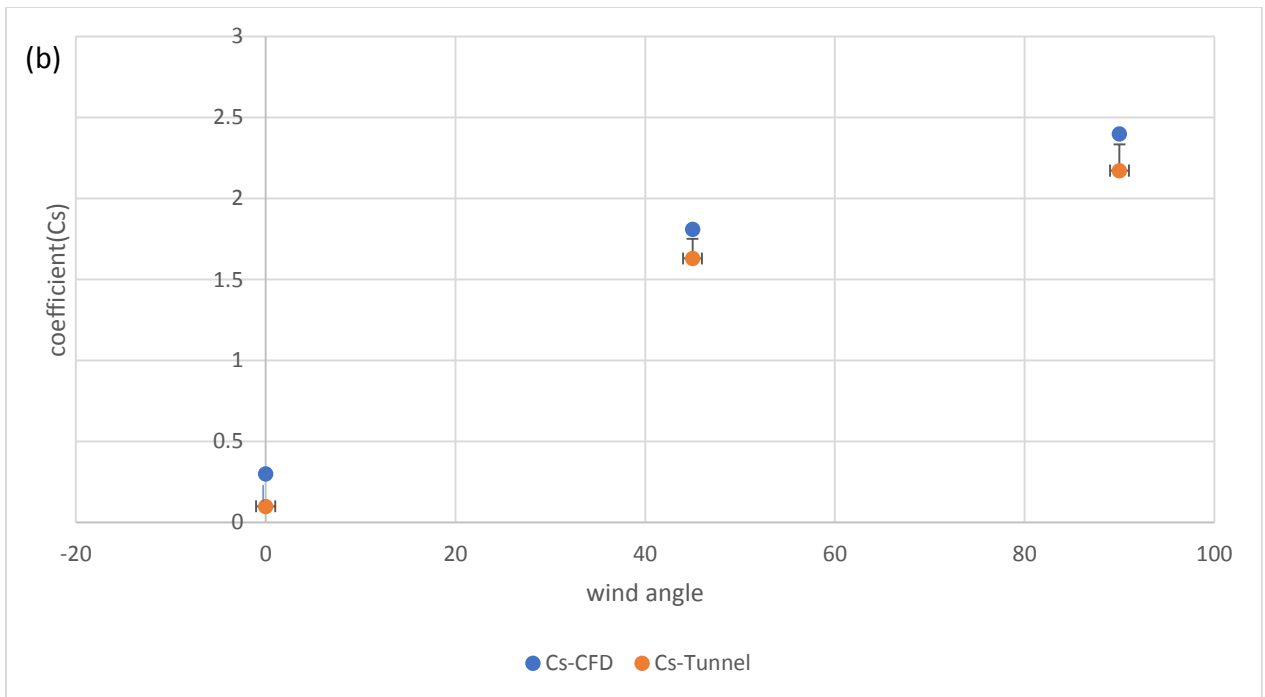
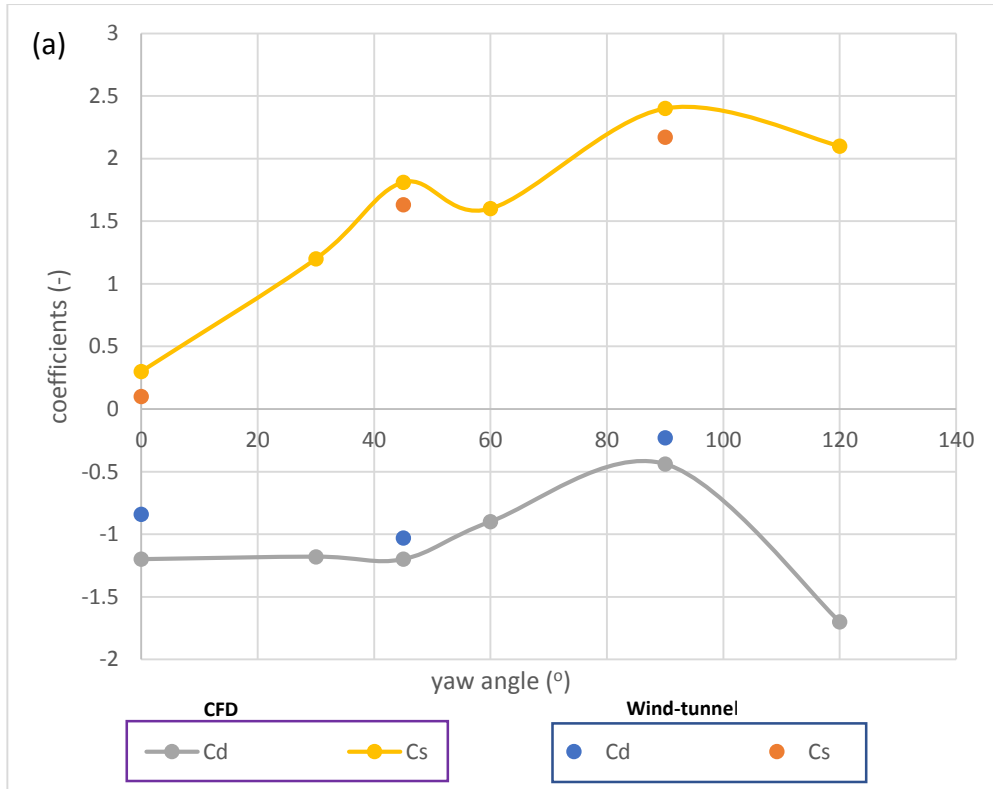


Figure 4-6: (a) CFD vs wind-tunnel side and drag aerodynamic coefficients; (b) data comparison

Moreover, as depicted in figures 4-6(b), data compression shows that the maximum difference of the aerodynamic force coefficients was found to be about 0.18 for the side coefficient at

the 90° yaw angle. Also, small standard deviations between measurement and simulation data were observed. In consideration of many uncertainties involved in both the CFD simulations and wind-tunnel experiments, the wind-tunnel results used in this study can be considered acceptable.

## **4.6 Multibody dynamics modelling of tractor-trailer combination**

As mentioned, the investigation of vehicle rollover based on real-world experiments can be very dangerous and expensive. As a result of this, multibody dynamic simulation (MBS) by using software is one of the methods that help to investigate vehicle rollover states, and constitute vehicle dynamic models close to a real system. The MBS software package ADAMS is well-known MBS used to analyse dynamic behaviour of complicated systems, as well as being widely used to validate simpler models developed for specific studies. Moreover, Adams gives the reliability of being accepted by industry and offers a 3D-based graphical interface supporting the user in pre- and post-processing of multibody models. The software interfaces to several other commercial programs. Based on this application, this section illustrates a brief introduction to the multibody modelling of tractor semi-trailer dynamic systems.

### **4.6.1 Theory of multibody dynamics**

ADAMS formulations for rigid body are based on those provided by Wielangta [143]. Assuming position of part  $n$  in a tractor-trailer model is specified by a position vector  $\{R_n\}$  from the Ground Reference Frame (GRF) and a frame that belongs to this part is  $O_1$ , as shown in Figure 4-7. The velocity expression for this  $n$ th part is given by [144]:

$$V_{n1} = \frac{d}{dt} R_n \quad (4-12)$$

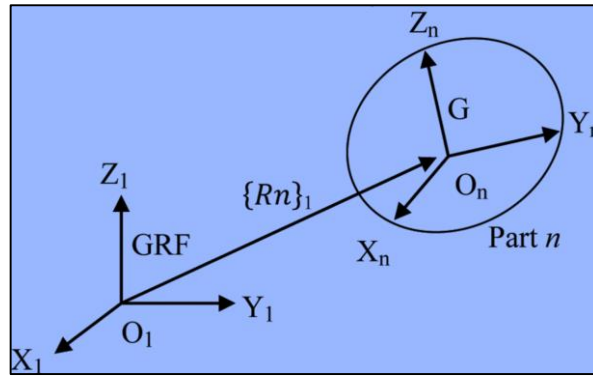


Figure 4-7: Ground Reference Frame (GRF) and a part frame[144].

A set of Euler angles ( $\Psi$ ,  $\Phi$ ,  $\theta$ ) is used to define the orientation of the part reference frame. There are three important frames of reference during transformation  $O1$ ,  $Oe$ ,  $On$ , where  $O1$  is the GRF ( $X Y Z$ ) reference frame,  $Oe$  is the Euler-axis frame ( $Z, X1, Z1$ ) and  $On$  is the resulting  $n$ th part frame. Assuming the Euler matrix for part  $n$  of the model given by matrix and by establishing the transformation from the part frame  $On$  to  $O1$ [144]:

$$[A_{1n}] = \begin{bmatrix} \cos\theta \cos\psi - \sin\psi \cos\theta \sin\theta & -\cos\psi \sin\theta - \sin\psi \cos\theta \cos\theta & \sin\psi \sin\theta \\ \sin\psi \cos\theta + \cos\psi \cos\theta \sin\theta & -\sin\psi \sin\theta + \cos\psi \cos\theta \cos\theta & -\cos\psi \sin\theta \\ \sin\theta \sin\theta & \sin\theta \sin\theta & \cos\theta \end{bmatrix} \quad (4-13)$$

Matrix  $[B]$  is the transformation from Euler-axis frame  $Oe$  to the part frame  $On$ .

$$[B] = \begin{bmatrix} \sin\theta \sin\theta & 0 & \cos\theta \\ \sin\theta \sin\theta & 0 & -\sin\theta \\ \cos\theta & 1 & 0 \end{bmatrix} \quad (4-14)$$

when  $Z$  and  $Z1$  are parallel and pointing in the same direction. The matrix  $[B]$  becomes singular. In this case, an internal adjustment is used to create a new part frame where the  $Z1$  axis is rotated through 90 degrees. Assume an infinitesimal change in orientation in the part frame of  $On$ . This change can be represented by a vector that will depend on  $\{\delta\gamma\}_n$ . Therefore, angular velocity of the part in the local part frame can be expressed as  $\{\omega\}_n$ . ADAMS requires the components of these vectors in the Euler-axis frame  $Oe$ . Thus, the angular velocity in the Euler-axis frame is actually the time derivative of the Euler angle [144]:

$$\{\omega_n\}_e = \frac{d}{dt} \{y_n\}_e \quad (4-15)$$

[B] matrix is used for transformation between the part frame and the Euler-axis frame. Now we have a set of kinematic position and velocity variables for the  $n$ th part with components measured in GRF. Also, we have a set of orientation and angular velocity variables measured about the Euler-axis frame [144]:

$$\begin{aligned} \{R_n\}_1 &= [R_{nx} \ R_{ny} \ R_{nz}]^T \\ \{V_n\}_1 &= [V_{nx} \ V_{ny} \ V_{nz}]^T \\ \{y_n\}_e &= [\psi_{nx} \ \phi_{ny} \ \theta_{nz}]^T \\ \{\omega_n\}_e &= [\omega_n\psi \ \omega_n\phi \ \omega_n\theta]^T \end{aligned} \quad (4-16)$$

By considering the equations of motions for a rigid body, the remaining part variables and equations can be obtained. Each part may be considered to have a set of six generalized coordinates given by [144]:

$$q_j = [R_{nx} \ R_{ny} \ R_{nz} \ \psi_n \ \theta_n \ \phi_n] \quad (4-17)$$

The translational coordinates are the translation of the centre of mass measured parallel to the axes of the GRF, while the rotational coordinates are provided by the Euler angles for that part. The translational forces for any parts are the summed in the X, Y and Z direction of the GRF. The moments summation takes place at the centre of mass and about each of the axes of the Euler-axis frame. This can be shown by Lagrange equations as:

$$\frac{d}{dt} \left( \frac{\partial T}{\partial \dot{q}_j} \right) - \frac{\partial T}{\partial q_j} - Q_j + \sum_{i=1}^n \frac{\partial \phi_i}{\partial q_j} \lambda_i = 0 \quad (4-18)$$

The kinetic energy  $T$  is written in terms of the generalized co-ordinates  $q_j$  and is given by

$$T = \frac{1}{2} \{V_n\}_1^T m \{V_n\}_1 + \frac{1}{2} \{\omega_n\}_e^T [B]^T [I_n] [B] \{\omega_n\}_e \quad (4-19)$$

Also,  $m$  is the mass of the part and  $[I_n]$  is the mass moment of inertia tensor for the part and provided by

$$[I_n] = \begin{bmatrix} I_{xx} & I_{xy} & I_{xz} \\ I_{yx} & I_{yy} & I_{yz} \\ I_{zx} & I_{zy} & I_{zz} \end{bmatrix} \quad (4-20)$$

The terms  $\Phi$  and  $\lambda$  represent the reaction force components acting in the direction of the generalised co-ordinate  $q_j$ . The term  $Q_j$  represents the sum of the applied force components acting on the part and in the direction of the generalised co-ordinate  $q_j$ . For simplicity a term for the momentum  $P_j$  associated with motion in the  $q_j$  direction and a term  $C_j$  to represent the constraints are given as:

$$P_j = \frac{\partial T}{\partial \dot{q}_j} \quad (4-21)$$

$$C_j = \sum_{i=1}^n \frac{\partial \phi_i}{\partial q_j} \lambda_i \quad (4-22)$$

This produced the below equation [144]:

$$\dot{P}_j = \frac{\partial T}{\partial q_j} - Q_j + C_j = 0 \quad (4-23)$$

The generalised translational momenta  $\{P_{nt}\}_1$  for the part can be obtained from [144]:

$$\{An\}_1 = \frac{d}{dt} \{Vn\}_1 \quad (4-24)$$

$$\{P_{nt}\}_1 = \frac{\partial T}{\partial \{Vn\}_1} = m \{Vn\}_1 \quad (4-25)$$

The equations indicate  $\{An\}_1$  is the acceleration of the centre of mass. Also one should note that the kinetic energy is dependent on the velocity but not the position of the centre

of mass  $\frac{\partial T}{\partial \{Rn\}_1}$  is equal to zero. Then the equation can be written in more familiar format [144]:

$$m \{An\}_1 = \sum \{Fn_A\}_1 + \sum \{Fn_C\}_1 = 0 \quad (4-26)$$

where  $\{Fn_A\}_1$  and  $\{Fnc\}_1$  are the individual applied constraint reaction forces acting on the body. The rotational momenta  $\{Pnr\}_e$  for the part can be obtained from [144]

$$\{Pnr\}_e = \frac{\partial T}{\partial \{\omega_n\}_e} = [B]^T [I_n] [B] \{\omega_n\}_e \quad (4-27)$$

Finally, we can write the equations associated with rotational motion in the form

$$\{Pnr\}_e - \frac{\partial T}{\partial \{\gamma_n\}_e} - \sum \{Mn_A\}_e + \sum \{Mn_C\}_e = 0 \quad (4-28)$$

## 4.7 Modelling of tractor semitrailer systems based on ADAMS/car application

### 4.7.1 Co-ordinate systems

Co-ordinate systems are used in the modelling of vehicle dynamics to calculate the vehicle's position, orientations, velocities, forces, and accelerations. There are two types of co-ordinate systems worthy to mention here, an inertial axis system (also known as global / earth-fixed coordinate system) and a vehicle axis system (also known as body-fixed coordinate system)[145]. The inertial axis system is fixed to the earth and is a non-moving system. It is primarily used to calculate the position of a vehicle. However, the vehicle axis system is assumed to be fixed to the centre of gravity of a vehicle and it is primarily used to calculate the velocities and accelerations of a vehicle. Initially these two systems are aligned with each other at the origin. As the vehicle moves the position and the orientation of the vehicle is calculated as a difference between these two systems.

ADAMS employs global coordinate formulation, that is, each part in the system is referenced to inertial reference frame for its generalised co-ordinates. This allows sparse matrix numerical techniques to be applied, along with a direct solution of differential-algebraic equations (DAE) rather than converting those to original differential equations (ODE) first,

[146]. The whole vehicle model is built in ISO coordinate system, and vehicle axis system is assumed to be fixed to the centre of gravity of each moving part of the vehicle [147].

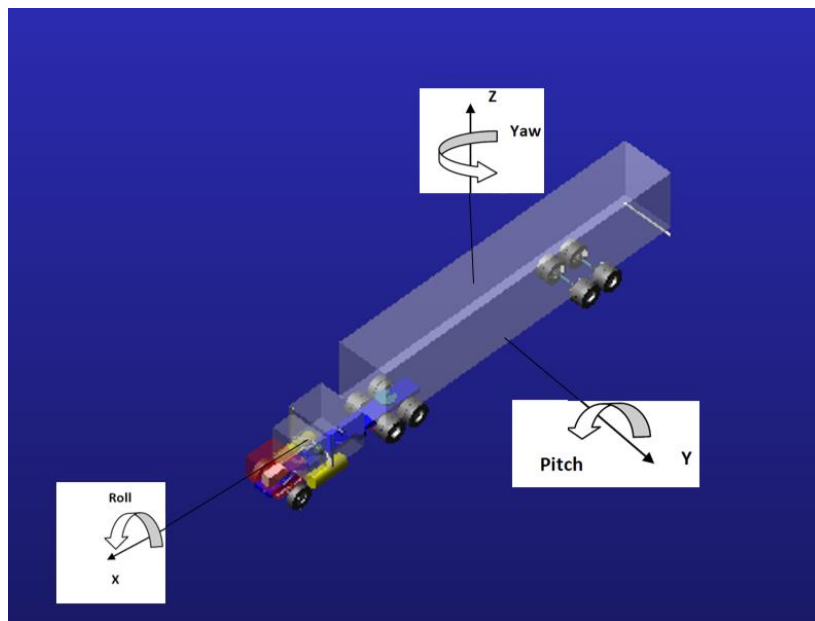


Figure 4-8 : ISO Vehicle Axis System





Figure 4-9 : ADAMS fixed coordinate system

As depicted in Figure 4-10, for vehicle modelling there are three system files in ADAMS [147]; Template file, Subsystem file and Assembly file. The user assembles each subsystem file to set up an assembly file under the standard interface. The assembly file of the vehicle includes a series of sub-files and a test-file, then the ADAMS Solver is used to simulate and analyse the assembly.

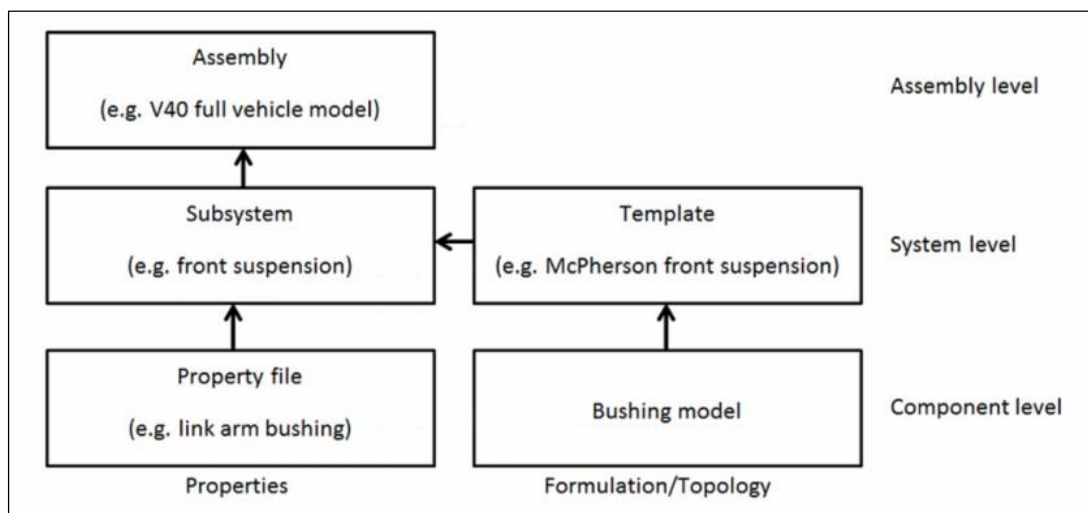


Figure 4-10 : Database structure for MSC ADAMS /car

Furthermore, templates include all necessary geometry, constraints, forces and measurements. All forces require two interacting parts, orientation reference and a property file. Subsystems are based on templates and allow the user to change the parametric data of the template. One or several subsystems can be grouped together to form assemblies. The final step in creating a template is creating and defining communicators. This is perhaps the least intuitive aspect

of ADAMS templates [147]. Communicators provide the mounting locations for subsystems upon assembling the full-vehicle model. They can also transmit forces from one subsystem to another. Input communicators in one subsystem must have corresponding output communicators in another. Some, such as mount communicators, are created automatically while most must be created separately.

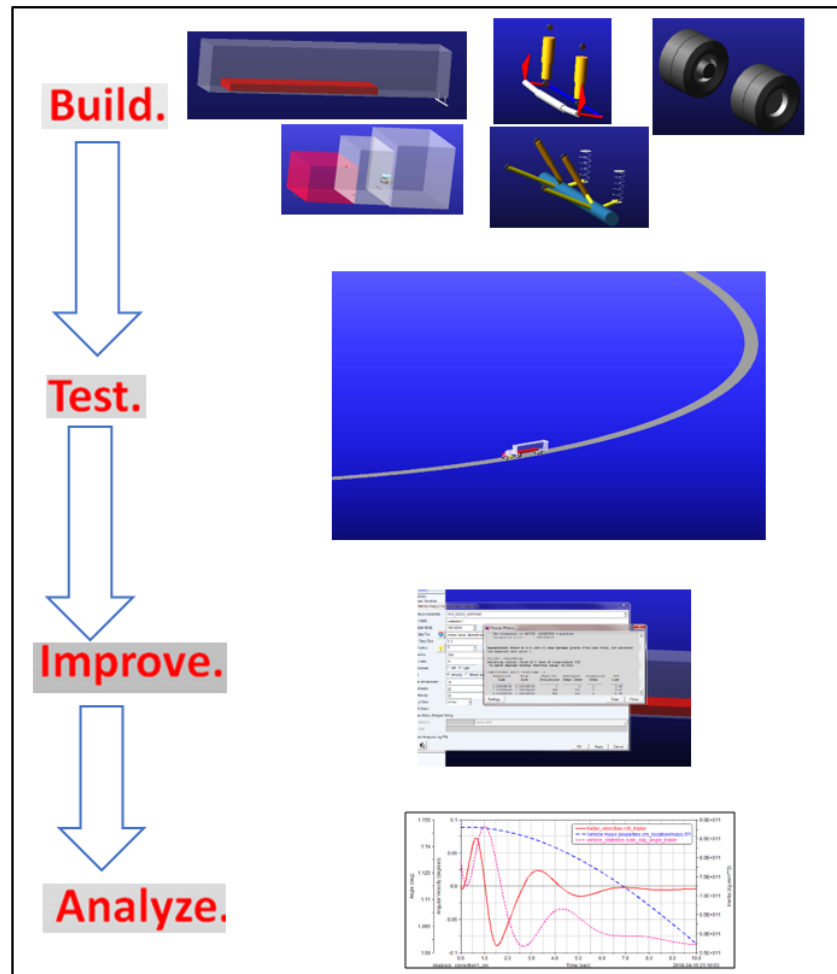


Figure 4-11: Schematic outline for ADAMS work

Moreover, for each rigid body in the system, it is necessary to include a part statement defining the mass, centre of mass location and mass moments of inertia. Each part will possess a set of markers which can be defined in global or local coordinate systems and are considered to move with the part during the simulation. Markers are used to define centre of mass locations, joint locations and orientations, force locations and directions. In every ADAMS model, it is

also necessary to include one non-moving part which is referred to as the ground part. Figure 4.11 shows the schematic outline of ADAMS/car procedure used to analysis vehicle dynamic in this work . These main steps are:

- Build or assemble the vehicle model by connect vehicle subsystems
- Test model performance
- Improve vehicle dynamics and maneouvers (e.g., import external aerodynamic forces)
- Analysis vehicle dynamics and maneouvers

#### **4.7.2 Virtual prototyping modelling**

For tractor semi-trailer analysis, the prototype of the vehicle consists of two main parts; the first part is the tractor and the second part is the trailer. The tractor model was divided into nine subsystems: steering system, brake system, front suspension, rear suspension, front wheel, front tire, powertrain, tractor body and the fifth wheel. The trailer model was divided into seven subsystems: trailer body, rear and front independent suspension of the trailer. Attached to the suspension subsystem is the subsystem representing the rear and front tires. The trailer was joined to the tractor using a revolute joint in vertical direction. The chassis of the tractor and the trailer were both rigid. To allow a relative angular roll motion between both parts of the vehicle, the revolute joint was modelled in the horizontal direction at the fifth wheel position and attached to a dummy part, with a torsional spring damper combination to simulate the torsional stiffness of the trailer chassis. The complete multibody dynamic model of the tractor semi-trailer vehicle consists of 189 moving parts and 627 degrees of freedom. The details of the vehicle parameters are presented in Appendix A.

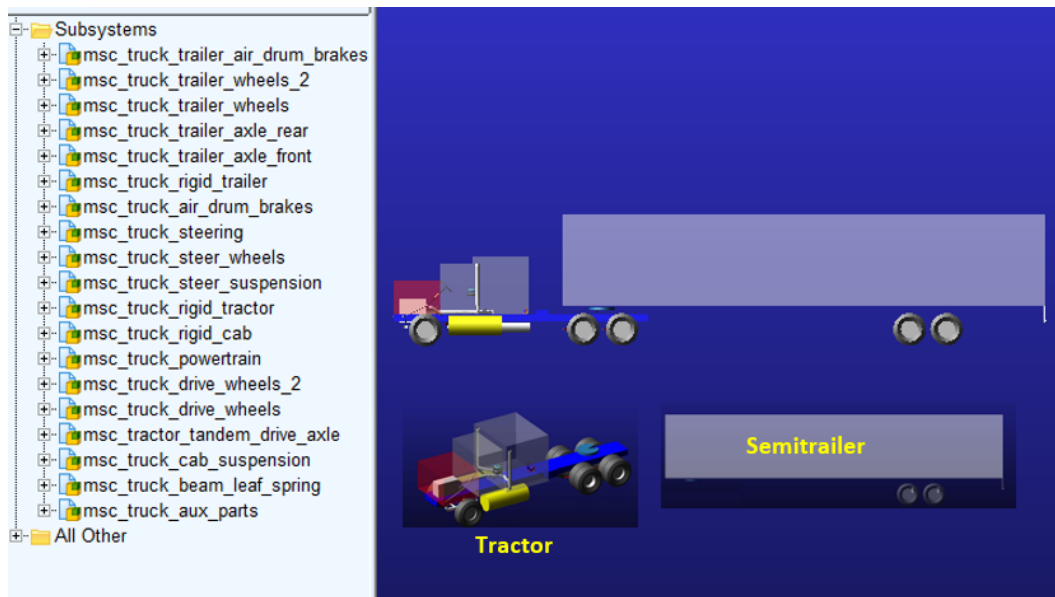


Figure 4-12 : Subsystems of the complete multibody dynamic model for the tractor semitrailer vehicle

#### 4.7.2.1 Tire Model

ADAMS car tire models were determined to be excessively complicated to justify an in-depth analysis. For example, a typical tire model available in the <acar\_shared> database contains over 100 different coefficients to define the geometry and dynamic behaviour of the tire [148]. The tire model used in this analysis was the standard tire module within the ADAMS shared library for a tire with dimension 315/12.0R22.5, which is similar to those fitted on tractor semi-trailer vehicles. It (wheel template) was selected based on Magic Formula [2], and the wheels were connected to the axle wheel carriers using revolute joints. The coefficients in the tire model are derived from measured data collected from a physical tire, which makes the model realistic.

#### 4.7.2.2 Suspension model

The vehicle suspensions were modelled in detail, including non-linear parts such as air springs and bump stops. The front suspension of the tractor unit and suspension system of trailer axle were constructed as shown in Figure 4-13 and Figure 4-14 respectively. The front suspension

is a rigid axle mounted on two leaf springs. The leaf spring model was built using nine discrete beam elements, from which the ADAMS software computes, using the geometry and the material characteristics, the deflection of the elements due to the vertical load. The height of the spring was calculated based on the simple beam theory. The front spring eye, at the front end of the leaf spring, was modelled as being attached to the chassis via a revolute joint lateral to the vehicle longitudinal axis. The front axle was connected to the leaf spring via a fixed joint at the mid-point of the leaf spring. The rear end of the leaf spring was fixed to the shackle also via a revolute joint, while the shackle was connected to the chassis in the same manner. Both joints were parallel to the front revolute joint, and the suspension oscillation motion is governed by the Lagrange equations of motion [101].

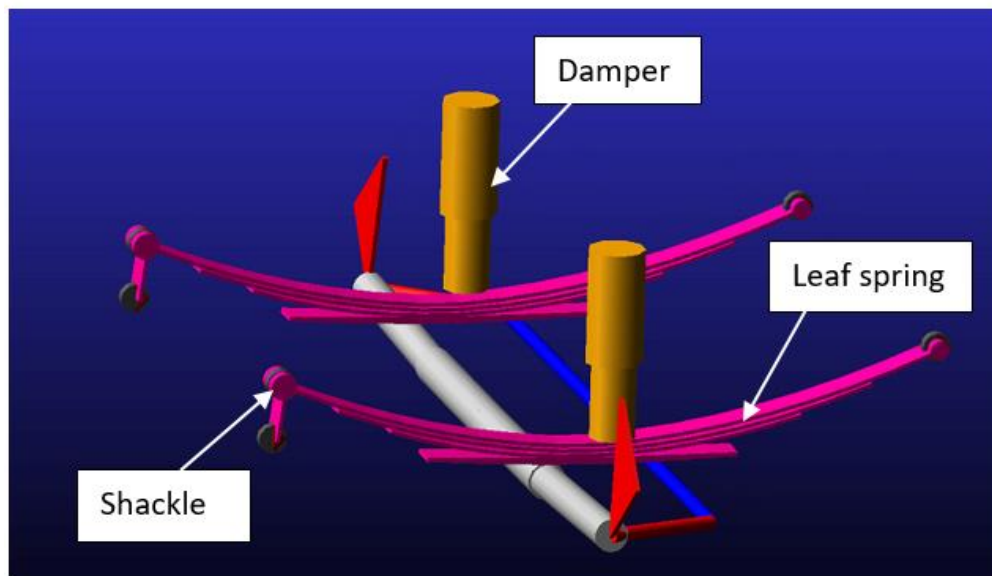


Figure 4-13: Front suspension for tractor unit

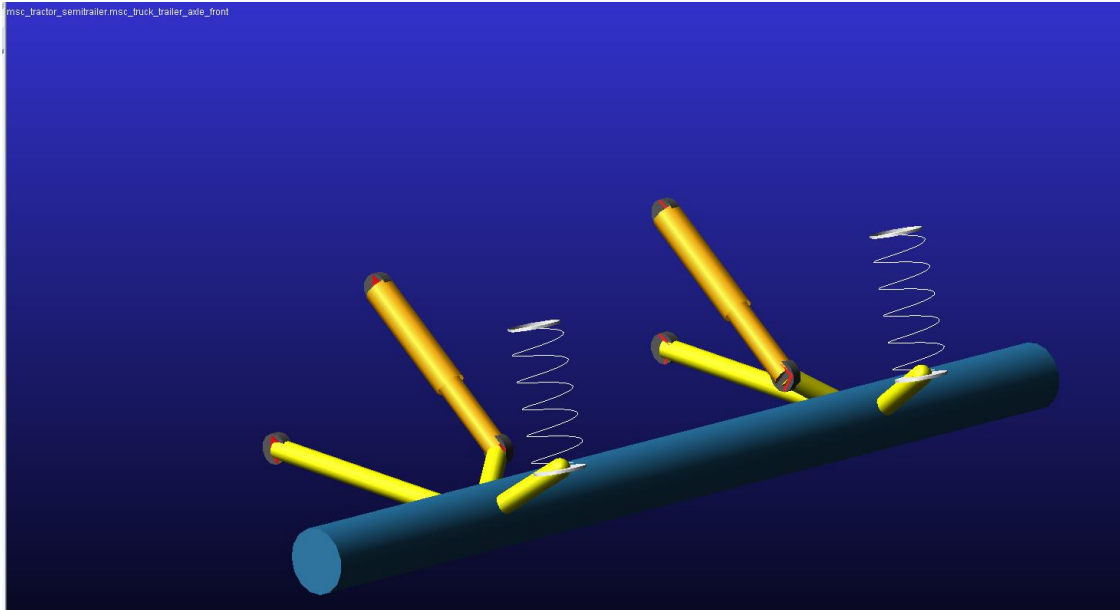


Figure 4-14: Suspension of trailer axle

#### 4.7.2.3 Road model

ADAMS/car application offers “Road Builder” function to develop different types of road models. This tool also allows the user to create multiple sections of a road with dissimilar geometry and properties. The road friction, road bank angle (the angle at which the road is elevated) and the road width can be varied along the length of the road. The Road Builder also contains a transition function that can automatically generate a length of road to join two dissimilar road geometries. This was particularly useful for the banked road model as, for example, it comprised a flat section at the start of the road and a banked section at the end. As shown in Figure 4-15, the Road Builder does not require the manual generation of road points, but rather allows the user to generate sections of the road by specifying its width, bank angle, and friction, etc.

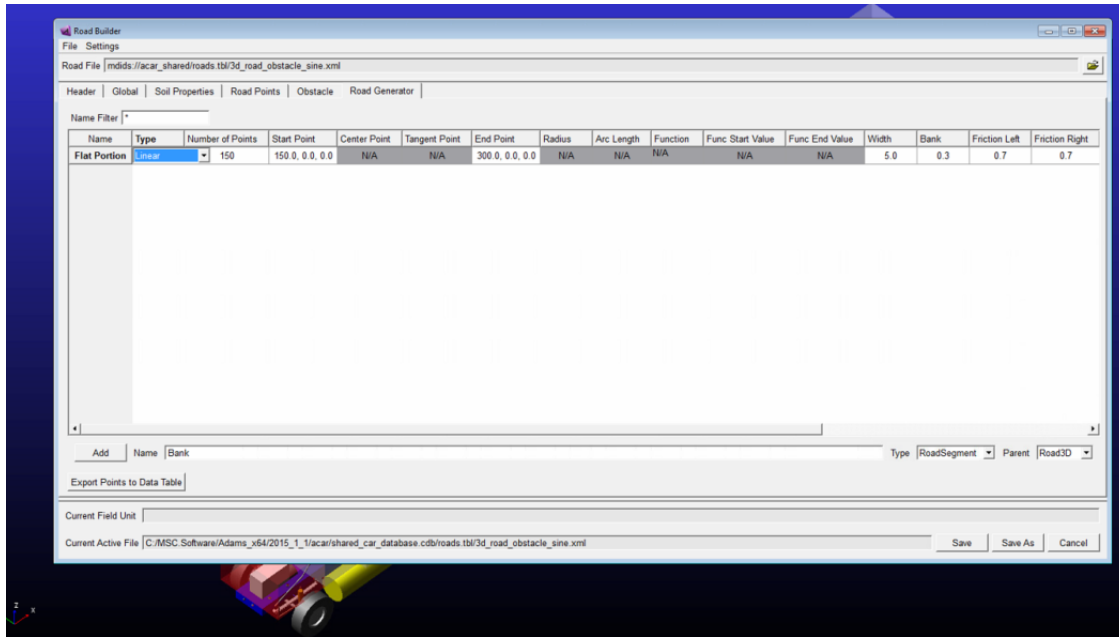


Figure 4-15: Road builder

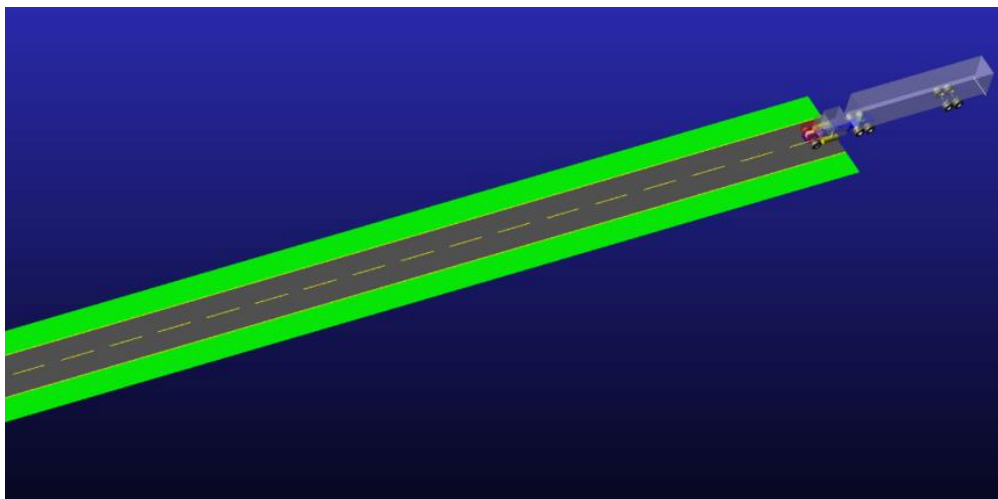


Figure 4-16: Road model

#### 4.7.2.4 Driver Controls Model

To emulate the test driver performing in ADAMS, driver controls model can be created within the Event Builder. The Event Builder combines all of the inputs into an efficient GUI (Graphical User Interface). Custom events can be built as a sequence of mini-manoevres; manoeuvres are defined by steering, throttle, brake, gear, and clutch input, (see Figure 4-17). When a set of end conditions is reached for a particular mini-manoevre, it triggers the start of the next mini-manoevre.

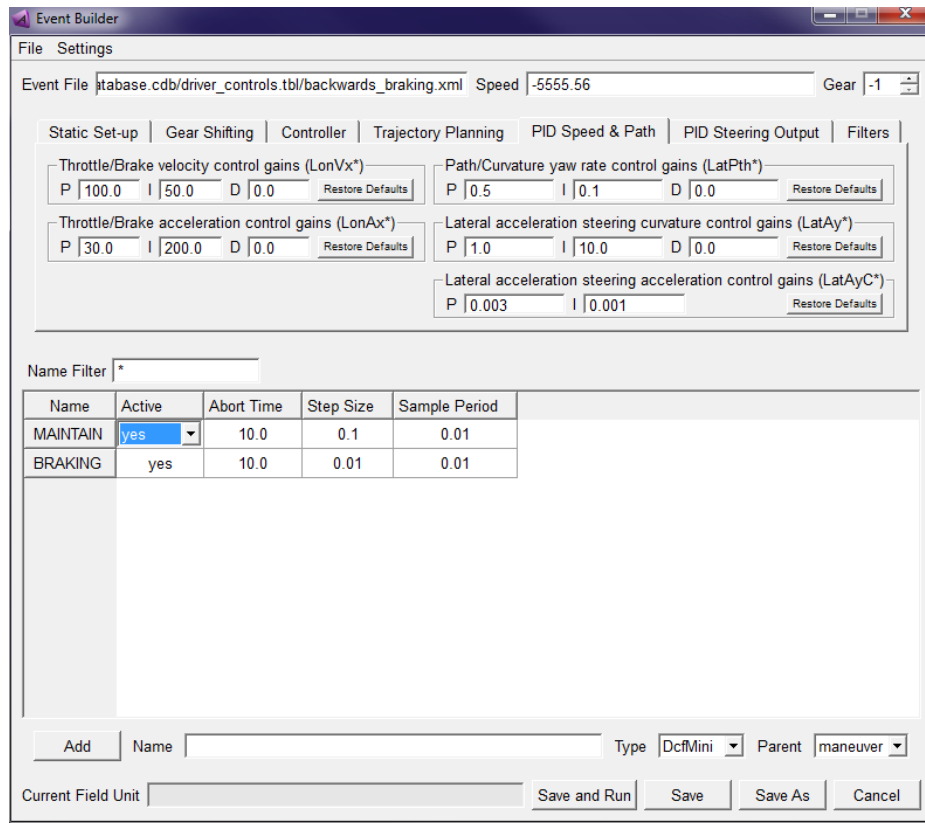


Figure 4-17 : Event builder

#### 4.8 Model analysis

Once the model has been assembled, the main ADAMS code may be used to carry out kinematic, static, quasi-static or dynamic analyses. For static analysis, ADAMS sets the velocities and accelerations to zero and the applied loads are balanced against the reaction forces until an equilibrium position is found. This may involve the system moving through large displacements between the initial definition and the equilibrium position. Therefore, ADAMS will perform a number of iterations until it converges on the solution closest to the initial configuration. Static analysis is often performed as a preliminary to a dynamic analysis [101].

Dynamic analysis is performed on systems with one or more degrees of freedom. The differential equations representing the system are automatically formulated and then numerically integrated to provide the position, velocities, accelerations and forces at

successively later times. Although the user will select output at various points in time, the program will often compute solutions at many intermediate points in time. The interval between each of these solution points is known as an integration time step. In ADAMS, the size of the integration time step is constantly adjusted using internal logic, although the user may override the system defaults if so desired [101]. Moreover, these results can be resolved globally or relative to any other part in the system. By using the ADAMS post-processor, users can also formulate their own customised output using any mathematical combination of the normal request output. The output can be presented as tabular data or as X-Y plots where results can be displayed in the time or frequency domain. It is also possible to visualise the results of a simulation either as still frames or continuous graphic animation.

#### **4.9 Validation of ADAMS Tractor Semitrailer Model**

In any computer model, the accuracy of the simulation relies on the accuracy of the model and the vehicle parameters used to build the model. Therefore, validation of the computer model (ADAMS model) is one of the most important aspects of simulations. The validation process ensures that the model's dynamic behaviour created follows closely the dynamic behaviour of the real tractor-trailer vehicle. It is important to note that the responses of the simple models considered in many previous works are not expected to be identical with the responses of a more sophisticated ADAMS -full-vehicle model, as the multibody model includes several additional details of vehicle properties. During this study, it is not possible to have experimental measurements for validating the ADAMS model. As a result, in this section the author has endeavoured to discuss two representative and valuable studies in the field.

The first study [144] directly compares the results of an ADAMS simulation with a real tractor-trailer test data, obtained by the use of an actual test track. The trailer was fitted with four displacement sensors, and the relative displacement between the trailer chassis and wheel

were recorded by the Data Acquisition Systems placed in the truck. The aim was to collect the vehicle dynamics data at the specified speed, which is 20km/h as the vehicle passed through the test track. The speed of 20km/h is chosen in order to minimise the inertia effect of the load that might contribute to the inaccuracy of the signal being recorded. Also, at this lower speed, the displacement sensors used in the test can operate effectively and give better results. In the experiment, the truck was driven forward and gradually increased its speed. Once the desired speed of 20km/h was reached and maintained, the vehicle was driven through the test track. During this manoeuvre, the vehicle's tires on its left side passed through the smooth road surface while all tires on its right passed through the sine road surface, as shown in Figure 4-18.



Figure 4-18: On road experimental facilities for testing of vehicle dynamics [144]

Plots in Figure 4-19 show the model simulation and test data of trailer roll angle, left rear suspension deformations, and velocity in vertical direction respectively. As shown in the figures, the experimental results are in close agreement with those predicted by the simulation analysis with slight variations. The variations arise mainly due to the real driver of the tractor having difficulty in maintaining the speed at 20km/h and a straight path during the experiment

on the test track. The study summarized that dynamics behaviour of the tractor-trailer vehicle can be investigated via various manoeuvres available or created in ADAMS.

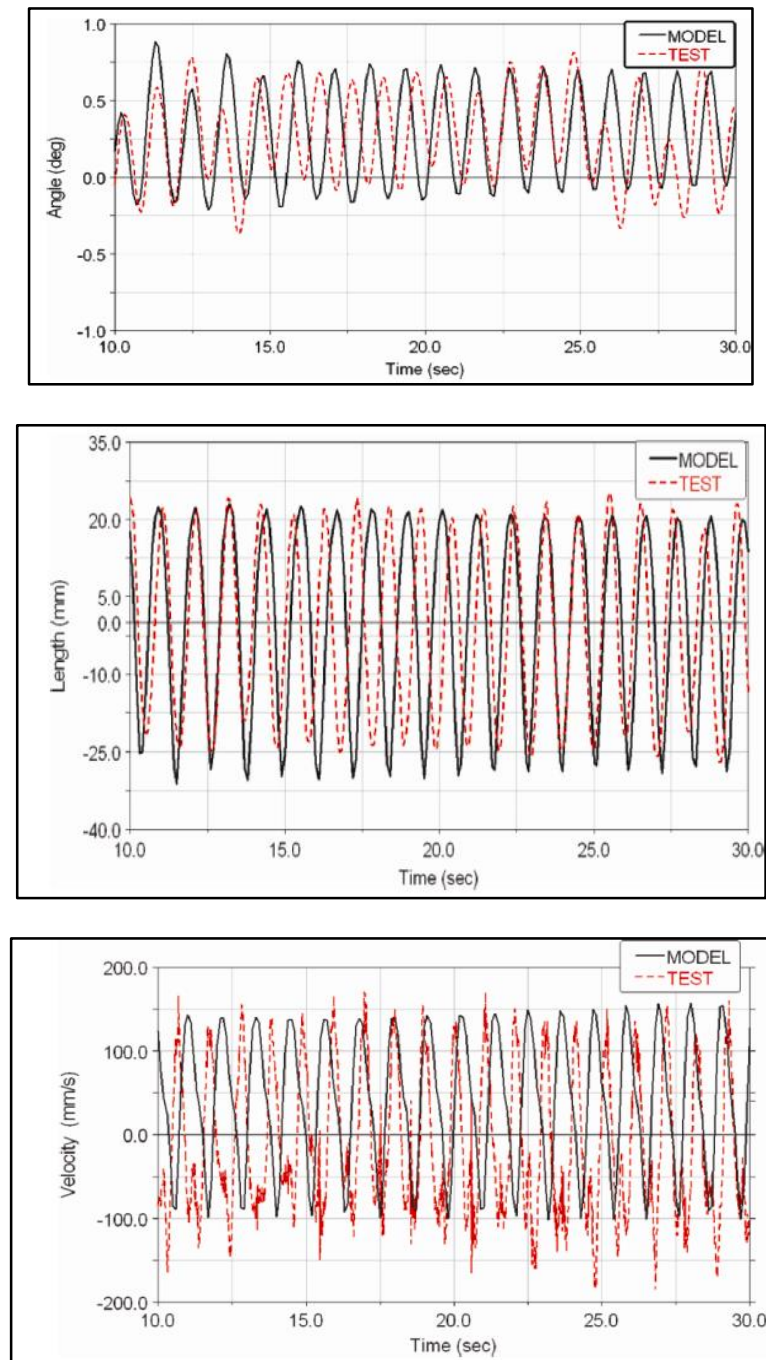


Figure 4-19: Validation of ADAMS dynamic simulation of tractor semitrailer vehicle [144]

In the second study [149], results from the simulations with the axle motions driven by test data were compared to measured accelerations collected on the test vehicle over various routes. The test vehicle had been instrumented with 70 accelerometers strategically distributed

over the tractor and trailer to capture the dynamics of the primary systems affecting ride quality.

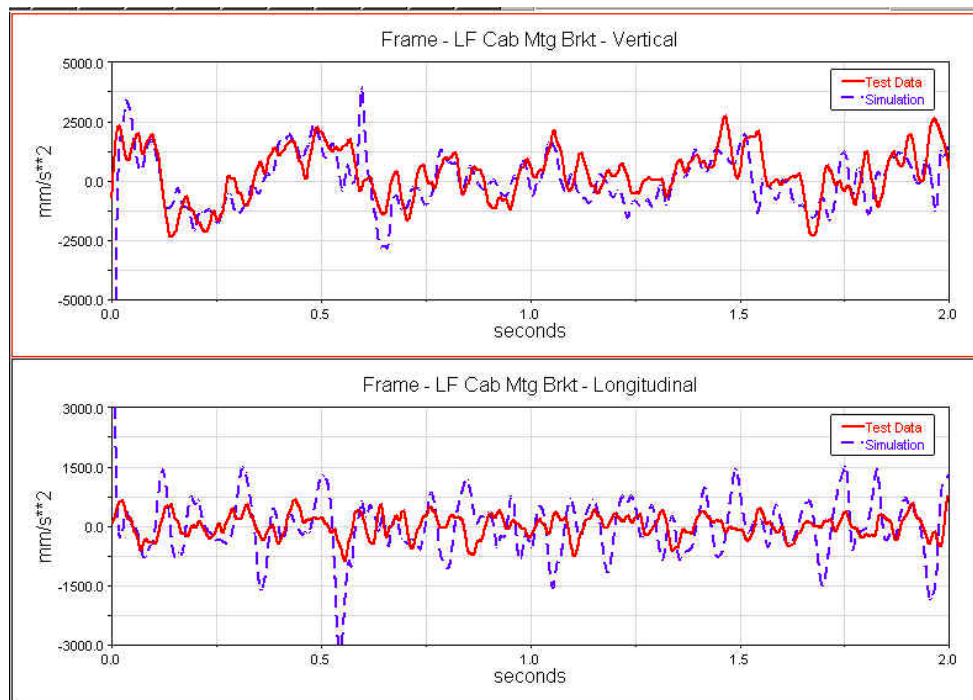


Figure 4-20 : Test and ADAMS simulation results for tractor semitrailer vehicle performance for validation purpose [149]

Figure 4-20 shows plot of selected measurement channels compared to corresponding simulation results for a small portion of one of the highway routes. The data has been low-pass filtered to remove high-frequency signal content coming from engine firing disturbances and measurement noise. In general, the plots show good correlation for vertical channels while in the longitudinal direction, correlation is moderate.

#### 4-10 Summary

This chapter provides a detailed explanation of CFD parameters used in this study for numerical simulation, such as vehicle geometry, mesh generation, LES technique and solver setup. The setup of CFD simulation based on Ansys Fluent application was built with the same geometrical features and boundary conditions used in the experimental models.

The CFD results show good agreements with experimental ones on both side and drag aerodynamic force coefficients. After numerically simulating the air flow of wind-tunnel, various results will be gathered from experimental and CFD techniques. Detailed discussions on these results will be presented in the proceeding chapters.

Furthermore, this chapter introduces a multibody method that was developed in ADAMS/Car software for modelling dynamic system behaviour of the tractor semitrailer vehicle. This technique will help to couple the complex vehicle dynamic with transient aerodynamic forces under various driving manoeuvres.

## **Chapter 5 : Unsteady aerodynamic forces of a tractor semitrailer vehicle moving in gusty crosswind conditions**

---

In order to improve the performance of rollover prevention devices (based on prediction of rollover indices) for a high-sided tractor semitrailer vehicle moving under high crosswind conditions, it is necessary to evaluate unsteady aerodynamic forces exerted on the vehicle. For this purpose, this chapter will present the results obtained after conducting wind-tunnel tests and CFD simulations for the tractor-semitrailer aerodynamics under gusty crosswind conditions. The study will cover development of two critical crosswind scenarios that involve a sudden change in wind speed (transient aerodynamic conditions). The first scenario represents a high-sided tractor semitrailer moving on a road in moderate wind and immediately being hit by wind gusts that originated due to topology of road surroundings. This scenario has been developed based on simulated transient-flow experienced by the vehicle model in the wind-tunnel. The second wind gust scenario describes a high-sided tractor semitrailer moving in wind condition at exposed locations such bridges or embankments. This scenario was represented by TSI gust, which was applied as time-dependent boundary condition to the lateral input of the CFD numerical domain. Furthermore, in this work, for both methods, only pure crosswind, i.e. wind perpendicular to the vehicle ( $\beta=90^\circ$ ), is considered; which the worst case of wind angle [43, 57].

### **5.1 Analysis of wind-tunnel gust flow**

As mentioned earlier, a ground vehicle can be affected by different turbulent wind conditions in real operating conditions and it also depends on the type of terrain where the road is located. When the crosswind turbulence is large, the fluctuations of the wind velocity cannot be neglected or reduced to indicators. Therefore, to evaluate vehicle aerodynamic behaviour at high transient wind speeds, two crosswind conditions were simulated in wind-tunnel, to represent naturally occurring windy conditions and extreme wind gusts.

In natural windy conditions, the aerodynamic model has been tested in low speed flow, which corresponds to the wind-tunnel test section neutrally without a gust generator. For extreme gust, high turbulent flow conditions ( $Re= 5.7 \times 10^5$  at  $U=18$  m/s) were generated by using passive techniques (oblique plate) of gust generation as explained in Chapter 3. In both conditions, the crosswind was modelled on wind hitting perpendicular to the trailer lateral side. Detailed analysis of the flow parameters in the wind-tunnel test section are provided in following subsections.

### 5.1.1. Vertical velocity Profile

Figures 5-1 and 5-2 compare low-speed wind-tunnel flow conditions against gusty wind flow. In these conditions, the wind flow is characterised by a normalised stream wise vertical velocity profile. It can be observed from Figure 5-1 that when the flow is at low speed, the boundary layer rises gradually a few centimetres above the bottom surface of the wind-tunnel (about 2 cm), and out of this region, the mean value of the wind velocity remains constant. However, under gust condition and as observed in Figure 5-2, the measured wind velocity contains high turbulences due to the wake of oblique plate and the profiles do not reach a constant speed value at the reference height ( $z=3.5$  cm).

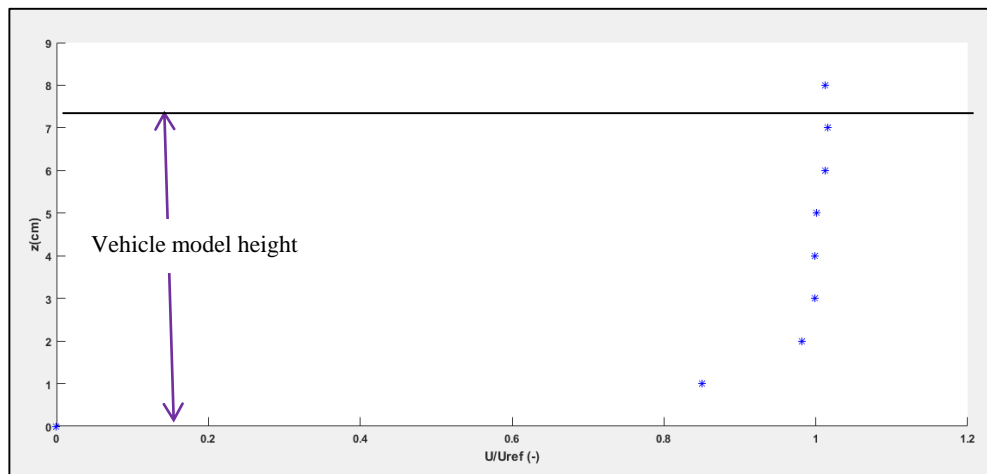


Figure 5-1: Time-average boundary layer velocity profile at sampling point in wind-tunnel without gusty flow (i.e. cobra probe velocity profile)

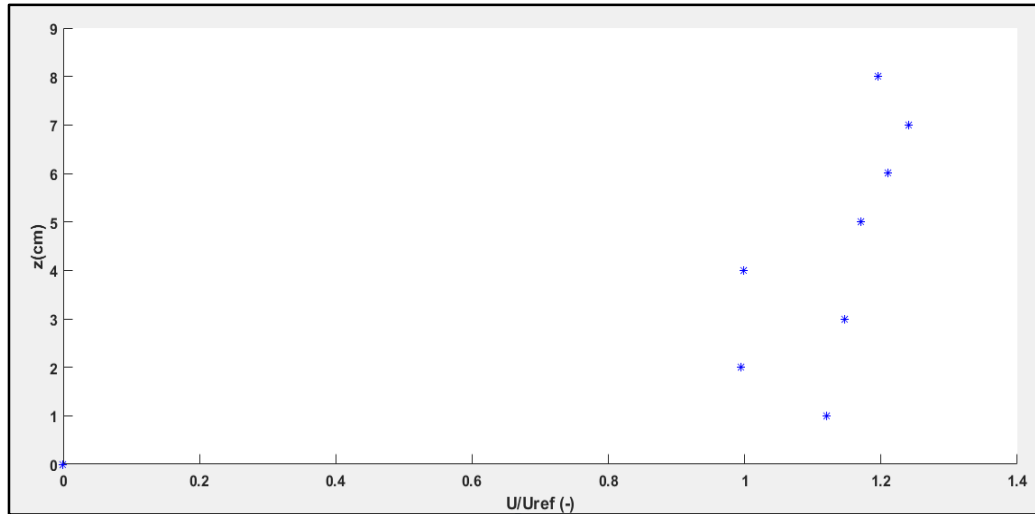


Figure 5-2: Boundary layer (transient) velocity profile at sampling point in wind-tunnel under gusty flow conditions

### 5.1.2 Wind-tunnel flow field

Flow visualization is an effective means to understand the concept of flow physics. Figure 5-3 depicts time-varying CFD flow field in terms of velocity contours, which are presented in the test section of the wind-tunnel with gust generator based on the LES turbulent model. The velocity contour is illustrated in a vertical plane, which was created at the mid-width of the flow domain. The contours show that flow field of the wind-tunnel is multi-dimensional and complex thus making its measurement difficult. It also separates the wind flow at both the lower and the upper leading edges of the plate. The effect of subsequent changes induced by the gust generator leads to the flow being forced to quickly accelerate in the regions above and below the plate which recreates a gust flow condition in those regions. The vehicle model is placed into the accelerated flow region, this is increase the turbulence of the flow incurred by the interaction between the flow and the vehicle. Moreover, the velocity contour illustrates that the upstream flow velocity of the plate and particularly at the domain inlet is uniform and steady but in the wake plate region, a high circulation was observed.

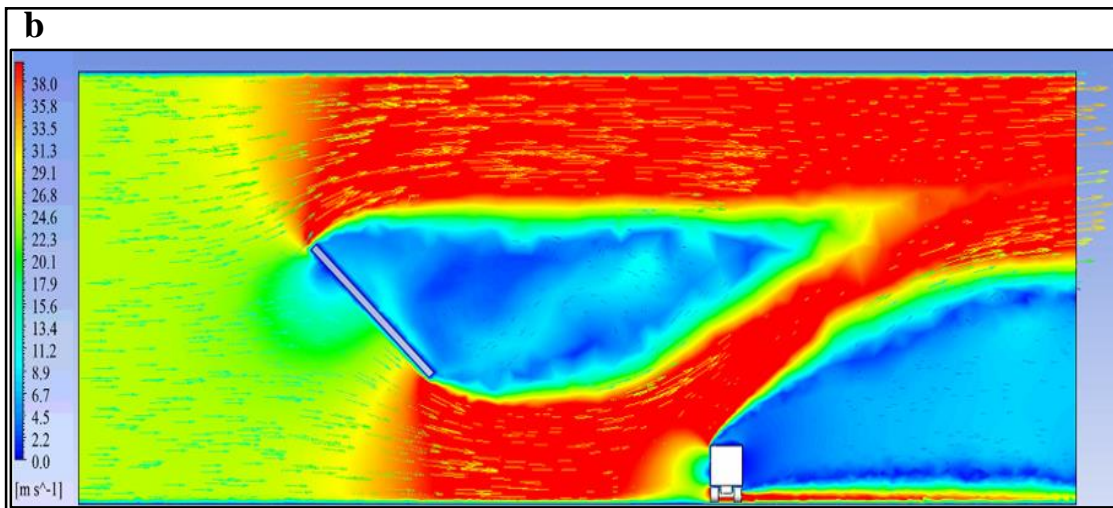
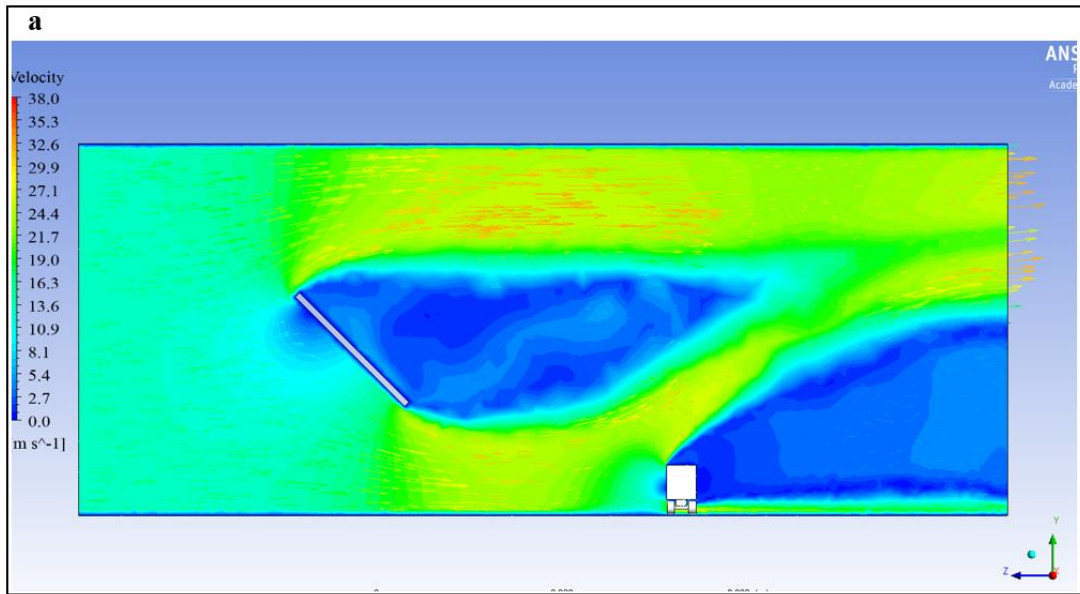


Figure 5-3: Velocity contour of wind-tunnel gust flow: a) extracted at  $t=1\text{sec}$ ; b) at  $t=10\text{ sec}$

For low-speed wind-tunnel flow, Figure 5-4 depicts experimental results of the wind velocity distribution within the test section, without the gust generator. It can be seen that the upstream flow velocity of the vehicle model is uniform in the majority of the flow domain (i.e. the same velocity direction at every point in the flow) with an average magnitude of about 16 m/sec. Under this steady flow conditions, tractor semi-trailer aerodynamic coefficients have been measured in the wind-tunnel test section, as has been discussed in Chapter 3.

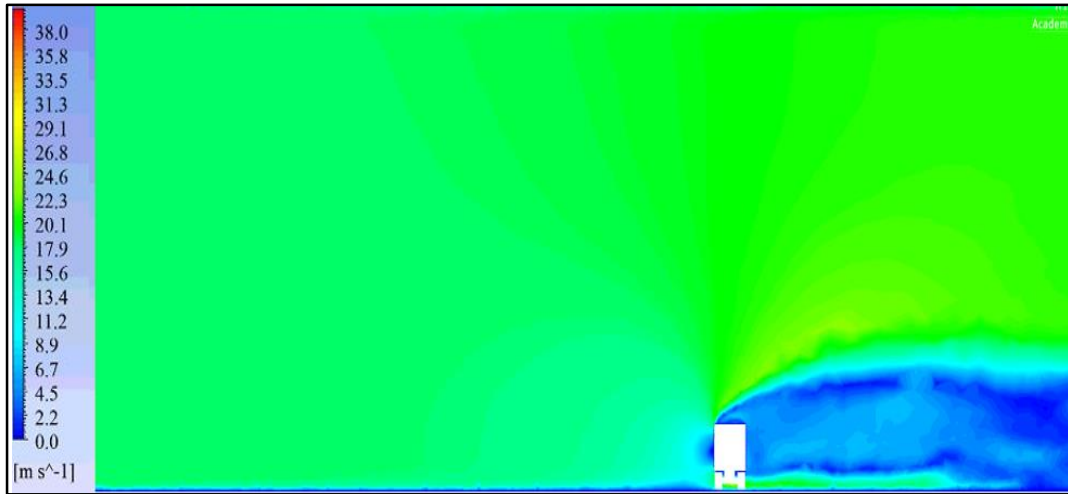


Figure 5-4: Velocity contour of wind-tunnel flow (without gust generator)

## 5.2 Wind speed time series

For a certain point at height ‘z’ in space, the wind speed  $U(z, t)$  is usually considered to comprise of 3 components and can be described as follows [74]:

$$U(z, t) = \begin{pmatrix} u_u(z, t) \\ u_v(z, t) \\ u_w(z, t) \end{pmatrix} = \begin{pmatrix} \bar{U}(z) + u'_u(z, t) \\ \bar{U}(z) + u'_v(z, t) \\ \bar{U}(z) + u'_w(z, t) \end{pmatrix} \quad (5-1)$$

Where  $u_u(z, t)$ ,  $u_v(z, t)$  and  $u_w(z, t)$  refer to the 3 components of wind speed in longitudinal, lateral and vertical directions respectively.  $\bar{U}(z)$  refers to the mean wind speed and  $u'_u(z, t)$ ,  $u'_v(z, t)$  and  $u'_w(z, t)$  denote the corresponding wind turbulences in each direction.

Figures 5-5, 5-6 and 5-7 show the time history of wind velocity components. They were measured by cobra probe in the wind-tunnel under a low-speed condition at the sampling point. The sampling frequency was 1250 Hz and the number of the sampled data was 12500, and the total time (T) is 10s. The recorded values of the flow velocity revealed that the longitudinal fluctuations i.e. the wind component in the mean wind flow direction is the most significant component when compared with vertical and lateral components.

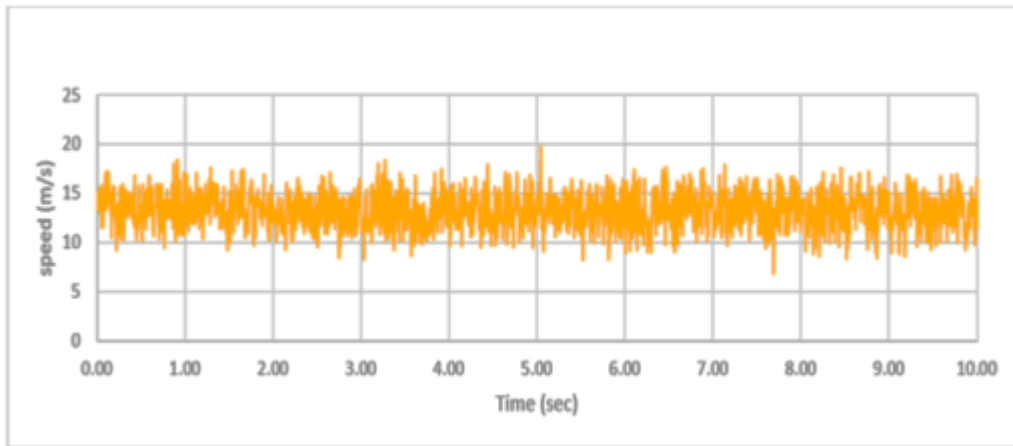


Figure 5-5 : Longitudinal wind velocity component recorded in wind-tunnel

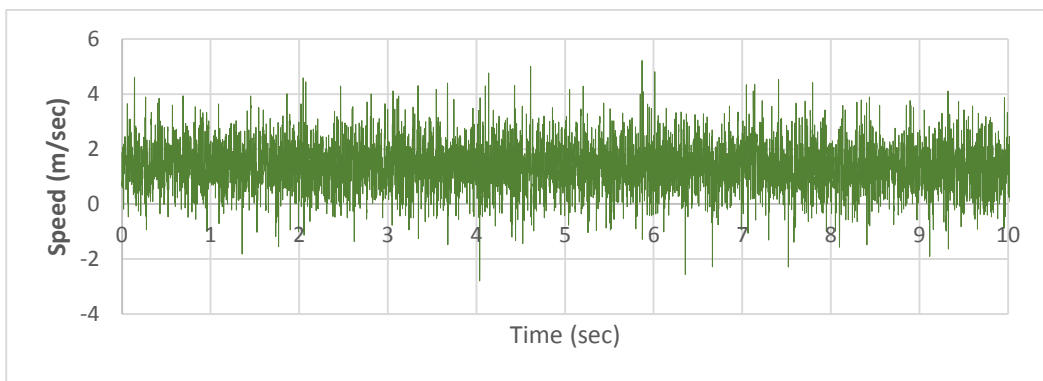


Figure 5-6: Lateral wind velocity component recorded in wind-tunnel

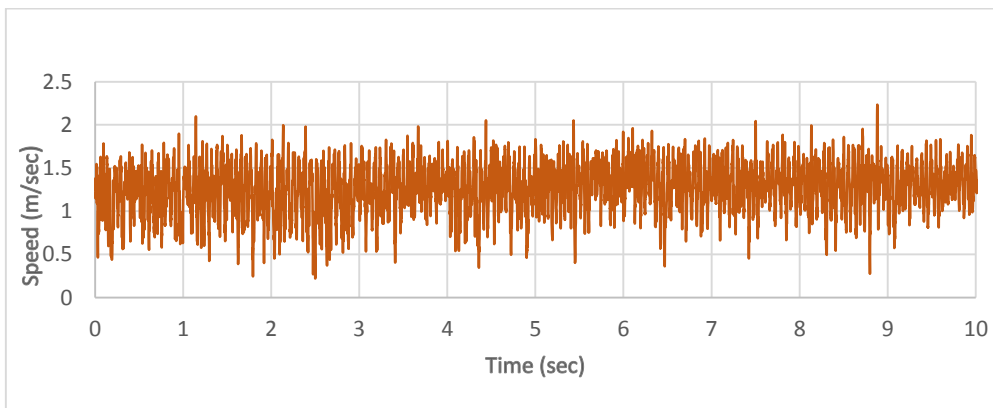


Figure 5-7: Vertical wind velocity component recorded in wind-tunnel

In this study under gusty wind conditions, two general assumptions about the wind direction have been considered:

- The direction of longitudinal wind component is always perpendicular to the vehicle model. This means that when the vehicle is driven on a curve (will be discussed further

in the next Chapter); the direction of the wind changes with respect to the inertial reference system.

- The wind direction is always parallel to the road plane.

### 5.2.1 Parameters of wind-tunnel turbulent flow

In this sub-section, parameters of gusty air flow generated in wind-tunnel are represented. In the traditional approach for predicting the wind-induced response of ground vehicles, the stationary wind speed of atmospheric boundary layer is just an assumption. In this approach, the wind speed at a given height is described as the sum of the mean speed  $\bar{U}$ , which is a function of height ( $z$ ) above the ground and a fluctuating component,  $u'$  ( $z, t$ ), which is a function of both height and time ( $t$ ).

$$u(z, t) = \bar{U}(z) + u'(z, t) \quad (5-2)$$

The mean wind speed (Time-average wind speed) can be approximated as [21]:

$$\bar{U}(z) = \frac{u_*}{\kappa} \ln\left(\frac{z}{z_o}\right) \quad (5-3)$$

where  $u_*$  is the surface friction velocity,  $\kappa$  is the Von Karman constant ( $\sim 0.41$ ) and  $Z_o$  is the surface roughness length which is dependent on topography [150]. However, due to the existence of high turbulences, wind speed can be modelled as a stochastic process. Therefore, realistic assumptions on the nature of crosswinds are required to take its non-stationary characteristics into account.

Shown in Figure 5-8, is the measured longitudinal wind speed time-histories of the high turbulent flow conditions recorded under wind gust generator at the reference point (i.e., sampling point see Figure 3-10) in the wind-tunnel. Instead of constant mean wind speed, the figure shows time-varying mean wind speed  $U(t, z)$  and fluctuation components.

$$u(z, t) = \bar{U}(t, z) + u'(z, t) \quad (5-4)$$

In previous investigations on wind speed measurements, different methods were used to define the time-varying mean wind speed characteristics (e.g. [151],[152]). In this analysis, a method described by Bottasso et al. [153] has been employed to extract the longitudinal time-varying mean wind speed from the recorded wind data. This has been done by filtering the wind speed time history with a moving average filter on a window of 10 seconds [152]. Also, the filtered wind speed (red line curve in Figure 5-8) illustrates that a moving average is capable of eliminating the faster (high frequency) fluctuations, and revealing the presence of high change in values of wind speed.

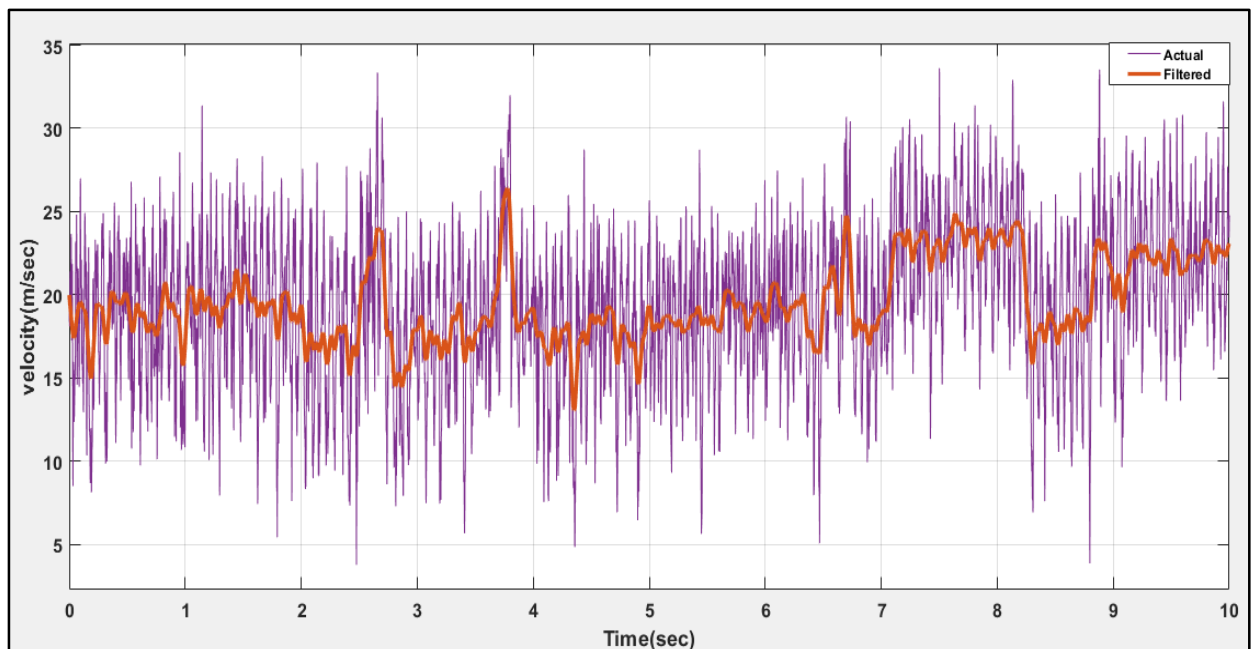


Figure 5-8: Longitudinal wind velocity component recorded in wind-tunnel under gust conditions

As shown in the Figure 5-9, the constant mean wind speed,  $\bar{U}(z)$ , described by Equation 5-3, is about 18.79m/s for the high wind flow, whereas the maximum and minimum values of the time-varying mean wind speed ( $\bar{U}(t, z)$ ) are 26.5 m/s and 13.21m/s respectively. Therefore, it is observed that the time-varying mean wind speed is more suitable for representing the basic trend of wind gust speed than the constant mean wind speed.

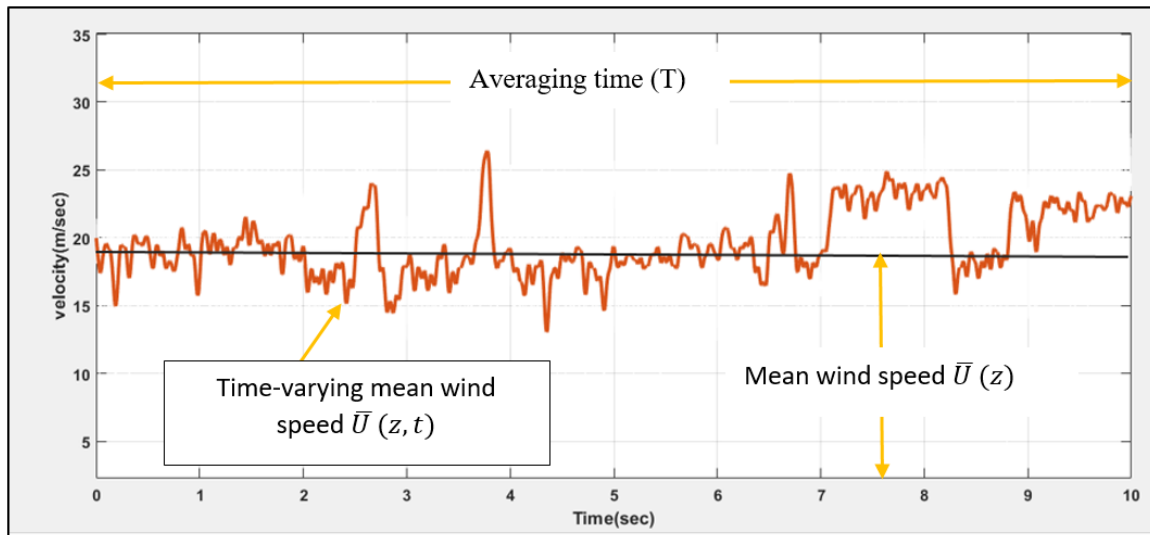


Figure 5-9: Time-average and time-varying mean wind speed recorded in wind-tunnel under gust condition

Another turbulent flow parameter in the longitudinal direction is quantified by their standard deviations  $\sigma_u$ . This parameter represents the general level of turbulence or ‘gustiness’ in the wind speed. Mathematically, the formula for standard deviation can be expressed as [21]:

$$\sigma_u^2 = \frac{1}{T} \int_0^T u^2(t) dt \quad (5-5)$$

Furthermore, Turbulence intensity ( $I_u$ ) is a measure of the strength of wind-tunnel turbulent fluctuations with respect to the mean velocity. Hence, it is defined as the ratio of the standard deviation of the mean flow direction to the mean velocity measured in the main flow direction.

$$I_u = \frac{\sigma_u}{\bar{U}} \quad (5-6)$$

Table 5-1 summarises the maximum turbulence intensity associated with low and high turbulence conditions generated in the wind-tunnel.

Table 5-1: Turbulence intensity

Parameter	Low wind speed	High wind speed
Overall turbulence intensity (%)	11.5	25.0
$I_u$ (%) ,i.e. in u direction	13.9	30.3

### 5.2.1.1 Amplitude and period of wind gusts

In fact, the estimation of gust amplitude, as well as other characteristic parameters of the gust, is not easy due to the variability of wind speed [80]. In reality, the gust is always a stochastic process, and the time-series wind speed shown in Figure 5-10 consists of a series of gusts, where a sharp change in wind velocity over a short time period are observed.

Each gust has amplitude and period. An example for maximum wind gust event is presented in Figure 5-10. The gust event is marked with a black rectangle, and it is expected to cause transient aerodynamic forces on the high-sided truck vehicle.

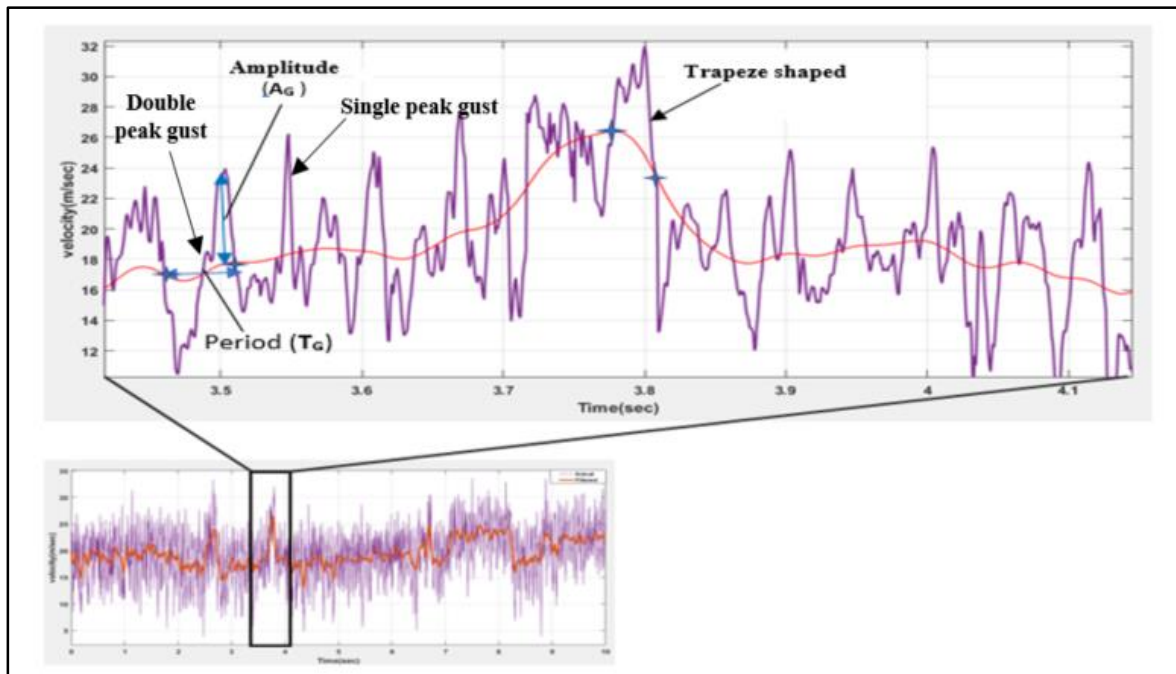


Figure 5-10: Discrete gusts of stochastic wind data

### 5.2.1.2 Gust amplitude (Gust factor)

At the sampling point, maximum gust speed,  $\hat{u}(t)$ , in wind speed time series, having a mean value of  $U(z,t)$  and a standard deviation of  $\sigma_u$ , is illustrated by the following [154]:

$$\hat{u}(t) = \bar{U}(t) + g_p I_u \quad (5-7)$$

Here,  $g_p$  is the expected peak factor (also known as normalized gust). The relationship between mean wind speed and the gust speed is often expressed in terms of a gust factor (amplitude)  $G$  [70].

$$G = \frac{\hat{u}(t)}{\bar{u}(t)} = 1 + g_p I_u \quad (5-8)$$

Using this formula, values of  $G$  can be obtained from appropriate values of  $I_u$  and a statistically-based estimate of  $g_p$ . According to Kristensen et al [155], the normalized gust  $g_p$  can be defined as:

$$g_p = [2\ln(\frac{T_g \sigma_{\dot{u}}}{2\pi \sigma_u})]^2 \quad (5-9)$$

where  $\sigma_{\dot{u}}$  is the variance of the derivative  $u$ , and  $T_g$  is the gust period.

### 5.2.1.3 Gust length (duration)

The beginning (start point) and the end (finish point) of the gust can be defined in different ways:

- One possibility is to define a certain time period (e.g. several seconds), and maximum wind speed in the flow as total gust (see for example, [156]). In this case, the maximum value coincides with the centre of the gust and all gusts have the same duration.
- Another way which is considered in this analysis is to define the intersection of the wind signal with the mean wind value as gust edges. After applying a moving average filter (length 0.1625 sec), the majority of gust profiles can be classified into two categories: single peak gusts, double peak gust, i.e. two consecutive peaks with opposite directions, and trapeze shaped peak. Each gust is defined by its amplitude  $A_G$  and duration  $T_G$  (see Figure 5-10).

## 5.3 Development of transient gusty crosswind scenario

Based on the results, which have been obtained in this chapter, prediction model for wind gust condition can be developed. For this purpose, data of transient crosswind “gusty” flow, which was developed in the experimental study have been employed in combination with steady flow data. Figure 5-11 depicts the wind speed time series of the transient crosswind scenario, i.e. mean and turbulent (longitudinal) components. The wind condition period is 10 seconds, divided into two intervals: the first one (from 0 sec to about 6.3 sec) is for modelling of moderate wind

conditions, and the second interval (from 6.3 sec to 10 sec) is for modelling of gusty flow situation. The proposed scenario represents the case where the tractor semi-trailer unit moving on a road under moderate wind conditions and, it being exposed to wind gusts. Example for this situations is that a gust generated due to slope of surrounding topography in high wind conditions. Moreover, in this scenario effects of sudden increases in wind speed and then aerodynamic forces will be considered.

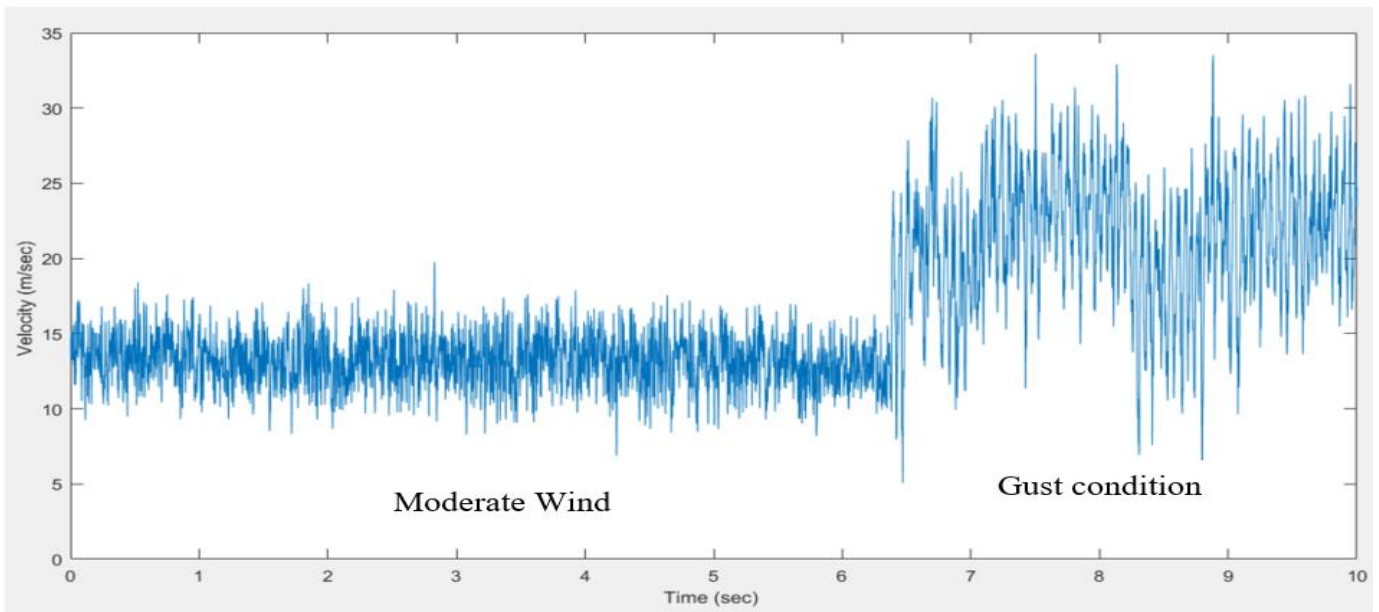


Figure 5-11: Transient crosswind scenario developed based on wind-tunnel data

It can be noted that , theoretically, the time-history of the longitudinal component of the wind speed  $u(t)$  shown in Figure 5-11 can be reproduced by a Fourier series according to the following formula[157]:

$$u_{ref}(t) = \sum_{n=0}^{n_{max}} u(\omega_n) \cos(\omega_n t + \varphi_n) \quad (5-10)$$

where  $\omega_n$  is given by  $\omega_n = n\omega_o$ , which is the  $n$ th harmonic having indicated with the fundamental harmonic ( $\omega_o$ ), where  $\omega_o$  defined as a function of the length of the time history  $T$  (i.e. total time of the scenario).  $\varphi_n$  is a random phase, ranged between 0 to  $2\pi$  while  $n_{max}$  is the total number of considered harmonics.

### 5.3.1 Development of new mean time-varying wind gust model

In this section, the curve-fitting technique was performed with the aid of MATLAB program for developing a functional relationship that could be adopted to describe the wind gust scenario (Figure 5-11). In this technique, Fourier model has been used to fit a function to data of the transient wind scenario. Figure 5-12 plots the function curve (i.e., time-varying wind speed) along with the original data. As it can be seen from the figure, in moderate wind conditions; the wind profile has an average (nearly constant) speed of about 13.81 m/s. However, in the gusty period, there is an extreme variation in the average wind speed, and this may result in a significant increase in the vehicle aerodynamic loads. This scenario will be also applied for different vehicle speeds to examine dynamic responses of the vehicle (Chapter 7 will provide further explanation).

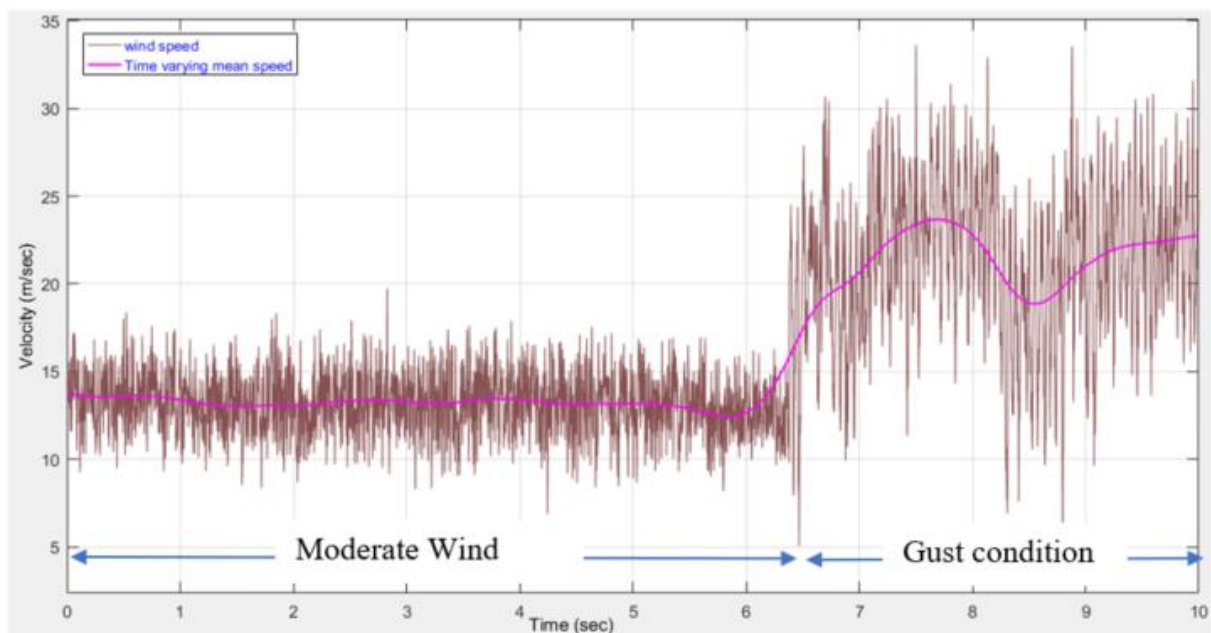


Figure 5-12: Mean and fluctuation crosswind speed of the transient scenario

Furthermore, as depicted in Figure 5-13, along with constant/moderate wind speed (from  $t_1$  to  $t_3$ ), the gust shape introduces two parameters: gust amplitude and gust duration. Also, the average speed of the gust scenario includes a linear rise from  $t_2$  to  $t_3$ . After that the trailer is loaded in extreme gusty flow, in this interval (i.e. from  $t_3$  to  $t_4$ ), wind speed fluctuates corresponding to a double peak gust scenario.

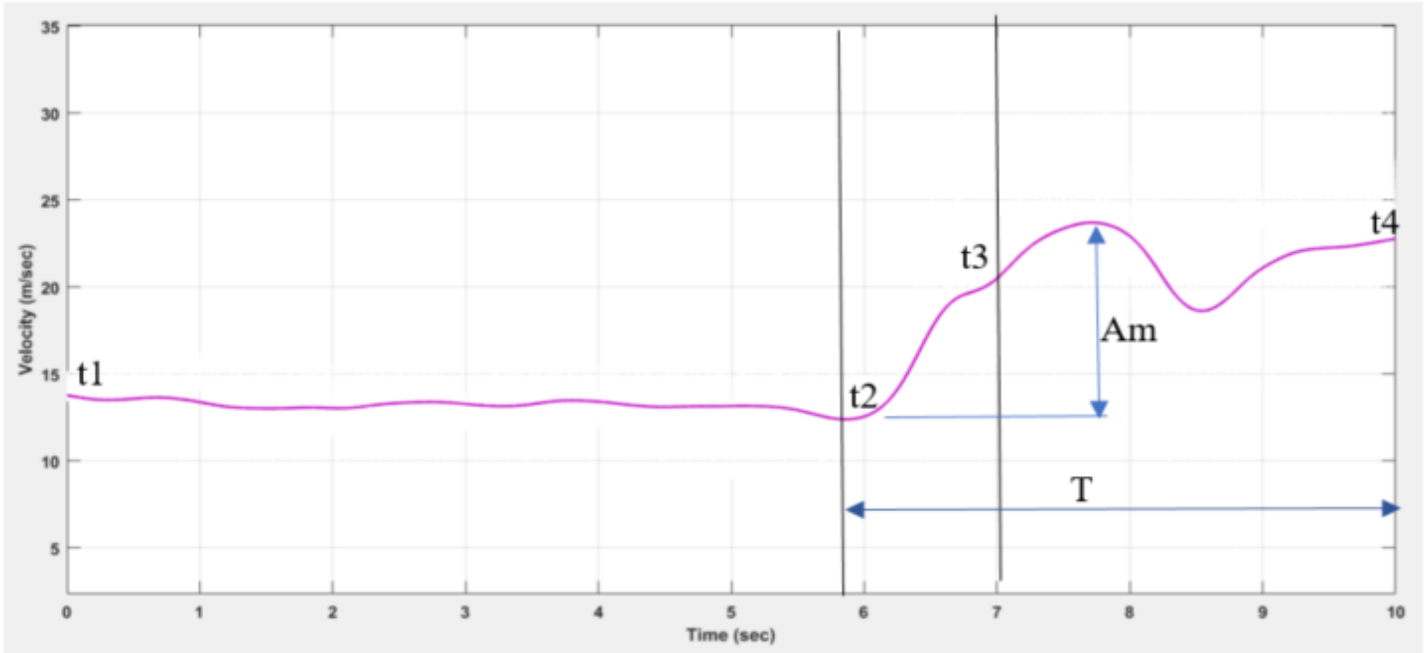


Figure 5-13: Parameters of mean time-varying wind gust model

Therefore, from the realistic fit of the wind data, the new gust profile can be formulated as follows:

$$u(t) = \begin{cases} \bar{U}(z) & t_1 \leq t \leq t_2 \\ \frac{\bar{U}_g(z)}{t_3-t_2}(t-t_2) & t_2 \leq t \leq t_3 \\ a_g \sin(b_g t + c_g) & t_3 \leq t \leq t_4 \end{cases} \quad (5-11)$$

$$u_G(t) = \bar{U}(z) + \frac{\bar{U}_g(z)}{t_3-t_2}(t-t_1) + a_g \sin(b_g t + c_g) \quad (5-12)$$

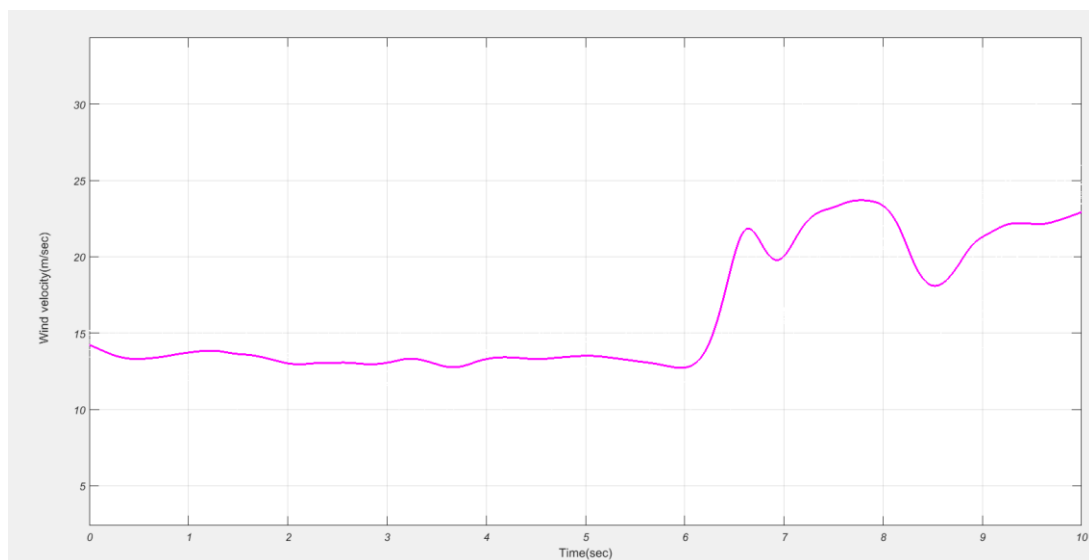
where  $u_G(t)$  is wind speed of gusty period in the scenario,  $\bar{U}(z)$  is the mean wind speed,  $\bar{U}_g(z)$  is the average wind speed of the gust period and  $(a_g, b_g, c_g)$  are wind gust parameters. From the values of wind gust parameters have been calculated by fitting technique and based on the gust profile of Bierbooms & Cheng [80], these parameters can be introduced as :

$$a_g \cong A_m, b_g \cong \frac{2\pi}{T}, c_g \cong T$$

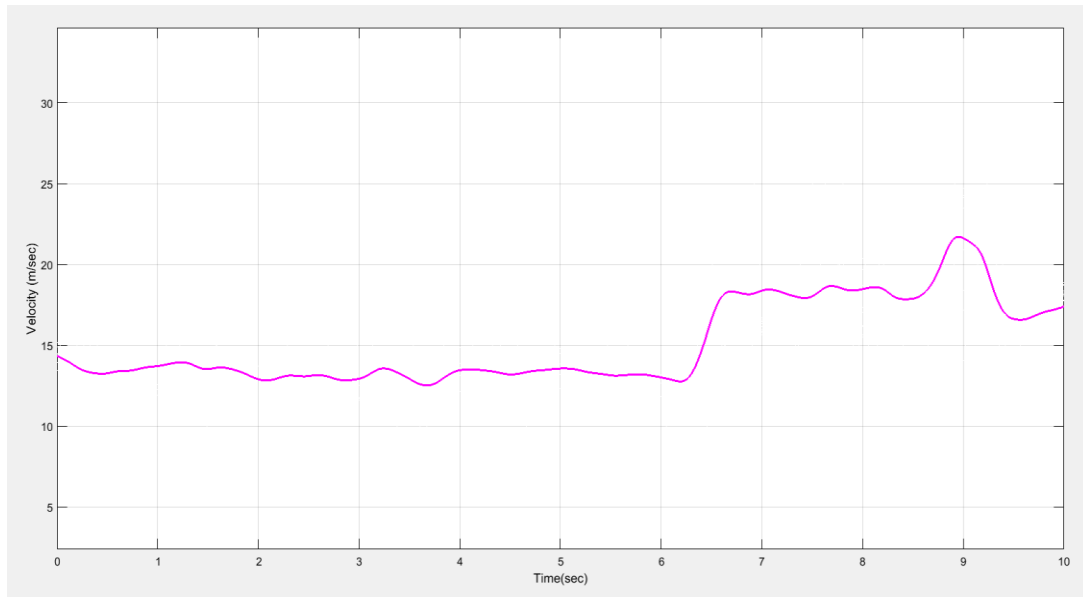
where  $A_m$  is the maximum gust amplitude (yielding a maximum wind gust speed), and  $T$  is the duration (time period) of the gust. Practically, these parameters can be determined in the laboratory or in a wind field by using advanced wind speed measurement devices. For this work, these gust parameters are:

$a_g=22.49$ ;  $T=4.07$  sec. Appendix D includes more details about the curve fitting and the wind speed properties.

As previously mentioned, the gusty flow conditions have been produced in the wind-tunnel test section based on mechanism of fixed plate gust generator with inclination angle of  $30^\circ$  (relative to the horizon, see Figure 3-8). As shown in Figure 5-14, when the gust generator angle increases or decreases, new gust shape can be developed. Therefore, the wind gust characteristics (e.g., gust amplitude and gust period) is a function in this angle. However, a roughly sinusoidal trend is observed for all gusts generated by using this mechanism. For further investigations on this phenomena, the section 5-5 will discuss another approach (standard gust) for analyse gusty wind conditions.



(a) Time-varying mean wind gust scenario generated with inclination angle of  $45^\circ$



(b) Time-varying mean wind gust scenario generated with inclination angle of 15°  
 Figure 5-14: Effects of inclination angle of gust generator on gust properties.

## 5.4 Calculation of aerodynamic forces acting on a tractor-trailer vehicle in transient gusty crosswind environment

### 5.4.1 Relative wind speed

Figure 5-15 represents a vector diagram of the relative crosswind speed (perpendicular to the vehicle) for a moving as well as a static vehicle. These diagrams show mean and fluctuating wind speeds in the stream-wise direction only. There will, of course, be the component of these normal fluctuations to the mean velocity. However, as observed from wind-tunnel tests and reported in [158], these components are not of great significance. From the vector diagrams, it can be seen that for both the stationary and the moving case [158]:

$$\bar{V}_{rel} \cdot V'_{rel} = \bar{U}u' \quad (5-13)$$

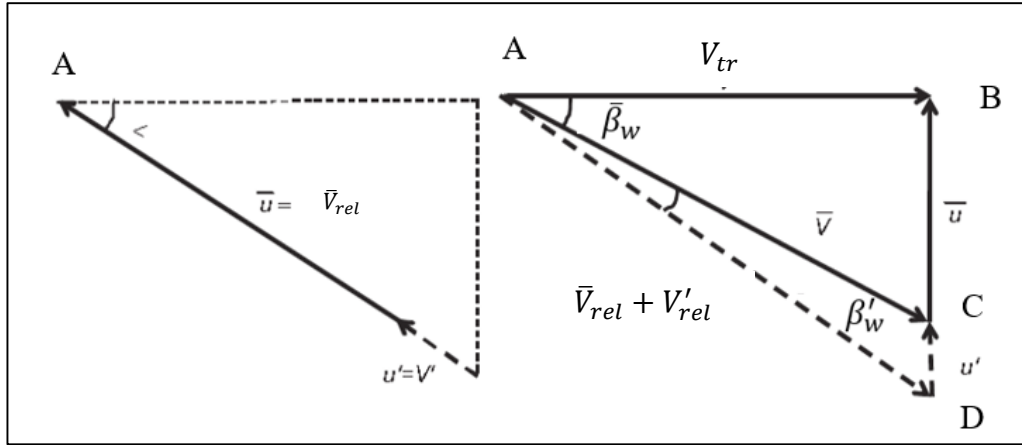


Figure 5-15 : Longitudinal ( $u$  direction) velocity vector diagram for instantaneous wind speed (i.e., mean ( $\bar{U}$ ) and fluctuating ( $u'$ )): triangle ABC for the mean wind speed  $\bar{U}$ , and triangle ABD includes the  $u'$ ,

The relative wind speed on the vehicle is the result of the sum of the vectors of trailer velocity and cross wind absolute velocity and is represented by:

$$V_{rel} = \bar{V}_{rel} + V'_{rel} = \bar{U}^2 + 2\bar{U}u'(t) + u'(t)^2 + V_{tr}^2 \quad (5-14)$$

Moreover, the relative wind speed and angle will change due to the wind gust and it is represented by:

$$\beta_w = \bar{\beta}_w + \beta'_w = \arctan\left(\frac{\bar{U}+u'}{V_{tr}}\right) \quad (5-15)$$

#### 5.4.2 Calculation of unsteady side aerodynamic force

In this part, the vehicle aerodynamics forces obtained by using conventional quasi-steady method are discussed. The Quasi-Steady approach is widely used for vehicle aerodynamic forces predictions. In this method, the unsteady aerodynamic force  $F(t)$  of a high speed vehicle moving of  $V_{tr}$  in a crosswind is given by the sum of mean value  $\bar{F}$  and fluctuating value  $F'(t)$ . It is assumed that the force fluctuations follow the velocity fluctuations in the ideal scenario i.e. they are fully correlated. Thus, the aerodynamic force can be defined according to the well-known quasi-steady expression as follows [150]:

$$\bar{F}(t) + F'(t) = \frac{1}{2} \rho_{air} A_r [(\bar{U}(t) + u'(t))^2 + V_{tr}^2] \bar{C}_l$$

$$= \frac{1}{2} \rho_{air} A (\bar{U}^2 + V_{tr}^2) \bar{C}_F + \frac{1}{2} \rho A (2u'\bar{U} + u'^2(t)) \bar{C}_i \quad (5-16)$$

where:

- $\rho_{air}$  is the air density,
- $V_{tr}$  is truck speed
- $A_r$  is Vehicle reference area,
- $\beta$  is the yaw angle,
- $\bar{C}_i$  is the mean aerodynamic force coefficients (measured in wind-tunnel),  $i=S, D$  and  $L$ ;
- $u'$  is the fluctuation of the wind velocity relative to the vehicle.

The aerodynamic coefficient measured through wind-tunnel tests on still models which is a function of the yaw angle  $\beta$  was introduced in previous chapter.

The quasi-steady force as defined in Equation 5-16 incorporates second order terms associated with the turbulent velocity  $u'(t)$ , i.e. a non-linear quasi-steady approximation. Now assuming that the fluctuating component  $u'(t)$  in Equation 5-16 is considerably smaller than the mean value  $\bar{U}$ , in this case the higher order fluctuations can be neglected [158]. As a consequence, Equation 5-16 leads to the formula for unsteady aerodynamic force as [150]:

$$F(t) = \frac{1}{2} \rho_{air} A_r (\bar{U}^2 + V_{tr}^2) \bar{C}_F + \frac{1}{2} \rho_{air} A u'(t)^2 \bar{U} \bar{C}_F \quad (5-17)$$

Time series of side aerodynamic force generated due to the transient gust condition in terms of the longitudinal velocity at a yaw angle of  $90^\circ$  are displayed in Figure 5-16. In this calculation, the tractor semitrailer is assumed to be going straight on a flat surface at constant high speed ( $V_{tr}$ ) of 25 m/s. As can be seen from the figure, wind gust speed has large impact on the fluctuating values of the side aerodynamic force. Also, sudden increase in the force indicating a significant effect on the vehicle dynamic stability can be occurred. Trend of the variation in the side force was observed to be similar to that of the transient gust speed. As well as, the force magnitudes are large due to the high gust flow generated in wind-tunnel.

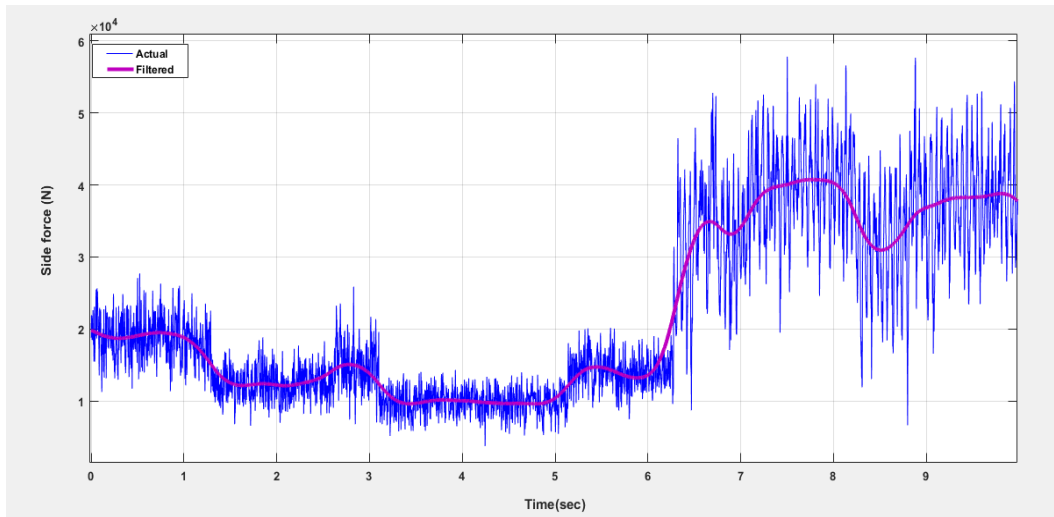


Figure 5-16: Side aerodynamic force due to developed transient crosswind scenario

In this study, the experimental findings have been verified against the numerical (CFD) model for the time varying side aerodynamic force. For this purpose, Large-Eddy Simulations (LES) was used to predict vehicle aerodynamic forces. The Navier-stokes equations are solved numerically using the ANSYS-FLUENT 17.0.0. The numerical simulation of a realistic atmospheric wind as similar as possible to the crosswind wind experienced by the tractor semitrailer was carried out by using the spectral synthesizer algorithms [159]. This algorithm is available in ANSYS\_FLUENT package to model the fluctuating velocity at velocity inlet boundaries. The approach is based on a random flow generation technique, originally proposed by [160] and modified in [161]. All CFD parameters used for the simulation, such as trailer geometry, dimensions of computational domain (see Figure 5-17) and boundary conditions were based on those of the experimental setup reported in Chapter 3.

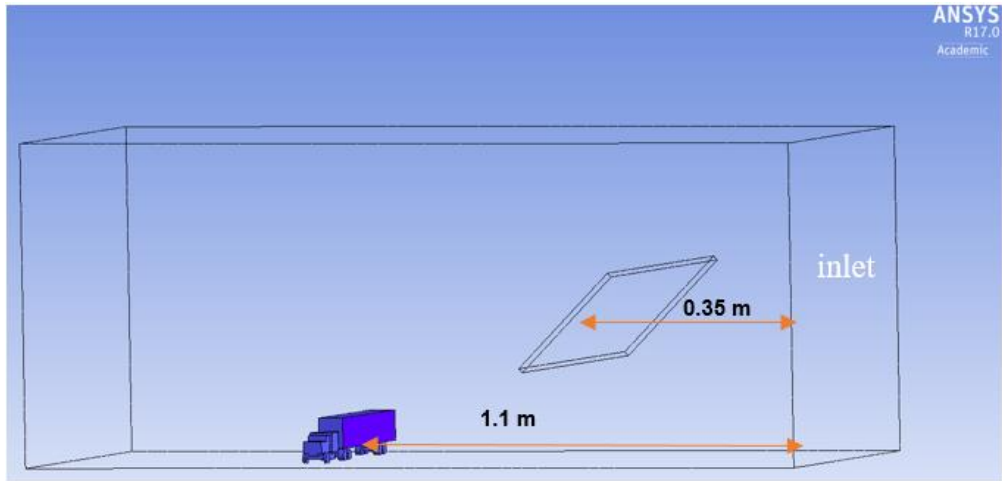


Figure 5-17: CFD computational domain and trailer model (with gust generator)

Figure 5-18 depicts the variations in the CFD results with respect to the time-varying mean aerodynamic side force. This force has been calculated by commercial code Fluent from total force (i.e., mean and turbulent force). It can be clearly seen that during the steady flow (i.e., moderate wind period) the difference between the experimental (see Figure 5-16) and numerical results are reasonably good. However, in gusty flow period of the scenario, the difference between the results increase, this most likely due to differences in air flow distribution in the flow domain computed by the two methods (i.e., differences in turbulence modelling and measuring techniques). In spite of these differences, the measured and simulated results show similar trend for both models.

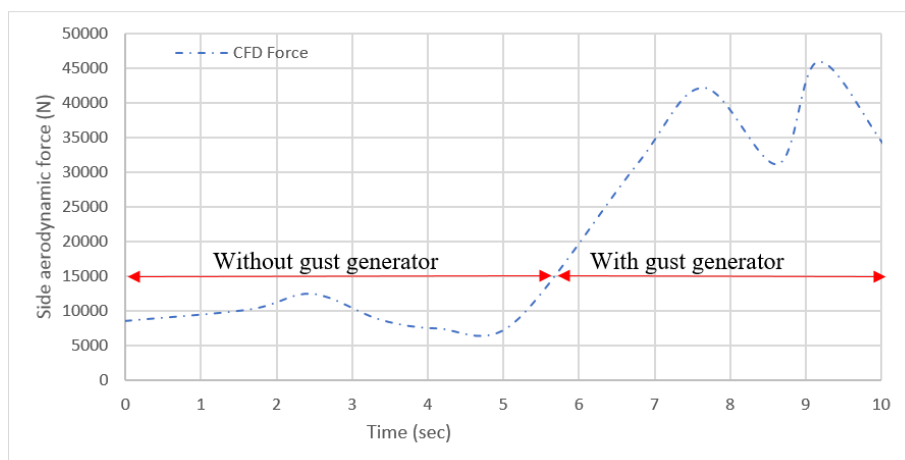


Figure 5-18: Time-varying mean aerodynamic side-force (CFD based results)

## 5.5 Deterministic modelling of extreme wind gust condition

High-sided trailers at exposed locations such as bridges or embankments are more vulnerable to the crosswind gusts than flat roads [92]. The reason is that in a windy environment, a high-sided vehicle may experience a suddenly strengthened crosswind when they enter a bridge that is usually more open than the road. This is especially true when compared with roads that have trees or bushes on both sides. Furthermore, high wind velocities are expected on bridges, because of the height above the ground (i.e. outside the ground boundary layer) [67].

Another critical situation for vehicles on bridges is the very short period of time that vehicles have to pass by bridge towers along with extremely gusty winds. Thereby, a higher wind speed at the top of bridges/embankments corresponds to higher aerodynamic forces acting on high-sided vehicles and as a consequence, the greater rollover risk.

As already observed, since wind is a random process, several space–time distributions of the absolute wind speed which satisfy the same statistical properties (mean wind speed, turbulence intensity, integral length scale) can be generated [157]. Also, wind gust effects described above are not easy to forecast or quantify precisely by practical road tests. However, the effects can be described and quantified deterministically. In the deterministic approach, gust model includes a variation of the wind velocity defined by a simple and usually analytical function of time. Such variation occurs in the same direction of (or “following”) the main wind speed (longitudinal gust).

According to the frozen turbulence hypothesis, a gust does not evolve and is transported with the mean wind velocity, which is assumed constant in the deterministic analysis. This approach is usually utilized when the maximum dynamic response of the body to wind forces has to be assessed, which is one of the main objectives of this study.

As previously discussed, Standard and also European law in form of the Technical Specification for Interoperability (TSI) [162] prescribes a deterministic wind gust model based on a bi-exponential function, also referred to as a “Chinese hat”, to be used for crosswind analysis. The

TSI scenario that has been applied to the rail vehicles represents a train traveling on an embankment or a bridge under constant mean wind speed and suddenly being hit by an extreme wind gust.

Then, the sudden change in ‘TSI’ gust model leads to an extreme change in train aerodynamic performance. This situation is applicable to road vehicles as well. Therefore, from a research point of view, it is of interest to examine effects of TSI gust on a high-sided tractor semitrailer.

In this section, an attempt to use the CFD simulations in combination with the TSI deterministic gust scenario will be discussed. The possibility to apply the TSI gust for predicting aerodynamic forces acting on the high sided trailer is investigated based on the LES turbulent model. The gust scenarios are introduced into a CFD simulation by creating an external velocity data file according to gust’s equation and imposing this to the lateral inlet boundary face.

### 5.5.1 Deterministic wind gust-characteristic

Recently, an efficient way to simulate a wind gust model by means of the so called constrained-simulation approach has been proposed for wind turbine reliability analysis (cf. [80]). The main advantage of this method is that the turbulent wind process with the superimposed gust characteristic is statistically indistinguishable from the natural wind process. Based on this approach, the total wind speed  $u(t)$  can be defined as follows [75]:

$$u(t) = (\bar{U} + u'(t)) + u_G(t - t_G) \left( A_p - u'(t_G) \right) - \frac{u_G(t-t_G)u'(t_G)}{\bar{u}_G(t_G)} \quad (5-18)$$

where  $u_G(t)$  is the gust characteristic based on the coherence function,  $A_p$  is wind gust amplitude and  $t_G$  is the gust time. It allows a simulation of gusts with different durations for the moving vehicle.

As can be seen, the first term of the equation 5-18 contains the non-stationary wind turbulence and the second term generates a mean gust shape with a target amplitude  $A_p$ . Additionally, the third term makes sure that the gust reaches its maximum at time  $t_G$ .

According to [71], the gust characteristic can be given by:

$$u_G(t) = \exp\left(-\frac{1}{2T\bar{U}}\sqrt{(C_{ux}\Delta x)^2 + (C_{uy}\Delta y)^2}\right) \quad (5-19)$$

in which  $C_{ux}$  and  $C_{uy}$  are the corresponding coherence coefficients in a plane above the ground (the vertical direction is not considered). The coefficient's value can be obtained based on experimental measurements. 'T' describes the duration of the gust, and ' $\Delta x$ ' and ' $\Delta y$ ' is the relative distances of two points in space.

According to the famous Taylor's hypothesis 'frozen turbulence', it assumes that the turbulence field can be considered as frozen in both space and time and the field of turbulence past a fixed point can be taken entirely by the mean flow [67]. Figure 5-19 shows the geometrical relationship of a vehicle running in the turbulent wind. For example, P is the fixed point at the vehicle which moves along a straight line and with a constant speed of  $V_{tr}$ . With time delay  $\Delta t$ , the physical point P will move to  $P'$ , and  $P_e'$  is an equivalent point for  $P'$  in the frozen turbulent field. So, the coherence function of  $P'$  and P for a moving vehicle can be obtained by calculating the coherence function between the equivalent point  $P_e'$  and P [75]. Therefore, one obtains

$$\Delta x = (\bar{U} + V_{tr} \sin(\alpha_w)) \Delta t, \Delta y = V_{tr} \cos(\alpha_w) \Delta t \quad (5-20)$$

And equation 5-20 leads to

$$u_G = \exp\left(-\frac{1}{2T\bar{U}}\sqrt{(C_{ux}(\bar{U} + V_{tr} \sin(\alpha_w)) \Delta t)^2 + (C_{uy}(V_{tr} \cos(\alpha_w)) \Delta t)^2}\right) \quad (5-21)$$



following the gust function. Finally, an additional time stage involving a constant wind speed takes place between  $t_5$  and  $t_6$ .

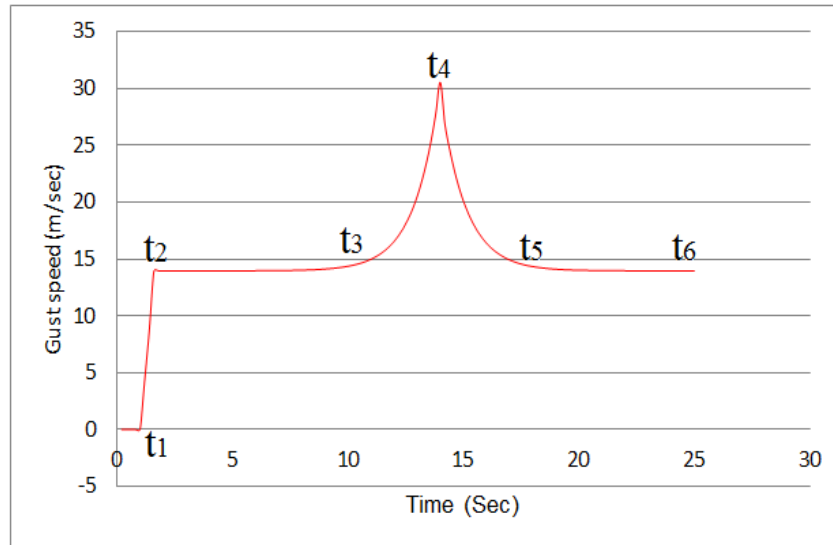


Figure 5-20: TSI gust scenario

As seen from the Figure 5-20, the TSI wind gust generated corresponds to fixed amplitude (corresponding to a probability level of amplitude  $\sim 99\%$ ) and a probability level exceeding 50% for the gust duration (mode of the distribution). The gust model also has the following characteristics:

- The Gust time-space model (bi-exponential) is based on a gust model investigated in Deufrako [69] and corresponds to the best approximation of a random process in a maximum local vicinity.
- Mean wind is horizontal (only the longitudinal component  $U$  is used). This component represents the prominent part of wind fluctuations and it is the projection of the instantaneous wind vector in the mean wind direction.
- Variations of wind direction are not taken into account.

The mathematical description of the TSI gust in the TSI [163] and BS EN 14067-6 [71] standards refers only to the decaying section of the exponential function. The gust is completed with the increased segment by mirroring the function with respect to the vertical axis of coordinates. The

method describes it as a spatial distribution since the wind gust is fixed in space. Hence, the transformation to calculate the temporal distribution is only possible when the vehicle speed is constant [9]. TSI gust speed,  $u_{TSI}(t)$ , impacting perpendicularly to the side surface of the vehicle is calculated by the following formula [163]:

$$u_{TSI}(t) = \bar{U}(z) + \tilde{A} \cdot \sigma_u \cdot B(t) \quad (5-24)$$

where some of the parameters fixed by the method, which are [71]:

Table 5-2: Fixed parameters of TSI standard wind gust

Parameter	value
Reference height of the site (embankment/bridge) (z)	4 m
Normalized gust amplitude ( $\tilde{A}$ )	2.84 m/sec
Roughness length of the site( $z_0$ )	0.07 m
Probability of a gust duration(T) for a given amplitude	0.5sec

The input data for the scenario are wind direction, vehicle speed ( $V_{tr}$ ) and maximum wind speed  $u_{max}$ . In this paper the maximum wind speed is assumed as 23.7 m/s. The TSI Standard reported at a site is of height  $z = 4$  m, the turbulence intensity equals to 0.245, the gust factor (G) is calculated from the turbulence intensity and the normalized gust amplitude as [71]:

$$G = 1 + \tilde{A} \cdot I = 1.6946 \quad (5-25)$$

From the gust factor, the mean wind ( $\bar{U}$ ) can be deduced from a given maximum wind  $u_{max}$ :

$$\bar{U} = \frac{u_{max}}{G} \quad (5-26)$$

The standard deviation of longitudinal component (following the mean wind speed) of the wind  $\sigma_u$  is then deduced from the mean wind speed and the turbulence intensity.

The autocorrelation function,  $B(t)$ , is the complex factor of the equation 5-24. From the coherence decay, exponential coefficient of the gust parallel and perpendicular to the mean wind speed, the correlation function at an instant  $t$  can be calculated by[163]:

$$B(t) = \exp\left(-\sqrt{(C_u^x u_x P_u^x)^2 + (C_u^y u_y P_u^y)^2}\right) \quad (5-27)$$

$C_u^x$  and  $C_u^y$  are the coherence decay coefficients in the mean wind direction and perpendicular to the mean wind direction respectively.

$P_u^x$  and  $P_u^y$  are the exponential coefficients in the mean wind direction and perpendicular to the mean wind direction respectively. The values of these coefficients are predicted based on measurements of realistic wind flow, and more details can be found in Appendix B. After substituting the coefficients values in Equation 5-27, the correlation function can be calculated as:

$$B(t) = \exp\left(-\sqrt{(5u_x)^2 + (16u_y)^2}\right) \quad (5-28)$$

The calculation of the gust time constants is derived from the power spectral density(PSD)of the turbulence for the longitudinal component  $S_u(n)$ , which is given by Von Karman expression[71]:

$$S_u(n) = \frac{4.f_u.\sigma_u^2}{(1+70.07.f_u^2)^{\frac{5}{6}}} \cdot \frac{1}{n} \quad (5-29)$$

where n are the frequency range limits of the data (either measured or calculated). In this case, they are between  $n_1=1/300$  Hz and  $n_2=1$  [71].  $F_u$  stands for normalized frequency using the characteristic length  $L_u^x$  as in follows equation:

$$f_u = \frac{n.L_u^x}{U_{mean}} \quad (5-30)$$

The characteristic length  $L_u^x$  can be explained as the spatial wavelength of the gust in the wind direction and accordance with TSI standard the value of  $L_u^x$  can be calculated as [70]:

$$L_u^x = 50 \cdot \frac{z^{0.35}}{z_0^{0.063}} \quad (5-31)$$

The mean time constant ( $\bar{T}$ ) can be obtained by integrating the PSD between the  $n_1$  and  $n_2$  limits:

$$\bar{T} = \frac{1}{2} \left[ \frac{\int_{n_1}^{n_2} n^2 \cdot S_u(n) dn}{\int_{n_1}^{n_2} S_u(n) dn} \right]^{-0.5} \quad (5-32)$$

The duration of the maximum gust depends on measurement factor and mean time constant, and it is given by [70]:

$$T = 4.182 \cdot \bar{T} \quad (5-33)$$

Wind velocities of the u-component are [70]:

$$u_x(\tilde{x}) = \frac{1}{2} \tilde{x} \cdot \cos(\beta) \cdot \frac{1}{T \cdot U_{mean}} \quad (5-34)$$

$$u_y(\tilde{x}) = \frac{1}{2} \tilde{x} \cdot \sin(\beta) \cdot \frac{1}{T \cdot U_{mean}} \quad (5-35)$$

where the  $\tilde{x}$  term in the equation is a function of the distance along the road towards the position of the maximum amplitude of the gust that can be calculated by[70]

$$\tilde{x} = v_t(t - t_{max}) \quad (5-36)$$

where  $t_{max}$  is the time instance at which the maximum of the gust takes place.

Finally, the coherence function can be calculated via linear interpolation since the  $u_x$  and  $u_y$  terms can now be substituted in equation 5-28. The specific case in which the wind is perpendicular to the road can be resumed here. If  $\beta=90$ , then the value of  $u_x$  is zero, and the coherence function is simplified to[71]:

$$B_{(\beta=90)} = e^{16u_y} \quad (5-37)$$

Thus, the final equation of the TSI gust model is:

$$u_{TSI}(t) = \bar{U}(z) + \tilde{A} \cdot \sigma_u \cdot e^{16u_y} \quad (5-38)$$

## 5.6 CFD Aerodynamics simulation of full- scale tractor-semitrailer unit under TSI gust scenario

Aerodynamic development of a full-scale semi-trailer tractor presents a challenge for experimental testing due to the scale of the vehicle relative to most wind-tunnel test facilities. For this problem, Computational Fluid Dynamics is an attractive approach as it allows reproducing the conditions typical of crosswind gusts at a fraction of the cost of a full (on-road) experimental setup. Moreover, CFD can provide a large amount of data and detailed information

on the flow field and that can help to understand the mechanism by which unsteady aerodynamic forces due to wind gust develops.

This section presents a summary of Large-Eddy Simulations (LES) that was carried out to predict unsteady vehicle aerodynamic forces in combination with the TSI deterministic gust scenario. The Navier-stokes equations are solved numerically using the ANSYS-FLUENT 17.0.0 solver. An incompressible Newtonian fluid was supposedly used and the time-dependent Navier-Stokes equations were spatially filtered to acquire the governing equations of the LES. Details of this model are provided in chapter three.

### **5.6.1 Vehicle Model and Computational domain**

The target vehicle in the present calculations is a full-scale model of a tractor semi-trailer unit that was built in ADAMS/Car software version 2015.1.1. The model is based on geometry of a real commercial vehicle and it has been chosen to predict accurate vehicle dynamic response to the wind forces through ADAMS simulations as the crosswind aerodynamic forces are depend strongly on vehicle geometry[18] .

Figure 5-21 depicts the full-scale model with length (L), width (B), and height (H) taken as 21.84m, 2.6 m, and 4.31m, respectively. The vehicle is anticipated to move directly ahead at a continuous speed of 25 m/s which is the high speed limit for heavy vehicle, according to many legislations [18].

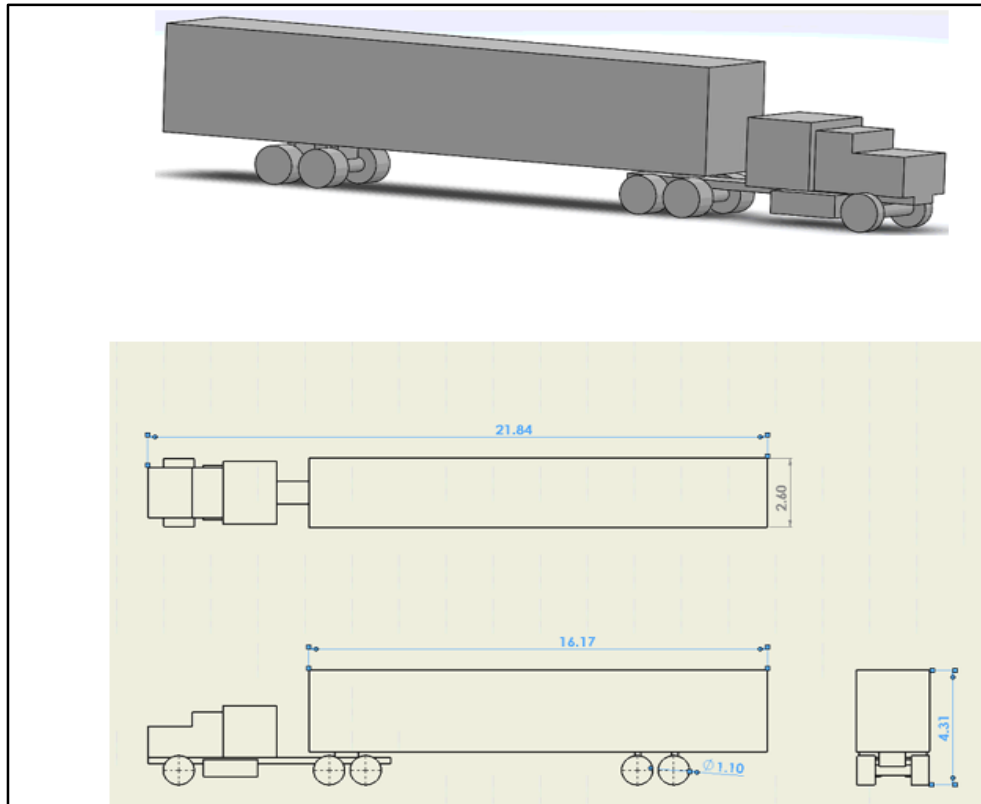


Figure 5-21: 3D full-scale model of a tractor semitrailer vehicle(ADAMS model)

Furthermore, as shown in Figure 5-22(a), the conventional computational domain (box shape) has been created around the vehicle model to simulate the crosswind conditions. The larger domain with 126.5m length (i.e.,6L), 124m width , and 32.0m height was used to capture the essential flow features [103].

Tetrahedral unstructured meshing scheme was used to discretise the computational fluid domain into about 27.6 million finite volumes. The number of elements has been chosen after several meshes were tested to check the grid independency. Also, the maximum skewness of the meshed geometry was 0.79, and the topology of these meshes is illustrated in Figure 5-22 (b). In the figure, two refinement zones are shown i.e. the fine cells zone and the upstream zone. The fine cells are created to capture the small flow structures around the vehicle.

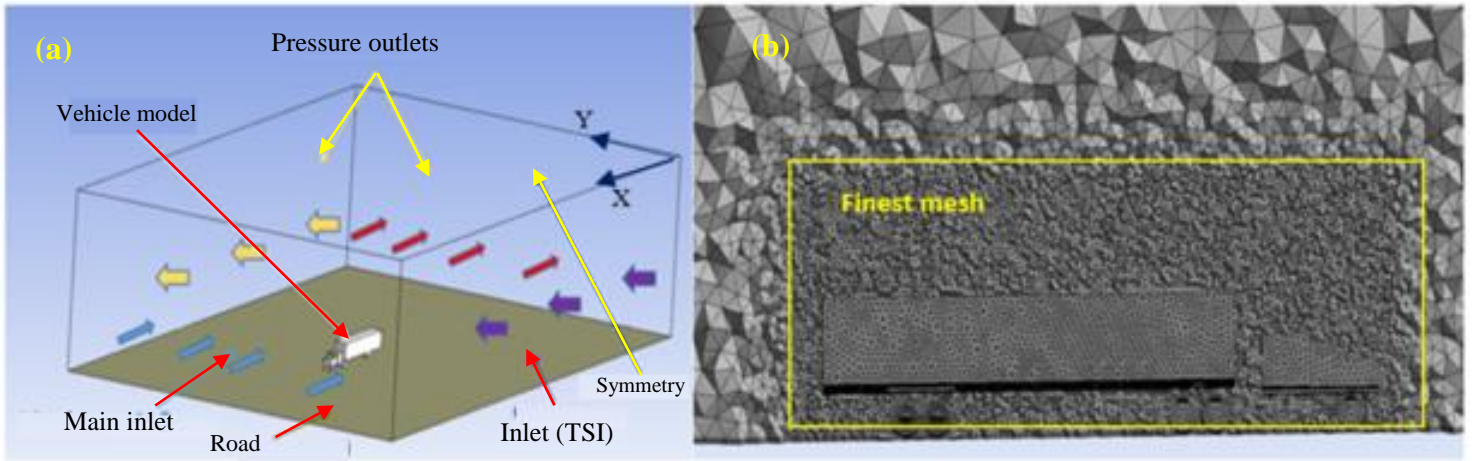


Figure 5-22: (a) computational domain (b) mesh topology

Furthermore, in order to reproduce a strong crosswind across the pathway of the trailer, the TSI crosswind gust scenario was imposed on the side boundary of the domain as second flow inlet [18]. A symmetry boundary condition (i.e. zero normal velocity) is assigned to the top boundary and the uniform atmosphere pressure is imposed at the main and lateral outlet walls of the domain. To simulate the vehicle movement, no-slip condition is used at the trailer surfaces while velocity of 25 m/sec is applied at main domain inlet and road boundary condition, see Figure 5-22 (a).

The SIMPLE method is used for solving the pressure velocity coupling. The spatial discretization schemes are used as second order for the pressure equation and the bounded central difference for the momentum equation. A bounded second order implicit scheme is chosen for the transient terms. A constant time step of  $\Delta t = 12 \times 10^{-4}$  s was used to achieve the Courant-Friederich-Lewy (CFL) number below 1.

### 5.6.2 TSI gust flow fields

Figures 5-24 illustrates the complexity of vehicle crosswind aerodynamics in terms of instantaneous lateral velocity. In this figure, the instantaneous flow field have been computed at

90o yaw angle for two planes - A horizontal plane at the trailer's mid-height and cross-section (vertical plane) taken along the trailer's mid-length. Additionally, as shown in the Figures 5-23,

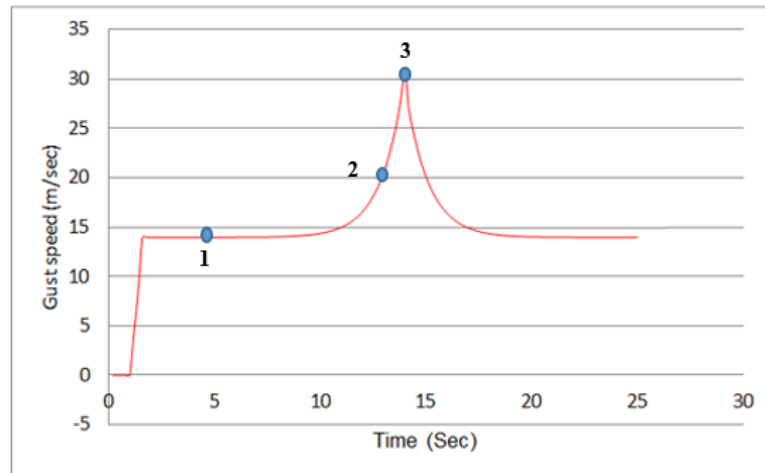
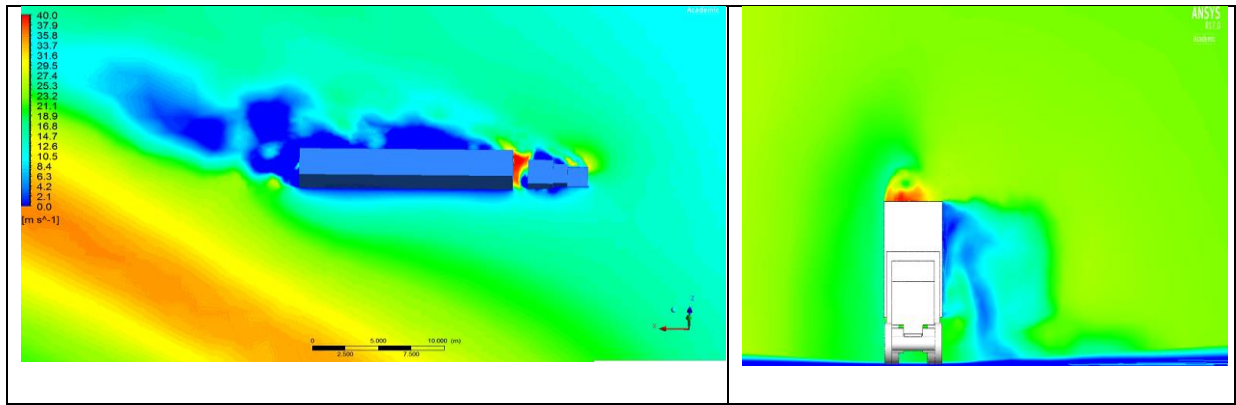


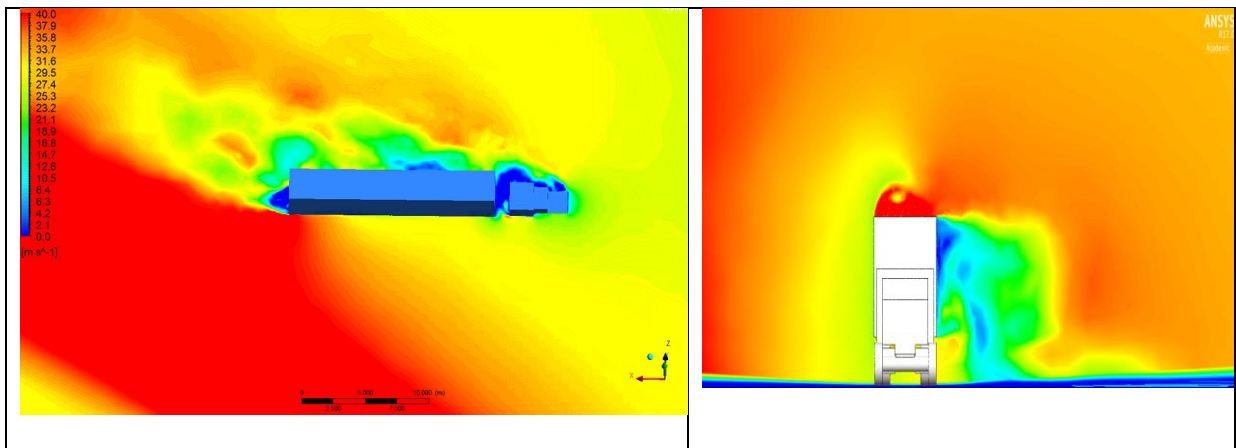
Figure 5-23: Monitoring points over the TSI gust period

wind velocities were monitored at three different instants of time during the TSI gust which are at  $t = 5\text{sec}$  (before the vehicle exposed to the gust region),  $t=13\text{sec}$  (when the vehicle exposed to the gust region three times as long as the vehicle length) and  $t=15\text{sec}$  (at which the vehicle exposed to the maximum gust speed). Over these time periods, the gust speed increased dramatically from about 13m/sec to a maximum gust speed of about 31 m/sec.

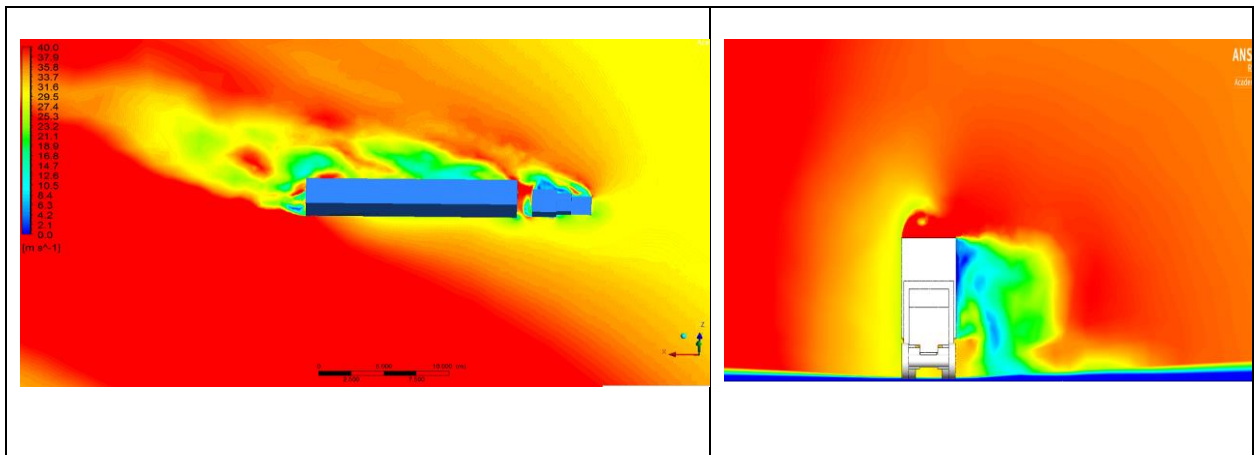
As depicted in the Figure 5-24, the TSI gust caused a turbulent wake region to form at the leeward side of the vehicle. This leads to creation of a low-pressure region at the leeward side of the trailer. Thus, the side aerodynamic force acting on the vehicle is dominated by the pressure differences induced by high-flow velocity with massive flow separation (see left side of Figure 5-24).



a) Velocity contour at monitor point 1 (at  $t \approx 5$  sec): top view (left), front view (right)



b) Velocity contour at monitor point 2 (at  $t \approx 13$  sec): top view (left), front view (right)



c) Velocity contour at monitor point 3 (at  $t \approx 15$  sec): top view (left), front view (right)

Figure 5-24: Velocity contours of the TSI gust flow.

Furthermore, the velocity contours clearly explain how the gust is evolved from a moderate event (at  $t=5$ sec), where the maximum wind speed surrounding the trailer was about 16 m/sec (Figure 5-24 (a)), to highly critical condition at  $t= 15$  sec, with maximum gust speed between 30 m/sec to 35 m/sec(Figure 5-24 (c)). It can be also seen that the flow velocity at the road (bottom wall

of the domain) is almost zero, and this is due to the no-slip boundary condition has been applied to this boundary.

For a comparison, Figure 5-25 depicts velocity contour computed in uniform crosswind field. In this case a constant wind speed (it was assumed as 14 m/sec which is the speed of TSI gust at steady period) has been applied to the lateral side of the computational domain. It can be noted from the figure that Unlike the gusty flow, in this situation the vehicle experiences a stably and uniform crosswind (lateral) flow, because of no sudden increases in crosswind speed. This stable crosswind flow may has no negative effects on the large vehicle's running stability. Therefore, this method (i.e., constant crosswind velocity) which has been employed in several previous study is limited for investigating the vehicle crosswind stability.

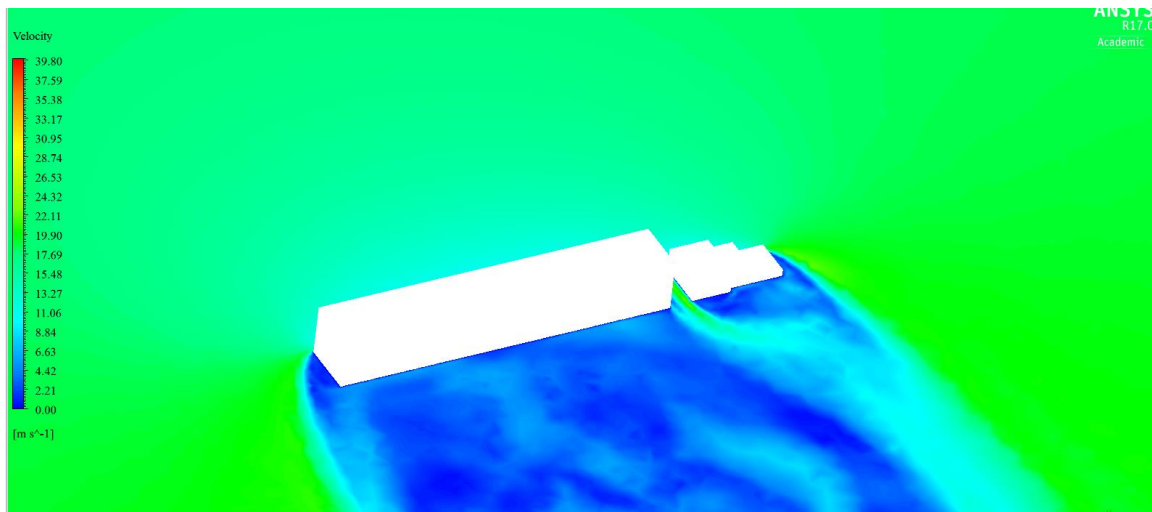
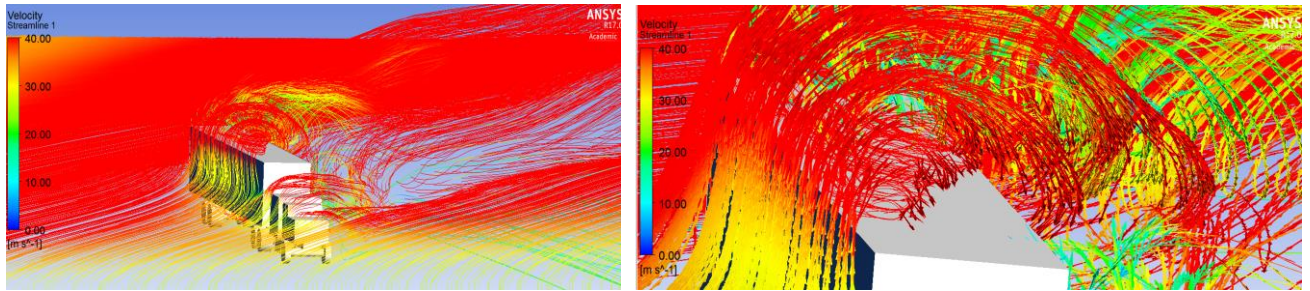


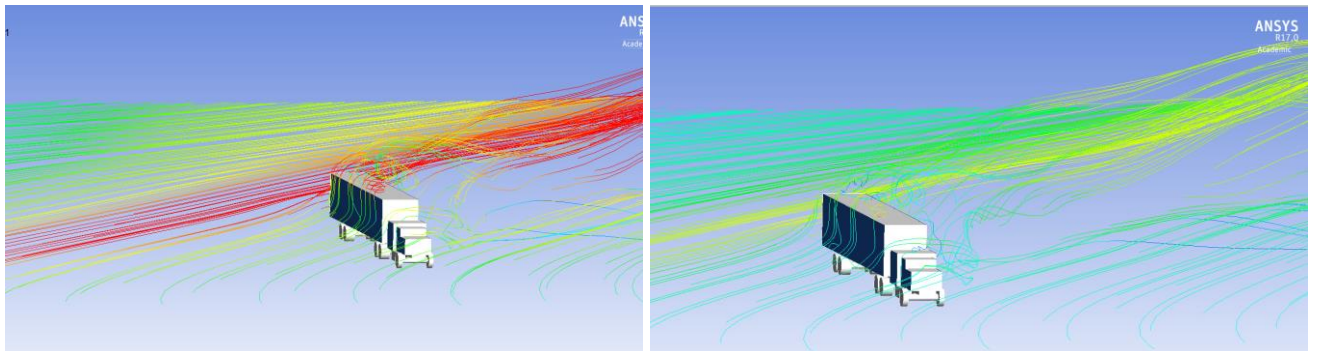
Figure 5-25 : Velocity contours of time-average crosswind flow

For further investigation on the influence of TSI gust flow on local velocity field, Figure 5-26 depicts flow path analysis in terms of velocity streamlines for the vehicle. The figure also compares the strength of the gust at monitoring points shown in Figure 5-23. At the gusty period of the scenario (i.e., at the point 3 of the Figure 5-23), the flow pattern clearly shows that the gusty flow increases the vorticity levels dramatically and a large counter rotating vortex region formed by the semitrailer body at the top surfaces is observed. The gust flow also rotates over the bottom and leeward surfaces of the trailer, but in less severity. Therefore, this local flow behaviour

affects the global instability of flow field variables, and it may lead to high drag and side aerodynamic forces. Also, as the contours indicated, the front part of the vehicle body resists the air flow to pass through this gusty environment. This means that the vehicle needs to overcome a high longitudinal drag force, and that leads to increase in fuel consumption under this condition



a) Velocity streamlines computed at maximum TSI gust speed (at monitoring point 3)



b) Velocity streamlines computed at: monitoring point 2 (left); minimum TSI gust speed (right)

Figure 5-26 : Flow divergence at semitrailer edge shown by path lines colored by velocity magnitude

Furthermore, as shown in Figure5-27, the TSI gust flows smoothly (i.e., no significant flow circulation is observed ) at the spacing gap between the tractor and trailer units as well as over the top of the tractor unit due to differences in the height of the vehicle components. However, this smooth flow has high velocity of about 30 m/sec to 37 m/sec. Such high variations in speed of the local flow may cause significant differences in lateral motion between tractor and trailer units, and may affect strongly the vehicle yaw stability.

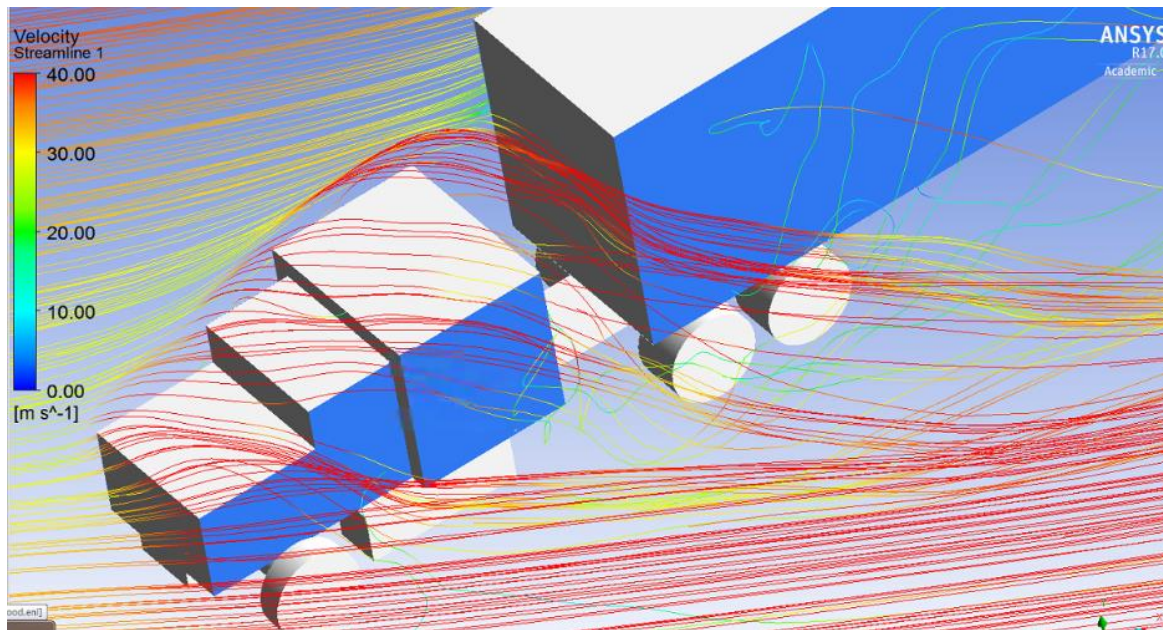


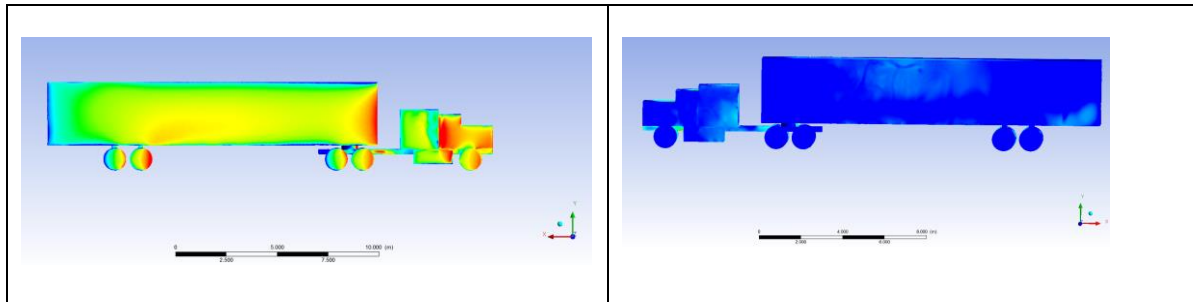
Figure 5-27: Local TSI gust flow

### 5.6.3 The TSI wind gust pressure distribution over the vehicle

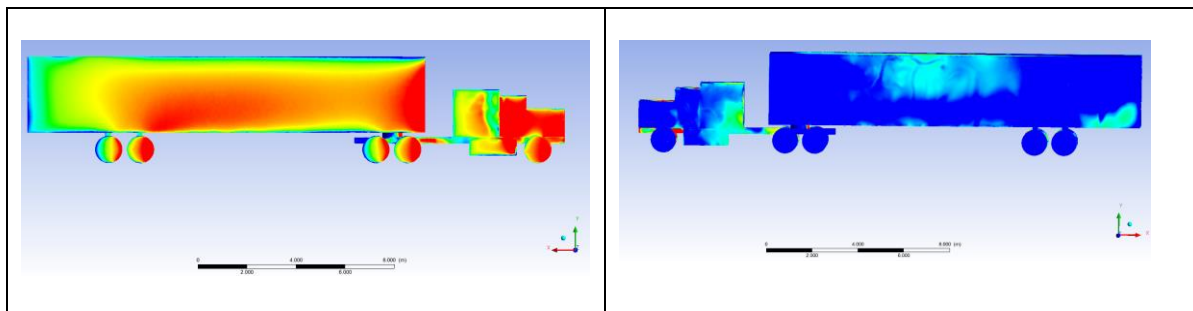
Lateral sides of the tractor semi-trailer combination are important in the overall flow field analysis. This is because these faces having the largest area of the vehicle's external surface that exposed to wind actions. The windward side in particular, has greater significance due to the fact that this side experiences the direct impact of the larger portion of the oncoming gust flow. The velocity contours at various time points during TSI gust scenario described in Section 5.6.2 show that the variation in gust speed causes increased interaction between the surfaces of the vehicle and the gust flow. In order to analyse this in terms of vehicle aerodynamic forces, contours of the total pressure distributions due to TSI gust conditions have been computed for the leeward and windward sides of the trailer in this section.

Figure 5-28 shows variations of the total pressure distribution on the leeward side (left) and windward side (right) of the trailer for three different instants of time during the TSI gust as described in Figure 5-23. As expected, the total pressure acting on windward side of the trailer was observed to be significantly higher than that of the leeward side. A very-low and sometimes

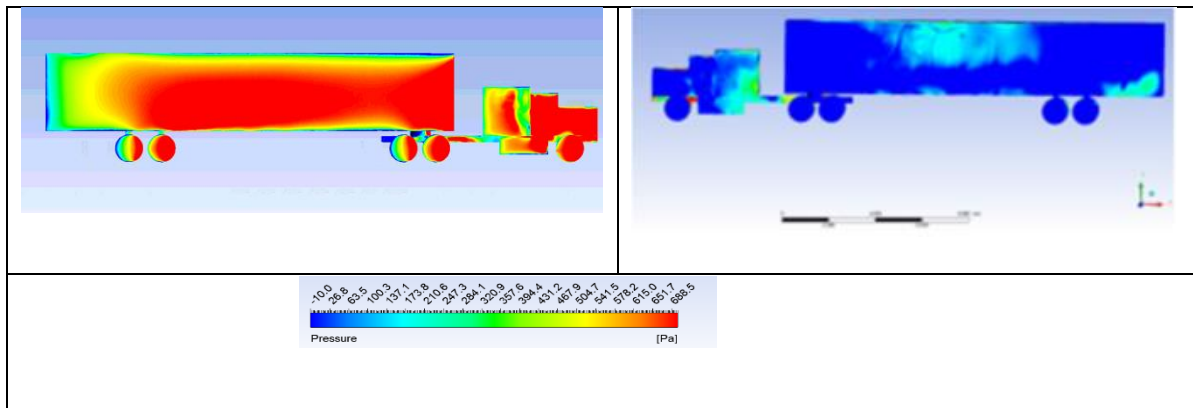
negative pressure zones that were developed on the leeward side during the TSI gust event are due to the development of flow vortices and flow separation on the surface.



a) Pressure contour at monitor point 1 (i.e., at  $t \approx 5$  sec): leeward side (right), windward side (left)



b) Pressure contour at monitor point 2 (i.e., at  $t \approx 13$  sec): leeward side (right), windward side (left)



c) Pressure contour at monitor point 3 (i.e., at  $t \approx 15$  sec): leeward side (right), windward side (left)

Figure 5-28: Snapshots of the total pressure distribution on sides of the trailer

Moreover, this pressure difference increased gradually over period of the TSI gust condition (i.e., from  $t = 5$  second to  $t = 14$  sec). As shown in Figure 5-28, at the mean speed of the TSI gust (i.e. from  $t = 1$  sec to  $t = 10$  sec), only small high-pressure zones (i.e.  $650 \text{ Pa} \leq P \leq 690 \text{ Pa}$ ) were developed on the windward side. The worst-cases of the scenario occurs when the vehicle

experienced high speed gust at  $t = 14$  sec. At this time, large stagnation area can be observed clearly on the windward surface of the vehicle on which high positive wind pressure was developed.

Over other surfaces of the vehicle, there are all low and negative wind pressures because of flow separations and wakes. The majority of the windward side is covered by high pressure (See Figure 5-28). The existence of the lower pressure region on the leeward side of the trailer explains the increase in aerodynamic side force and roll moment.

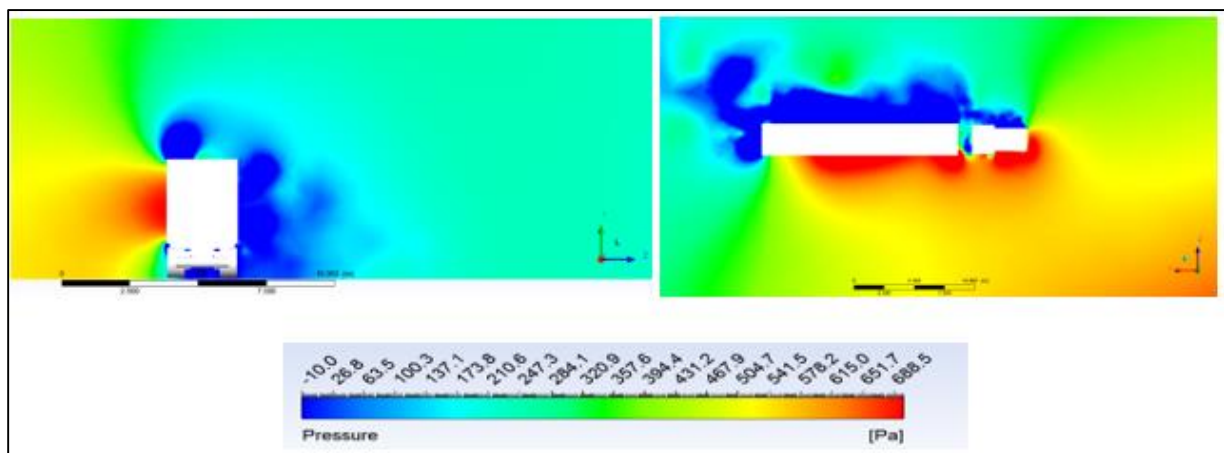


Figure 5-29: Distribution of total pressure in flow field of TSI gust .

In Figure 5-29, contours of total pressure distributions have also been computed at the middle-height plane of the domain. The pressure contour illustrates variation in the TSI gust pressure values over the vehicle's body. Again, it is apparent from the figure that high-pressure region is concentrated near the vicinity of the windward side of the vehicle whereas on the other side, low pressure region is formed at the leeward side and back surfaces. As it will be discussed in the next section, high differences in pressure field generated by the wind gust plays an important role for the development of unsteady aerodynamic forces as well as vehicle dynamic instability.

For more details on TSI wind gust pressure, the pressure coefficient  $C_p$  acting on leeward and windward sides of the trailer is also calculated in this investigation. Figure 5-30, depicts time-dependent pressure coefficients acting on leeward and windward sides of the trailer under the

TSI wind scenario. The calculation of pressure coefficient was along the lines on the leeward and windward surfaces of the trailer. The lines are parallel to the ground at height equal to the height of trailer box centre. It can be seen from the figure that the variations in the pressure coefficients are significant large (i.e., from about  $C_p=0.03$  to about  $C_p=5.8$ ) with positive values on the windward side of the trailer. The figure also demonstrate that the value of the pressure coefficients change monotonically and consistently with the size of the TSI wind gust speed. Therefore, effects of this parameters (pressure coefficient) on the vehicle roll stability will investigate further in Chapter 7.



Figure 5-30 : Time dependent pressure coefficients along a line on the leeward and windward sides of trailer in the TSI gust scenario

The average  $C_p$  on the windward and leeward faces of the tractor and semitrailer units under the TSI gust scenario were also computed (for the monitoring points shown in Figure 5-24) and are shown in Table 5-3. The resulting difference in pressure coefficient ( $\Delta C_p$ ) between windward and leeward faces for each unite of the vehicle was calculated and is shown in Table 5-3. For all monitoring point, the differential pressure coefficient  $\Delta C_p$  was found to be dramatically higher for the trailer faces than those of the tractor. This conclusion proves that practically for

developing vehicle crosswind stability/control system it is sufficient to consider wind pressure acting on a trailer unit.

Table 5-3: Pressure difference between windward side and leeward side of the tractor and semitrailer unites

Monitoring points	Average pressure Coefficient $C_p$				Average Differential Pressure Coefficient $\Delta C_p$	
	Tractor faces		Semitrailer faces		Tractor	Semitrailer
	Leeward	Windward	Leeward	windward		
1	0.02	0.07	0.47	1.80	0.05	1.33
2	0.06	0.23	0.85	2.17	0.17	1.32
3	0.19	0.72	3.11	5.32	0.53	2.21

#### 5.6.4 Unsteady aerodynamics loads due to TSI gust condition

Equations 1–8 and 1-9 were used to calculate the unsteady aerodynamic forces acting on the trailer. Figure 5-31 plots these forces acting on the truck, which were predicted based on CFD method by using LES turbulence model. The figure also illustrates that the side and drag forces monotonically increase and decrease consistently with the scale of the gusts speed.

However, the fluctuation of the lift force is marginally different. Also, the vehicle is affected by the maximum gust speed (exponential parts of the TSI gust) for 8 seconds. In this condition, the crosswind speed rises from 13.5 m/sec to maximum 30 m/s ,and the gust effect observed on the aerodynamic side force is practically 2.5 times higher than its effects on the drag and lift forces.

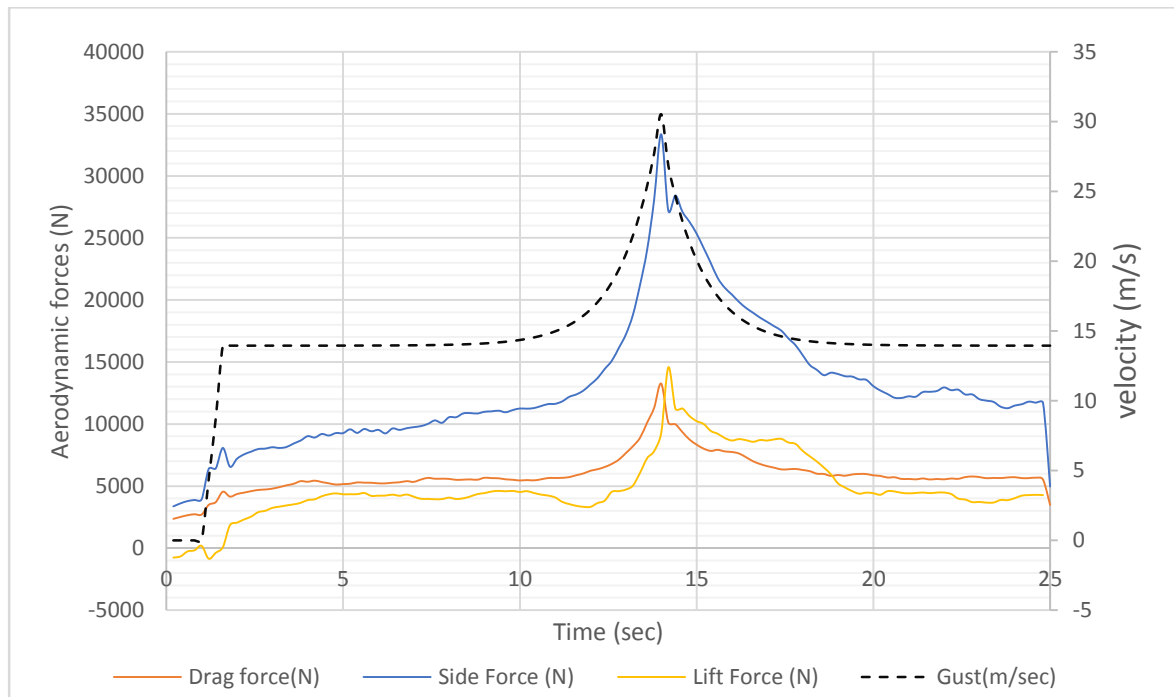


Figure 5-31: Time-history of the unsteady aerodynamic forces under effect of the TSI wind scenario

Under this scenario, the unsteady effects can be more visibly perceived in the reaction of aerodynamic moments (Figure 5-27). Among these, the rolling moment (calculated about roll centre as it will be explained in the next chapters) displays severe instability, when the vehicle was travelling in and out of the gust region. Additionally, the yaw moment also displays the penchant of instability. Regarding duration, such non-linear escalation and reduction of moments are particularly notable and valuable for the appraisal of vehicular movement stability.

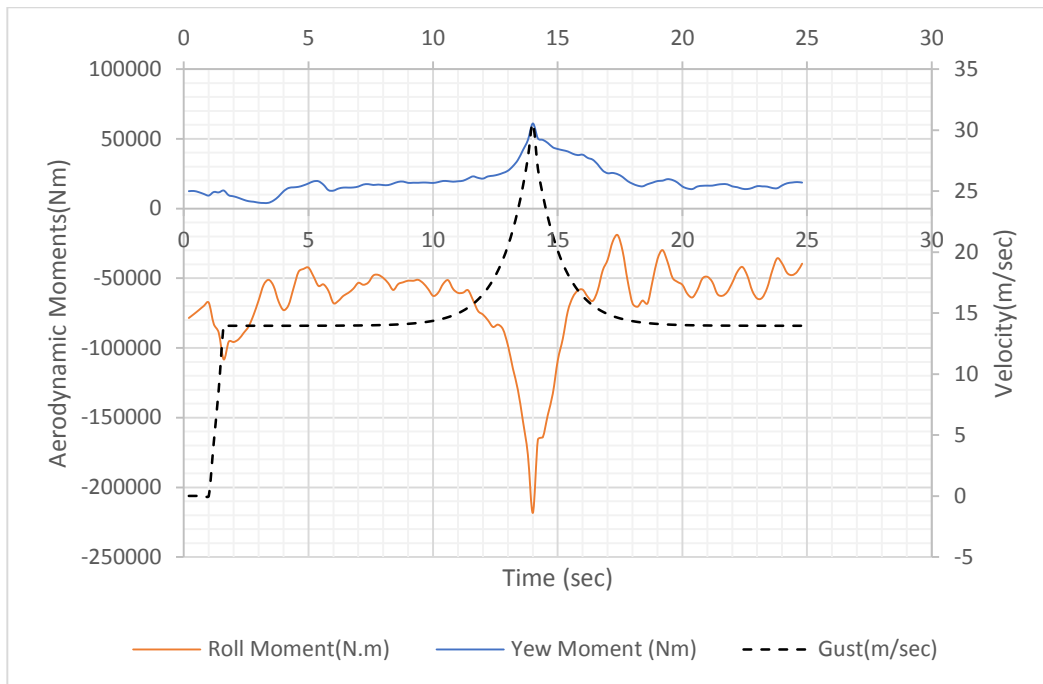


Figure 5-32: Duration of the unsteady aerodynamic rolling and yawing moments in the TSI wind scenario

### 5-7 Summary

This chapter provides prediction of transient crosswind forces acting on a high-sided tractor semitrailer vehicle moving in high crosswind conditions. Two different wind gust scenarios (empirical and standard (TSI)) were applied to the vehicle to predict the aerodynamic forces in two different situations. For comparison between the two methods/scenarios, the wind-tunnel scenario represents a real wind turbulence (not modelling) signal for this condition, which play important roles in prediction of crosswind aerodynamic forces. However, based on wind-tunnel flow, several space-time distributions of the wind speed which satisfy the air turbulent flow properties can be generated. Therefore, the extreme wind loads were predicted by deterministic gust model that was developed in the TSI standard for design purpose.

Moreover, both full scale and scaled vehicle model have been taken into consideration. A series of time-dependent aerodynamic interactions on the tractor-trailer unit have been recorded and investigated. The transient aerodynamic side force and rolling moment were observed to be significantly higher than other aerodynamic forces. As well as, there are significant variations in

aerodynamic forces, in particular side force consistent with the gust's strength. Also, the obtained results based on flow field analysis, give some insight into the aerodynamic behaviour of commercial vehicles under gusty crosswind environment. From this analysis for example, it has been noted that the gust flow distribution around the trailer body is very complex and non-uniform. It accelerates dramatically at the upper surface of the vehicle with high circulation, in contrast, the flow speed is very low at the leeward side surface

Furthermore, based on wind-tunnel data, new wind gust model has been developed. These conclusions strongly suggested the significance of considering the unsteady aerodynamic forces in the analysis of large vehicle roll stability.

## **Chapter 6 : Effects of gusty crosswind conditions on tractor semitrailer vehicle dynamics and its roll stability**

---

As high crosswind forces are a road safety issue for a high-sided commercial vehicle, in this chapter, detailed information about the behaviour of the vehicle at crosswind (i.e. dynamic responses) is desirable. Moreover, since an accurate rollover index is necessary for a precise rollover threat detection and prevention ‘control’ system, unsteady aerodynamic forces based on experimental and numerical results will be applied at the tractor semitrailer vehicle under several manoeuvres. In addition, improvement in performance of the traditional LTR has been introduced.

## 6.1 Coupling unsteady aerodynamic forces to a tractor semitrailer motion

Based on multi-body dynamics and aerodynamic forces, a general equation of motion of the vehicle system is obtained which is as follows [164]:

$$\mathbf{M}\ddot{\mathbf{X}} + \mathbf{C}\dot{\mathbf{X}} + \mathbf{K}\mathbf{X} = \mathbf{P} + \mathbf{P}_w$$

where the symbols  $\mathbf{M}$ ,  $\mathbf{C}$ , and  $\mathbf{K}$  are the mass, damping and stiffness matrices respectively.  $\mathbf{X}$ ,  $\dot{\mathbf{X}}$  and  $\ddot{\mathbf{X}}$  are the displacement, velocity and acceleration vectors respectively.  $\mathbf{P}$  is the generalized load vector and  $\mathbf{P}_w$  is the vector of wind loads.

The aerodynamic loads can be coupled to the vehicle dynamic model via a full dynamic coupling (two-way) or via a static coupling (one-way). For the two-way coupling approach, the position of the vehicle is chosen to be updated at every instant from the vehicle dynamics model. For the one-way coupling approach, the aerodynamic loads are first computed without feedback from the vehicle dynamics model and then used as an input to the vehicle dynamics model in computing the motion of the vehicle [46]. Fully and one-way coupled approaches were compared in [165] for a ground vehicle, the results show that the differences in tested dynamic responses of the vehicle between the methods were small.

In this study, a one-way coupled simulation of unsteady aerodynamics and vehicle dynamics has been applied to a high-sided tractor semitrailer vehicle which has been subjected to sudden crosswind loads. Furthermore, ADAMS solver allows the user to write customized FORTRAN/C++ routines or to import experimental/numerical data to incorporate forces, constraints, and motions that are not included in the ADAMS libraries. In current work, time-dependent splines tool has been used to incorporate the tractor semitrailer aerodynamic forces into the ADAMS model. The spline tool (see Appendix C) contains the x and y data points, which were used for applying external (e.g., aerodynamic) forces and ADAMS spline functions “AKISPL” was used to interpolate the discrete data.

Based on this method (as shown in Figure 6-1), the aerodynamic loads were applied to the system through a V-FORCE element which was located at the wind pressure centre. Figure 6-2 shows an example of aerodynamic forces (calculated from wind-tunnel data), and was imported to the full ADAMS model and acting on the trailer at pressure centre, (i.e. output of VFORCE element).

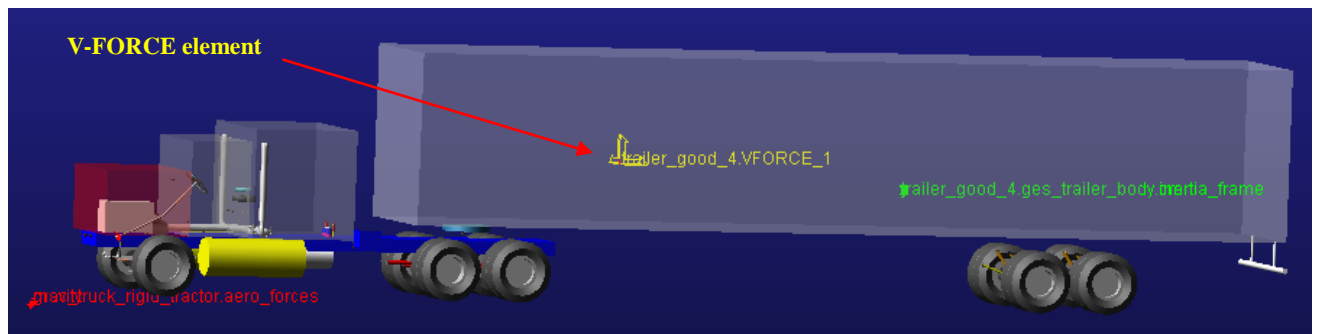


Figure 6-1: Aerodynamic center on ADAMS model

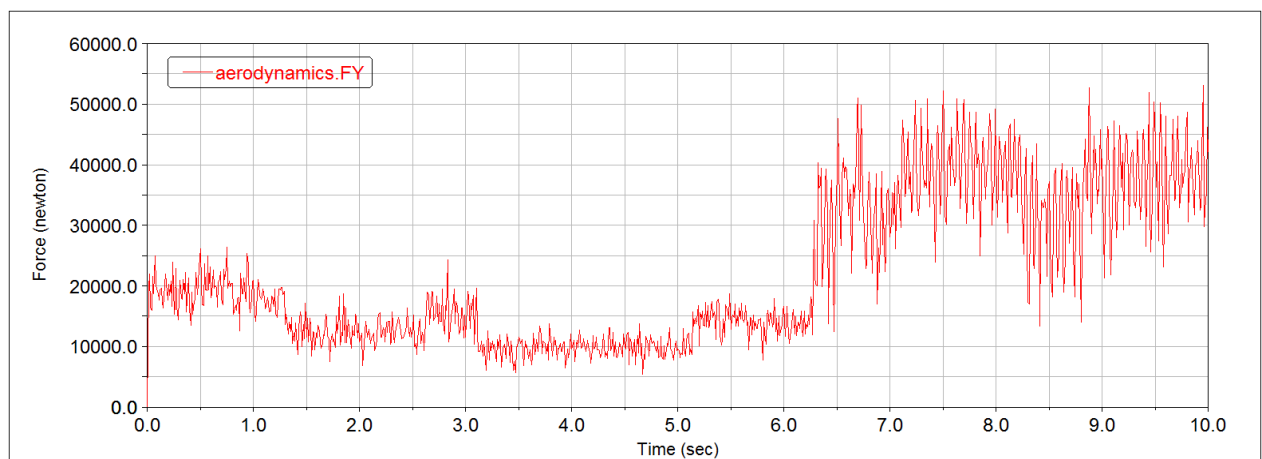


Figure 6-2: Transient crosswind scenario imported to ADAMS environment to perform dynamic analysis

## 6.2 Dynamic responses of a high sided tractor semi-trailer vehicle to gusty wind conditions

In this section, investigations were carried out to assess the influence of gusty crosswind forces on dynamic behaviour of a semi-trailer tractor vehicle. The vehicle dynamic state such as lateral displacement, roll angle and yaw angle are often used as indicator for evaluation of the

vehicle crosswind stability[166]. Therefore, for the purpose of this study, these parameters have been chosen for dynamic analysis and were calculated at the mass centre of each unit of the vehicle.

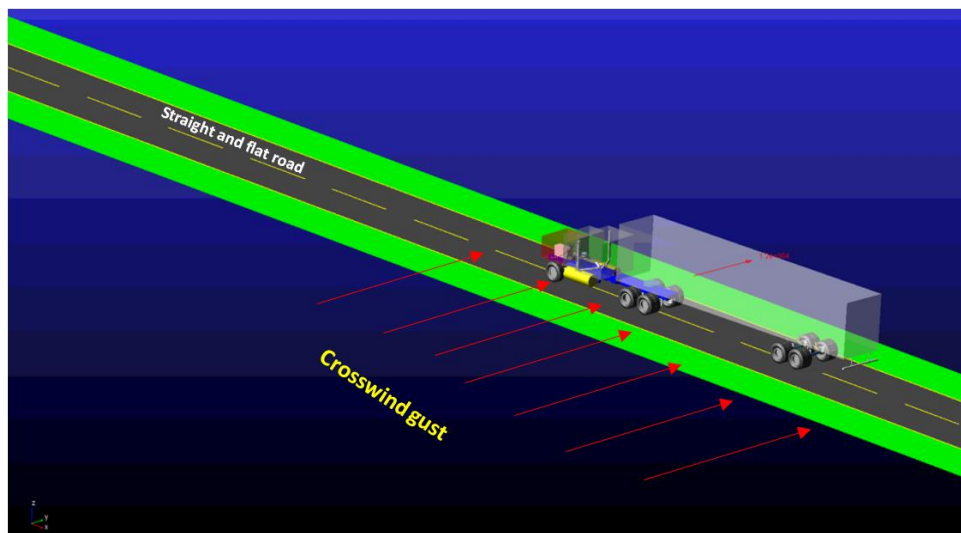


Figure 6-3: Schematic view of objective simulation test

Initially, the aerodynamic loads will be considered as main destabilising factors (i.e. road geometry effects were ignored), and straight-road test manoeuvres have been simulated using the coupled wind –vehicle model which is presented in section 6.1.

As shown in Figure 6-3, in this simulation, the vehicle is driving with a constant velocity of 25 m/sec and assumed to be going straight ahead under wind excitations on a flat road, with zero slip ratio (i.e., no accelerating or braking). During the manoeuvre, the tractor semitrailer moves a total longitudinal distance of 200m, over which it experiences moderate to strong wind loads (see Figure 6-4).

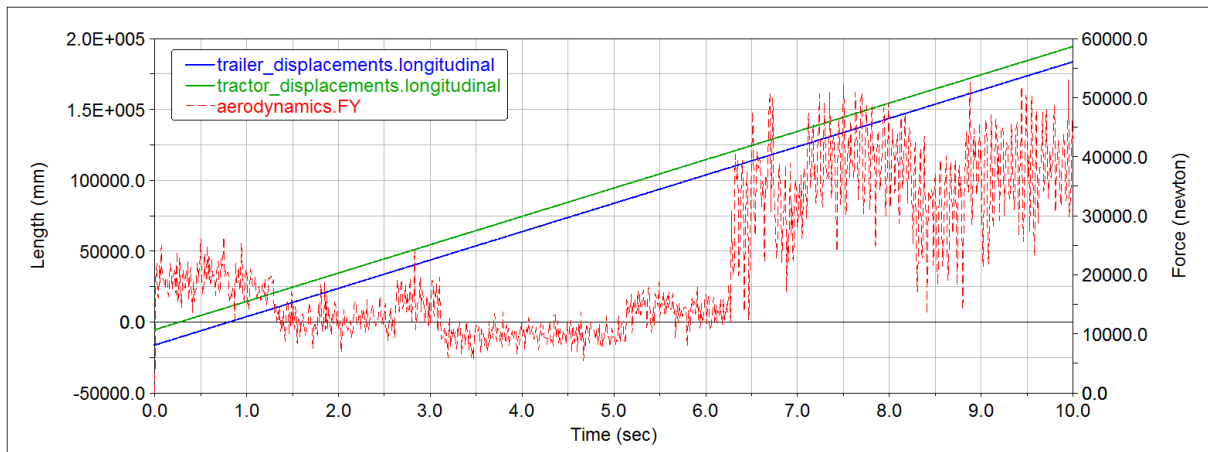


Figure 6-4: Time-history of a longitudinal displacement travelled by the tractor and trailer units during straight-road maneuver in random wind-gust scenario

In addition, the simulations are conducted for transient vehicle aerodynamic forces under both the TSI gust scenario and wind-tunnel gust environment that were computed in the previous chapter. The vehicle's aerodynamic centre (wind pressure centre) was assumed as fixed to the trailer body. For the TSI gust, location of the pressure centre was calculated at the maximum wind speed of the gust, based on option available in the ANSYS fluent solver (further discussion in next chapter).

For the wind-tunnel gust, the pressure centre is assumed at a point just opposite to the sampling point. Further details about effects of pressure centre locations on the vehicle responses to wind conditions are presented in Chapter 7.

### 6.2.1 Effect of crosswind gust on tractor semitrailer lateral dynamics

Figure 6-5 describes the lateral displacement of the tractor and trailer units during the straight manoeuvre in normal condition without crosswind effects. The graph shows that there has been a slight difference (not more than 20mm) between the lateral displacement of tractor and trailer units. Also, the results of this manoeuvre do not show any significant increase in the lateral displacement of the combination, and maximum lateral displacement of 10 cm for the mass centre of the trailer unit in normal operation is acceptable value [1]. This small-deflection

from the initial position (at t=0 sec) is due to lateral forces generated by tire and suspension components. As well as, this results confirm the lateral stability of this model in normal operation (without wind effects).

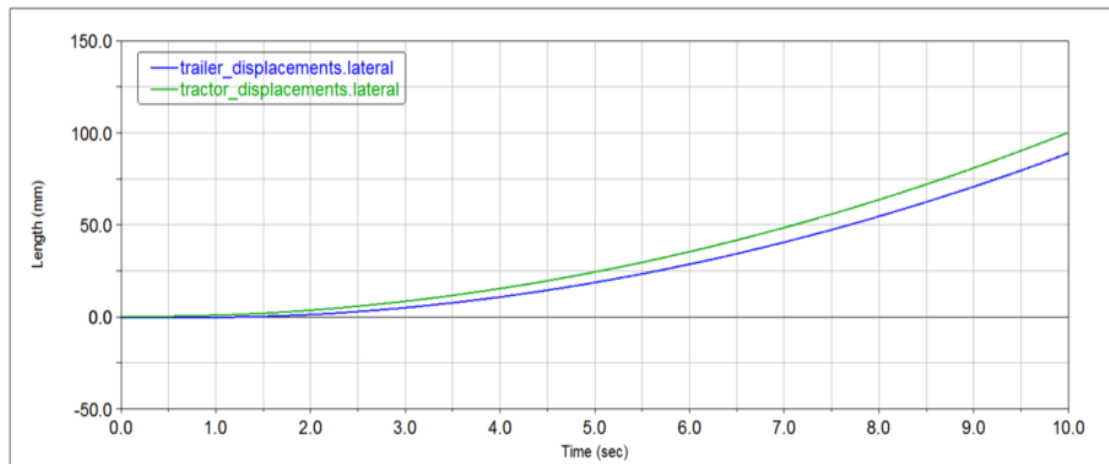


Figure 6-5: Lateral displacement of tractor and semitrailer units without crosswind effects

For comparison, the simulation was run under the same straight manoeuvre but in different gusty crosswind conditions. Depicted in Figures 6-7 and 6-8, are the time histories of the lateral displacements of the vehicle under the transient wind-tunnel gust scenario and the TSI gust respectively.

In both cases, due to unsteady aerodynamic forces caused by the crosswind, the vehicle drifts in the lateral direction and deviates from the original path. Figure 6-6 shows the lane offset (the lateral displacement between the longitudinal central lines of the vehicle in the initial status and in the end of manoeuvre). This variable gives an indication of the level of lateral control that driver has to apply over the vehicle under such conditions.

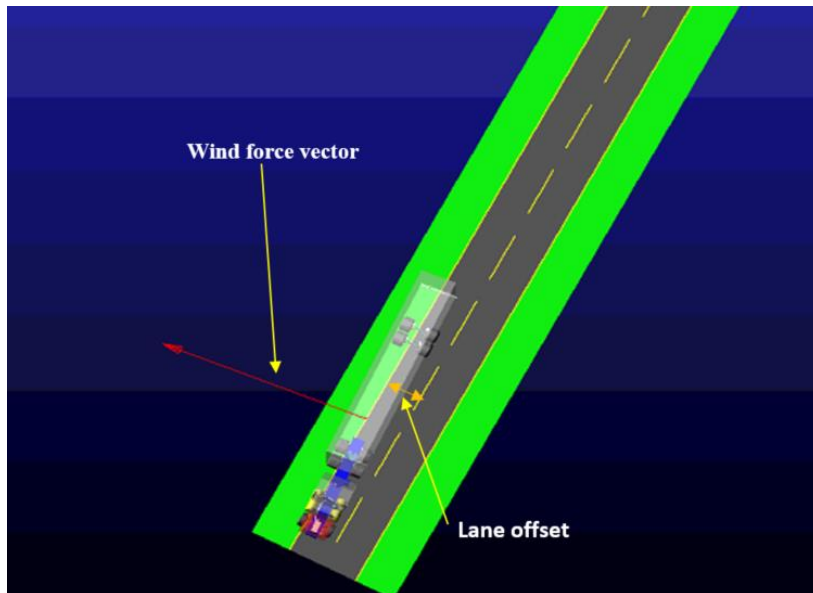


Figure 6-6: Snapshot of vehicle lateral position at the end of maneuver (under transient (wind-tunnel) wind scenario)

In the transient wind gust scenario (Figure 6-7), the vehicle experiences large lateral displacement when exposed to extreme crosswind loads which is from  $t=6.5$  sec to  $t=10$  sec. In this period, the lateral displacement of the trailer unit starts to vary dramatically from about 800 mm at  $t=6.5$  to 2500 mm at the end of the manoeuvre.

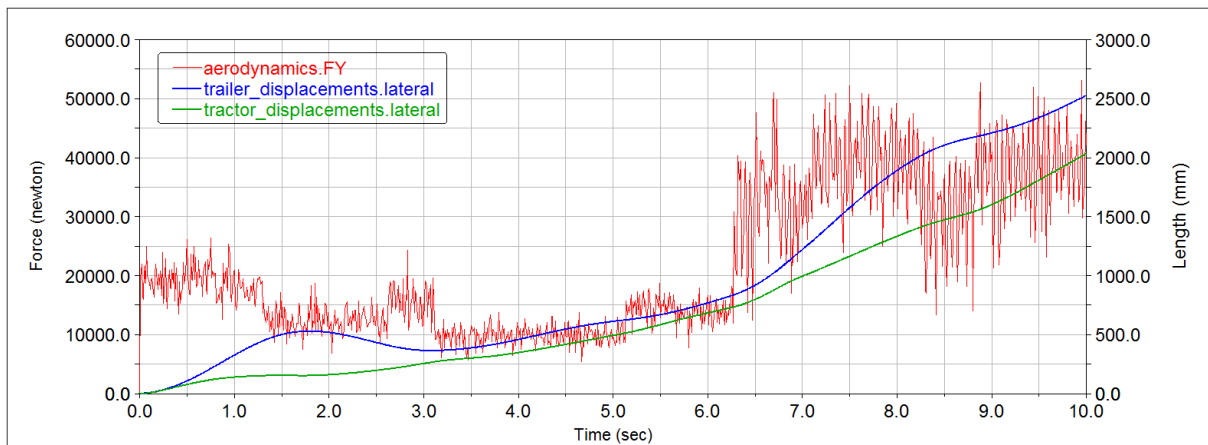


Figure 6-7: Lateral displacement of tractor and semitrailer units under transient crosswind scenario

Figure 6-8 presents the simulation results obtained during the straight manoeuvre under the TSI gust. The results are for lateral responds of the trailer and tractor unites. For the both units,

lateral displacements increase gradually from 0 mm to about 750mm. as the figure indicated, regardless of transient actions acting on the vehicle's body under the TSI gust, smooth lateral responses were observed for this manoeuvre. for the trailer unit(blue line of the graph), however, at the maximum wind gust period (from 13 sec to 16sec), the lateral response is affected slightly by the transient side aerodynamic force . Furthermore, a similar trend in the lateral displacement under the previous gust scenario was observed from the above figure. However, side displacement values and fluctuations are about 25% higher in the random gust scenario particularly for the trailer unit. These differences are because of variation in wind loads that are exerted on the vehicle's body during the random gust scenario.

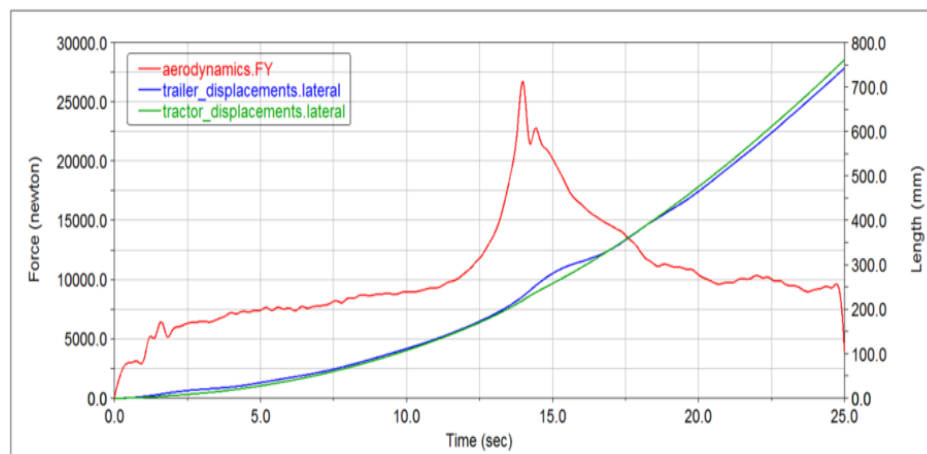


Figure 6-8: Lateral displacement of tractor and semitrailer units under TSI gust model

### 6.2.2 Effect of crosswind gust on tractor semitrailer rotational dynamics

Time series of the yaw angle for the tractor semitrailer driven in straight road under wind-tunnel and TSI gust effects are plotted in Figures (6-9 and 6-10) respectively. In both scenarios, the simulation results for yaw response of the tractor units show a trend similar to that observed for the trailer. However, variations in yaw displacement show lower amplitude for the trailer unit with a time delay compared with the tractor.

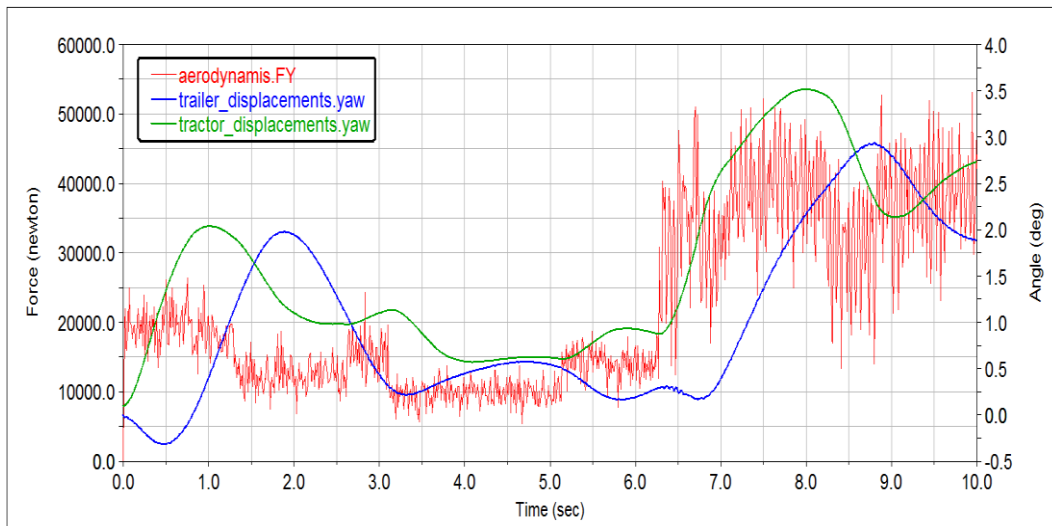


Figure 6-9: Yaw response of tractor and semitrailer units under transient crosswind scenario

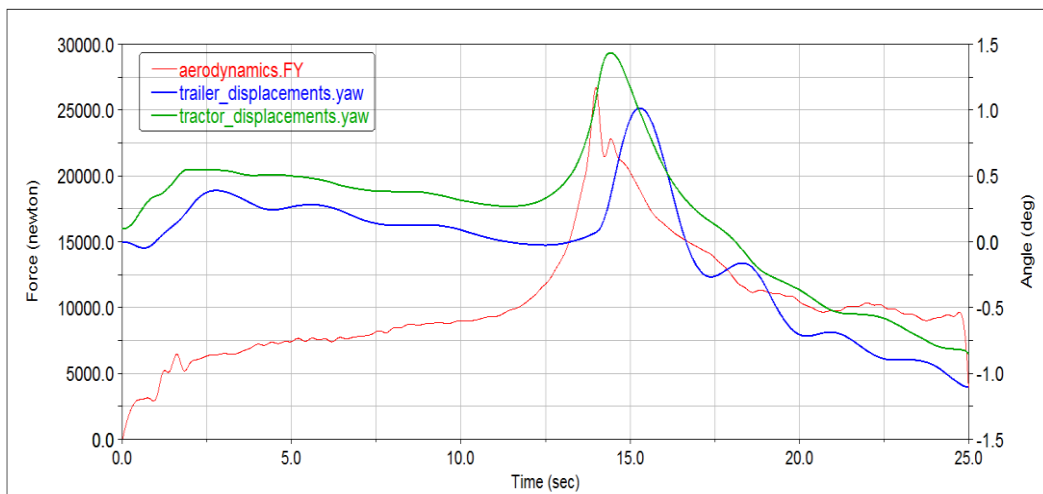


Figure 6-10: Yaw responses of tractor and semitrailer units under TSI gust model

The graphs also show that variations in yaw angle over time during random wind gust (wind-tunnel gust) are higher than those under the TSI gust. In spite of that, these variations in both cases are relatively small with maximum yaw angle of 3.7 degree under the artificial (wind tunnel) gust, and ~1.4 degree in TSI gust. These results show that crosswind yaw instability of the vehicle is not significantly because considerable changes in the yaw angle can be produced by changing the vehicle speed or changing in the wind attack angles.

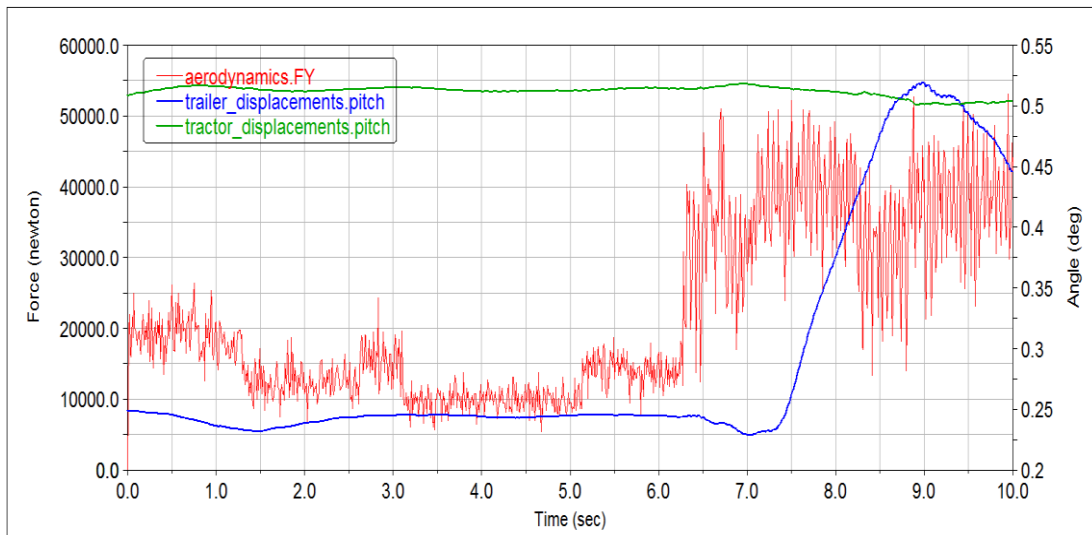


Figure 6-11: Pitch motion of tractor and semitrailer units under transient crosswind scenario

Moreover, as shown in Figures 6-11 and 6-12, the results suggest that the pitching motion of the vehicle may have weak coupling effect with transient crosswind conditions. Thus, pitching motions are neglected in formulating a model focused mainly on study of roll propensity.

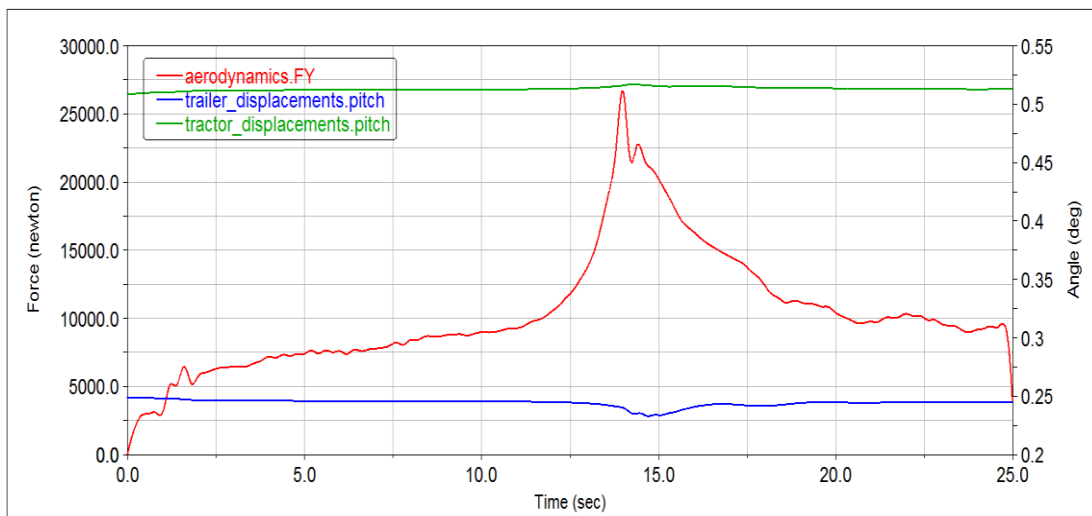


Figure 6-12: Pitch motion of tractor and semitrailer units under TSI gust model

In the case of semitrailer tractor roll dynamic response, Figures 6-13, 6-14 and 6-15 provide simulation data of straight manoeuvring with and without wind effects. As can be seen from the figures below, under wind loads, substantial differences are evident between the relative rolling displacement of the trailer and that of the tractor.

Moreover, the changes in roll displacement due to random gust conditions (wind-tunnel gust) are larger than those of the TSI gust scenario. Compared with Figure 6-14, the rolling response of the vehicles in the random gust (i.e., Figure 6-13) increases dramatically over the gust period (i.e. from 6 to 10 seconds). These differences in the roll angle are caused by the differences in aerodynamic forces coming from the change in wind velocity under each crosswind scenario. To verify this observation, Figure 6-15 shows slight increase in the roll angle (nearly 0.02 degree) during simulation of straight manoeuvre without crosswind actions when compared with the former two displacements.

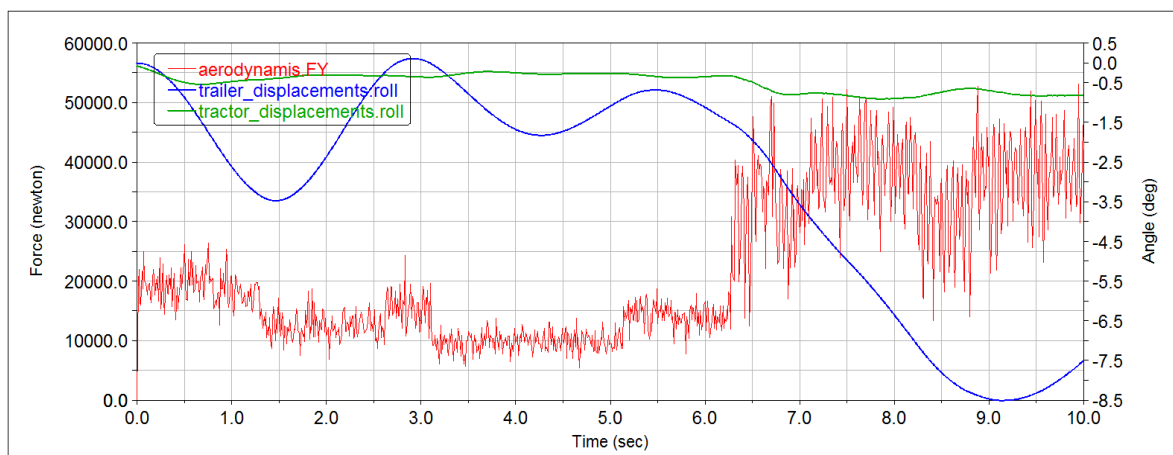


Figure 6-13: Variation in roll angle of tractor and semitrailer units under transient crosswind scenario

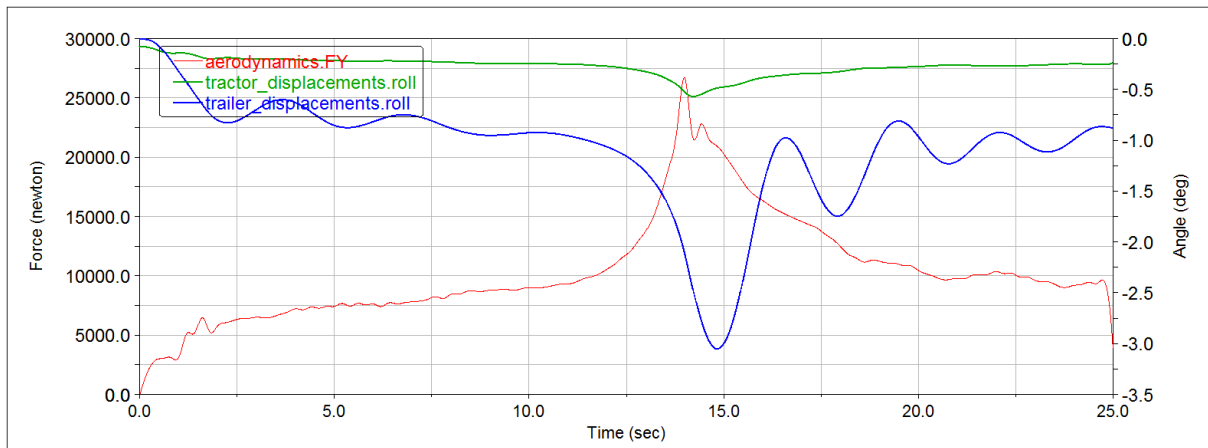


Figure 6-14: Variation in roll angle of tractor and semitrailer units under TSI gust model

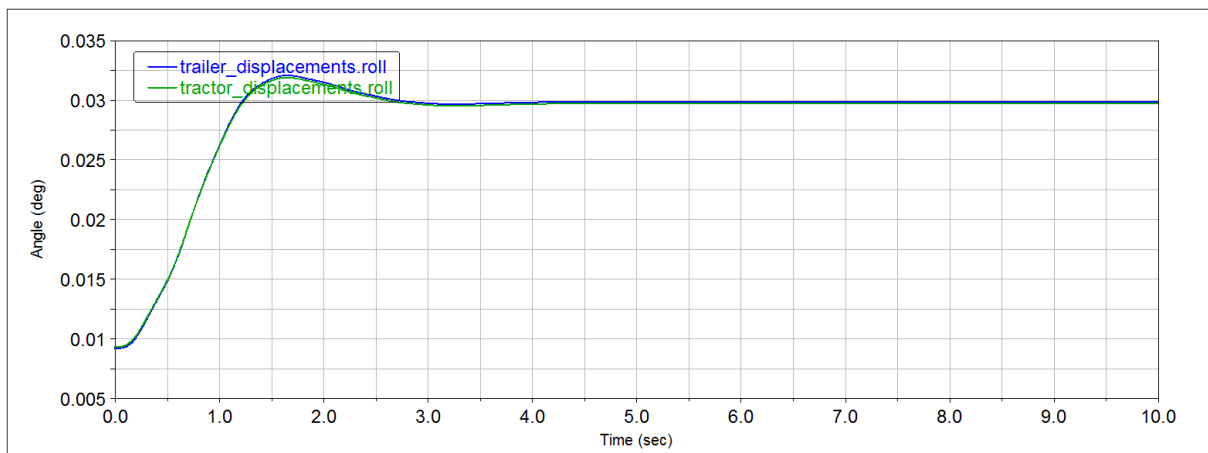


Figure 6-15: Variation in roll angle of tractor and semitrailer units without crosswind effects

### 6.3 Effects of crosswind actions on vehicle steering dynamics

Apart from the wind speed and vehicle speed, the driver's behaviour also has an influence on vehicle crosswind stability. The directional performance of the trailer unit is indirectly controlled from the steering wheel action of the tractor. In this simulation, multibody dynamic program removes the real driver from the simulation and instead uses a closed-loop driver model or open-loop inputs.

In order to investigate how aerodynamic forces, influence dynamic parameters of the high-sided semitrailer tractor, all the simulations were carried out by using the open-loop driver model, i.e. driver feedback is not involved. For example, in Figure 6-16, under random gust, steering angle is recorded as the driver manipulation applied on the steering wheel in the form of an angle.

The figure gives an indication of the driver's behaviour of adjusting a vehicle heading in a straight line to avoid rollover or side-slip events. Also, large variations in the steering angle prove the sensitivity of high-sided tractor semitrailer vehicle to crosswind forces. The amplitude of the steering wheel angles is reported as a parameter strongly related to the driver's perception, and thus the running stability of the vehicle in crosswinds.

Therefore, in such an environment, the vehicle requires accurate steering actions which can be achieved with the help of steering control systems. In contrast, from the data in Figure 6-17, during the same manoeuvre without wind effects, no steering angle input was required to maintain the vehicle on the straight road. The figure shows small initial suspension oscillation from  $t=0$  sec to  $t=4$  sec, but in general the vehicle moves under constant steering angle of  $-10.2^\circ$ .

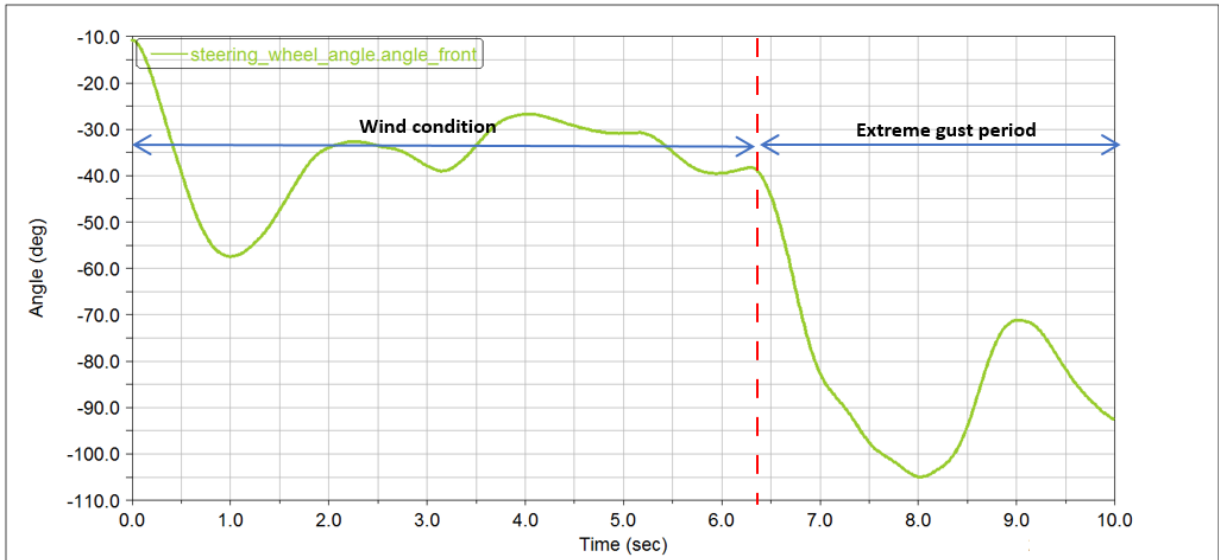


Figure 6-16: Steering angle required for keeping the vehicle on course under transient crosswind actions

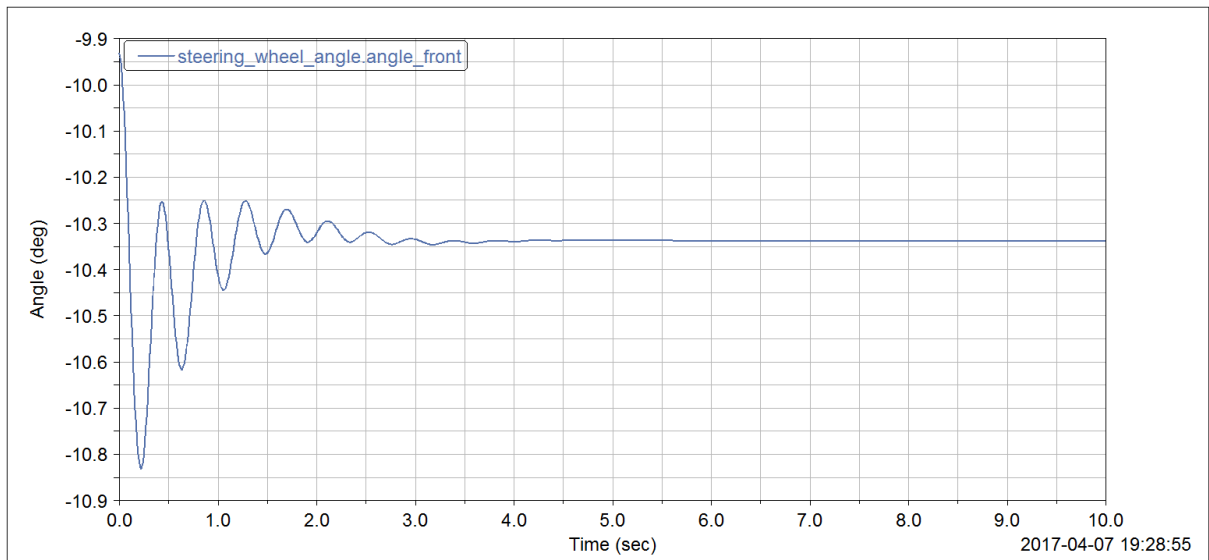


Figure 6-17: Steering angle input without crosswind effects for keeping the vehicle on course

Furthermore, Figure 6-20 also provides demonstration on how steering actions and steering control systems play an essential role for improving vehicle crosswind stability. The figure represent results of straight manoeuvre in random (wind-tunnel) gust scenario without any steering actions (inputs) applied to the vehicle by driver, i.e. steering system was locked (see Figure 6-18).

Consequently, a value of about  $-10.8^\circ$  steering angle was maintained over the simulation period with small fluctuation increases due to suspension dynamics (see figure 6-19). As depicted in figures, results from this condition revealed a critical increase in roll angle of the trailer unit during gust period, i.e. from  $t=6.5$  sec to  $t=10$  sec until rollover occurred (Figure 6-21). Under these conditions, driver's misjudgement may raise concern about the general stability and safety of the vehicle.

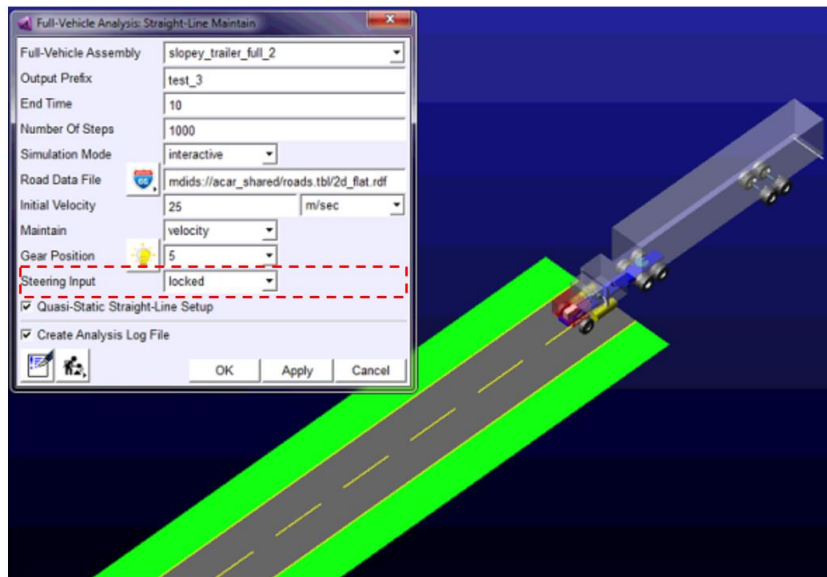


Figure 6-18: De-activate steering input

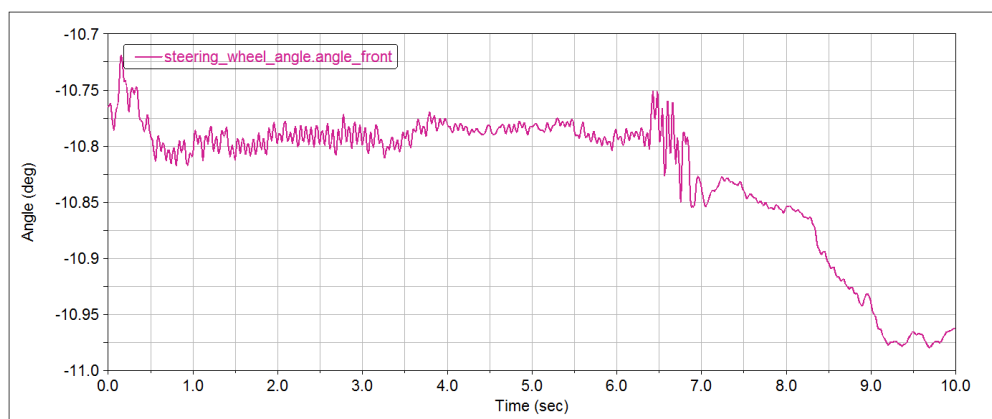


Figure 6-19: Fluctuations in locked steering wheel

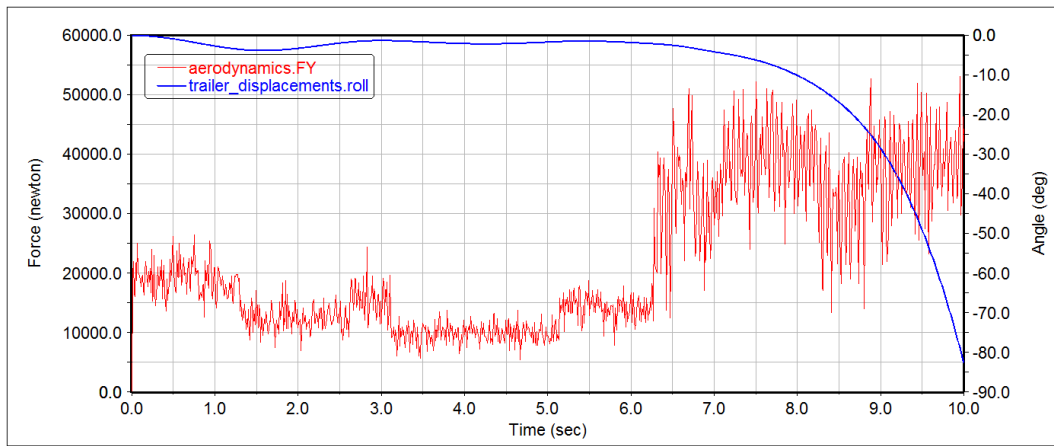


Figure 6-20: Trailer unit roll angle response in straight maneuver under transient crosswind without driver actions

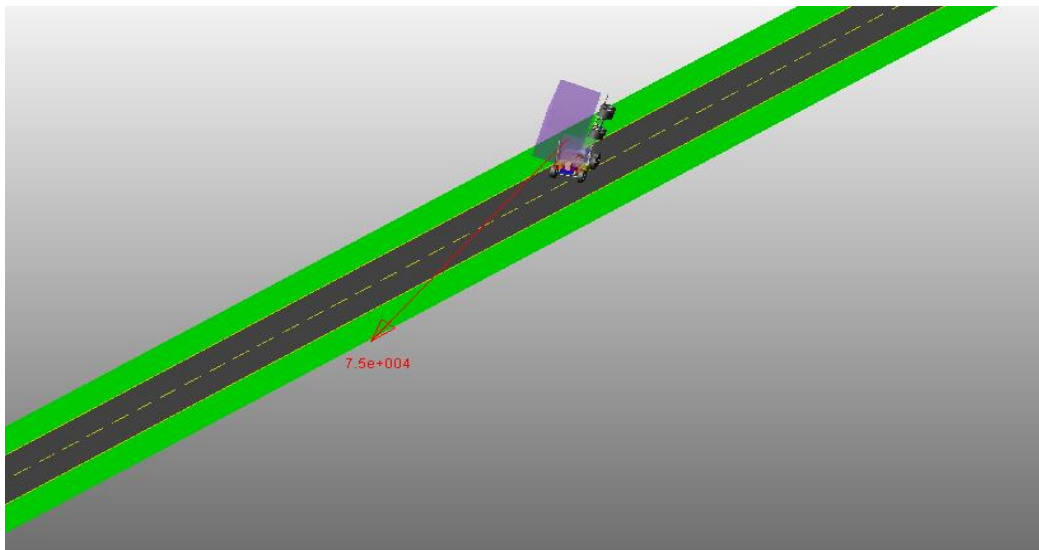


Figure 6-21: Snapshot of rollover event for the trailer unit under transient crosswind conditions without driver actions

## 6.4 Crosswind rollover index

The lateral load transfer (LTR) of the trailer unit in nature differs from the lateral load transfer of the tractor unit. However, according to Boettiger et.al. [167], for vehicles with units partly decoupled, load transfer ratio calculations apply better within a single suspension unit.

In addition, during path-change manoeuvre, the trailer unit is more prone to rollover than the tractor due to the rear ward amplification tendency of the combination [168]. Hence, in this calculation, the contribution due to the tractor unit is neglected. Therefore, the LTR for the

trailer axles ( $R_i$ ) is used as a rollover threat index in this analysis as suggested by the ratio and defined as[37]:

$$R_i = \frac{F_{Zr} - F_{Zl}}{F_{Zr} + F_{Zl}} - 1 \leq R_i \leq 1 \quad (6-1)$$

where  $F_{Zl}$  and  $F_{Zr}$  are the vertical loads of the dual tires on the left and right sides respectively, and  $i$  represents the front and rear axle of the trailer (see Figure 6-22). However, under crosswind condition, the intention is to prevent any wheel from lift-off conditions and so, the normalized lateral load-transfer index for the entire trailer,  $R_t$ , is:

$$R_t = \max(R_i) , i \text{ is rear or front axle} \quad (6-2)$$

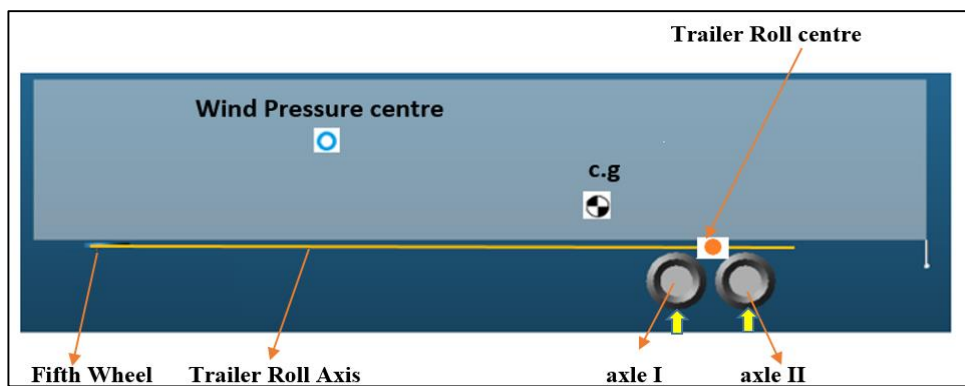


Figure 6-22: Free body diagram of the trailer body

An implementable formula of the LTR can be developed by establishing the balance of vertical forces and roll moments of the sprung and un-sprung mass at roll centre [8, 169]. The roll centre is dependent on the kinematic properties of the suspensions and typically located between the height of the centre of gravity above the ground [170]. Roll model of a forward moving vehicle negotiating a turn is depicted in Figure 6-23. With the assumption of constant roll and pressure centres, the summation and difference of tire forces can be calculated based on forces and moments equilibrium about the longitudinal vehicle axis at roll centre as:

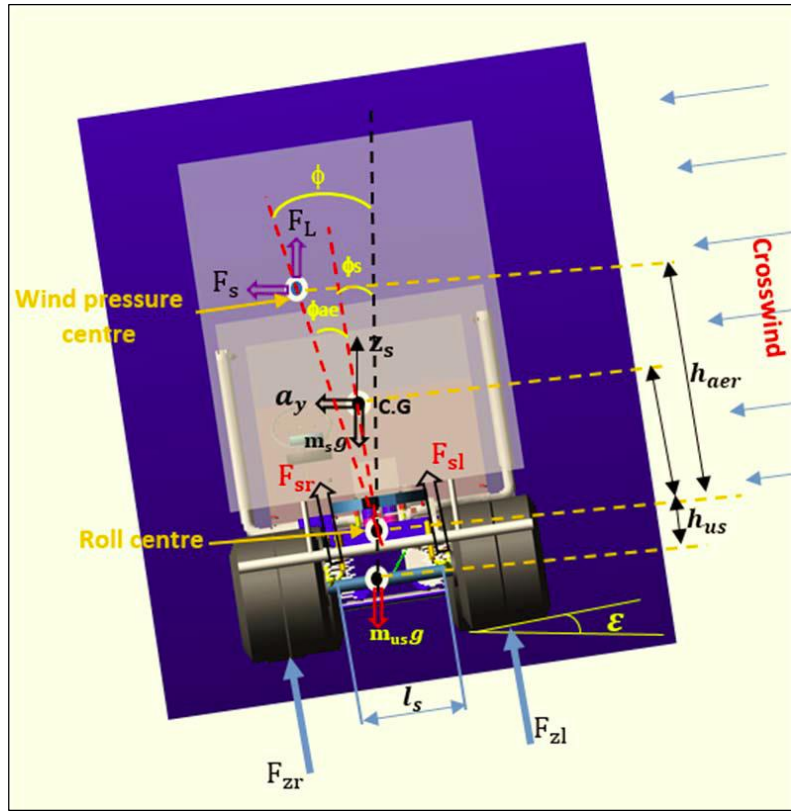


Figure 6-23: Free body diagram for the trailer's roll model

$$F_{zl} - F_{zr} = \frac{l_s}{l_w} (F_{sl} - F_{sr}) + \frac{2}{l_w} [(F_S \cdot h_{aer} \cdot \cos\phi) - (F_L \cdot h_{aer} \cdot \sin\phi) + m_s \cdot g \cdot h_s \cdot \sin\phi_s + a_y (m_s \cdot h_s \cdot \cos\phi_s - m_u \cdot h_{us})] \quad (6-3)$$

$$F_{zl} + F_{zr} = F_{sl} + F_{sr} - F_L + m \cdot g \quad (6-4)$$

the suspension forces are given as [145]:

$$F_{sr} = -k \left( z_s - \frac{l_s}{2} \sin\phi \right) - d \left( \dot{z}_s - \frac{l_s}{2} \dot{\phi} \cos\phi \right) \quad (6-5)$$

$$F_{sl} = -k \left( z_s + \frac{l_s}{2} \sin\phi \right) - d \left( \dot{z}_s + \frac{l_s}{2} \dot{\phi} \cos\phi \right) \quad (6-6)$$

where k is the suspension stiffness, d is the suspension damping and  $Z_s$  is the sprung mass position (monitor point on trailer). Furthermore, as the vehicle is entering a turn of radius R, a centripetal lateral acceleration,  $a_y$ , is generated at vehicle's mass centre, and it is given by [145]:

$$a_y = \dot{v}_y + v_x r_t - (h_s \ddot{\phi}_s + h_{aer} \ddot{\phi}_{ae}) = \frac{v_t^2}{R} \cos \varepsilon + g \sin \varepsilon \quad (6-7)$$

where,  $v_y$  and  $r_t$  are vectors of longitudinal, lateral and yaw velocities at vehicle's mass centre respectively, and  $\varepsilon$  is road camber. This acceleration includes the influence of the lateral tire dynamics.

### 6.4.1 Simulation results

The necessity of a coupled analysis of vehicle aerodynamics and vehicle multi-body dynamics to investigate the vehicle roll stability with a higher accuracy is demonstrated below. The LTR indicator for the trailer's axles when the empty trailer moves straight on a road at high speed of 25 m/sec, with and without crosswind condition are compared in Figure 6-24 for the TSI gust.

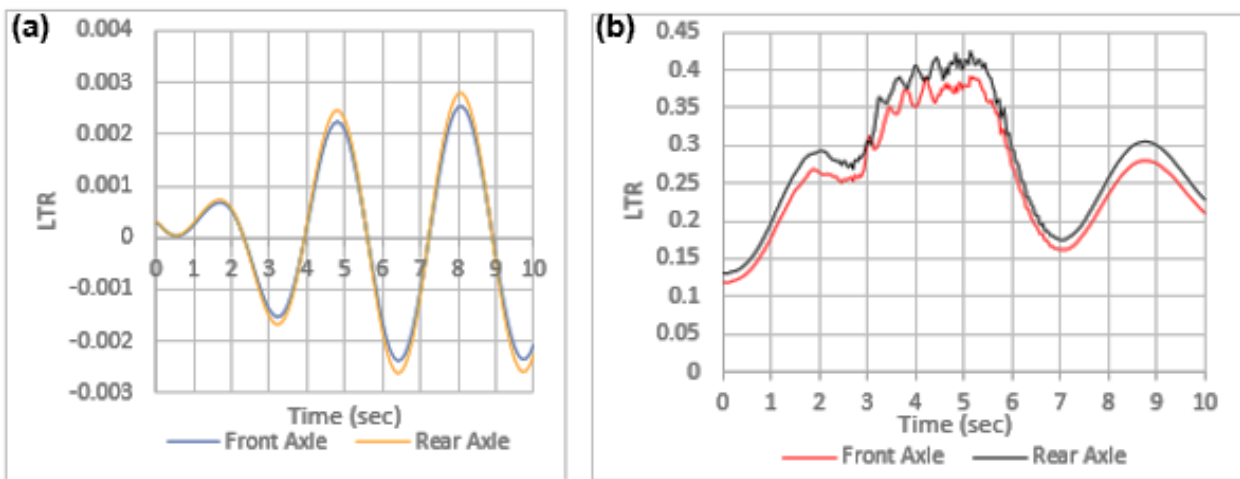


Figure 6-24: Time dependent of the LTR index of the trailer axles (a) Crosswind ignored (b) crosswind considered

As can be seen from the figure, the variations in the LTR coefficient in the presence of crosswind loads are significantly higher than the equivalent LTR coefficient with crosswind ignored. The peak value of the crosswind LTR indicator is nearly 0.43 for the rear axle of the trailer, suggesting a greater aerodynamic moment caused by the wind loads. Moreover, the results (Figure 6-24 (a)) clearly confirm that when the trailer is travelling in a straight road without crosswind, the tires on both sides have equal loads, and the LTR value is nearly zero.

For evaluating the LTR indicator for the trailer axles under crosswind in critical scenario, a rollover manoeuvre was simulated in the ADAMS/Car. The manoeuvre (Figure 6-25) involved a constant radius turning, in which the vehicle is exposed to a high level of centripetal acceleration. In this critical scenario, it is assumed that the vehicle negotiates the curve at high constant speed of 25 m/sec and the wind loads acting at the direction of centripetal force. Although, the crosswind is assumed to be perpendicular to the driving direction of the vehicle all the time, the ADAMS solver can consider the variation in wind directions during curved motion.

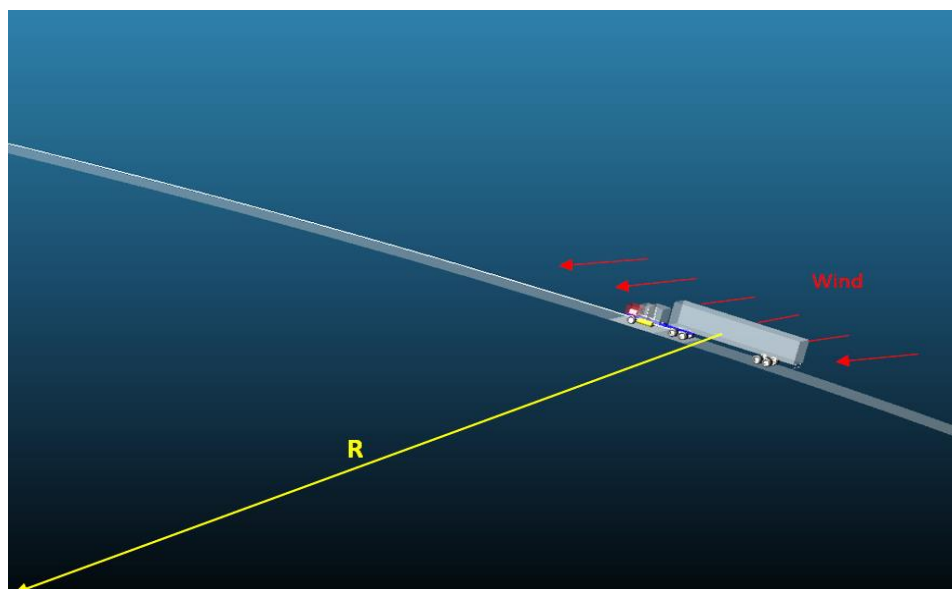


Figure 6-25: Constant radius turning maneuver

Figures 6-26,6-27 illustrate the variation of the LTR index of the trailer axles with/without crosswind actions, when the trailer moves through a curved road with a typical radius of 260 m [27]. In Figure 6-26, at the steady-turning manoeuvre without crosswind effects, the LTR index values for both axles do not change. Under this condition, safety performance of the trailer unit is relatively high, and under the maximum/danger limit of the LTR index, which is at  $LTR = 1$ .

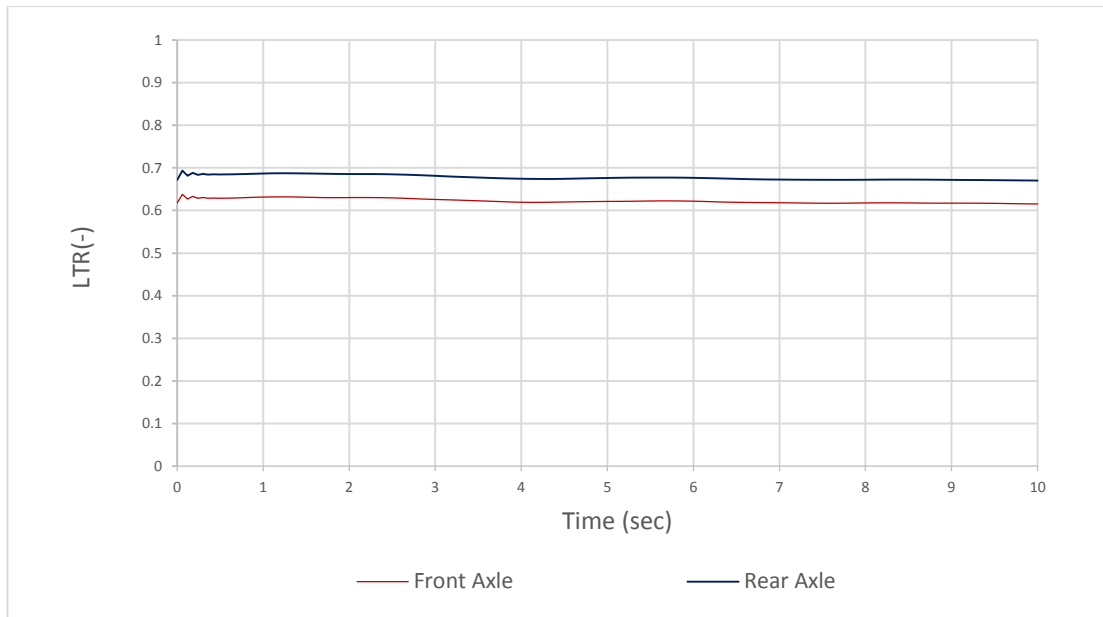


Figure 6-26: Time-history of LTR during a steady-turning maneuver without crosswind loads

However, under a similar manoeuvre, but in crosswind conditions, the results in Figure 6-27 show that the unsteady crosswind actions add transient effects to the steady-state turning manoeuvre. As a result of that, the values of crosswind LTR indices for both axles of the trailer have increased and wheel lift-off condition has been detected for the rear axle of the trailer, see figure 6-27.

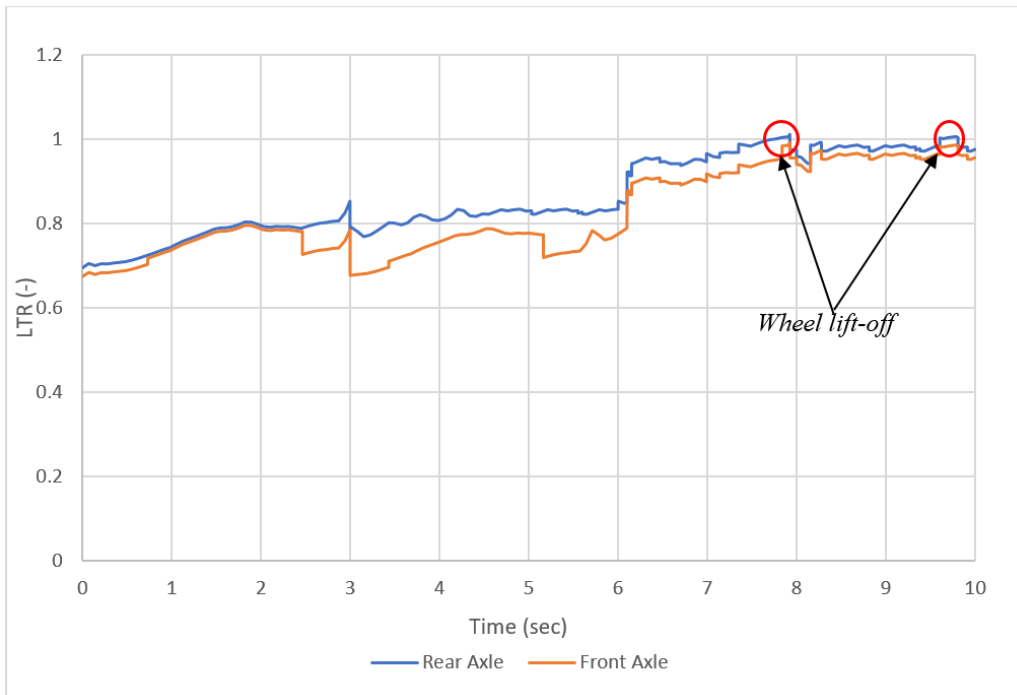


Figure 6-27: Time-history of LTR during a steady-turning maneuver with transient crosswind loads

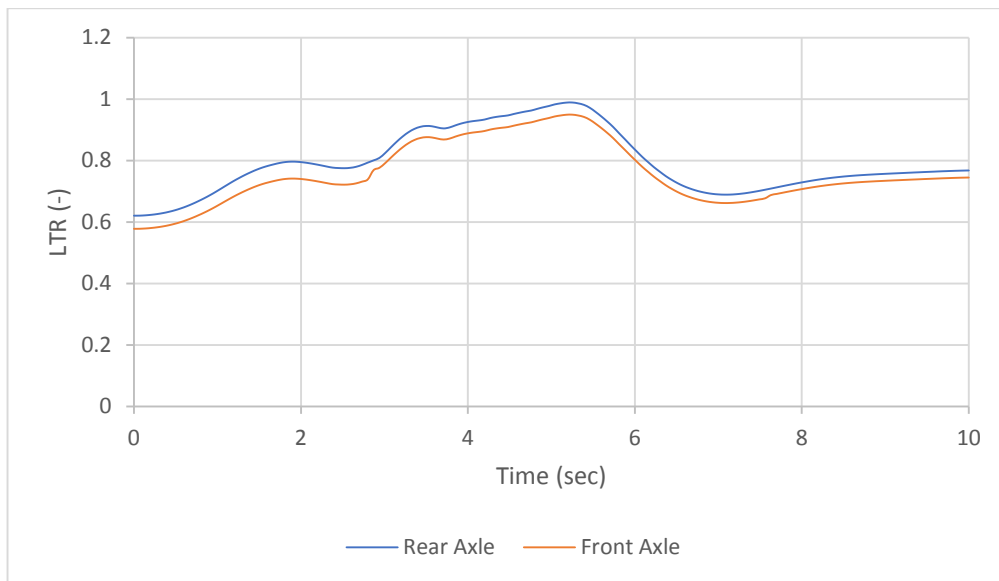


Figure 6-28: Time-history of LTR during a steady-turning maneuver under TSI gust scenario

As shown in Figure 6-28, the trailer is exposed to significant roll moment due to high aerodynamic forces that are imparted into the vehicle from the environment. However, no

wheel lift-off condition has been observed, and LTR response to this artificial gust is with a smooth response curves.

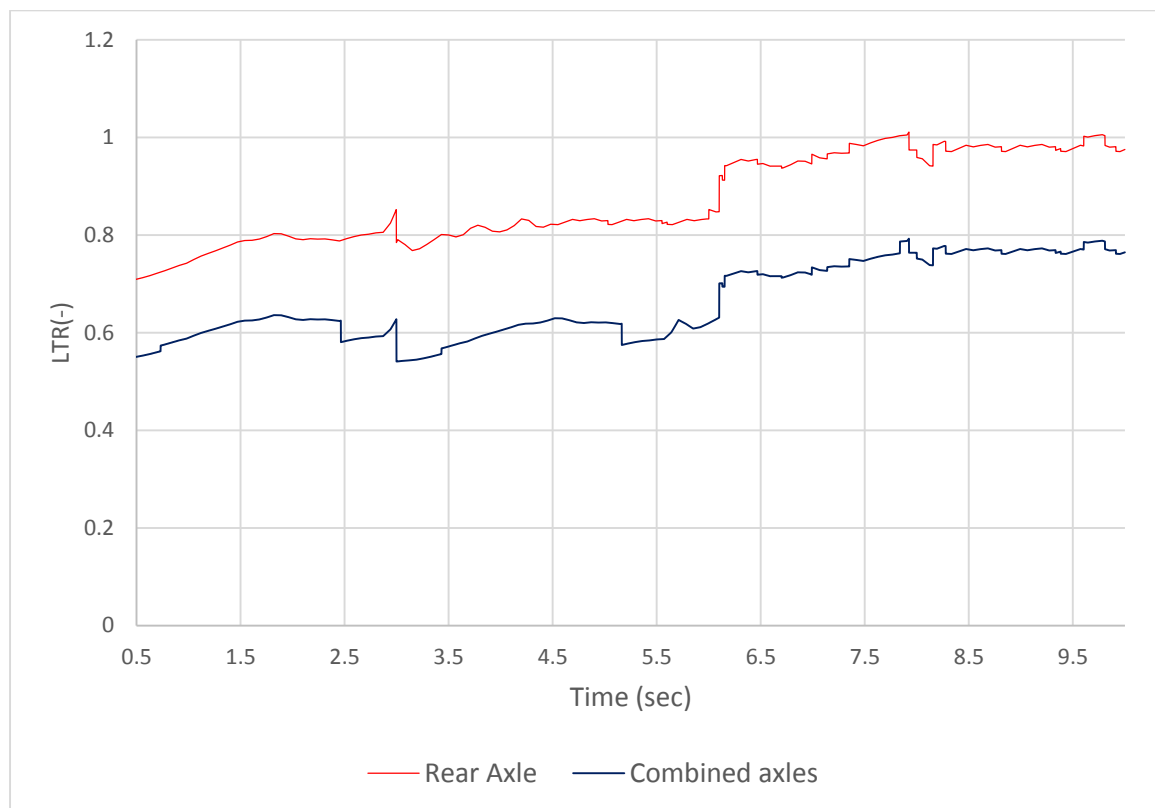


Figure 6-29 : Differences in the trailer's LTR values for rear axle (most affected by wind forces) and LTR values of the trailer computed by traditional definition (i.e., combined axles).

Moreover, a comparison has been shown in Figure (6-29) to justify the use of equation (2-6) in which the estimation of trailer rollover conditions in crosswind are depend on index of each trailer axle individually instead of a traditional method in which the axles are assumed as one axle. It has been seen from the figure that the trend of LTR index predicted by using these two different methods were observed to be similar. However, the maximum value of the index calculated by traditional method (combined axles) is about 20% lower than the LTR index improved by the suggested method in this study. Therefore, the LTR index that calculated based on equation (2-6) is preferred for vehicle rollover monitoring when the transient aerodynamic loads are acting on the trailer's body.

## 6.5 Comparison investigation on coupled aerodynamic and dynamic method

To establish the level of accuracy of the ADAMS results throughout this text, the results obtained from coupled method that has been carried out in ADAMS environment were compared against results of another standard test. For this purpose, in this work, MATLAB/SIMULINK application was used to record and analyse the aerodynamic (CFD) data and ADAMS full vehicle model outputs without aerodynamic effects separately. This approach was established for the purpose of predicting the LTR that can be calculated from equations 6-1,6-3 and 6-4.

By combining ADAMS /Car and MATLAB/Simulink, it is possible to add control algorithms or other forces/velocity to a model developed in ADAMS/Car. The synchronized simulation of the two systems is called a co-simulation (see Figure 6-30). In order to set up the co-simulation environment, ADAMS/Car has to be provided with two modules[171]:

- ADAMS/Controls
- ADAMS/Solver

The ADAMS/Controls module generates a simulation model based on the ADAMS/Car model, which can be imported into Simulink. ADAMS/Solver's purpose is to calculate the result from the equations of motion. During a co-simulation, a closed loop between the ADAMS/Car model and SIMULINK is formed. ADAMS/Car inputs of a model enter the ADAMS/Solver, which calculates the output signals from the model [171].

The ADAMS/Solver output signals enter the SIMULINK model, where MATLAB calculates the model signals and a new iteration starts by sending the model signals as inputs to the ADAMS/Car model. The ADAMS/Solver module is a numerical analysis application that automatically solves the equations of motion for kinematics, static and dynamic simulations for an ADAMS/Car model. The result of the co-simulation can be imported into ADAMS/Car, where plots and animations from the simulation are available [171]. However, in this analysis, this method (co-simulation) is valid only when the aerodynamic pressure centre is fixed.

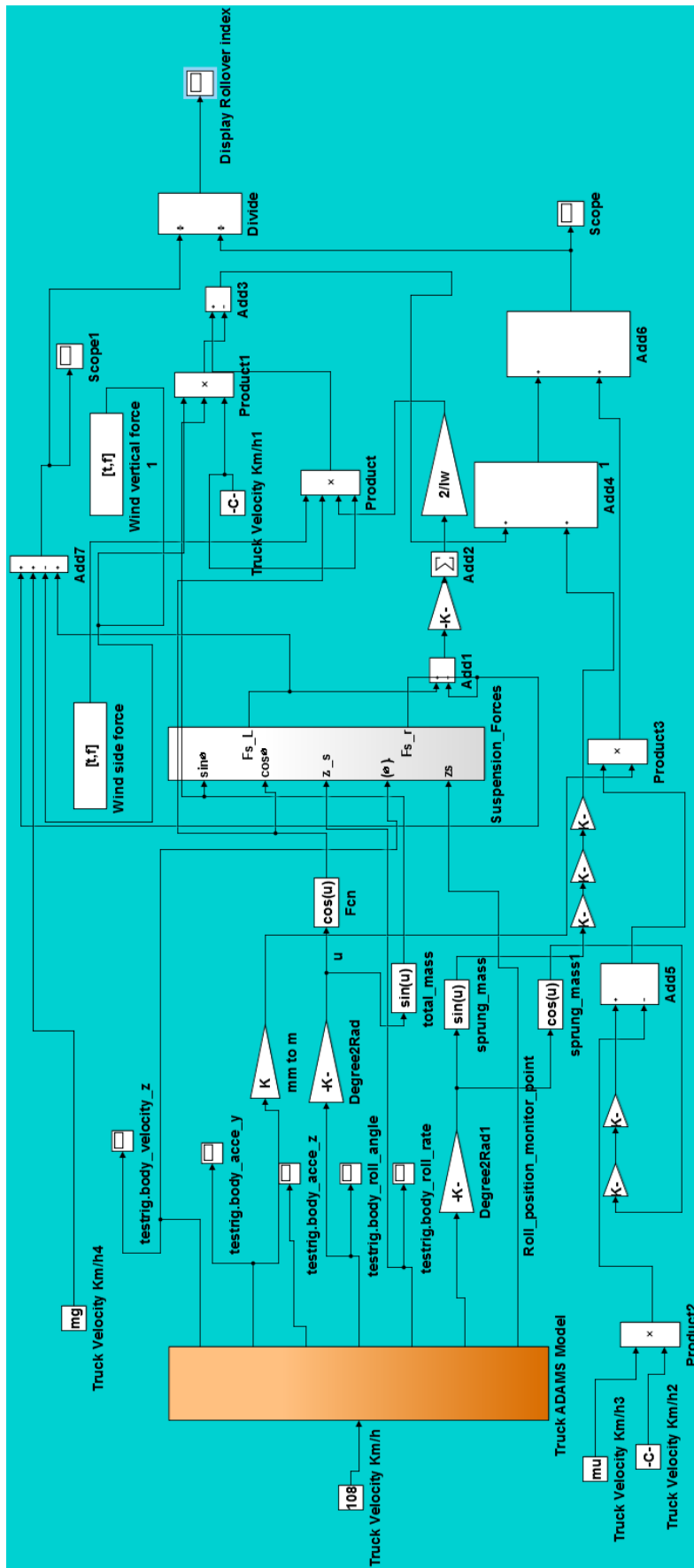


Figure 6-30: Co-simulation method for predicting of LTR index

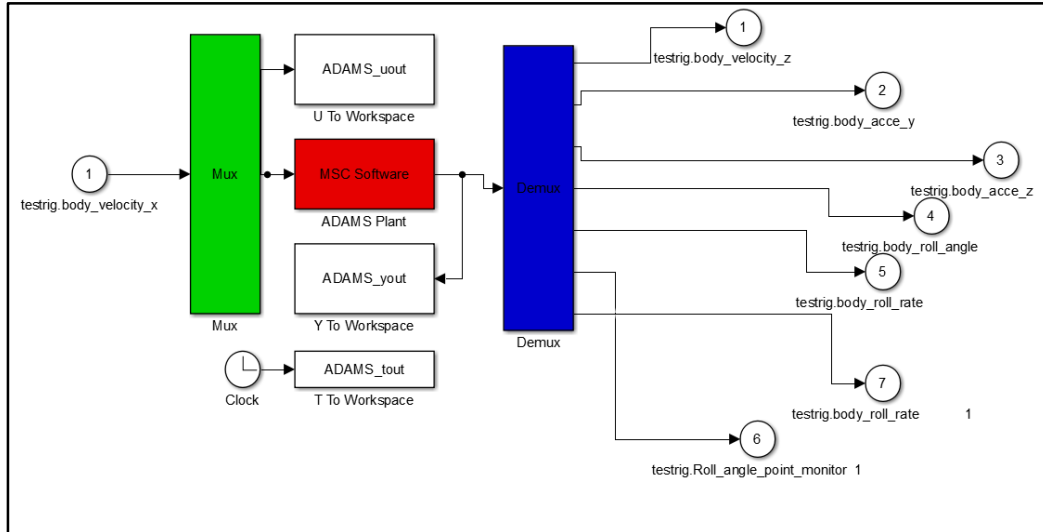


Figure 6-31: Block diagram of truck ADAMS model (state parameters of tractor semi-trailer) estimated with full-order observer in Simulink

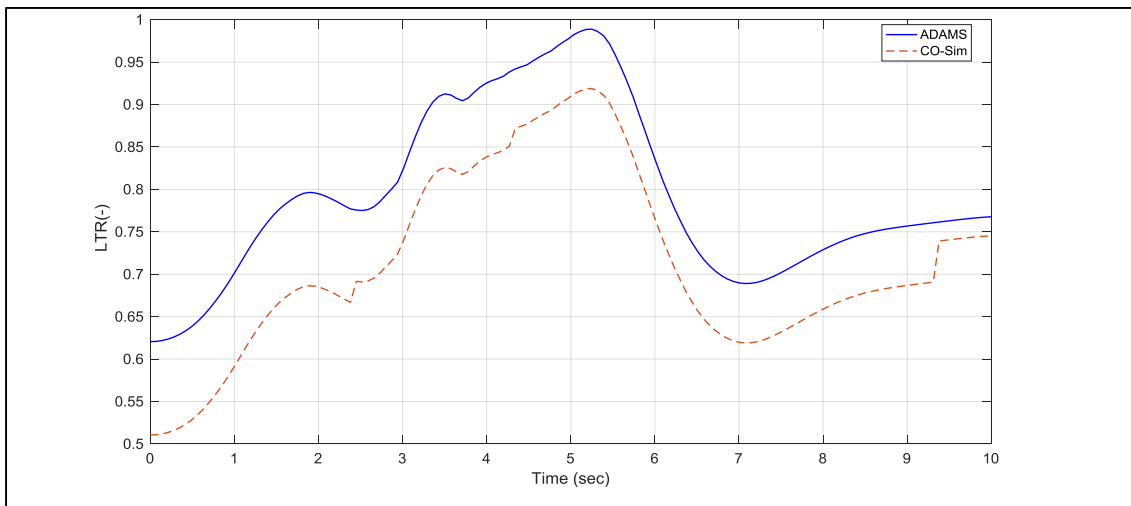


Figure 6-32: Comparison between co-simulation and ADAMS data for LTR of the trailer's rear axle

LTR of the trailer's rear axle is obtained by incorporating aerodynamic characteristics into ADAMS dynamic simulation and is compared with the computed by using the co-simulation method for the TSI gust scenario. Figure 6-32 illustrates the time history of the LTR and it can be seen that LTR computed by co-simulation model correlates very well with that of ADAMS. The slight difference in the responses and the deviation that occurs may be due to the fact that the roll centre in ADAMS is assumed to be fixed with respect to the ground

whereas in the model developed here, the roll centre is assumed to be at a fixed distance from the mass centre of gravity. It can be concluded that the ADAMS software is reliable to provide sufficient accuracy for the purpose of the present work.

### **6-7 Development of characteristic crosswind curve**

Due to the stochastic excitation, it is not possible to determine an exact certain wind speed at which the vehicle rollover can be occurred [157]. However, based on this research's findings, it is possible to develop a characteristic wind curve which represents the relation between wind speed and the rollover safety limit (i.e., LTR as a function of wind speed). To investigate this relation, Figure 6-33 and table 6-1 show values of time-dependent LTR rollover index (for rear axle at where the maximum LTR was observed) corresponding to different wind velocities, which have been selected from the wind-tunnel data. This assumption (i.e., selecting data) has been made to simplify the stochastic distribution of the recorded wind speed.

Table 6-1: wind-tunnel data &LTR

T	velocity (m/s)	LTR(-)
0	14.5217	0.694538
0.5	17.537	0.709692
1	14.6015	0.744542
1.5	12.4118	0.787178
2	11.8305	0.794678
2.5	13.732	0.791438
3	11.7714	0.785994
3.5	14.9679	0.800224
4	12.9918	0.807188
4.5	13.2902	0.822025
5	12.9321	0.829368
5.5	11.8863	0.829112
6	14.5511	0.833103
6.5	22.3	0.946101
7	16.34	0.964874
7.5	30.45	0.984142
8	23.71	0.959053
8.5	21.83	0.982768
9	24.132	0.983707
9.5	25.752	0.977268
10	24.768	0.975427

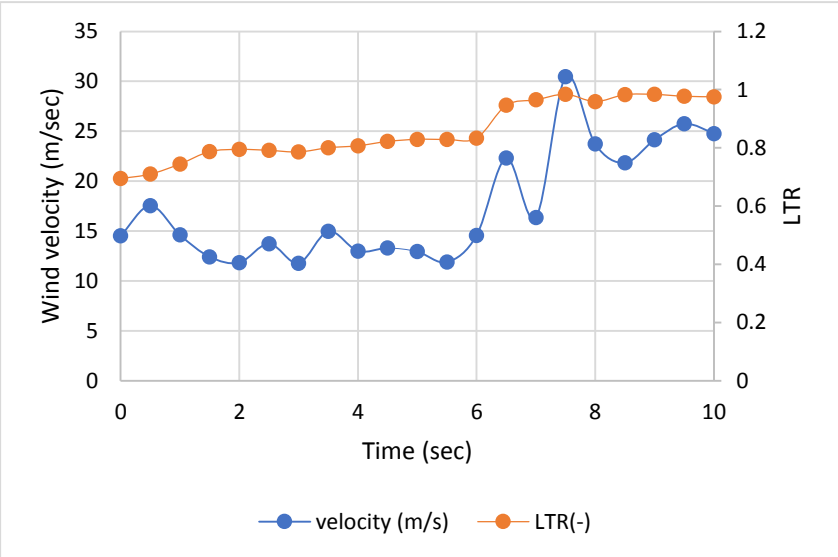


Figure 6-33: Velocity data and corresponding LTR values

Based on this data, Figure 6-34 introduces a curve relating the LTR rollover index and wind speed under constant vehicle speed of 25 m/sec. As it can be seen, the curve passes through the most of selected data, and mathematical relation can be approximated between the rollover indicator and wind speed. This curve is important for investigating of the vehicle operation safety in crosswind, it can be also used for (control) design purpose.

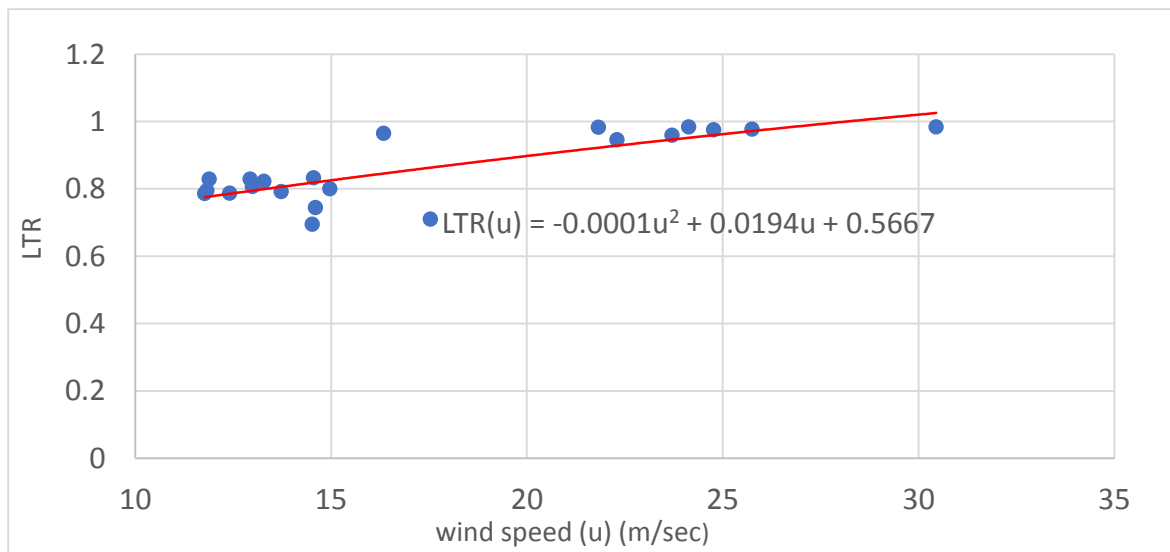


Figure 6-34: Characteristic wind curve

## 6-8 Summary

In this chapter, multi-body simulations coupling with unsteady aerodynamic forces have been performed for high-sided tractor semitrailer vehicle. Based on one-way coupled analysis, dynamic responses of the vehicle to high crosswind conditions have been predicted. The results show that in straight road manoeuvre with wind actions, the trailer experience high roll moment and lateral displacement, comparing with the same manoeuvre, in the absence of crosswind forces. Moreover, steering-wheel inputs required for the manoeuvre with wind conditions have been reported to illustrate the steering effort of the driver through high or sudden wind situation.

Furthermore, an improved LTR rollover criteria for a tractor semitrailer vehicle has been developed. All parameters of the LTR index such as body roll angle and lateral acceleration were estimated through simulation of a critical turning manoeuvres with effects of crosswind actions. As well as, new relation between this indicator and wind speed has been suggested. In the next chapter, effects of vehicle parameters, such as trailer mass, pressure centre location, roll centre height on the vehicle rollover (i.e., on LTR) under crosswind condition will be investigated.

## **Chapter 7 : Parametric and comparison study on performance of LTR index under crosswind loads**

---

In this chapter, investigations have been carried out to assess the influence of key destabilising factors on roll stability of a high-sided articulated vehicle, based on the LTR stability criteria discussed earlier. The influence of vehicle speed, vehicle mass, wind pressure centre location, and roll centre location, on the LTR in crosswind have been discussed. For the investigation of each parameter other parameters have been kept constant at reasonable values which have been described in each section separately. Moreover, three roll indices used for estimating a vehicle roll stability have been compared under crosswind actions. They are: Energy-Based Rollover indicator, Rollover Critical Factor (RCF) and the improved LTR. Finally, the possibility of applying the improved LTR to passive rollover warning system has been suggested.

## **7.1 Parametric Study of Vehicle Rollover Stability**

In this study, some vehicle and road parameters are varied, in order to investigate effects of these parameters on crosswind stability of the tractor semitrailer vehicle. Parameters variations include vehicle speed, vehicle mass, the location of rollover centre and pressure centre location. All parameter variations are performed for curve negotiation at a vehicle speed of 25m/sec (apart from the parameters of section 7.1.1) in conjunction with wind gust scenario.

### **7.1.1 Effects of tractor semitrailer speed on roll stability**

In this section, multi-body dynamic simulations were performed for the high-sided tractor semitrailer vehicle, which is being subjected to the transient crosswind gust scenario (wind-tunnel gust) during curve negotiation. The constant radius curve that was designed in section (6-4) has been used, with the road adhesion coefficient of 0.6 (average coefficient for dry roads [145]). The vehicle speeds were set as 15m/sec, 25m/sec, and 30 m/sec. Accordingly, the LTR under these different speeds and in random transient wind gust scenario (wind-tunnel scenario) was obtained, as shown in Figure 7-1. This figure also illustrates that the maximum value of LTR can reach up to 0.99 for a vehicle speed of 25 m/s. This critical roll condition decreases to 0.74 as the vehicle negotiates the curve at a speed of 15 m/s, according to results also observed in [172]. Furthermore, at the highest vehicle speed of 30m/sec, the vehicle experiences extreme wheel unloading and rollover occurs at the beginning of the gusty period.

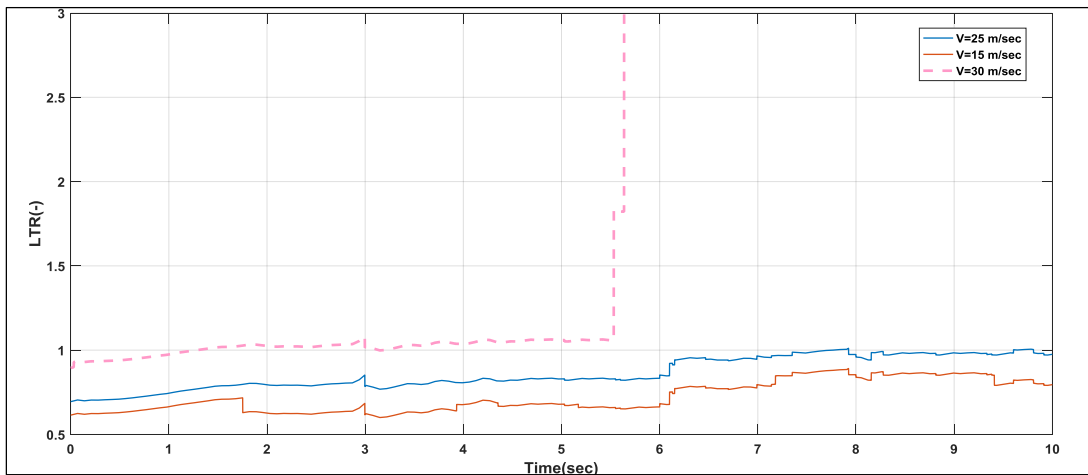


Figure 7-1: Effects of vehicle speed on rollover indicator, LTR

Furthermore, variations in the roll angle of the trailer unit at a vehicle speed of 30 m/sec are shown in Figure 7-2. From this figure, it can be seen that the trailer’s roll angle increases rapidly from about  $10^\circ$  to  $180^\circ$  in 1.5 sec (i.e., from  $t=4\text{sec}$  to  $t=5.5\text{ sec}$ ), after that, the trailer rollover conditions are occurred. This relation shows the significance of vehicle speed on the roll stability of the vehicle in crosswind conditions.

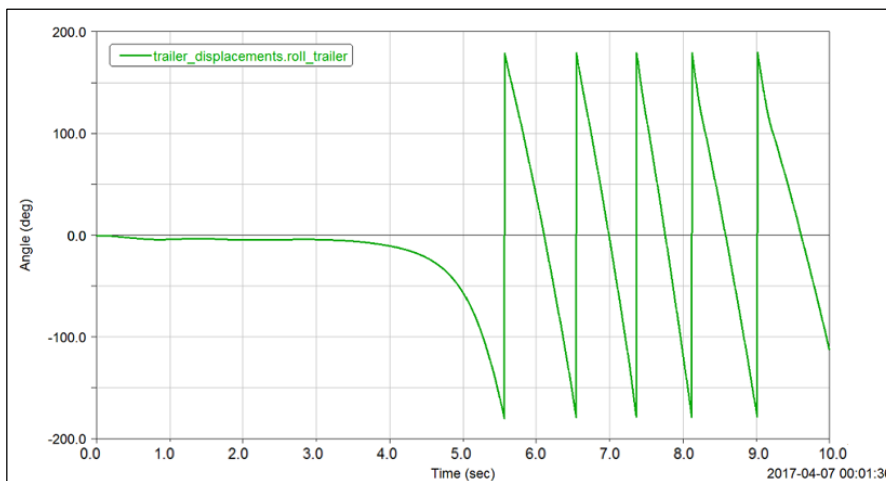


Figure 7-2: Roll angle of the trailer when negotiating a curve with speed of 30 m/sec under crosswind effects

### 7.1.2 Effects of roll centre Location

The roll centre is defined as a point at which the forces developed by the wheels are transferred to the body [173]. In addition, the aerodynamic roll moment in Equation 1-9 should be about

the roll centre [174]. However, in most of the previous studies discussed earlier, the aerodynamic roll moment was calculated about the vehicle body's centre of gravity. Thereby, the roll centre is an important parameter in the analysis of vehicle roll dynamics. In reality, this centre moves according to the variation in suspension geometry [107]. To indicate the influence of the roll centre position on vehicle roll behaviour, the height of the roll centre for the trailer's rear axle is varied within 20% from the original position of  $h_s = 1.78\text{m}$  (i.e. at this height, the LTR is predicted in section 6-4).

Figure 7-3 shows variation in the maximum LTR with different roll centre heights, at a trailer speed of 25 m/sec in the curving manoeuvre with same driving inputs for each height. Note that LTR values were computed in the transient (empirical) crosswind scenario, and a positive value of  $\Delta h/h_s$  represents an increase in the height. Moreover, roll moment generated by the fifth wheel component has been added to the Equation 6-3, and considered in the calculation of LTR. It can be seen from the figure that changes in vertical position of the roll centre has a large influence on the crosswind stability. This is because of the roll centre location is directly related to the suspension dynamics and, hence, to the rolling behaviour of a vehicle as well as to rollover warning algorithms (indicators).

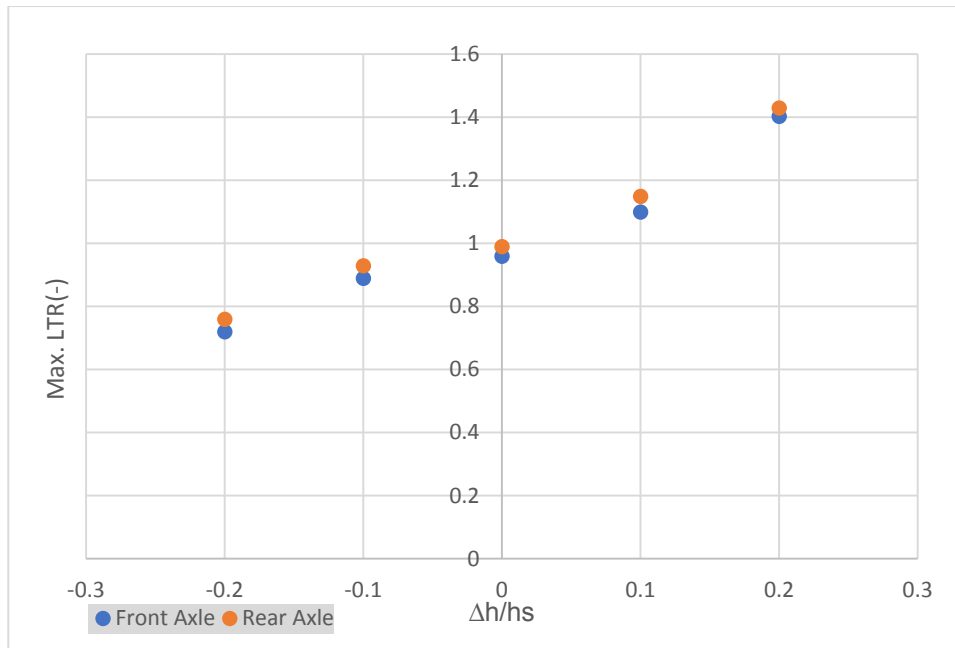


Figure 7-3: Variation in the maximum LTR with different roll center heights

### 7.1.3 Effects of Pressure Centre

The pressure centre is defined as the point about which the roll aerodynamic moment of selected cross-section is zero. In most of the former simulation studies, regarding the stability of ground vehicles in crosswind, it is assumed the wind pressure centres are fixed to the vehicle body [175]. However, this is often inconsistent with the actual situation. In real vehicle examinations, when the vehicle is passing through a gusty crosswind region, the speed of the air stream can change, thus the location of wind pressure centre also changes. To simulate this phenomenon, some researchers use the step of function-fitting a curve to simulate the movement of the wind pressure centre [176]. However, this method is too complex and the precision of the curve is not enough [175].

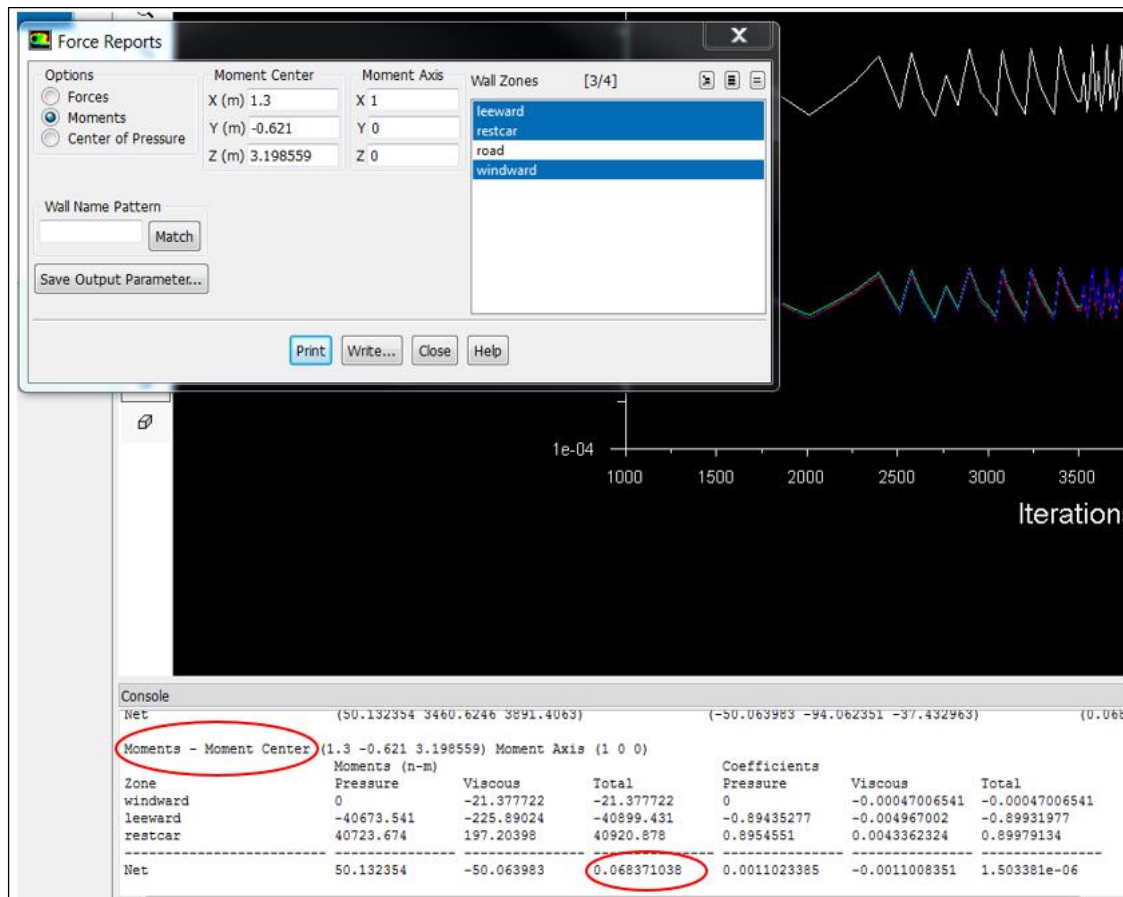


Figure 7-4 Calculation of pressure center location by Fluent software

Focusing on this problem, this investigation uses multiple discrete wind pressure centres to simulate the shift of the wind pressure centre [175]. The TSI gust scenario was subdivided into five intervals (Figure 7-5), with five discrete wind pressure centres for each interval. The locations of a wind pressure centre over the trailer's body at different times are calculated by ANSYS Fluent software (see Figure 7-4). As shown in Figure 7-6, each pressure centre is acting on a longitudinal plane of the trailer in different vertical heights. Then, lateral aerodynamic force will be applied to the trailer in ADAMS /Car software through V-Force elements that were created at these five positions.

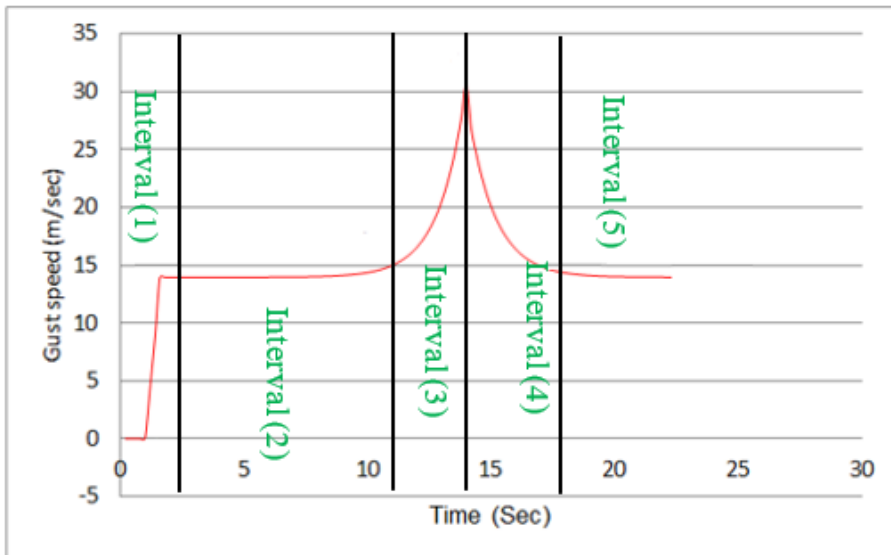


Figure 7-5 : Five intervals for calculating wind pressure centres



Figure 7-6 : V-Force elements created at location of gust pressure centres

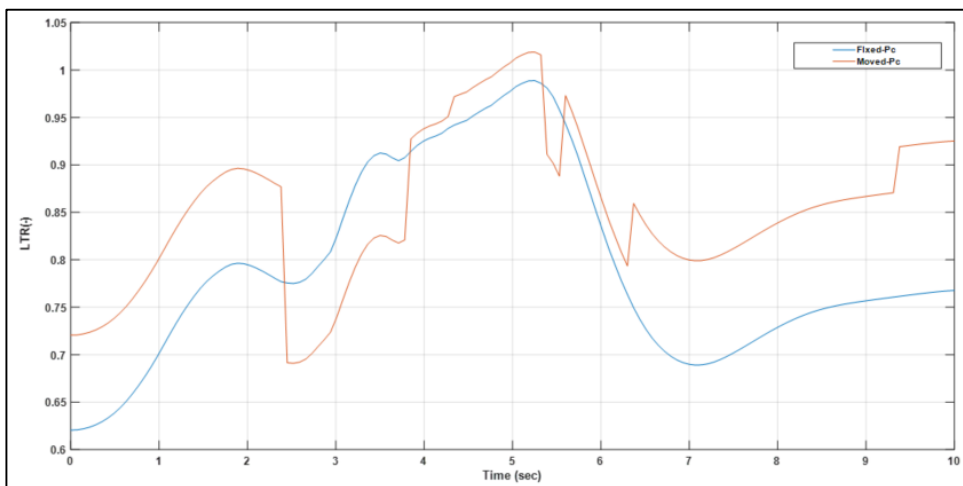


Figure 7-7: LTR in crosswind with moved and fixed aerodynamic center

Figure 7-7 shows effects of the TSI gust pressure centre's varying location on the LTR rollover indicator during a curve negotiation manoeuvre. As it can be seen, when the wind pressure centre shifting is considered, the crosswind rolling stability is worse than in the case of the pressure centre being fixed during the majority of the gust period. This is because, when the wind pressure is acting on the vehicle's body at several locations during the gust event, it enlarges the fluctuation in the vehicle's roll angle and leads to an additional reduction rolling stability. This also reflects the potential of this parameter (i.e. wind pressure location) in predicting crosswind stability in large commercial vehicles.

#### **7.1.4 Effects of Vehicle Mass**

Investigating the influence of vehicle mass (i.e. centre of gravity) on the overall stability is important to be able to predict vehicle behaviour in normal operating conditions. Figure 7-8 shows the influence of vehicle mass on the roll stability for a vehicle running at speed of 25 m/s under a TSI crosswind gust. It is seen that an increase in the vehicle's mass causes a corresponding increase in the roll stability condition. For an unloaded vehicle with a mass of 10000 kg, the maximum LTR indicator of the rear axle is predicted to be 0.98. This index decreases to 0.6 for a fully laden vehicle with a mass of about 40000 kg for the same wind speed. This variation in the roll stability indicator with the vehicle's mass shows that the wind loads should be considered in the design of the vehicle's body and chassis. However, the effects of trailer load distribution (goods or materials) on its crosswind stability need further investigation.



Figure 7-8 : LTR for rear axle of the trailer under TSI wind gust

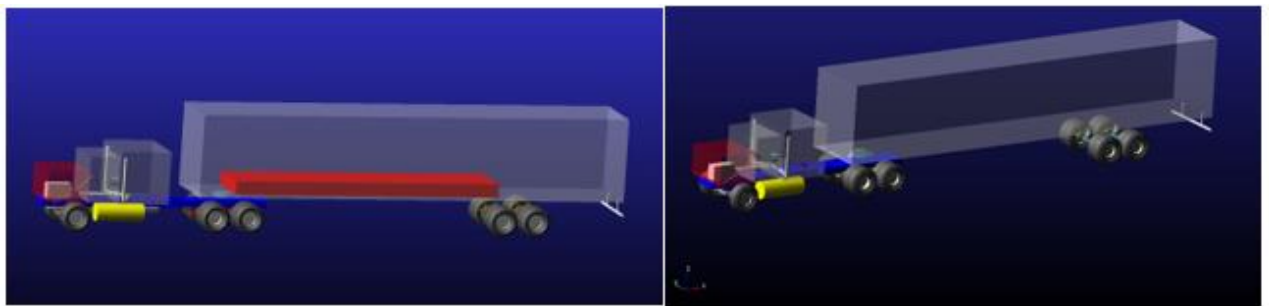


Figure 7-9: Laden and empty trailer for dynamic simulations

Thus, the stability model discussed in this work has the potential to reliably determine the rollover characteristics of HCVs under a variety of destabilising factors. This is especially useful for predicting such stability characteristics as critical vehicle speeds under varying conditions.

### 7.1.5 Effects of multi-parameters (vehicle mass and radius of road-curvature) on performance of LTR rollover indicator

In this section, transient roll stability of articulated tractor-semitrailer vehicles has been examined through analysis of their responses during curved manoeuvres for different road-

curvature radii ( $R_{ii}$ ) and carried load (trailer mass). Vehicle speed was set at constant value of 25 m/sec, and values of LTR index were reported for cargo load conditions of 20000kg, 40000kg and 80000kg that under effects of the TSI wind gust. The variations in the LTR index are presented in Figure 7-10 as a function of time and the mentioned parameters. It can be shown that in general, for the variable cargo load, the variations in vehicle roll motion are more stabilizer for the heavier trailers.

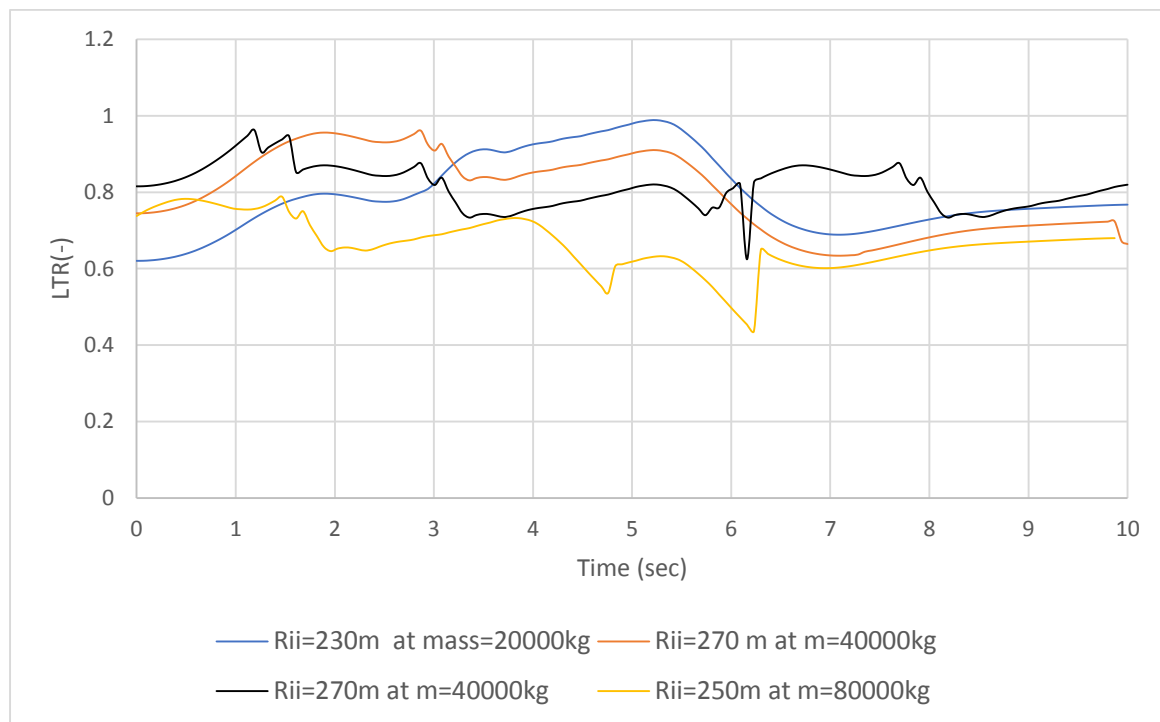


Figure 7-10 : effects of multi-parameters on performance of LTR rollover indicator under TSI wind gust

Furthermore, the oscillations in amplitude of the LTR index corresponding to the radius of road-curvature of 270 m for the constant cargo load (40000kg), are also more pronounced than those corresponding to the road-curvature of 250m. This results confirm the greater influences of vehicle speed and radius of road-curvature on the crosswind roll stability of high-sided trailers.

## **7.2 Comparative analysis of Rollover Indicators for a tractor semitrailer vehicle under wind gust condition**

As discussed, in previous studies various types of vehicle rollover indices have been proposed; these indexes depend on various factors such as roll angle, roll centre of vehicle, the height of a vehicle's centre of gravity (C.G), suspension parameters, and external road inputs, amongst others. The second research area presented in this chapter is an investigation on the effectiveness of LTR coefficient. To achieve that, a comparative analysis of the rollover stability behaviour based on three different rollover indexes has been undertaken to identify which one is the most sensitive indicator to detect a rollover event for a large class vehicle in a windy environment. These indexes are Energy-Based Rollover indicator, Rollover Critical Factor (RCF), and the improved LTR. The purpose of this analysis was also to establish a preliminary set of results for confidence in the performance of the improved LTR index when used in the design of vehicle rollover avoidance technology.

### **7.2.1 Energy-Based Rollover indicator**

The approach used is inspired by [177, 178] and is based on energy considerations. In this method, a rollover occurs when the rotational energy generated by an external force is larger than the potential energy required to shift the centre of gravity towards the rollover point [163]. In the following analysis, it is assumed that the load transfer at the trailer's front axle is the same as the load transfer at the rear axle. Just before wheel lift-off, all the load has been transferred to one side (see Figure 7-11). In this situation, the lateral force is assumed to be the maximum possible force, given the vertical force, i.e.,  $F_y = \mu F_z$ , and rotational vehicle dynamics are given as [179]:

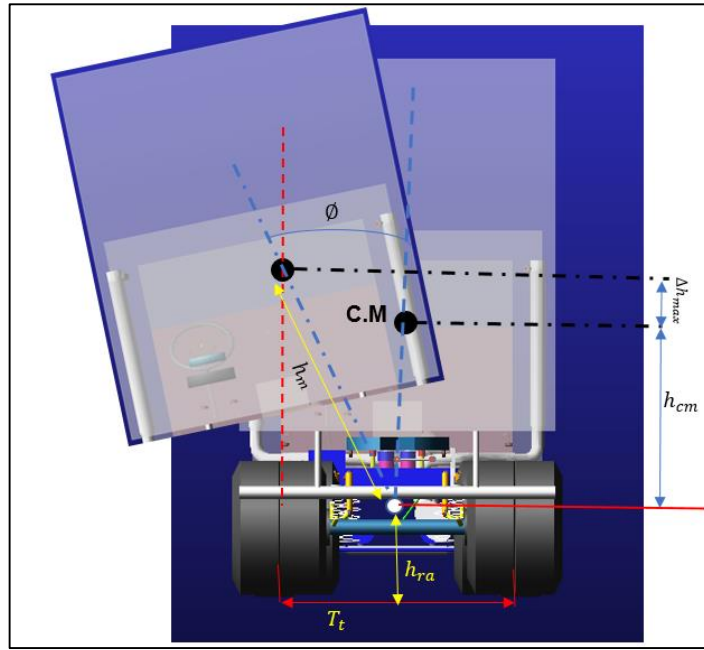


Figure 7-11 : Critical roll condition

$$T_{roll} = \frac{1}{2} (I_{xx} + mh_m^2) \dot{\phi}^2 \quad (1-7)$$

$$U_e = \frac{1}{2} \phi^2 C_\phi - mgh_m(1 - \cos\phi) \quad (2-7)$$

$$E_{roll} = \frac{1}{2} \phi^2 C_\phi - mgh_m(1 - \cos\phi) + \frac{1}{2} (I_{xx} + mh^2) \dot{\phi}^2 \quad (3-7)$$

where ( $I_{xx}$ ) is moment of inertia of the vehicle's sprung mass about the x-axis, other parameters like horizontal and vertical distances between roll centre and mass centres are displayed in Figure 7. Now, in the critical situation, or in critical position, the rollover energy boundary,  $E_{crit}$ , can be expressed as [180]:

$$E_{crit} = \eta \cdot mg\Delta h_{max}, \Delta h_{max} = \sqrt{h_{cm}^2 + (T_t/2)^2} - h_{cm} \quad (4-7)$$

where  $\Delta h_{max}$  is the maximum increase of gravity center's height caused by roll motion,  $\eta$  is coefficient. Considering the lateral motion of vehicle, the value of this coefficient is smaller than unity. To get indicating values, a normalized measure is defined as [181]:

$$W_L = \frac{E_{crit} - E_{roll}}{E_{crit}} \quad (5-7)$$

where  $W_L$  is a warning (wheel lift off) indicator.

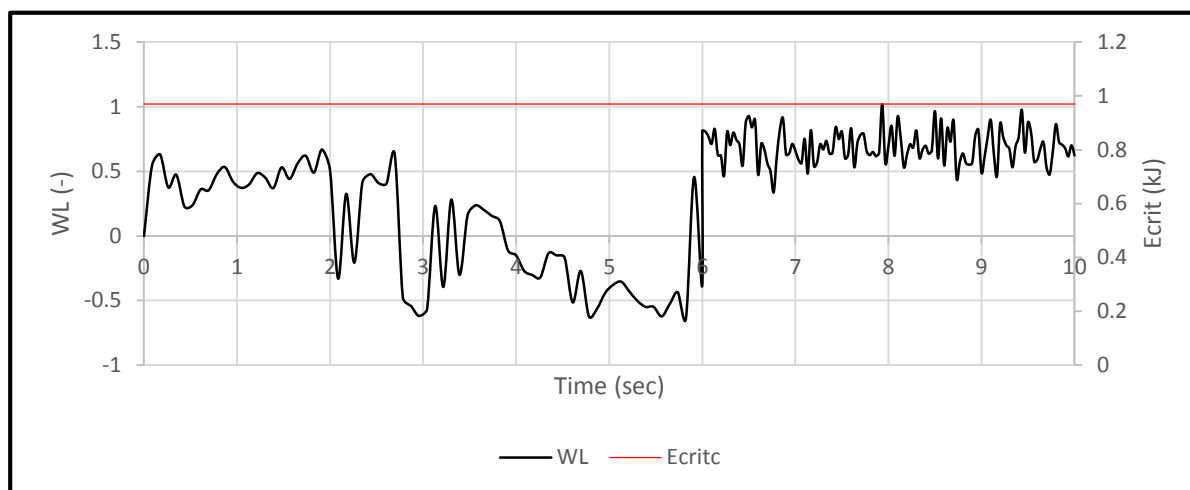


Figure 7-12: Behavior of Energy-Based Rollover indicator in crosswind

Figure 7-12 shows the energy analysis of the un-tripped rollover under crosswind conditions, which was conducted at the same driving condition (i.e., vehicle speed, road curve geometry, wind direction) that have been considered for development of LTR index. It can be concluded from the figure that both LTR rollover indicator and Energy-Based Rollover follow the same pattern throughout the entire wind scenario (transient scenario). However, according to the results reported in Figure 6-27, it is clearly seen that LTR indicator is more efficient than Energy-Based Rollover in the detection of wheel lift-off conditions.

## 7.2.2 Rollover Critical Factor

The Rollover Critical Factor (RCF) developed by Zhang et al.[182] compares the available restoring moment normalised for mass – the Equation's (6-7) first square brackets – with moments due to lateral and roll acceleration. The authors developed Rollover Critical Factor *RCF* as follows[182]:

$$RCF = g \cdot \left[ \frac{(t_f + t_r)}{2} - h_{cm} \cdot |\phi| \right] - |a_y| \cdot [(h_{cm} + h_{ra}) - z_s] - (I_{xx}) \frac{|\ddot{\phi}|}{m_s} \quad (6-7)$$

where  $t_f$  and  $t_r$  is half width of the front and rear axles, respectively,  $a_y$  is vehicle lateral acceleration and  $g$  the gravity acceleration. Also,  $h_{cm}$  is height of the sprung mass CG above the roll axis,  $h_{ra}$  is height of the roll axis above the ground (see Figure 7-10), and  $z_s$  is vertical displacement of sprung mass.

By substituting the vehicle's lateral acceleration and roll acceleration (predicted by ADAMS/car simulation for curving manoeuvre) into equation 6-7, a measure of instantaneous rollover margin can be predicted. As described by equation (6-7), smaller RCF indicates a low rollover resistance capability in a vehicle and rollover will occur when RCF becomes negative.

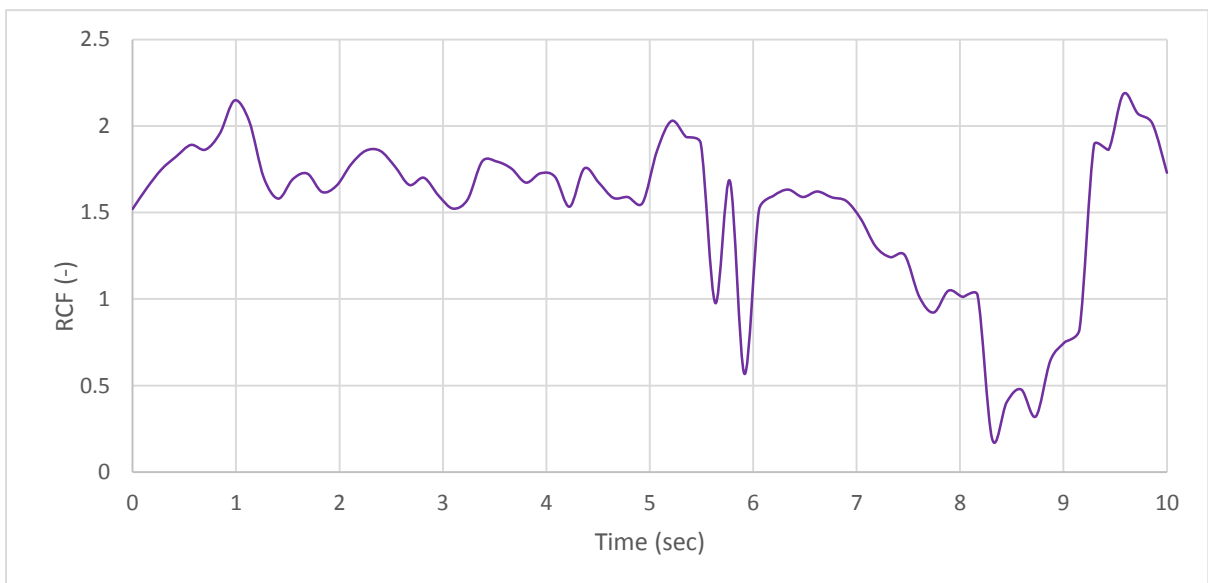


Figure 7-13: Behavior of RCF rollover index in crosswind conditions

The RCF for the trailer unit during the curving manoeuvre (developed in section 6-4) under the wind-tunnel gust scenario was computed and shown in Figure 7-13. As can be seen in the figure, the RCS have failed to detect wheel lift condition (i.e. no negative value) that was observed by using LTR indicator (see Figure (6-27)). The results further show higher amplitude oscillations in the trailer body which is due to the higher fluctuation of the gust flow.

## **7.3 Evaluation of the Performance of a Passive Rollover Warning System in Crosswind Conditions**

Public road agencies are investigating the potential for intelligent safety systems to reduce the number of rollover accidents, thus improving the commercial vehicle as well as bus safety on highway systems. Intelligent rollover safety systems (passive system) are designed to calculate the rollover potential for the specific vehicle and direct a warning if required. The directed message is achieved by activating a sign or flashing lights only when a potential rollover is detected. In this way, warning signs alert the drivers of a high probability of entering a rollover situation.

This section describes the system design for a Rollover Warning System (RWS), and investigates the possibility of improving the performance of the system in windy environments. The RWS is being deployed by road agencies across North America; for instance, three rollover-warning sites are installed in Virginia and Maryland. These locations have had no rollover accidents since the systems were installed in 1994 and the newer site in Pennsylvania has had similar short-term results [183].

### **7.3.1 Description of RWS system**

The intent of the RWS is to alert vehicles that are travelling too fast for an upcoming curve in the road to reduce speed in order to prevent a costly rollover. The alarm system includes meteorological sensors on the road infrastructure and a risk assessment software. Weigh in Motion (WIM) sensor arrays, which are located in up to two lanes prior to the start of the critical curve, are used to collect vehicle information. As a vehicle passes over WIM1, its weight and speed are recorded by the system. The vehicle then passes over WIM2, and likewise has its speed and weight recorded. The vehicle information is then used in the determination of whether or not the vehicle has the potential to roll over. A warning indicator

is activated to alert the vehicle to reduce its speed if it is determined to be exceeding a defined harmless speed for the important curve. A typical site layout is shown in Figure 7-14.

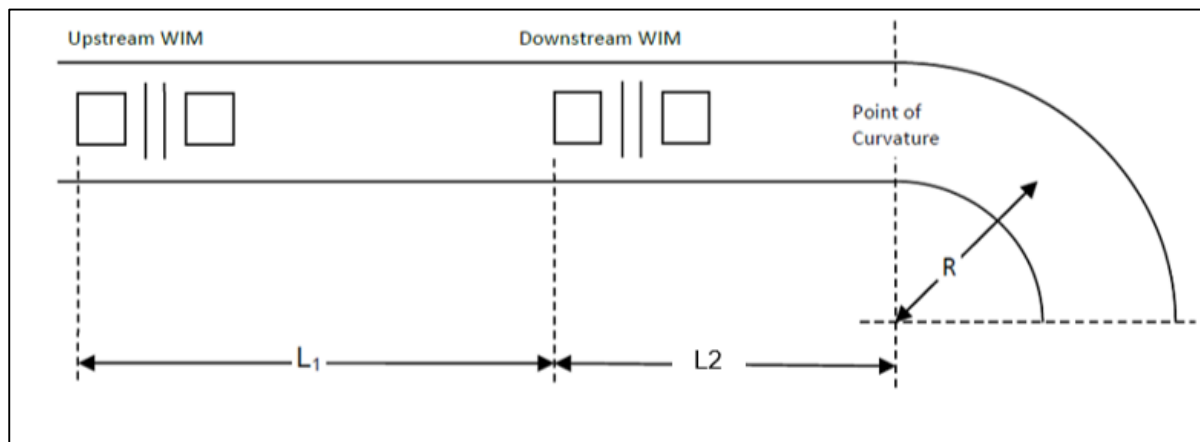


Figure 7-14 :Layout of Rollover warning system [183]

From the sensors located upstream of the curve, the trucks deceleration ( $d_c$ ) is determined from the following equation[184]:

$$d_c = \frac{v_1^2 - v_2^2}{2L_1} \quad (7-7)$$

where  $V_1$  and  $V_2$  are speeds at each upstream sensor location and  $L_1$  is the distance between them. Then, based on the deceleration rate ( $d$ ), the speed of the tractor at the point of curvature is calculated as follows [183]:

$$V_{PC} = \sqrt{V_2^2 - 2d L_2} \quad (8-7)$$

Where  $L_2$  is the distance from the second station to the point of curvature. The maximum values of lateral acceleration  $a_{max}$  beyond which the truck will roll over is calculated as follows [184]:

$$a_{max} = \frac{(RT - SM)g}{1.15} \quad (9-7)$$

where  $RT$  is rollover index, and  $SM$  is the safety margin (the safety margin ( $SM$ ) is normally 0.1 [183]). Furthermore, the maximum rollover threshold speed ( $V_{max}$ ) is determined from the following equation[183]:

$$V_{max} = \sqrt{(a_{max} + ge)R} \quad (10-7)$$

where  $e$  is the super-elevation of the curve, and  $R$  is the radius of the curve.

### 7.3.2 Case study

In an attempt to investigate increase of the effectiveness of a rollover warning system (RWS), the crosswind parameter, which affects the rollover situation of a vehicle, can be incorporated into the RWS. This can be done by using the improved LTR, which has been developed in Chapter 6. Moreover, the tractor semitrailer speed relative to the crosswind speed has been used in equation 7-7 instead of absolute vehicle speeds ( $V_1, V_2$ ). This has been investigated through developing a case study, in which deceleration (braking) manoeuvres were simulated for the tractor semitrailer vehicle running on a curved road of  $R=150\text{m}$ .

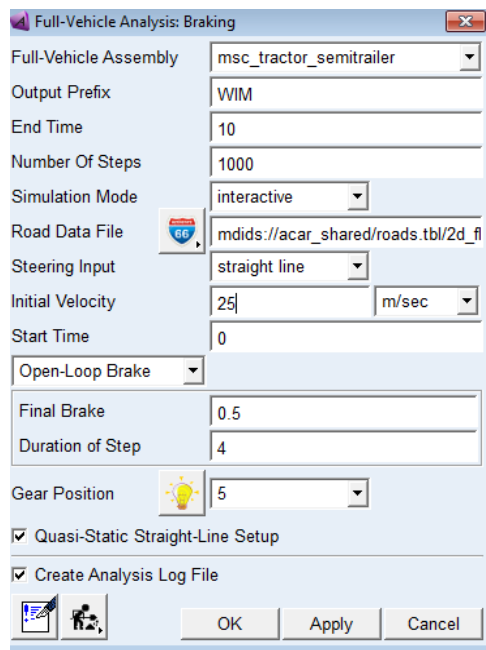


Figure 7-15: Set-up of a deceleration maneuver

As shown in Figure 7-15, the deceleration (braking) manoeuvres have been performed in ADAMS software with an initial speed of 25 m/sec. Then brake forces will be applied gradually to the vehicle. Also, the road super-elevation angle was set as  $0.05^\circ$  [183], and the simulations run for nine base weights of the vehicle with/without wind gust effects, see Table 7-1. Furthermore, the random wind gust scenario was applied to the vehicle during the

manoeuvres. Based on the weight of the vehicle, the rollover threshold (RT) is taken from Table 5.

Table 7-1: LTR indicator for different weights

Vehicle weight (Kg)	Average rollover index (LTR) without wind	Average rollover index (LTR) with wind
15,000	0.6	0.78
19,000	0.52	0.71
23,000	0.58	0.71
27,000	0.63	0.74
32,000	0.56	0.81
36,000	0.63	0.68
38,000	0.54	0.61
40,000	0.47	0.59
42,000	0.53	0.64

As mentioned, practically, some type of sensor is used to detect the presence and speed of a vehicle. However, in this simulation, this data was monitored/recorded at different locations over the road (before, at and after point of road curvature) (see Figure 7-16).

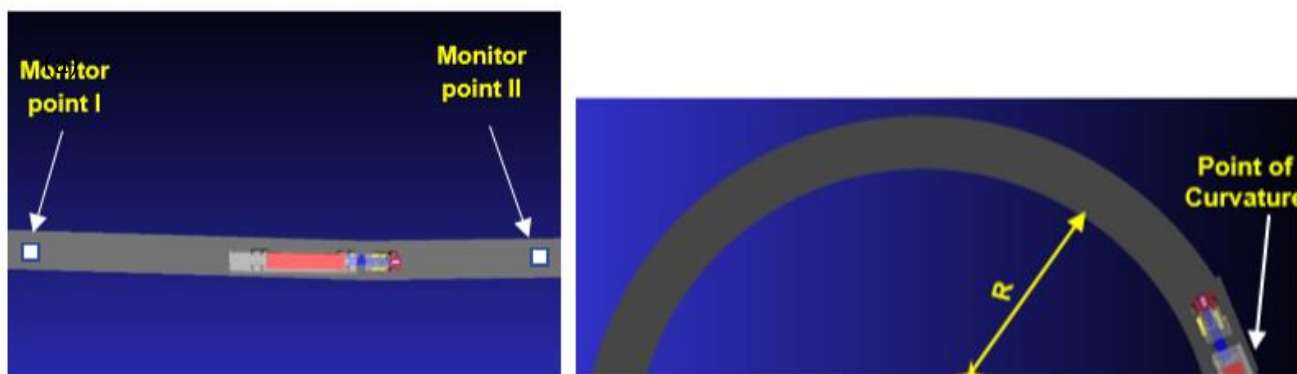


Figure 7-16: Location of vehicle speed monitors

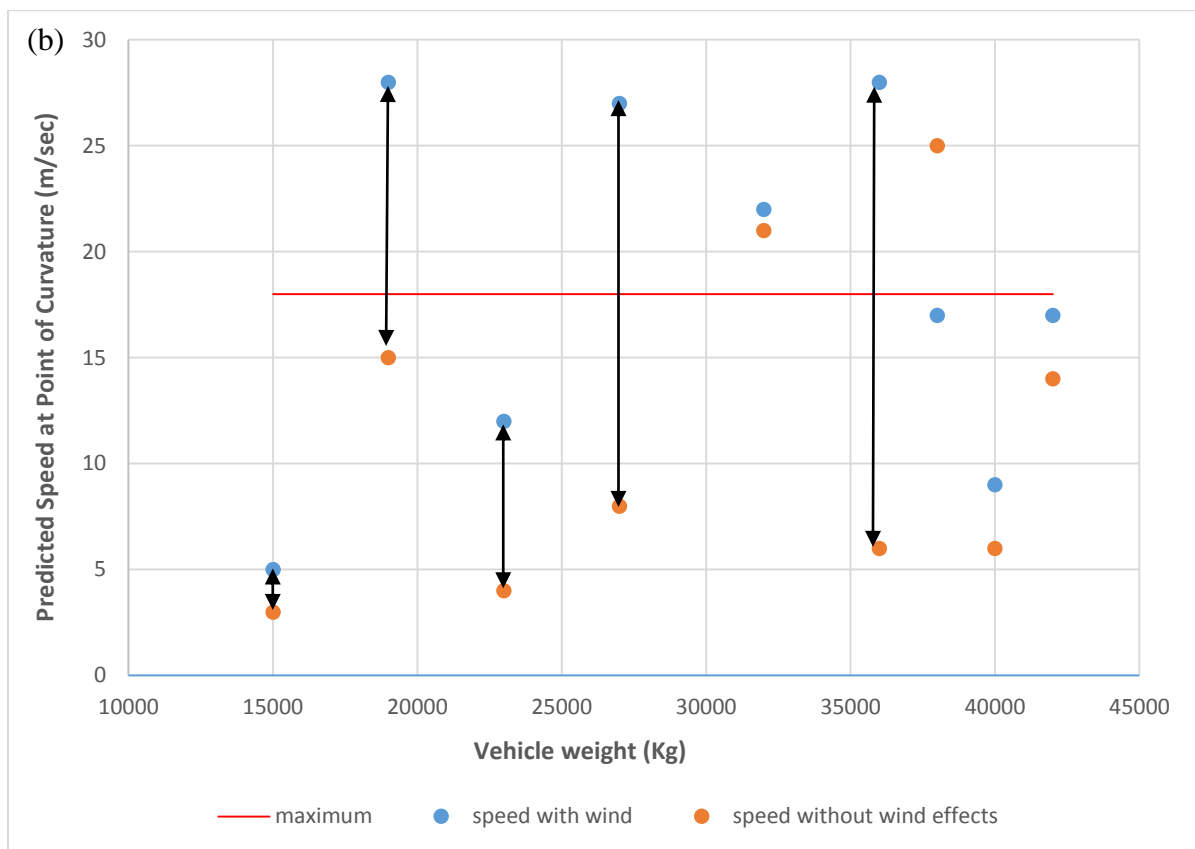
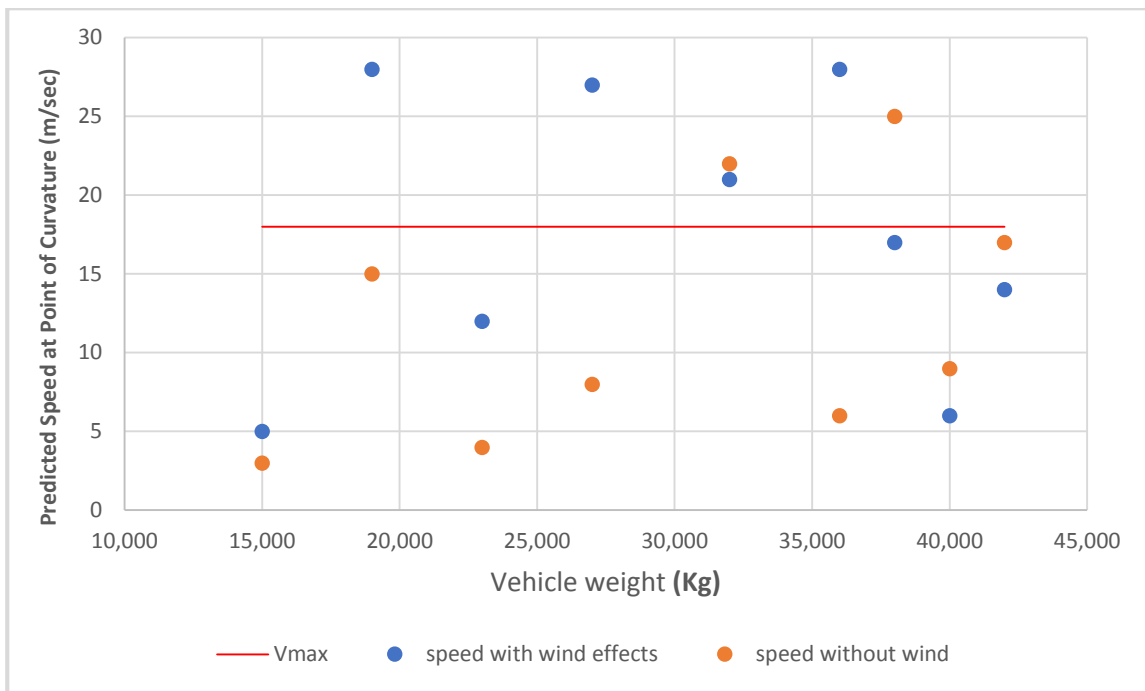


Figure 7-17: (a) Performance of warning algorithm with /without wind consideration, (b) data compression

In Figure 7-17, the warning speed of 18 m/sec was used (maximum speed) as the activation speed for the speed-based rollover system. The simulation results and data compression show significant differences (up to 5 times) in performance of RWS when using LTR index that consider wind effects on the vehicle roll dynamics. Furthermore, the observation of this analysis (Figure 7-17 a), demonstrates that when crosswind actions are considered, the warning system (i.e., RWS) will generate signal that can detect four vehicle rollover cases. However, in the same driving manoeuvre, the traditional warning system (i.e., RWS system that ignored the wind forces) can detect only two rollover cases. This analysis shows that high improvement in performance of vehicle rollover warning systems can be achieved if detection of crosswind aerodynamic forces is incorporated to rollover control systems of high-sided vehicles.

#### **7.4 Summary**

There are many design parameters which can affect the crosswind roll stability of a large class vehicle. It is really hard to understand influence of each parameter to the vehicle rollover under crosswind actions. However, this chapter provide analysis of key parameters that strongly influence the vehicle roll dynamics. The results emphasized that control of vehicle mass and speed play an important role in improvement of vehicle crosswind stability. Also, the results reported that rollover indicator (LTR) in crosswind is dominated by changing in locations of the roll and of wind pressure centres. Furthermore, brief investigation on the possibility for applying the improved rollover indicator (LTR) to the rollover warning system has been provided.

## **Chapter 8 : Conclusions**

---

This chapter concludes the thesis by summarising the achievements of this research. In this thesis, experimental and numerical investigations have been conducted on a tractor semitrailer vehicle to predict the vehicle's aerodynamic forces in extreme crosswind conditions. Moreover, due to the difficulty of reproducing real running conditions of the vehicle in a wind-tunnel, a coupled simulation method between the motion of the vehicle and unsteady aerodynamics was developed. Based on this method, the dynamic responses of the tractor semitrailer vehicle to the gusty crosswind conditions have been investigated. In addition, improvement of a traditional rollover index, LTR under gusty crosswind environment has been achieved. Furthermore, requirements have been defined for future work in the field of large vehicle crosswind stability.

## 8.1. Research Problem Synopsis

Articulated commercial vehicles such as tractor semitrailer combinations are usually designed and manufactured with large bodies and high payload capacities. As a result of this, improvement of control and operational safety of these vehicles are important research fields in recent years. Investigations on crosswind stability of such large vehicles, for example, have attracted much attention both in research and industry fields. However, the effects of gusty crosswind aerodynamic on a vehicle's motion/stability have not been clarified quantitatively enough. This is because the unsteady aerodynamic forces are difficult to estimate in on-road tests, and also wind-tunnel tests with vehicle motion is difficult to set up.

Furthermore, although there are many research studies investigating the roll stability of heavy commercial vehicles, most of these studies use oversimplified equations for vehicle dynamics. Thus, the complexity (nonlinearity) of the vehicle's system (i.e. suspension dynamics, tire dynamics, chassis dynamics, etc.), which have significant impact on a large vehicle's roll behaviour, are not considered. Also, in the majority of these studies, the contribution of external forces, such as road and wind loads to the roll instability of the vehicle, were neglected.

According to the literature review in Chapter 2, a number of objectives have been formulated, which determined the scope of the present research study. The main aim of the thesis is to investigate the roll stability of a high-sided tractor semitrailer vehicle under gusty crosswind conditions, as well as to improve the LTR rollover index of the vehicle to be more efficient in such environments. The main aims of this study, and the major achievements and contributions that have been achieved during this study, have been presented in a summary form in the following sections of this chapter.

## 8.2. Research Aims and Major Achievements

The main aims of the thesis outlined in Chapter 1 are given below with a summary of how these aims have been achieved.

**Research Aim #1: Predicting unsteady aerodynamic forces acting on a high-sided tractor semitrailer vehicle that is under gusty crosswind conditions.**

**Achievement #1:** Many previous studies reported that vehicle rollover is most likely to occur under strong wind conditions. Therefore, in this study, two wind gust scenarios were considered for simulating high crosswind conditions. For the first scenario, an artificial wind gust condition with high turbulence wind has been developed for the analysis. Wind-tunnel equipment has been used to generate the gusty flow domain over a scale-model of tractor semitrailer vehicle. The gust velocity along with other turbulence flow parameters were recorded by Cobra probe sensor. In addition, in low-wind speed (i.e. without gust conditions), the aerodynamic force coefficients have been obtained by integration of the pressure distributions over the vehicle surfaces. The effects of yaw angle were analysed in terms of force and pressure coefficients. It is observed that when increasing the yaw angle, the pressure distribution around the vehicle varies especially at the windward side. For example, all vehicle surfaces show the presence of a negative pressure for yaw angles of  $45^\circ$  and  $0^\circ$ , but for  $90^\circ$  yaw angle, a positive pressure at windward surface has been observed. The pressure difference between the windward side and the leeward side at yaw angle of  $90^\circ$  gives rise to a corresponding variation in side aerodynamic force. Consequently, the roll moment of the vehicle increases.

Moreover, a commercial CFD package has been used to create a virtual domain of the wind-tunnel test section. The model makes use of the control volume numerical technique for solving the governing equations of wind pressure and velocity coupling. The experimental results have been verified against the numerical model, which show a good agreement.

Therefore, based on experimental findings, a transient gust wind scenario has been developed for predicting aerodynamic forces due to sudden crosswind conditions. The scenario consists of two main periods: the initial wind period represents moderate wind conditions, and the second period represents the condition of extreme wind gusts. Under this scenario, a high lateral aerodynamic force which is mainly governed by the wind speed profile (i.e. the transient gust scenario) was predicted.

In the second scenario, a gusty wind condition has been evaluated based on a deterministic gust approach. The deterministic gust model generally describes the stochastic character of the turbulence with the shape of occasional occurring wind peaks [6]. For this study, the TSI (deterministic) gust scenario was applied to the full-scale tractor semitrailer model with a complicated geometry in combination with CFD based approach, using Large Eddy simulation (LES) for modelling air turbulence.

The results depicted in Chapter 5 have shown that the TSI gust scenario has significant unsteady effects on the side aerodynamic force and the roll moment of the vehicle. Also, there are significant variations in aerodynamic loads, consistent with the gust's strength. The discoveries made by using this scenario demonstrate a comparable propensity of time-dependent aerodynamic forces amassed from [185] numerical–experimental study. In this situation, the author used a rectangular gust profile with a higher maximum wind speed value of 25 m/sec, and a positive concurrence is observed between their results and the findings here.

**Research Aim #2: Developing a methodology to incorporate crosswind aerodynamic loads into a high fidelity multi-body model of the tractor semitrailer combination, analysing the effects of sudden crosswind conditions on its dynamic responses.**

**Achievement #2:** In this study, a high fidelity non-linear model for tractor semitrailer dynamics, which has been built in ADAMS/CAR environment based on multi-body dynamic

approach, was used. The chosen high level of dynamic model complexity meant that the limitations of simpler models that are commonly used in rollover research could be overcome. In addition, a one-way coupled simulation of unsteady aerodynamics and vehicle dynamics has been applied to a tractor semitrailer vehicle subjected to a sudden crosswind. Transient aerodynamic forces that were predicted under both the empirical wind gust scenario and TSI gust model were input into multi-body dynamic simulations of the tractor semitrailer vehicle. Furthermore, in order to represent as realistic a driving scenario as possible, straight and constant radius manoeuvres were performed through ADAMS/Car software. In these simulations, the vehicle was run on virtual roads passing a gusty crosswind region.

The simulation results were obtained based on both wind speed and vehicle speed. It has been shown that when the vehicle is affected by a crosswind gust, the roll and yaw angle experienced by the vehicle increased dramatically and the vehicle will deviate from its original path. The severity of these responses as well as the lateral deviations are dependent on the vehicle dynamic behaviour, the gust characteristics, and the aerodynamic characteristics of the vehicle. Also, when the vehicle deviates from its path in such environment, the driver will react and steer, and this will reduce or increase the severity of the wind disturbance depending on the driving situation.

To conclude, this work shows that the coupling of vehicle aerodynamic and dynamic is needed to capture the vehicle responses to crosswind actions, which are essential for the investigation of vehicle crosswind stability. Also, the driver response is shown to be an important aspect to consider when designing appropriate methods for crosswind stability.

**Research Aim #3: Improving the LTR rollover index that can effectively detect vehicle rollover events due to impacts of extreme wind disturbances.**

**Achievement #3:** Based on the coupled vehicle dynamics and aerodynamics method, an improved LTR rollover criterion for the tractor semitrailer vehicle has been introduced in this work. All parameters of this index such as body roll angle and lateral acceleration were estimated in critical turning manoeuvres with crosswind actions. The turning (constant radius) manoeuvres were simulated in ADAMS/Car software. The improved LTR rollover metric bears a close resemblance to the real world situation due to the use of a high fidelity non-linear model for tractor semitrailer dynamics with hundreds of degrees of freedom, and it employs wind data measured in a wind-tunnel. Moreover, as presented in Chapter 7, the metric is very sensitive to changes in vehicle parameters, which allows an evaluation of the influence of vehicle characteristics in rollover events with greater precision. Furthermore, simulation results show that, comparing to the traditional LTR index, the LTR under crosswind is more efficient in detecting manoeuvre-induced rollovers. Therefore, this trailer rollover indicator that has been improved upon by the proposed methodology can provide more reliable information to the warning or control system in the presence of wind conditions.

### **8.3 Thesis Conclusions**

A comprehensive study has been carried out to support the existing literature regarding the crosswind roll stability of high-sided tractor semitrailer vehicles. Additionally, it has provided new contributions to improve the current understanding of the operational characteristics and parameter-related effects for large class vehicle stability. The major conclusions from each facet of this research study are summarized as follows:

#### **Research Objective #1:**

- (a) Measure the crosswind time-averaged aerodynamic force coefficients of a high-sided tractor semitrailer vehicle (ADAMS model).

(b) Developing novel aerodynamic gust treatment method for crosswind conditions to predict unsteady aerodynamic loads acting on the high-sided tractor semitrailer vehicle.

**Conclusion #1:** From experimental investigations regarding the aerodynamic characteristics of the tractor semitrailer combination carried out in this study, it can be concluded that the variation of flow angle introduces differences in the behaviour of the side force and pressure coefficients acting on the vehicle. As the flow angle increases to  $90^\circ$ , the side force coefficient is seen to increase rapidly to 2.3. Also, the side force coefficient has been found to be maximum at  $90^\circ$  flow angle (perpendicular to the vehicle's side surface). As a result of this, this angle was considered in development of gusty crosswind scenarios under which the vehicle will experience the maximum aerodynamic forces that could lead to a vehicle rollover event.

In addition, in order to examine the stability and the serviceability of large commercial vehicles in wind conditions more rationally, wind-tunnel tests should be carried out in a turbulent flow similar to natural wind. For this purpose, the aim of the second half of the experimental investigation is to develop a method of generating wind flows related to extreme wind events. The approach involves the installation of a flat plate in wind-tunnel to generate stream-wise gusts. To this end, a 1:54 scale model of the vehicle that was built in ADAMS/Car software was subjected to the wind-tunnel gusty flow at a flow angle of  $90^\circ$ . The flow data has been measured and the flow configuration has been analysed in terms of flow turbulence intensity, mean speed, fluctuations in speed, and amplitude. According to features observed, the method (i.e. gust generator) provides a reasonable approach to the modelling of gusty wind conditions, and experimental results of simulated gust profiles add support to the literature in this regard.

**Research Objective #2:** Development of transient wind gust scenario based on wind-tunnel data.

**Conclusion #2:** From vehicle aerodynamic forces that were calculated due to the transient wind gust scenario developed based on wind-tunnel data , it can be concluded that:

- Under wind gust environment, transient aerodynamic loads acting on a high-sided vehicle fluctuate dramatically with high values and this causes sudden changes in overall lateral forces and roll moment of the vehicle.
- These effects are less obvious under moderate (steady) wind conditions of the scenario. Also, in moderate period, it is expected that fluctuation components of wind speed result in uniform effects on vehicle aerodynamics behaviour. Therefore, difficulties associated with the vehicle manoeuvring and the stability of road vehicles in terms of unsteady aerodynamic loads are expected to occur predominantly at the wind gusting frequency.

**Research Objective #3:** To conduct CFD simulations in combination with the TSI deterministic gust scenario to predict extreme wind loads that large ground vehicles at exposed locations, such as bridges or embankments, are likely to experience.

**Conclusion # 3:** In the CFD investigations, a set of boundary conditions for implementing an unsteady wind gust on the computational domain is provided. It contains parameters that allow simulating the TSI gust condition, which propagate along the side inlet of the domain. LES technique was applied to the full-scale high-sided tractor semitrailer vehicle, and the effects of unsteady aerodynamics were evaluated. Rapidly changes with high amplitude were found in the aerodynamic side force and rolling moment during the rushing in and out of the wind gust. Magnitudes of these loads have been several times larger than the longitudinal drag force and yawing moment. Furthermore, the study shows that the gust amplitude  $A$  and duration  $T$ , the side aerodynamic force as well as the aerodynamic rolling moment, are the most important

parameters that have an influence the crosswind stability of large class vehicles. Moreover, comparing with the aerodynamic performance of the scale-vehicle in gusty wind-tunnel flow, the crosswind stability of road vehicles depends strongly on the vehicle type and gust characteristics.

**Research Objective #4:** To understand the wind-tunnel (empirical) and TSI gust flow field behaviour and pressure distribution around the tractor semitrailer vehicle.

**Conclusion #4:** Effects of time-dependent aerodynamic forces acting on the tractor-trailer vehicle have been investigated through the visualization of instantaneous gust flow structures around the vehicle. It can be concluded that gusty wind conditions result in the development of vortex structures around the vehicle's body. Additionally, due to high gust speed, the flow accelerates dramatically over the trailer's top and bottom surfaces and through the gap between the tractor and trailer. The high speed flow over the top and bottom surfaces of the vehicle leads to an increase in the rolling moment, and this explains why the vehicle will encounter more rollover risk in gusty crosswind environment. In addition, from the investigations regarding the pressure distributed over the vehicle surfaces, it can be concluded that the gusty flow conditions result in large differences in pressure developed on the windward and leeward sides of the vehicle. Consequently: high side aerodynamic forces.

**Research Objective #5:** To establish a novel coupled analysis of unsteady aerodynamic forces and a full-vehicle model based on the multi-body method.

**Conclusion #5:** In the coupling methodology that has been developed in Chapter 7 based on multi-body approach, the developed crosswind scenarios were incorporated into 674 degrees-of-freedom equations of the vehicle's dynamic motion. Thereby, the model complexity needed to accurately capture the dynamic behaviour of the vehicle during a transient crosswind event has been achieved. Furthermore, the results presented in the chapter show that the tractor semitrailer aerodynamic forces from the wind field of the developed wind gust

scenarios were exactly imported to ADAMS/Car environment. The forces were acting on the trailer's body at aerodynamic centre, which was calculated in ANSYS Fluent software (e.g. for TSI gust scenario). From the coupling method, it can be concluded that ADAMS spline functions, such as AKISPL, can be successfully used to interpolate the discrete data of wind speed measurement devices or numerical data of wind flow computed by ANSYS Fluent software.

**Research Objective #6:** To investigate the response of a high-sided tractor semitrailer vehicle subjected to two different wind gust scenarios during straight manoeuvre.

**Conclusion # 6:** From the investigations regarding the effect of the crosswind unsteady aerodynamic forces on the dynamic responses of the vehicle during straight manoeuvre, carried out in this study, it can be concluded that the vehicle reacts with a strong roll response on the TSI and the empirical gusts. Also, the trailer unit experiences higher lateral deviation, yaw angle, and roll angle than the tractor unit. Variations in a steering wheel angle generated by the steering action of the driver are presented as well. The results indicate that steering angle is an essential factor that should be considered for accurately analysing vehicle crosswind stability.

**Research Objective #7:** Propose a predictive lateral load transfer ratio (LTR) that incorporated gusty crosswind actions.

**Conclusion #7:** This study has improved LTR rollover index of large class vehicles that can detect un-tripped rollovers under gusty crosswind conditions. The new rollover index utilizes side and left aerodynamic forces to predict aerodynamic external inputs acting on the system. Furthermore, the rollover indicator was examined under critical cornering manoeuvre in wind action. For comparison, under the same manoeuvre, the traditional LTR index (i.e. wind action ignored) has been tested too. The results show that the improved rollover index can reliably handle un-tripped rollovers of high-sided vehicles under crosswind environments.

**Research Objective #8:** To carry out a parametric study for investigating the influence of various road and vehicle parameters on the roll stability (rollover index) of the vehicle.

**Conclusion #7:** In this work, parametric analysis has been carried out to show the influence of various parameters on roll stability of the vehicle in crosswind. From the investigations, key observations show that vehicle speed is seen to strongly influence the predicted rollover indicator, which is seen to be higher for higher vehicle/wind speeds. It has been further noted that the vehicle speed of 25m/sec is sufficient to cause a rollover accident in high wind speed. Location of wind pressure centre on the vehicle is also seen to influence the vehicle rollover stability greatly. In the same crosswind area, when the shift of the wind pressure centre is considered, the rolling stability is worse than the case when the wind pressure centre is fixed. This also proves that this method is more realistic. Furthermore, the effects of suspension design parameters on vehicle roll stability have been investigated by changing the roll centre height of the vehicle's axle. A significant increase in the rollover indicator has been observed without greatly changing in roll centre height.

#### **8.4 Thesis Contributions and Novelties**

The major contributions of this research study are summarized below in which novelties of this research are described:

**Contribution #1:**

One of the major contributions of this study is the prediction of aerodynamic forces acting on a high-sided tractor semitrailer vehicle based on wind-tunnel experiments and CFD simulation in combination with TSI wind gust model. In the available literature, the TSI wind scenario has been applied to rail vehicles, representing a train traveling on an embankment under constant mean wind load and suddenly being hit by an extreme wind gust [12]. This situation applies to road vehicles as well, and from a practical point of view, it is of interest to examine the TSI gust in the road vehicle aerodynamics.

Furthermore, wind-tunnel tests on the evaluation of commercial vehicle aerodynamics are usually carried out in a smooth flow. However, in order to examine the stability of ground vehicles more rationally, wind-tunnel tests should be carried out in a turbulent flow similar to natural wind. Although simulation of a scaled boundary layer flow, similar to that of the natural wind, requires a large wind-tunnel with a long test section, this study contributes to this body of research by developing a gust generation system based on a small wind-tunnel with a short test section. The wind gust data measured in the wind-tunnel was used to develop new wind gust scenario which simplifies the complex real gust condition. As well as, new mathematical formula for estimating gusty wind condition generated for example due to slope topography has been developed in this research

**Contribution #2:**

Currently, there are limited studies found in literature for predicting road vehicle crosswind stability. The majority of these studies have employed single rigid body dynamics and associated mathematical formulations. Some of these investigations use oversimplified equations, thus affecting the accuracy of their results. Other studies are valid for a limited range of conditions. Focusing on this problem, this study predicts the dynamic responses of a high-sided tractor semitrailer vehicle to gusty crosswind conditions based on a high fidelity non-linear dynamic model. The model has been built in ADAMS/car software based on multi-body approach, which means that the strong effects of suspension kinematic and nonlinearity as well as tire nonlinearity on the vehicle crosswind stability have been considered. Furthermore, a one-way coupled simulation of unsteady aerodynamics and vehicle dynamics has been applied to the vehicle, under straight and constant radius managers.

Furthermore, since the shape of the vehicle greatly influences the flow field as well as the overall aerodynamic forces of the vehicle, unlike previous studies on coupled analysis of vehicle dynamic and aerodynamic forces, this work considers this factor. For this purpose, in

wind-tunnel experiments, a scaled model of ADAMS model for a tractor semitrailer vehicle (in full dimensions) was developed. As well as, a full-scale model has been used in CFD simulations for predicting the vehicle crosswind aerodynamics.

**Contribution #3:**

It can be seen from the literature review discussion that the parameters of the vehicle rollover reported in literature depend either on vehicle states or on road geometry factors. However, there has been limited investigation into other factors affecting particularly vehicle rollover index such as strong crosswind forces [186]. As a result of this, this study introduces improved LTR rollover index to effectively detect effects of crosswind forces on a vehicle rollover.

Furthermore, a new relation between the vehicle rollover indicator, LTR, and wind speed has been suggested. The new characteristic wind curves can foresee rollover condition based on worst wind case scenarios (i.e., prediction of rollover event for high wind speed).

**Contribution #4:**

The effects of a number of destabilising factors on rollover index (roll stability) of a high-sided tractor semitrailer vehicle have been investigated. These include the vehicle speed, the vehicle's mass, the wind pressure centre, and the location of roll centre. These destabilising factors have been described in detail, with a description of associated variables that influence vehicle stability. Moreover, a comparative analysis between three different rollover indicators has been carried out to quantify the effectiveness of LTR indicator in wind condition, compared with two other rollover indices.

## **8.5 Recommendations for Future Work**

The primary goal of this research has been to devise a method to improve the roll stability of large commercial vehicles under crosswind actions. Three key areas have been identified to achieve this. In light of the concluded remarks provided in the previous sections, a vast

potential for further research in this particular area of vehicle crosswind stability has been unlocked. The main areas identified for further work are described below.

**Recommendation # 1:** The CFD simulations in combination with the TSI deterministic gust scenarios, carried out in this study, were limited to constant gust amplitude. The allowance of varying amplitudes, however, does not result in further problems. Moreover, it appears to be feasible to extend this technique to apply on both bicycles and motorbikes traveling in wind-exposed environments.

**Recommendation # 2:** A detailed investigation on the effect of gusty crosswind conditions on lateral, yawing and pitching stability of large-class commercial vehicle.

**Recommendation # 3:** Design vehicle rollover warning “active” system based on crosswind LTR indicator in order to prevent vehicle rollover which occurred while driving under crosswind conditions.

**Recommendation # 4:** For better understanding of the correlation between the flow and the vehicle dynamic forces, further study on heavy vehicle crosswind stability based on two-way coupling approach is recommended.

**Recommendation # 5:** A detailed investigation on the effects of suspension dynamics on vehicle crosswind stability is recommended.

## References

---

- [1] S. Bennett, Heavy duty truck systems: Cengage Learning, 2015.
- [2] D. Oberoi, "Enhancing roll stability and directional performance of articulated heavy vehicles based on anti-roll control and design optimization," UOIT, 2011.
- [3] D. f. Transport, "Domestic Road Freight Statistics, United Kingdom 2015," 18/08/2016, 2016.
- [4] N. Statistics, "Vehicle licensing statistics: 2015. Department for Transport," 2015.
- [5] Z. Trivedi, and V. Lakhera, "Perceptible Roll," SAE International Journal of Commercial Vehicles, vol. 8, no. 2015-01-1585, pp. 147-151, 2015.
- [6] X. Kang, "Optimal tank design and directional dynamic analysis of liquid cargo vehicles under steering and braking," Concordia University, 2001.
- [7] M. N. Khajavi, V. Hemmati, and S. A. Shouredeli, "A novel approach to enhance roll stability of SUVs by a fuzzy logic controller," Proc World Acad Sci Engng Technol, vol. 37, pp. 1070-1075, 2009.
- [8] G. Phanomchoeng, and R. Rajamani, "New rollover index for the detection of tripped and untripped rollovers," IEEE Transactions on Industrial Electronics, vol. 60, no. 10, pp. 4726-4736, 2013.
- [9] A. S. TOMAR, "Estimation of Steady State Rollover Threshold for High Capacity Transport Vehicles using RCV Calculation Method," Chalmers University of Technology Goteborg, Sweden, 2015.
- [10] D. J. Sampson, and D. Cebon, "Achievable roll stability of heavy road vehicles," Proceedings of the Institution of Mechanical Engineers, Part D: Journal of Automobile Engineering, vol. 217, no. 4, pp. 269-287, 2003.
- [11] G. Isiklar, "Simulation of complex articulated commercial vehicles for different driving manoeuvres," 2007.
- [12] C. B. Winkler, "Rollover of heavy commercial vehicles," 1999.
- [13] M. P. Czechowicz, "Analysis of vehicle rollover using a high fidelity multi-body model and statistical methods," © Maciej Paweł Czechowicz, 2015.
- [14] D. van Dinther, O. K. Hartogensis, and A. F. Moene, "Crosswinds from a single-aperture scintillometer using spectral techniques," Journal of atmospheric and oceanic technology, vol. 30, no. 1, pp. 3-21, 2013.
- [15] C. Baker, "High sided articulated road vehicles in strong cross winds," Journal of Wind Engineering and Industrial Aerodynamics, vol. 31, no. 1, pp. 67-85, 1988.

- [16] C. Baker, "A simplified analysis of various types of wind-induced road vehicle accidents," *Journal of Wind Engineering and Industrial Aerodynamics*, vol. 22, no. 1, pp. 69-85, 1986.
- [17] C. Baker, "Measures to control vehicle movement at exposed sites during windy periods," *Journal of Wind Engineering and Industrial Aerodynamics*, vol. 25, no. 2, pp. 151-161, 1987.
- [18] V. Malviya, "Effects of a novel aerodynamic intervention for heavy commercial vehicles on fuel saving and stability," University of Huddersfield, 2011.
- [19] C. Baker, F. Cheli, A. Orellano, N. Paradot, C. Proppe, and D. Rocchi, "Cross-wind effects on road and rail vehicles," *Vehicle system dynamics*, vol. 47, no. 8, pp. 983-1022, 2009.
- [20] A. G. Ryan, "The simulation of transient cross-wind gusts and their aerodynamic influence on passenger cars," University of Durham, 2000.
- [21] Y.-L. Xu, *Wind effects on cable-supported bridges*: John Wiley & Sons, 2013.
- [22] C. Knigge, and S. Raasch, "Improvement and development of one-and two-dimensional discrete gust models using a large-eddy simulation model," *Journal of Wind Engineering and Industrial Aerodynamics*, vol. 153, pp. 46-59, 2016.
- [23] P. Cheng, and W. Bierbooms, "Extreme gust loading for wind turbines during operation," *Journal of Solar Energy Engineering*, vol. 123, no. 4, pp. 356-363, 2001.
- [24] C. Proppe, and C. Wetzel, "A probabilistic approach for assessing the crosswind stability of ground vehicles," *Vehicle System Dynamics*, vol. 48, no. S1, pp. 411-428, 2010.
- [25] A. J. Scibor-Rylski, *Road vehicle aerodynamics*, 1984.
- [26] R. Rajamani, D. Piyabongkarn, V. Tsourapas, and J. Y. Lew, "Parameter and state estimation in vehicle roll dynamics," *IEEE Transactions on Intelligent Transportation Systems*, vol. 12, no. 4, pp. 1558-1567, 2011.
- [27] G. Genta, *Motor vehicle dynamics: modeling and simulation*: World Scientific, 1997.
- [28] R. Eger, and U. Kiencke, "Modeling of rollover sequences," *Control Engineering Practice*, vol. 11, no. 2, pp. 209-216, 2003.
- [29] Z. Yao, G. Wang, X. Li, J. Qu, Y. Zhang, and Y. Yang, "Dynamic simulation for the rollover stability performances of articulated vehicles," *Proceedings of the Institution of Mechanical Engineers, Part D: Journal of Automobile Engineering*, pp. 0954407013501486, 2014.
- [30] H. Damian, "Multibody Systems Approach to Vehicle Dynamics," Great Britain, 2004.

- [31] W. Rulka, and E. Pankiewicz, "MBS approach to generate equations of motions for HiL-simulations in vehicle dynamics," *Multibody system dynamics*, vol. 14, no. 3-4, pp. 367-386, 2005.
- [32] M. ADAMS, "Automatic dynamic analysis of mechanical systems," MSC Software Corporation, 2005.
- [33] T. Shim, and P. C. Velusamy, "Improvement of vehicle roll stability by varying suspension properties," *Vehicle System Dynamics*, vol. 49, no. 1-2, pp. 129-152, 2011.
- [34] T. Chou, and T.-W. Chu, "An improvement in rollover detection of articulated vehicles using the grey system theory," *Vehicle System Dynamics*, vol. 52, no. 5, pp. 679-703, 2014.
- [35] M. van de Molengraft-Luijten, I. Besselink, R. Verschuren, and H. Nijmeijer, "Analysis of the lateral dynamic behaviour of articulated commercial vehicles," *Vehicle System Dynamics*, vol. 50, no. sup1, pp. 169-189, 2012.
- [36] N. H. T. S. Administration, Initiative to address the mitigation of vehicle rollover, Docket No, NHTSA-2003-14622-1, 2003.
- [37] J. Preston-Thomas, and J. H. Woodrooffe, "FEASIBILITY STUDY OF A ROLLOVER WARNING DEVICE FOR HEAVY TRUCKS," 1990.
- [38] M. Suzuki, K. Tanemoto, and T. Maeda, "Aerodynamic characteristics of train/vehicles under cross winds," *Journal of Wind Engineering and Industrial Aerodynamics*, vol. 91, no. 1, pp. 209-218, 2003.
- [39] B. Diedrichs, M. Sima, A. Orellano, and H. Tengstrand, "Crosswind stability of a high-speed train on a high embankment," *Proceedings of the Institution of Mechanical Engineers, Part F: Journal of Rail and Rapid Transit*, vol. 221, no. 2, pp. 205-225, 2007.
- [40] T. Chiu, and L. Squire, "An experimental study of the flow over a train in a crosswind at large yaw angles up to 90," *Journal of Wind Engineering and Industrial Aerodynamics*, vol. 45, no. 1, pp. 47-74, 1992.
- [41] L. Drugge, and M. Juhlin, "Aerodynamic loads on buses due to crosswind gusts: extended analysis," *Vehicle system dynamics*, vol. 48, no. S1, pp. 287-297, 2010.
- [42] R. Cooper, "The effect of cross-winds on trains," *Journal of Fluids Engineering*, vol. 103, no. 1, pp. 170-178, 1981.
- [43] M. Sterling, A. Quinn, D. Hargreaves, F. Cheli, E. Sabbioni, G. Tomasini, D. Delaunay, C. Baker, and H. Morvan, "A comparison of different methods to evaluate the wind induced forces on a high sided lorry," *Journal of Wind Engineering and Industrial Aerodynamics*, vol. 98, no. 1, pp. 10-20, 2010.

- [44] G. Matschke, and C. Heine, "Full scale tests on side wind effects on trains. Evaluation of aerodynamic coefficients and efficiency of wind breaking devices," TRANSAERO—A European Initiative on Transient Aerodynamics for Railway System Optimisation, pp. 27-38: Springer, 2002.
- [45] J. Kee, J. Rho, K. Kim, and D. Lee, "High speed driving stability of passenger car under crosswind effects," *International Journal of Automotive Technology*, vol. 15, no. 5, pp. 741-747, 2014.
- [46] N. Winkler, L. Drugge, A. S. Trigell, and G. Efraimsson, "Coupling aerodynamics to vehicle dynamics in transient crosswinds including a driver model," *Computers & Fluids*, vol. 138, pp. 26-34, 2016.
- [47] P. Theissen, "Unsteady Vehicle Aerodynamics in Gusty Crosswind," Institute of Aerodynamics and Fluid Dynamics, Technische Universität München, 2012.
- [48] H. Xiang, Y. Li, S. Chen, and C. Li, "A wind tunnel test method on aerodynamic characteristics of moving vehicles under crosswinds," *Journal of Wind Engineering and Industrial Aerodynamics*, vol. 163, pp. 15-23, 2017.
- [49] C. Baker, "Train aerodynamic forces and moments from moving model experiments," *Journal of Wind Engineering and Industrial Aerodynamics*, vol. 24, no. 3, pp. 227-251, 1986.
- [50] N. D. Humphreys, "High cross wind gust loads on ground vehicles from moving model experiments," University of Nottingham, 1995.
- [51] M. Boccione, F. Cheli, R. Corradi, S. Muggiasca, and G. Tomasini, "Crosswind action on rail vehicles: wind tunnel experimental analyses," *Journal of Wind Engineering and Industrial Aerodynamics*, vol. 96, no. 5, pp. 584-610, 2008.
- [52] Y. Li, P. Hu, Y.-L. Xu, M. Zhang, and H. Liao, "Wind loads on a moving vehicle-bridge deck system by wind-tunnel model test," *Wind and Structures*, vol. 19, no. 2, pp. 145-167, 2014.
- [53] F. Dorigatti, M. Sterling, C. Baker, and A. Quinn, "Crosswind effects on the stability of a model passenger train—A comparison of static and moving experiments," *Journal of Wind Engineering and Industrial Aerodynamics*, vol. 138, pp. 36-51, 2015.
- [54] J. Howell, "The side load distribution on a Rover 800 saloon car under crosswind conditions," *Journal of wind engineering and industrial aerodynamics*, vol. 60, pp. 139-153, 1996.
- [55] S. Sanquer, C. Barre, M. D. de Virel, and L.-M. Cléon, "Effect of cross winds on high-speed trains: development of a new experimental methodology," *Journal of Wind Engineering and Industrial Aerodynamics*, vol. 92, no. 7, pp. 535-545, 2004.

- [56] X. Liu, Y. Han, C. Cai, M. Levitan, and D. Nikitopoulos, "Wind tunnel tests for mean wind loads on road vehicles," *Journal of Wind Engineering and Industrial Aerodynamics*, vol. 150, pp. 15-21, 2016.
- [57] S. Coleman, and C. Baker, "An experimental study of the aerodynamic behaviour of high sided lorries in cross winds," *Journal of Wind Engineering and Industrial Aerodynamics*, vol. 53, no. 3, pp. 401-429, 1994.
- [58] C. Baker, and N. Humphreys, "Assessment of the adequacy of various wind tunnel techniques to obtain aerodynamic data for ground vehicles in cross winds," *Journal of Wind Engineering and Industrial Aerodynamics*, vol. 60, pp. 49-68, 1996.
- [59] D. Schröck, N. Widdecke, and J. Wiedemann, "Aerodynamic response of a vehicle model to turbulent wind."
- [60] S. Ahmed, G. Ramm, and G. Faltn, Some salient features of the time-averaged ground vehicle wake, 0148-7191, SAE Technical Paper, 1984.
- [61] A. Ryan, and R. G. Dominy, Wake surveys behind a passenger car subjected to a transient cross-wind gust, 0148-7191, SAE Technical Paper, 2000.
- [62] R. Volpe, V. Ferrand, A. Da Silva, and L. Le Moyne, "Forces and flow structures evolution on a car body in a sudden crosswind," *Journal of Wind Engineering and Industrial Aerodynamics*, vol. 128, pp. 114-125, 2014.
- [63] T.-h. Liu, X.-c. Su, J. Zhang, Z.-w. Chen, and X.-s. Zhou, "Aerodynamic performance analysis of trains on slope topography under crosswinds," *Journal of Central South University*, vol. 23, no. 9, pp. 2419-2428, 2016.
- [64] K. Hedegaard, and S. E. Larsen, Wind Speed and Direction Changes Due to Terrain Effects Revealed by Climatological Data from Two Sites in Jutland: Risø, 1983.
- [65] T.-h. Liu, and J. Zhang, "Effect of landform on aerodynamic performance of high-speed trains in cutting under cross wind," *Journal of Central South University*, vol. 20, no. 3, pp. 830-836, 2013.
- [66] H. Kozmar, K. Butler, and A. Kareem, "Downslope gusty wind loading of vehicles on bridges," *Journal of bridge engineering*, vol. 20, no. 11, pp. 04015008, 2015.
- [67] A. Carrarini, "Reliability based analysis of the crosswind stability of railway vehicles," *Mechanical Engineering and Transport Systems*, Berlin University of Technology, 2006.
- [68] B. Schulte-Werning, A. Deutsche Bahn, F.-u. Technologie-Zentrum, and B. Schulte, "The TRANSAERO Project-Joint European Railway Research on Transient Aerodynamics," *TRANSAERO: A European Initiative on Transient Aerodynamics for Railway System Optimisation*, vol. 79, pp. 11, 2013.

- [69] D. Consortium, "Common DEUFRAKO research on cross wind effects on high speed railway operation 2001–2004," Final Report of DEUFRAKO SIDE WIND project, Draft version, vol. 1, 2004.
- [70] O. J. o. t. E. Union, "Technical specification for interoperability," Effects of Crosswinds, 2008.
- [71] B. E. 14067-6:2010, "BS EN 14067-6:2010: Railway applications. ," Aerodynamics. Requirements and test procedures for cross wind assessment, Generic, British Standards Institute, 2010.
- [72] D. Thomas, B. Diedrichs, M. Berg, and S. Stichel, "Dynamics of a high-speed rail vehicle negotiating curves at unsteady crosswind," Proceedings of the Institution of Mechanical Engineers, Part F: Journal of Rail and Rapid Transit, vol. 224, no. 6, pp. 567-579, 2010.
- [73] C. Wetzel, and C. Proppe, "On reliability and sensitivity methods for vehicle systems under stochastic crosswind loads," Vehicle System Dynamics, vol. 48, no. 1, pp. 79-95, 2010.
- [74] X. Zhang, Crosswind stability of vehicles under nonstationary wind excitation: KIT Scientific Publishing, 2015.
- [75] C. Wetzel, and C. Proppe, "Crosswind stability of high-speed trains: a stochastic approach."
- [76] I. 61400-1, "International Standard-Wind turbines," External conditions, IEC 2005, 2005.
- [77] S. Lippert, "On side wind stability of trains," 1999.
- [78] S. Krajnović, "Numerical simulation of the flow around an ICE2 train under the influence of a wind gust."
- [79] M. Tsubokura, T. Nakashima, M. Kitayama, Y. Ikawa, D. H. Doh, and T. Kobayashi, "Large eddy simulation on the unsteady aerodynamic response of a road vehicle in transient crosswinds," International Journal of Heat and Fluid Flow, vol. 31, no. 6, pp. 1075-1086, 2010.
- [80] W. Bierbooms, and P.-W. Cheng, "Stochastic gust model for design calculations of wind turbines," Journal of Wind Engineering and Industrial Aerodynamics, vol. 90, no. 11, pp. 1237-1251, 2002.
- [81] V. Vandecauter, "CFD simulation of atmospheric wind gusts," Master Thesis, 2011.
- [82] J. Vlachopoulos, "Fundamentals of Fluid Mechanics," Dept. of Chemical Engineering, McMaster University, Hamilton, Canada, 2016.
- [83] T. Cebeci, J. P. Shao, F. Kafyke, and E. Laurendeau, Computational fluid dynamics for engineers: Springer Berlin Heidelberg, 2005.

- [84] S. V. Patankar, and D. B. Spalding, "A calculation procedure for heat, mass and momentum transfer in three-dimensional parabolic flows," *International journal of heat and mass transfer*, vol. 15, no. 10, pp. 1787-1806, 1972.
- [85] N. Markatos, "The theoretical prediction of external aerodynamics of road vehicles," *Vehicle Design SP3*, pp. 387-400, 1983.
- [86] F. R. Menter, "Two-equation eddy-viscosity turbulence models for engineering applications," *AIAA journal*, vol. 32, no. 8, pp. 1598-1605, 1994.
- [87] X. Tang, X. Ding, and Z. Chen, "Large eddy simulations of three-dimensional flows around a spur dike," *Tsinghua Science & Technology*, vol. 11, no. 1, pp. 117-123, 2006.
- [88] N. Patel, H. Hemida, and A. Quinn, "Large-Eddy Simulations of the airflow around a vehicle."
- [89] A. Quinn, M. Sterling, A. Robertson, and C. Baker, "An investigation of the wind-induced rolling moment on a commercial vehicle in the atmospheric boundary layer," *Proceedings of the Institution of Mechanical Engineers, Part D: Journal of Automobile Engineering*, vol. 221, no. 11, pp. 1367-1379, 2007.
- [90] H. Hemida, and C. Baker, "Large-eddy simulation of the flow around a freight wagon subjected to a crosswind," *Computers & Fluids*, vol. 39, no. 10, pp. 1944-1956, 2010.
- [91] S. Krajnović, P. Ringqvist, K. Nakade, and B. Basara, "Large eddy simulation of the flow around a simplified train moving through a crosswind flow," *Journal of Wind Engineering and Industrial Aerodynamics*, vol. 110, pp. 86-99, 2012.
- [92] T. Favre, and G. Efraimsson, "An assessment of detached-eddy simulations of unsteady crosswind aerodynamics of road vehicles," *Flow, Turbulence and Combustion*, vol. 87, no. 1, pp. 133-163, 2011.
- [93] C. Baker, "Ground vehicles in high cross winds part III: The interaction of aerodynamic forces and the vehicle system," *Journal of fluids and structures*, vol. 5, no. 2, pp. 221-241, 1991.
- [94] M. Tsubokura, T. Nakashima, T. Ikenaga, K. Onishi, K. Kitoh, N. Oshima, and T. Kobayashi, *HPC-LES for the Prediction of Unsteady Aerodynamic Forces on a Vehicle in a Gusty Cross-flow Condition*, SAE Technical Paper, 2008.
- [95] Z. Lozia, "Rollover thresholds of the biaxial truck during motion on an even road," *Vehicle System Dynamics*, vol. 29, no. S1, pp. 735-740, 1998.
- [96] T. Shim, and C. Ghike, "Understanding the limitations of different vehicle models for roll dynamics studies," *Vehicle system dynamics*, vol. 45, no. 3, pp. 191-216, 2007.

- [97] G. J. Forkenbrock, W. R. Garrott, M. Heitz, and B. C. O’Harra, “A comprehensive experimental examination of test maneuvers that may induce on-road, untripped light vehicle rollover–Phase IV of NHTSA’s light vehicle rollover research program,” Report No. DOT HS, vol. 809, pp. 513, 2002.
- [98] K. Hussain, W. Stein, and A. J. Day, “Modelling commercial vehicle handling and rolling stability,” Proceedings of the Institution of Mechanical Engineers, Part K: Journal of Multi-body Dynamics, vol. 219, no. 4, pp. 357-369, 2005.
- [99] H. Rahnejat, Multi-body dynamics: vehicles, machines, and mechanisms: Wiley, 1998.
- [100] S. Hegazy, H. Rahnejat, and K. Hussain, “Multi-body dynamics in full-vehicle handling analysis under transient manoeuvre,” Vehicle System Dynamics, vol. 34, no. 1, pp. 1-24, 2000.
- [101] M. Blundell, and D. Harty, The multibody systems approach to vehicle dynamics: Elsevier, 2004.
- [102] T. Nakashima, M. Tsubokura, T. Ikenaga, and Y. Doi, HPC-LES for Unsteady Aerodynamics of a Heavy Duty Truck in Wind Gust-2nd report: Coupled Analysis with Vehicle Motion, 0148-7191, SAE Technical Paper, 2010.
- [103] T. Nakashima, M. Tsubokura, M. Vazquez, H. Owen, and Y. Doi, “Coupled analysis of unsteady aerodynamics and vehicle motion of a road vehicle in windy conditions,” Computers & Fluids, vol. 80, pp. 1-9, 2013.
- [104] Y. Maruyama, and F. Yamazaki, “Driving simulator experiment on the moving stability of an automobile under strong crosswind,” Journal of Wind Engineering and Industrial Aerodynamics, vol. 94, no. 4, pp. 191-205, 2006.
- [105] E. Harwin, and L. Emery, The crash avoidance rollover study: A database for the investigation of single vehicle rollover crashes: NHTSA, 1989.
- [106] S.-K. Chen, N. Moshchuk, F. Nardi, and J. Ryu, “Vehicle rollover avoidance,” IEEE Control Systems, vol. 30, no. 4, pp. 70-85, 2010.
- [107] J. Jung, T. Shim, and J. Gertsch, “A vehicle roll-stability indicator incorporating roll-center movements,” IEEE Transactions on Vehicular Technology, vol. 58, no. 8, pp. 4078-4087, 2009.
- [108] B.-C. Chen, and H. Peng, “Rollover warning for articulated heavy vehicles based on a time-to-rollover metric,” Journal of dynamic systems, measurement, and control, vol. 127, no. 3, pp. 406-414, 2005.
- [109] D. Hyun, and R. Langari, “Modeling to predict rollover threat of tractor-semitrailers,” Vehicle System Dynamics, vol. 39, no. 6, pp. 401-414, 2003.

- [110] B. Zhu, Q. Piao, J. Zhao, and L. Guo, "Integrated chassis control for vehicle rollover prevention with neural network time-to-rollover warning metrics," *Advances in Mechanical Engineering*, vol. 8, no. 2, pp. 1687814016632679, 2016.
- [111] J. Yoon, D. Kim, and K. Yi, "Design of a rollover index-based vehicle stability control scheme," *Vehicle system dynamics*, vol. 45, no. 5, pp. 459-475, 2007.
- [112] A. G. Nalecz, *Intermediate Maneuver Induced Rollover Simulation (IMIRS) and Sensitivity Analysis*: National Highway Traffic Safety Administration, 1991.
- [113] M. Yu, J. Liu, D. Liu, H. Chen, and J. Zhang, "Investigation of aerodynamic effects on the high-speed train exposed to longitudinal and lateral wind velocities," *Journal of Fluids and Structures*, vol. 61, pp. 347-361, 2016.
- [114] Y. He, X. Yan, D. Chu, C. Wu, and Z. Chen, "Contribution of wind forces to rollover stability of heavy duty vehicle." pp. 173-176.
- [115] K. R. Cooper, *The wind tunnel testing of heavy trucks to reduce fuel consumption*, 0148-7191, SAE Technical Paper, 1982.
- [116] K. Cooper, "Bluff-body aerodynamics as applied to vehicles," *Journal of Wind Engineering and Industrial Aerodynamics*, vol. 49, no. 1-3, pp. 1-21, 1993.
- [117] D. V. Sumantran, and D. G. Sovran, "Vehicle Aerodynamics," Warrendale, PA: Society of Automotive Engineers, 1996. 688, 1996.
- [118] T. F. I. (2014). "COBRA PROBE," [https://www.turbulentflow.com.au/Downloads/Cat\\_CobraProbe.pdf](https://www.turbulentflow.com.au/Downloads/Cat_CobraProbe.pdf).
- [119] A. M. Aly, A. G. Chowdhury, and G. Bitsuamlak, "Wind profile management and blockage assessment for a new 12-fan Wall of Wind facility at FIU," *Wind & Structures*, vol. 14, no. 4, pp. 285-300, 2011.
- [120] K. Sehn, *Aerodynamic mitigation of extreme wind loading on low-rise buildings*: Iowa State University, 2008.
- [121] H. Kozmar, K. Butler, and A. Kareem, "Transient cross-wind aerodynamic loads on a generic vehicle due to bora gusts," *Journal of wind engineering and industrial aerodynamics*, vol. 111, pp. 73-84, 2012.
- [122] K. Butler, and A. Kareem, "Physical and numerical modeling of downburst generated gust fronts." pp. 791-798.
- [123] K. Butler, A. Kareem, S. Cao, and Y. Tamura, "Analysis of the Surface Pressure Characteristics of Prismatic Models in Gust Front and Downburst Outflows." pp. 22-29.
- [124] V. Malviya, N. Gundala, and R. Mishra, "Effect of cross wind on aerodynamic coefficients of ground vehicles," 2009.

- [125] F. Cheli, R. Corradi, E. Sabbioni, and G. Tomasini, "Wind tunnel tests on heavy road vehicles: cross wind induced loads—part 1," *Journal of Wind Engineering and Industrial Aerodynamics*, vol. 99, no. 10, pp. 1000-1010, 2011.
- [126] G. Franck, N. Nigro, M. Storti, and J. D'Elía, "Numerical simulation of the flow around the Ahmed vehicle model," *Latin American applied research*, vol. 39, no. 4, pp. 295-306, 2009.
- [127] K. H. Lo, and K. Kontis, "Flow around an articulated lorry model," *Experimental Thermal and Fluid Science*, vol. 82, pp. 58-74, 2017.
- [128] F. Cheli, F. Ripamonti, D. Rocchi, and G. Tomasini, "Aerodynamic behaviour investigation of the new EMUV250 train to cross wind," *Journal of Wind Engineering and Industrial Aerodynamics*, vol. 98, no. 4, pp. 189-201, 2010.
- [129] D. Rocchi, L. Rosa, E. Sabbioni, M. Sbroisi, and M. Belloli, "A numerical–experimental methodology for simulating the aerodynamic forces acting on a moving vehicle passing through the wake of a bridge tower under cross wind," *Journal of Wind Engineering and Industrial Aerodynamics*, vol. 104, pp. 256-265, 2012.
- [130] S. Oka, and T. Ishihara, "Numerical study of fluctuating aerodynamic characteristics of a square prism in a uniform flow."
- [131] X.-n. QI, Y.-q. LIU, and G.-s. DU, "Experimental and numerical studies of aerodynamic performance of trucks," *Journal of Hydrodynamics, Ser. B*, vol. 23, no. 6, pp. 752-758, 2011.
- [132] S. Bell, *A beginner's guide to uncertainty of measurement. Issue 2*, National Physical Laboratory, Report, 1999.
- [133] B. Freegah, "Design, development and optimisation of a novel thermo-syphon system for domestic applications," University of Huddersfield, 2016.
- [134] A. Alonso-Estébanez, J. Del Coz Díaz, F. P. Álvarez Rabanal, and P. Pascual-Muñoz, "Numerical simulation of bus aerodynamics on several classes of bridge decks," *Engineering Applications of Computational Fluid Mechanics*, vol. 11, no. 1, pp. 435-449, 2017.
- [135] T. Asim, "Computational Fluid Dynamics based Diagnostics and Optimal Design of Hydraulic Capsule Pipelines," University of Huddersfield, 2013.
- [136] M. Tsubokura, T. Kobayashi, T. Nakashima, T. Nouzawa, T. Nakamura, H. Zhang, K. Onishi, and N. Oshima, "Computational visualization of unsteady flow around vehicles using high performance computing," *Computers & Fluids*, vol. 38, no. 5, pp. 981-990, 2009.

- [137] M. B. Asress, and J. Svorcan, "Numerical investigation on the aerodynamic characteristics of high-speed train under turbulent crosswind," *Journal of Modern Transportation*, vol. 22, no. 4, pp. 225-234, 2014.
- [138] A. Fluent, "Ansys fluent," Academic Research. Release, vol. 14, 2015.
- [139] M. Noor, A. P. Wandel, and T. Yusaf, "Detail guide for CFD on the simulation of biogas combustion in bluff-body mild burner." pp. 1-25.
- [140] A. Fluent, "12.0 Theory Guide," Ansys Inc, vol. 5, 2009.
- [141] X.-m. Shao, J. Wan, D.-w. Chen, and H.-b. Xiong, "Aerodynamic modeling and stability analysis of a high-speed train under strong rain and crosswind conditions," *Journal of Zhejiang University-SCIENCE A*, vol. 12, no. 12, pp. 964-970, 2011.
- [142] T. Bruckmann, C. Sturm, and L. Wildan, "Wind tunnels and experimental fluid dynamics research," Tech, ch. Wire Robot Suspension Systems for Wind Tunnels, pp. 978-953, 2011.
- [143] T. Wielenga, "Analysis methods and model representation in ADAMS," MDI Technical paper, no. 41, 1987.
- [144] S. Kushairi, R. Schmidt, A. R. Omar, A. A. Mat Isa, and K. Hudha, "Tractor-trailer modelling and validation," *International Journal of Heavy Vehicle Systems*, vol. 21, no. 1, pp. 64-82, 2014.
- [145] R. Rajamani, *Vehicle dynamics and control*: Springer Science & Business Media, 2011.
- [146] N. Lewington, L. Ohra-aho, O. Lange, and K. Rudnik, *The Application of a One-Way Coupled Aerodynamic and Multi-Body Dynamics Simulation Process to Predict Vehicle Response during a Severe Crosswind Event*, 0148-7191, SAE Technical Paper, 2017.
- [147] M. Adams, and C. Documentation, "Msc," Software Corporation, 2005.
- [148] B. D. Schlueter, "Predicting Vehicle Dynamics for Roadside Safety Using Multibody Systems Simulations," 2012.
- [149] D. Anderson, G. Schade, S. Hamill, and P. O'Heron, *Development of a multi-body dynamic model of a tractor-semitrailer for ride quality prediction*, 0148-7191, SAE Technical Paper, 2001.
- [150] A. Bouferrouk, "Methods of calculating aerodynamic force on a vehicle subject to turbulent crosswinds," *American Journal of Fluid Dynamics*, vol. 3, no. 4, pp. 119-134, 2013.
- [151] M. Chay, R. Wilson, and F. Albermani, "Gust occurrence in simulated non-stationary winds," *Journal of Wind Engineering and Industrial Aerodynamics*, vol. 96, no. 10, pp. 2161-2172, 2008.

- [152] H. Wang, T. Wu, T. Tao, A. Li, and A. Kareem, "Measurements and analysis of non-stationary wind characteristics at Sutong Bridge in Typhoon Damrey," *Journal of Wind Engineering and Industrial Aerodynamics*, vol. 151, pp. 100-106, 2016.
- [153] C. Bottasso, A. Croce, and B. Savini, "Performance comparison of control schemes for variable-speed wind turbines." p. 012079.
- [154] I. Suomi, S. E. Gryning, R. Floors, T. Vihma, and C. Fortelius, "On the vertical structure of wind gusts," *Quarterly Journal of the Royal Meteorological Society*, vol. 141, no. 690, pp. 1658-1670, 2015.
- [155] L. Kristensen, M. Casanova, M. Courtney, and I. Troen, "In search of a gust definition," *Boundary-Layer Meteorology*, vol. 55, no. 1, pp. 91-107, 1991.
- [156] W. Bierbooms, J. B. Dragt, and H. Cleijne, "Verification of the mean shape of extreme gusts," *Wind Energy*, vol. 2, no. 3, pp. 137-150, 1999.
- [157] F. Cheli, R. Corradi, and G. Tomasini, "Crosswind action on rail vehicles: A methodology for the estimation of the characteristic wind curves," *Journal of Wind Engineering and Industrial Aerodynamics*, vol. 104, pp. 248-255, 2012.
- [158] C. Baker, "The simulation of unsteady aerodynamic cross wind forces on trains," *Journal of wind engineering and industrial aerodynamics*, vol. 98, no. 2, pp. 88-99, 2010.
- [159] J. García, J. Muñoz-Paniagua, A. Jiménez, E. Migoya, and A. Crespo, "Numerical study of the influence of synthetic turbulent inflow conditions on the aerodynamics of a train," *Journal of Fluids and Structures*, vol. 56, pp. 134-151, 2015.
- [160] A. J. Majda, and P. R. Kramer, "Simplified models for turbulent diffusion: theory, numerical modelling, and physical phenomena," *Physics reports*, vol. 314, no. 4, pp. 237-574, 1999.
- [161] A. Smirnov, S. Shi, and I. Celik, "Random flow generation technique for large eddy simulations and particle-dynamics modeling," *Transactions of the ASME-I-Journal of Fluids Engineering*, vol. 123, no. 2, pp. 359-371, 2001.
- [162] T. H. RST, "Commission decision of 21 February 2008 concerning a technical specification for interoperability relating to the 'rolling stock' sub-system of the trans-European high-speed rail system," *Official Journal of the European Union*, vol. L847132, no. L847132, pp. Directive 2008/232/CE, 26.03.2008.
- [163] H. TSI, "Technical specification for interoperability relating to the 'rolling stock' sub-system of the trans-European high-speed rail system," 2008.

- [164] A. Muyschondt, "Vehicle response to aerodynamic loads," Texas Tech University, 1988.
- [165] D. C. Forbes, G. J. Page, M. A. Passmore, and A. P. Gaylard, "A fully coupled, 6 degree-of-freedom, aerodynamic and vehicle handling crosswind simulation using the DrivAer model," 2016.
- [166] H. Ishioka, K. Onishi, K. Nakasato, T. Nakashima, and M. Tsubokura, "Coupled 6DoF motion and Aerodynamics Simulation of Road Vehicles in Crosswind gusts."
- [167] F. Boettiger, K. Hunt, and R. Kamnik, "Roll dynamics and lateral load transfer estimation in articulated heavy freight vehicles," *Proc. Instn Mech. Engrs*, vol. 217, no. Part D, 2003.
- [168] C. Mallikarjunarao, and P. Fancher, Analysis of the directional response characteristics of double tankers, 0148-7191, SAE Technical Paper, 1978.
- [169] Y. Sellami, H. Imine, A. H. El Hadri, and J. Cadiou, Probabilistic detection of rollover risk of heavy vehicles, 0148-7191, SAE Technical Paper, 2008.
- [170] M. G. Balsom, Contribution of Wind Forces to Lateral Acceleration of Tractor Semi-trailer Units: University of New Brunswick (Canada), 2004.
- [171] W. W. Wang, and J. F. Xu, "Virtual Prototype Co-Simulation of 4WS Vehicle." pp. 408-411.
- [172] D. Tan, H. Wang, and Q. Wang, "Study on the Rollover Characteristic of In-Wheel-Motor-Driven Electric Vehicles Considering Road and Electromagnetic Excitation," *Shock and Vibration*, vol. 2016, 2016.
- [173] S. F. van der Westhuizen, and P. S. Els, "Slow active suspension control for rollover prevention," *Journal of Terramechanics*, vol. 50, no. 1, pp. 29-36, 2013.
- [174] C. Baker, "A framework for the consideration of the effects of crosswinds on trains," *Journal of Wind Engineering and Industrial Aerodynamics*, vol. 123, pp. 130-142, 2013.
- [175] Q. Dong-chen, X. Yi-cun, Z. Qiang, and Y. Li, "Modeling and simulation study on crosswind stability of the high-speed bus," *Noise & Vibration Worldwide*, vol. 42, no. 11, pp. 44-50, 2011.
- [176] Z.-q. GU, H.-y. WANG, R.-f. LUO, and Y.-k. ZHOU, "Study on Automobile Cross-Wind Stability in Consideration of Pressure Center's Shift [J]," *Journal of Hunan University (Natural Science)*, vol. 3, pp. 016, 2005.
- [177] B. Johansson, and M. Gafvert, "Untripped SUV rollover detection and prevention." pp. 5461-5466.

- [178] I. Han, and K. Rho, "Characteristic analysis of vehicle rollover accidents: Rollover scenarios and prediction/warning," *International Journal of Automotive Technology*, vol. 18, no. 3, pp. 451-461, 2017.
- [179] A. G. Nalecz, "Influence of vehicle and roadway factors on the dynamics of tripped rollover," *International Journal of Vehicle Design*, vol. 10, no. 3, pp. 321-346, 1989.
- [180] S. B. Choi, "Practical vehicle rollover avoidance control using energy method," *Vehicle System Dynamics*, vol. 46, no. 4, pp. 323-337, 2008.
- [181] X. Wu, X. Ge, and H. Huang, "Study on vehicle rollover avoidance." pp. 681-684.
- [182] N. Zhang, G.-M. Dong, and H.-P. Du, "Investigation into untripped rollover of light vehicles in the modified fishhook and the sine maneuvers. Part I: Vehicle modelling, roll and yaw instability," *Vehicle System Dynamics*, vol. 46, no. 4, pp. 271-293, 2008.
- [183] D. Baker, R. Bushman, P. Eng, and C. Berthelot, "The Effectiveness of Truck Rollover Warning Systems," University of Saskatchewan, Department of Civil Engineering, 2000.
- [184] R. Strickland, and H. McGee, "Evaluation results of three prototype automatic truck rollover warning systems," *Transportation Research Record: Journal of the Transportation Research Board*, no. 1628, pp. 41-49, 1998.
- [185] M. Tsubokura, K. Takahashi, T. Matsuuki, T. Nakashima, T. Ikenaga, and K. Kitoh, HPC-LES for Unsteady Aerodynamics of a Heavy Duty Truck in Wind Gust-1st Report: Validation and Unsteady Flow Structures, 0148-7191, SAE Technical Paper, 2010.
- [186] I. TC88-MT, "IEC 61400-3: Wind Turbines–Part 1: Design Requirements," International Electrotechnical Commission, Geneva, 2005.

## APPENDIX A

Dynamic properties of Tractor Semitrailer model in the ADAMS/CAR package

\*\*\*\*\* ASSEMBLY INFO \*\*\*\*\*

Assembly Name : msc\_tractor\_semitrailer\_1  
Assembly Class : full\_vehicle  
File Name : <atruck\_shared>/assemblies.tbl/msc\_tractor\_semitrailer.asy  
VERIFY MODEL: . msc\_tractor\_semitrailer\_1  
627 Gruebler Count (approximate degrees of freedom)  
189 Moving Parts (not including ground)  
14 Cylindrical Joints  
23 Revolute Joints  
3 Spherical Joints  
1 Translational Joints  
1 Convel Joints  
46 Fixed Joints  
3 Hooke Joints  
1 Inline Primitive\_Joints  
1 Inplane Primitive\_Joints  
1 Parallel\_axes Primitive\_Joints  
16 Perpendicular Primitive\_Joints  
3 Motions  
6 Couplers

SUBSYSTEM NAME	MAJOR ROLE	MINOR ROLE
msc_truck_aux_parts	aux_parts	any
msc_truck_beam_leaf_spring	leaf_spring	front
msc_truck_cab_suspension	cab_suspension	any
msc_tractor_tandem_drive_axle	suspension	rear
msc_truck_drive_wheels	wheel	rear
msc_truck_drive_wheels_2	wheel	rear_2
msc_truck_powertrain	powertrain	any
msc_truck_rigid_cab	cab	any
msc_truck_rigid_tractor	body	any
msc_truck_steer_suspension	suspension	front
msc_truck_steer_wheels	wheel	front
msc_truck_steering	steering	front
msc_truck_air_drum_brakes	brake_system	any
msc_truck_rigid_trailer	body	trailer
msc_truck_trailer_axle_front	suspension	trailer
msc_truck_trailer_axle_rear	suspension	trailer_2
msc_truck_trailer_wheels	wheel	trailer
msc_truck_trailer_wheels_2	wheel	trailer_2
msc_truck_trailer_air_drum_brakes	brake_system	trailer

\*\*\*\*\* Trailer body Subsystem INFO \*\*\*\*\*

Location : 1.609526484E+004, 0.0, 2192.901803418 (mm, mm, mm)  
(LOC\_RELATIVE\_TO({0.0, 0.0, 0.0}mm, .trailer\_assy\_goodl.trailer\_good\_4.ground.hps\_Trailer\_body\_cm)) mm, mm, mm  
Orientation : 270.0, 0.0, 0.0 (deg)  
Ground Part : False  
Mass : 5600.0 kg  
Center Marker : .trailer\_assy\_goodl.trailer\_good\_4.ges\_trailer\_body.cm  
Inertia Marker : .trailer\_assy\_goodl.trailer\_good\_4.ges\_trailer\_body.inertia\_frame  
Mass Inertia Tensor :  
IXX : 1.4175E+011 kg-mm\*\*2  
IYY : 1.40899E+011 kg-mm\*\*2  
IZZ : 1.03308E+010 kg-mm\*\*2  
IXY : 0.0 kg-mm\*\*2  
IZX : 0.0 kg-mm\*\*2  
IYZ : 0.0 kg-mm\*\*2  
No Initial Velocities  
Exact Coordinates : None

\*\*\*\*\* Cab body Subsystem INFO \*\*\*\*\*

Object Type : Part  
Parent Type : Model  
Adams ID : 239  
Active : NO\_OPINION  
Location : 4011.7, 60.6, 2222.1 (mm, mm, mm)  
(LOC\_RELATIVE\_TO({0.0, 0.0, 0.0}mm, .trailer\_assy\_goodl.msc\_truck\_rigid\_cab.ground.hps\_cab\_cm)) mm, mm, mm  
Orientation : 0.0, 0.0, 0.0 (deg)  
(ORI\_RELATIVE\_TO({0.0, 0.0, 0.0}degrees, .trailer\_assy\_goodl.msc\_truck\_rigid\_cab.ground.cfs\_origin)) deg  
Ground Part : False  
Mass : 1000.0 kg  
Center Marker : .trailer\_assy\_goodl.msc\_truck\_rigid\_cab.ges\_cab.cm  
Inertia Marker : .trailer\_assy\_goodl.msc\_truck\_rigid\_cab.ges\_cab.inertia\_frame  
Mass Inertia Tensor :  
IXX : 2.35E+010 kg-mm\*\*2  
IYY : 7.0E+009 kg-mm\*\*2  
IZZ : 1.7E+010 kg-mm\*\*2  
IXY : 0.0 kg-mm\*\*2  
IZX : 0.0 kg-mm\*\*2  
IYZ : 0.0 kg-mm\*\*2  
No Initial Velocities  
Exact Coordinates : None

\*\*\*\*\* Wheels\_2 Subsystem INFO \*\*\*\*\*

Object Type : Part  
Parent Type : Model  
Adams ID : 209  
Active : NO\_OPINION  
Global :  
Location : 8705.9, -693.447, 758.4 (mm, mm, mm)

(LOC\_RELATIVE\_TO({0.0, 0.0, 0.0}mm, .trailer\_assy\_goodl.msc\_truck\_drive\_wheels\_2.ground.cfl\_spin\_axis)) mm, mm,  
 mm  
 Orientation : 0.0, 90.0, 0.0 (deg)  
 (ORI\_RELATIVE\_TO({0.0, 0.0, 0.0}degrees, .trailer\_assy\_goodl.msc\_truck\_drive\_wheels\_2.ground.cfl\_spin\_axis)) deg  
 Ground Part : False  
 Mass : 150.0 kg  
 Center Marker : .trailer\_assy\_goodl.msc\_truck\_drive\_wheels\_2.whl\_inside\_wheel.cm  
 Inertia Marker : None  
 Mass Inertia Tensor :  
 IXX : 1.3E+007 kg-mm\*\*2  
 IYY : 1.3E+007 kg-mm\*\*2  
 IZZ : 2.0E+007 kg-mm\*\*2  
 IXY : 0.0 kg-mm\*\*2  
 IZX : 0.0 kg-mm\*\*2  
 IYZ : 0.0 kg-mm\*\*2  
 No Initial Velocities  
 Exact Coordinates : None

\*\*\*\*\*Steer SuspensionSubsystem INFO \*\*\*\*\*

Object Type : Part  
 Parent Type : Model  
 Adams ID : 247  
 Active : NO\_OPINION  
 Global :  
 Location : 2100.0, 422.34, 587.5 (mm, mm, mm)  
 (LOC\_CENTERED({.trailer\_assy\_goodl.msc\_truck\_steer\_suspension.ground.hpr\_lower\_kingpin\_axis.loc,  
 .trailer\_assy\_goodl.msc\_truck\_steer\_suspension.ground.hps\_axle\_center.loc}, 2)) mm, mm, mm  
 Orientation : 180.0, 88.3059940745, 180.0 (deg)  
 (ORI\_IN\_PLANE(trailer\_assy\_goodl.msc\_truck\_steer\_suspension.ger\_axle,  
 .trailer\_assy\_goodl.msc\_truck\_steer\_suspension.ground.hpr\_lower\_kingpin\_axis,  
 .trailer\_assy\_goodl.msc\_truck\_steer\_suspension.ground.hps\_axle\_center, "Z\_ZX")) deg  
 Ground Part : False  
 Mass : 110.0 kg  
 Center Marker : .trailer\_assy\_goodl.msc\_truck\_steer\_suspension.ger\_axle.cm  
 Inertia Marker : .trailer\_assy\_goodl.msc\_truck\_steer\_suspension.ger\_axle.inertia\_frame  
 Mass Inertia Tensor :  
 IXX : 4.8E+007 kg-mm\*\*2  
 IYY : 4.7E+007 kg-mm\*\*2  
 IZZ : 2.7E+006 kg-mm\*\*2  
 IXY : 0.0 kg-mm\*\*2  
 IZX : 0.0 kg-mm\*\*2  
 IYZ : 0.0 kg-mm\*\*2  
 No Initial Velocities  
 Exact Coordinates : None

\*\*\*\*\*Trailer\_axle\_front Subsystem INFO \*\*\*\*\*

Object Type : Part  
 Parent Type : Model  
 Adams ID : 298  
 Active : NO\_OPINION

Global :  
 Location : 1.834442E+004, 0.0, 835.73 (mm, mm, mm)  
 (LOC\_RELATIVE\_TO({0.0, 0.0, 0.0}mm, .trailer\_assy\_goodl.msc\_truck\_trailer\_axle\_front.ground.hps\_axle\_cg)) mm,  
 mm, mm  
 Orientation : 0.0, 0.0, 0.0 (deg)  
 (ORI\_RELATIVE\_TO({0.0, 0.0, 0.0}degrees, .trailer\_assy\_goodl.msc\_truck\_trailer\_axle\_front.ground.cfs\_axle\_ori)) deg  
 Ground Part : False  
 Mass : 83.274 kg  
 Center Marker : .trailer\_assy\_goodl.msc\_truck\_trailer\_axle\_front.ges\_axle.cm  
 Inertia Marker : .trailer\_assy\_goodl.msc\_truck\_trailer\_axle\_front.ges\_axle.inertia\_frame  
 Mass Inertia Tensor :  
 IXX : 2.8547455198E+007 kg-mm\*\*2  
 IYY : 2.8402492278E+007 kg-mm\*\*2  
 IZZ : 3.9216539048E+005 kg-mm\*\*2  
 IXY : 0.0 kg-mm\*\*2  
 IZX : 0.0 kg-mm\*\*2  
 IYZ : 0.0 kg-mm\*\*2  
 No Initial Velocities  
 Exact Coordinates : None

## APPENDIX B

### Exponent coefficients of the TSI gust

From the coherence decay and exponent coefficients of the gust parallel and perpendicular to the mean wind speed a correlation function at an instant t can be calculated as:

$$C(t) = \exp \sqrt{(C_u^x P_u^x)^2 + (C_u^y P_u^y)^2}$$

with

C(t) being the correlation function between the amplitude of the gust at instant t and the maximum amplitude of gust;

$C_u^x$  is the coherence decay coefficient in the mean wind direction (parameter value: 5,0);

$C_u^y$  is the coherence decay coefficient perpendicular to the mean wind direction (parameter value: 16,0);

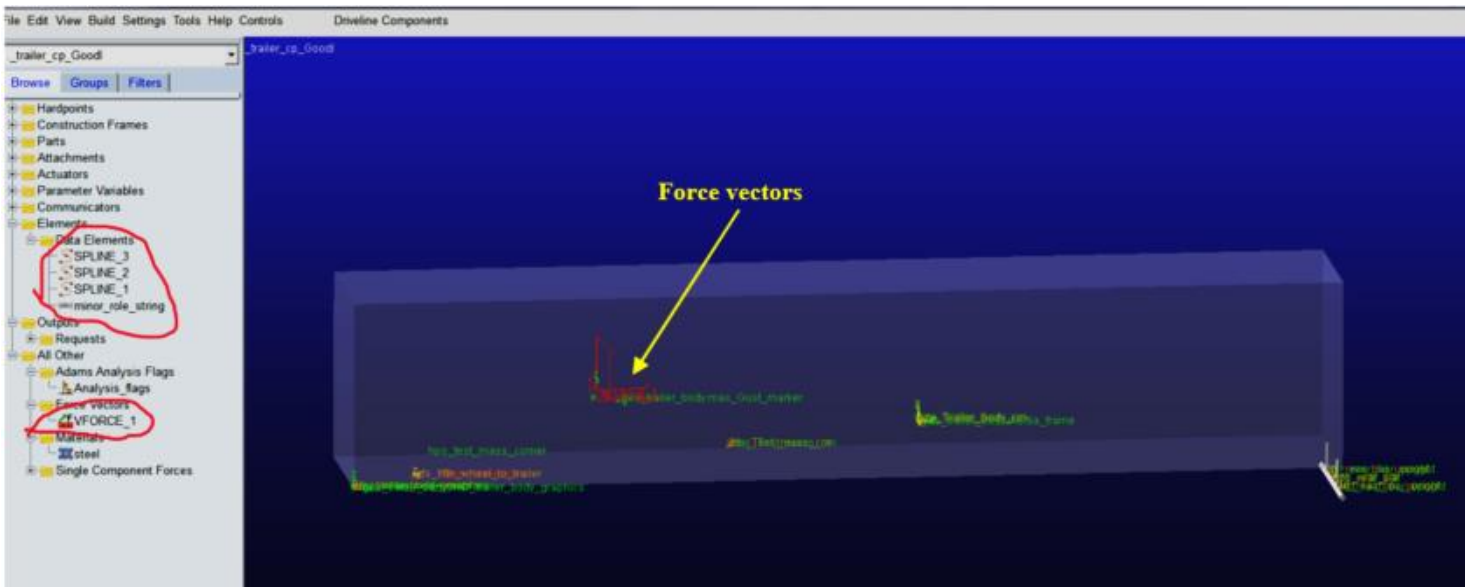
$P_u^x$  is the exponent coefficient in the mean wind direction (parameter value: 1,0)

$P_u^y$  is the exponent coefficient perpendicular to the mean wind direction (parameter value: 1,0).

All the parameters values are based on measurements in [71]

## APPENDIX C

This appendix provides more information on the method of coupling vehicle aerodynamics with vehicle dynamics. Figures below show the force vectors applied to the trailer body at aerodynamic/pressure centre. Spline tools were used to import the values of these forces (i.e., measured or computed aerodynamic forces) to the model.



Force vectors

	X	Y
1	1.111111E-002	344.5666721
2	2.222222E-002	387.4869294
3	3.333333E-002	446.259242
4	4.444444E-002	481.736536
5	5.555552E-002	392.3475158
6	7.777773E-002	600.7572463
7	8.888884E-002	390.3516697
8	0.099999994	462.6954774
9	0.111111104	463.1673669
10	0.122222215	462.6126839
11	0.133333325	476.0489666
12	0.144444436	474.5217372
13	0.155555546	484.2460482
14	0.166666657	487.2363887
15	0.177777767	493.3304044
16	0.188888878	508.0703348
17	0.199999988	511.3129422
18	0.211111099	521.8385393
19	0.222222209	526.4170034
20	0.233333319	532.0074243
21	0.24444443	541.3840605

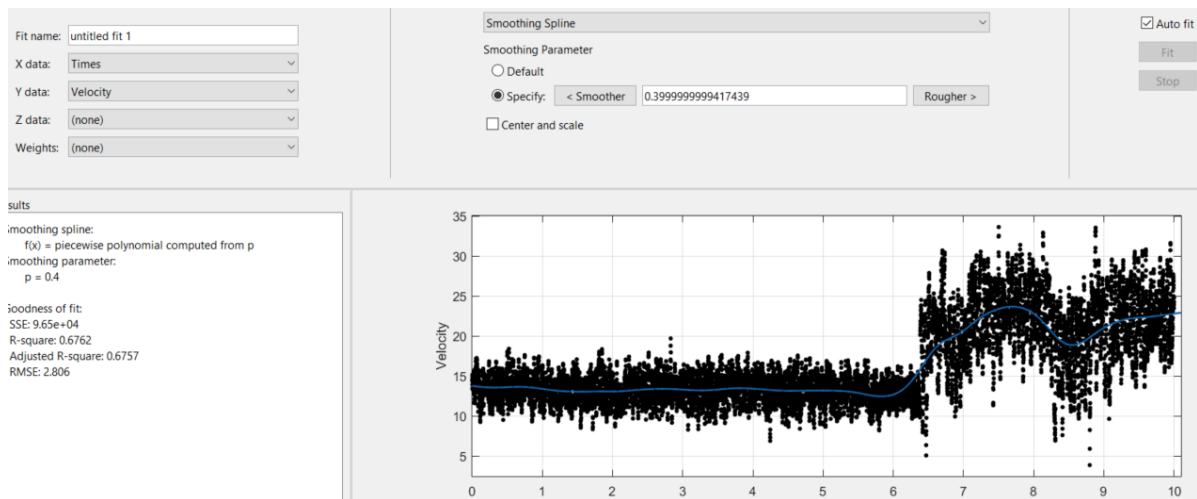
Spline tools (x=time, Y=force)

## APPENDIX D

This appendix provides more information about the characteristics of sampling wind-tunnel flow data collected by Cobra Probe. Also, curve fitting method based on Matlab application that used to develop new gust model is reported.

```
Zero1 (Ve).txt - Notepad
File Edit Format View Help
Device name : Cobra 162
Device type : Four-hole Cobra Probe
Device ID : 162
First sample date : 04-Nov-16
First sample time : 20:33:52.416
Sampling time (s) : 104.858
Number of samples : 131,072
Number of good samples : 131,072 (100.0%)
Data output rate (Hz) : 1,250.0
Output block size : 16,384
Mean temperature (°C) : 19.0
Barometric pressure (Pa) : 101,385.7
Mean reference pressure : 0.0
Mean flow speed, pitch angle, yaw angle and Pstatic (m/s, ° and Pa) :
18.8 4.0 -2.7 105.2
Mean u, v and w (m/s) :
18.4 -0.885 1.30
Minimum and maximum velocities (m/s) :
11.9 35.3
Turbulence intensities - overall, Iuu, Ivv, Iww (%) :
6.64 8.94 5.33 4.88
Reynolds normal stresses - Ruu, Rvv, Rww (Pa) :
-3.33 -1.18 -0.992
Reynolds shear stresses - Ruv, Ruw, Rvw (Pa) :
0.227 -0.0492 -0.000171
Please refer to the user's Guide for definitions of terms.
```

Properties of wind-tunnel flow reported by Cobra Probe



Curve fitting method performed in Matlab

Fit name:

X data:

Y data:

Z data:

Weights:

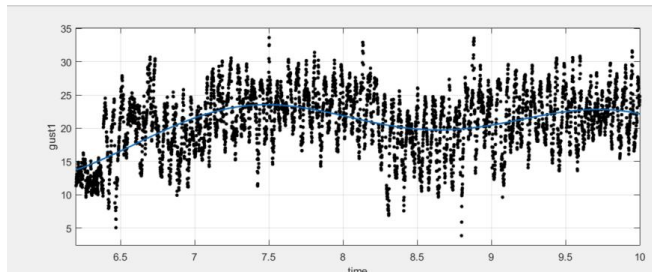
---

Results

General model Sin1:  
 $f(x) = a1 \cdot \sin(b1 \cdot x + c1)$

Coefficients (with 95% confidence bounds):

a1 = 22.48 (22.31, 22.65)  
b1 = 0.3225 (0.308, 0.337)  
c1 = 5.07 (4.962, 5.178)



Curve formula and parameters for gusty period of the wind scenario.